THESE de DOCTORAT

de l'INSTITUT DE PHYSIQUE DU GLOBE DE PARIS

Spécialité: GEOPHYSIQUE PLANETAIRE

présentée par

Ana Rita Baptista

pour obtenir le titre de

DOCTEUR DE L'INSTITUT DE PHYSIQUE DU GLOBE DE PARIS

Permanence du volcanisme sur Mars; Caractérisation de la Province de Tharsis par imagerie et altimétrie

Longstanding volcanism on Mars; surface and lithosphere studies of the Tharsis region using imagery and altimetry data

---

Soutenue le 12/03/2009, devant le jury composé de

Monsieur Steve Tait . . . . . Président du jury

Monsieur Christophe Sotin . . . . . .Rapporteur

Monsieur Daniel Mège . . . . . .Rapporteur

Monsieur François Costard . . . . . .Examinateur

Monsieur Nicolas Mangold. . . . . .Co-Directeur de Thèse

Monsieur Philippe Lognonné . . . . . .Directeur de Thèse

Département de Géophysique Spatiale et Planétaire,

Institut de Physique du Globe de Paris

Remerciements

Je voudrais d'abord remercier tous ceux qui ont contribué au développement de ce travail. Au Professeur Ivo Alves qui dès le début m'a soutenue dans mes choix ainsi qu'à Vera Fernandes et Mark Wieczorek qui m'ont ouvert la possibilité de réaliser ma thèse à l'IPGP. Un énorme merci à Nicolas Mangold, avec qui j'ai beaucoup appris, ainsi qu'à Philippe Lognonné d'avoir partagé son énorme expérience scientifique dans plusieurs domaines. Merci à François Costard de m'avoir très bien reçu à Orsay.

Je voudrais aussi remercier mes collègues de travail et « partageurs d'aventures » ; Sandrine pour son énorme sens de l'humour et esprit pointu. Damien pour sa constante « aura » de paix et avec qui il n'y a jamais de difficultés. Sylvain qui ira certainement changer le visage du monde (même d'autres mondes ?). Lucie et Joséphine deux très sages « écouteuses » de mes états d'esprit et sans qui la production finale de cette thèse n'aurait pu être littéralement possible. A Mathieu et Antoine pour votre amitié avec toujours un très raffiné sens de l'humour. A D. Vaz pour son amitié et sa disponibilité à résoudre les problèmes. Et à tous ceux ou celles qui avec tendresse et/ou professionnalisme ont partagé leurs connaissances et leur amitié ; Laure, Véronique, Hélène, Chiara, Julien, Émeline, Bénédicte, David, Renee, Essam, Chloé, Corinne, Giovanni, Cédric, Pierdavide, Olivier, Sylvain, Tanguy, André et Patrick. Un grand merci à Christiane pour son remarquable professionnalisme, ainsi que à Taoufik pour être toujours disponible et prêt à résoudre les problèmes logistiques. Merci aussi à Jeannine pour les mots si sages et agréables.

Merci aussi à mes amis « parisiens » avec qui j'ai partagé tant d'histoires et qui connaissent aussi bien mes états d'âme ; Patricia, Catarina, Luisinho, Yann, Claudia, Marina, Michelle, Vero, Rafael, Raquel, Samuel, Pedro. Et tous mes amis qui sont plus loin mais aussi présents, *não é gajas* ? *Tininha não me esqueci de ti !*

Enfin, il me reste à remercier ma famille et mes parents, *pelo vosso apoio incondicional em cada fase da minha vida*. A mes beaux parents pour l'encouragement et leur soutien dans la dernière ligne droite de cette thèse. *The last but not the least*, à Régis, avec qui, ensemble, nous allons conquérir le monde!

"L'Homme doit s'élever au-dessus de la Terre,
aux limites de l'atmosphère et au-delà,
ainsi seulement pourra-t-il comprendre tout à fait
le monde dans lequel il vit."

Socrate

Table des matières 1

Généralités sur Mars et Objectifs de ce mémoire de Thèse

La planète Mars et la Terre étaient très semblables il y a 4 milliards d'années. A cette époque comme la Terre, Mars possédait un champ magnétique principal d'origine interne, un volcanisme intense, une atmosphère dense et relativement chaude (grâce à un effet de serre important), de l'eau à la surface et peut-être même une tectonique des plaques. Pourquoi donc ces deux planètes ont-elles évolué si différemment ? Cette question est au centre des recherches menées en planétologie comparée.

L'étude de la structure (noyau, manteau, lithosphère, croûte) et de l'évolution géologique de Mars est réalisée avec l'aide des données des missions spatiales actuelles et passées, qui nous permettent aussi d'élaborer des modèles explicatifs des phénomènes. Concrètement, dans cette étude, et à l'aide de l'analyse des données de topographie et d'imagerie, nous compléterons l'étude de la formation et de la déformation de la croûte et de la lithosphère sous l'effet des gigantesques volcans martiens, notamment ceux du plateau de Tharsis. Ceci nous permet alors de cerner le rôle de la lithosphère, de son épaisseur en particulier, dans la formation des terrains volcaniques de Tharsis. Cela nous donnera aussi des informations sur l'évolution du flux thermique de la planète, sur son intensité et sur l'effet qu'il a pu jouer dans la localisation du volcanisme Martien.

Pour cela nous nous appuierons également sur les derniers modèles de composition chimique et minéralogique de la surface Martienne, ainsi que sur la géomorphologie des structures de la surface. Toutes ces contraintes sont déterminées à distance par les expériences de télédétection embarquées lors des missions de la NASA et de l'ESA.

La mise en place du plateau de Tharsis a contribué d'une façon importante à l'environnement de Mars, en libérant près de 1.5 bar de CO_2 et l'équivalent d'une hauteur d'eau de plus de 100 mètres à l'échelle globale [Phillips et al. 2001]. Par la suite, des épisodes de volcanisme intense furent peut-être à l'origine des périodes plus chaudes et humides [ex. Greeley et Spudis, 1981]. A l'inverse, l'arrêt de la dynamo planétaire et avec elle de la protection de la planète par un champ magnétique [Connerney, 2001], ont entraîné un échappement atmosphérique massif et aussi, probablement, les changements climatiques correspondants [Phillips et al. 2001]. Les vestiges de ce passé chaud et humide se trouvent à la surface de la planète.

Dans l'attente d'un observatoire Géophysique comme le GEP, qui fournira une première estimation du flux de chaleur et des mesures sismiques (et donc des contraintes sur une éventuelle sismicité associée à de la tectonique, [Lognonné et al. 2003] les modèles de lithosphère, critiques pour comprendre l'évolution et la structure des volcans martiens - doivent donc être réalisés à partir des données envoyées par les sondes spatiales orbitales et aussi par des mesures indirectes.

Ces études nous permettent aussi de mieux comprendre le fonctionnement des planètes, les conditions qui règnent à leur surface (température de surface, présence d'eau), leur évolution correspondant à la mise en place de leurs volcans, et la formation des structures de surface qui prouvent l'évolution planétaire et les changements climatiques que la planète a dû subir.

Le volcanisme est un processus fondamental dans le système solaire et est responsable de la formation des surfaces des corps telluriques. Sur Mars, la présence d'éruptions volcaniques récentes est maintenant acceptée (e.x. Neukum et al. [2004]). Elle tient compte des évidences géologiques de la surface, des mesures par comptage de cratères et est aussi prévue par les modèles de conduction thermique paramétrés [Schumacher et Breuer, 2007].

La littérature scientifique reflète les amples débats sur l'origine du volcanisme des grands centres volcaniques : il pourrait avoir été formé par des panaches ou des super-panaches géants [e.x. Esposito et al. 1992], qui auraient apporté assez de chaleur à la lithosphère et auraient ainsi maintenu le volcanisme dans le couvercle convectif. Si

l'origine de ces panaches a été associée aux discontinuités éventuelles entre manteau supérieur et inférieur (Harder, 1998, Breuer et al. 1997, van Thienen et al. 2006) Reese et al [2002] proposent cependant une origine liée à un impact géant alors que Zhong [2008] propose une rotation différentielle de la lithosphère. Toutefois, si ces processus peuvent être envisagés pour le début de Mars, ils sont peu vraisemblables pour expliquer le volcanisme de la planète depuis un milliard d'années. Les processus responsables du maintien d'une activité volcanique jusqu'à aujourd'hui dans une planète de petite taille comme Mars font donc l'objet de cette étude.

La province de Tharsis, avec celle d'Elysium (Figure 1), est la province volcanique la plus importante sur Mars [e.x. Greeley et Spudis, 1981]. Elle inclut une succession de volcans bien développés (Olympus Mons, Arsia, Pavonis, Ascraeus Montes et Alba Patera) en association avec des figures volcaniques de moindre échelle, formées à proximité de figures tectoniques gigantesques telles que les canyons profonds (Valles Marineris), des fossae étendues (Noctis Labyrintus and Claritas) et des grabens radiaux.

Entourée au nord par Noctis Labyrinthus et à l'ouest par Claritas Fossae, une autre région volcanique élevée est présente : Syria Planum (Figure 2).

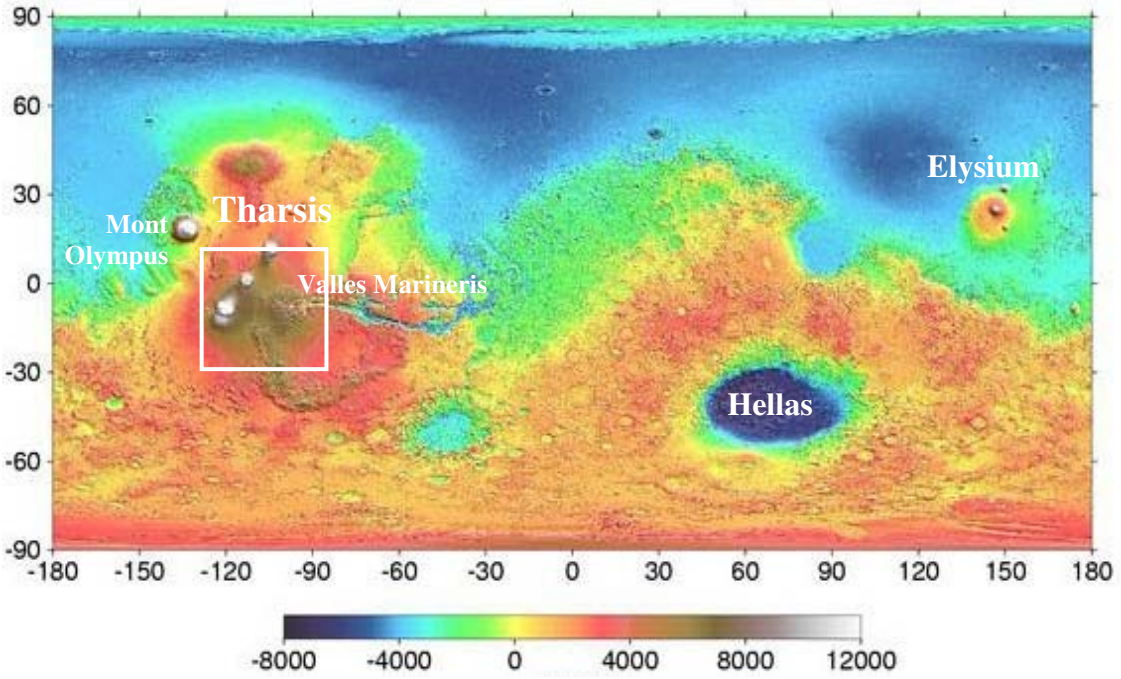

FIG 1 – *Carte de relief de Mars à partir des données MOLA 1/128_ DEM, avec l'échelle d'altitudes. Le carré blanc délimite la carte MOLA agrandie et présentée dans la Figure 2.*

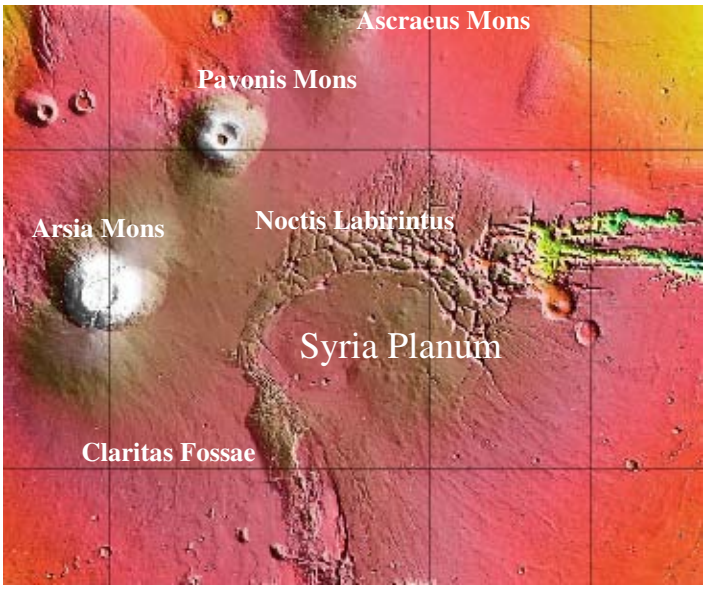

FIG 2 – *Carte de relief MOLA 1/128_ DEM de Syria Planum. Agrandissement du carré blanc en Figure 1.*

Le rôle de l'activité tectonique sur l'évolution de Syria par rapport au rôle principal de l'activité magmatique sur l'évolution des Tharsis Montes et de leur voisinage d'une part, et la relation entre ces deux régions géographiquement proches d'autre part, semblent cruciaux pour comprendre l'évolution thermique et la formation volcanique sur Tharsis et plus généralement sur Mars.

Ainsi, et avec les données, principalement d'imagerie, disponibles, nous pouvons mener une étude approfondie de la région de Syria Planum (Figure 2) : cette zone constitue le dôme volcanique le plus élevé des environs de Tharsis (voir Figure 1) et une étude approfondie de cette zone est nécessaire.

En conséquence, la première partie de cette étude concerne l'analyse de l'histoire volcanique de Syria Planum, grâce aux données topographiques extraites des images stéréoscopiques de haute résolution de la caméra HRSC (à bord de la Mission Mars Express), ainsi que des données altimétriques provenant de l'altimètre laser MOLA (de la Mission Mars Global Surveyor).

Nous avons ainsi identifié et décrit un modèle pour les petits volcans boucliers assemblés en tenant compte de leurs caractéristiques morphologiques. Cette formation est unique sur Mars.

Une étude détaillée a donc été menée, sur leur forme, les contacts aux frontières, leurs pentes, leur rhéologie, leur âge, leur morphologie et leur relation par rapport au modèle de tectonique régionale. Ces volcans sont en contact avec des écoulements de lave étendus, longs et lobés, qui diffèrent en âge, rhéologie et morphologie des volcans boucliers. Syria Planum a été dominée par des petits volcans boucliers accolés, et par un plus grand édifice singulier qui est la source des longues coulées de lave.

Nous avons supposé que Syria Planum a joué un rôle important sur le volcanisme principal primordial de Tharsis mais a cessé son activité tôt dans l'histoire géologique de la planète. La cessation progressive de l'activité pourrait avoir été due à l'augmentation de l'épaisseur de la croûte, formée tôt dans la genèse de Mars, dans le cadre du processus magmatique de cette région.

L'épaisseur la plus élevée de la croûte martienne se trouve sous Syria Planum, ce qui nous a amenés à réfléchir quant à son rôle principal sur l'origine mais également

sur le déclin du volcanisme dans ce secteur. Il s'est ensuite prolongé au nord-ouest de Tharsis, menant à la formation de l'état actuel des Tharsis Montes. Afin d'évaluer cette hypothèse, décrite dans la deuxième partie de cette étude, une simulation numérique du transfert de chaleur par conduction a été effectuée, dans la lithosphère thermique du plateau de Tharsis, où seule la conduction de la chaleur est en œuvre. La topographie obtenue par MOLA et l'épaisseur de croûte - qui ont été précédemment dérivées de la gravimétrie - ont été employées pour modéliser le Plateau de Tharsis en 3D. L'équation de transfert thermique a alors été appliquée et a été résolue dans le cas du régime permanent. Les effets des variations de flux et de chauffage radioactifs sont cependant discutés.

L'influence de la topographie fut le premier paramètre analysé, utilisé pour contraindre des modèles des conditions thermiques et de flux de chaleur sur Tharsis.

Nous avons ainsi analysé les régions comportant des variations d'épaisseur de croûte, et étudié les conséquences de ces variations sur l'élévation locale des températures et leur influence sur la durée du volcanisme. En modélisant la conduction de la chaleur sur le plateau de Tharsis, nous avons discuté:

(1) la présence d'importantes anomalies de flux de chaleur autour des pics volcaniques de Tharsis, qui semblent être localement corrélées avec une variation locale de l'épaisseur de la croûte mais aussi avec des escarpements exposés (comme sur les flancs d'Olympus Mons) ;

(2) la dépendance des figures géomorphologiques existantes à la base des flancs des volcans et formées probablement à partir de l'action de l'eau, avec une augmentation du flux de chaleur nécessaire à la surface de ces volcans (le cas d'Olympus Mons) ;

(3) les paramètres thermiques qui influencent l'augmentation de la température de la croûte autour des volcans ;

(4) l'augmentation locale de la température nécessaire pour former une fusion partielle dans le manteau supérieur.

Nous concluons enfin avec les conditions des modèles thermiques pour la province de Tharsis nécessaire pour maintenir un volcanisme de longue durée en accord avec les conditions géomorphologiques de surface.

Volcanism is the fundamental process in the solar system responsible for creating the surfaces of terrestrial bodies. As predicted by several thermochemical convective models [e.g Schubert et al., 1990; Weizman et al., 2001; Hauck and Phillips, 2002; Breuer and Spohn, 2003], Mars didn't seem to have experienced an extensive volcanic longevity. However, recent volcanic eruptions are now accepted, taking into account surface geological evidences with crater-counting measurements [e.g. Neukum et al., 2004] and as predicted by parameterized thermal conductive models [Schumacher and Breuer, 2007]. It has been debated if volcanism of large volcanic centers could have been sustained by giant plumes or superplumes [e.g. Esposito et al. 1992] bringing enough heat to the mantle and causing volcanism within the stagnant lid. If these processes may be considered for the early Mars, they are hardly accepted to explain the recent conditions of the planet. The processes to keep or to enhance a longstanding volcanic activity in a small size planet like Mars are object of study in this dissertation.

The Tharsis Province is, as like Elysium, the most important volcanic province on Mars. It includes a succession of well developed volcanoes (Olympus Mons, Arsia, Pavonis and Ascraeus Montes and Alba Patera) in association with low scale volcanic features, formed close to vast important tectonic features such as deep canyons (Vallis Marineris), extensive fossae (Noctis Labyrintus and Claritas) and radial grabens.

Surrounded on the North by the Noctis Labyrinthus and on the West by Claritas Fossae, another volcanic high region takes place; Syria Planum. The main role of the tectonic activity on the evolution of Syria Planum compared with the main role of the magmatic activity on the evolution of the Tharsis Montes and surroundings, and the relation between these two geographically close magmato-tectonic regions seems crucial to understand the thermal evolution and volcanic formations on Mars. Also, new

HRSC imagery permits now to study this area with a better resolution, and so with a better detail, than ever done in this area.

Consequently, in the first part of this dissertation, it was analyzed the volcanic history of the very high Syria Planum on Mars, by extracting topographic information from high-resolution stereo pairs obtained from HRSC and MOLA data. Also, THEMIS, HIRISE and MOC images were used to help in the interpretation of this area. We identified and described a pattern of coalesced shield volcanoes, which, taking into account their morphological characteristics, are not known anywhere else on Mars. It was done a detailed study of their shape, border contacts, slopes, rheology, age, morphology and relation to the main tectonic pattern. They are in contact with extensive long and lobate shape lava flows that differ in relative age, rheology and morphology from the shield volcanoes. Syria Planum was dominated by both swarms of small shields and a single larger edifice as the source of long lava flows.

We hypothesized that Syria Planum played an important role on the primordial Tharsis main volcanism and ceased their activity early in its geological history. The progressive cessation of activity might have been due to the enhanced crustal thickness in the magmatic processes of this region, formed early in the Martian's formation. The highest crustal thickness beneath Syria Planum led us to think on its principal role on the origin but also on the decline of the volcanism in this area, and it's continuation on the northwestern side of Tharsis, leading to the formation of the present state Tharsis Montes.

To test this hypothesis, it was done, in the second part of this dissertation, a numerical simulation of the heat transfer within the elastic part of the lithosphere of the Tharsis Plateau. The MOLA topography and the crust thickness derived from gravimetry were used to simulate the Tharsis Plateau in 3D, for which the heat transfer equation was solved in a steady state case for the crust and upper mantle.

The influence of the topography was the first analyzed parameter, as a constraint for the thermal and heat conductive model conditions on Tharsis. Also, it was analyzed the boundaries where there are crustal thickness variations and its role on local temperatures elevation and its influence on the volcanism duration.

By modeling the heat conduction on the Tharsis plateau, we discuss: 1) the presence of important heat flow anomalies around Tharsis peaks, which seems to be locally correlated with crustal roots variations and also on the surface with exposed scarps; 2) the dependence of water-formed features with a necessary heat flow increasing (the case of the Olympus Mons flanks); 3) the thermal parameters that most influence the increasing of the temperature around the volcanoes' crust; 4) the necessary local temperature increasing to form a melt on the upper mantle.

We conclude with the thermal model conditions on the Tharsis province necessary to enhance a longstanding volcanism and that are in agreement with the studied surface morphology.

Part I - Introduction

1. Le Flux Thermique sur Mars

2. La Topographie de Mars déduite à partir des satellites

1. Le flux thermique martien

Les contraintes sur les modèles thermiques martiens ainsi que celles associées au développement du volcanisme sur cette planète sont nombreuses. Dans ce chapitre d'introduction, nous dressons un panorama des différentes caractéristiques martiennes et des paramètres nécessaires à la compréhension de l'histoire thermique et donc du développement du volcanisme martien.

(1) Les observations géologiques, géophysiques et géochimiques nous renseignent sur la composition, la structure interne et les événements majeurs de l'évolution de Mars (i.e. différentiation globale, dégazage atmosphérique, formation de la dichotomie Nord/Sud et de Tharsis). Elles sont donc utilisées pour contraindre les modèles de l'évolution thermique de Mars. Les isotopes des météorites SNC[1] suggèrent que la formation du noyau martien est contemporaine de l'accrétion de la planète [ex. Righter, 2004]. Par ailleurs, les terrains fluviaux anciens et le rapport atmosphérique D/H [2] élevé indiquent qu'une atmosphère martienne dense était déjà formée dans les premières centaines de millions d'années de l'histoire de la planète et qu'elle a subi un dégazage important [Barabash et al. 2007]. Mars a donc commencé son évolution avec une très forte activité volcanique et un fort dégazage mantellique.

Par la suite, l'évolution thermique a conduit au refroidissement du manteau et du noyau, la différenciation de la croûte et à l'épaississement d'une lithosphère élastique [Schubert et al. 1992].

(2) La majorité de la production crustale s'est déroulée pendant le premier milliard d'années de l'histoire de Mars [ex. Breuer and Spohn, 2006]. Ceci est cohérent avec les évidences géologiques d'une décroissance temporelle du flux volcanique

[1] SNC = Shergottites, Nakhlites, Chassignites
[2] D/H = Deutérium/Hydrogène

martien, avec le phénomène de contraction globale de la croûte souligné par les structures tectoniques des rides de compression présentes au niveau des surfaces géologiques anciennes [ex. Andrews-Hanna et al. 2008].

(3) l'analyse des anomalies de gravité prédit une épaisseur actuelle de la croûte de 32 km pour l'hémisphère nord et de 58 km pour l'hémisphère sud [Neumann, 2004]. Cela est en accord avec les estimations de l'épaisseur de la lithosphère élastique déduites grâce à la réponse de celle-ci à une surcharge en surface [ex. Belleguic et al. 2005]. Par ailleurs, les modélisations numériques de la convection dans le manteau martien suggèrent que la formation du plateau de Tharsis est associée à la présence d'un ou plusieurs panaches mantelliques (ex. Esposito et al. [1992] ; Redmond and King, [2004]) ayant généré un apport basaltique important. La lithosphère située sous Tharsis présenterait donc un épaississement par rapport à la lithosphère de l'ensemble de la planète.

(4) Enfin, la mesure du magnétisme rémanent (engendré par une dynamo martienne qui se serait arrêtée il y a 4 Ga [Connerney et al. 2001, Lillis et al. 2008]) enregistré par les roches est un outil supplémentaire à la compréhension de l'histoire thermique de Mars et est un témoin des épisodes qui ont affecté la structure interne de cette planète (activité du noyau). Là encore, l'arrêt de la dynamo s'explique par la baisse de l'intensité de la convection.

1.1 La Planète Mars

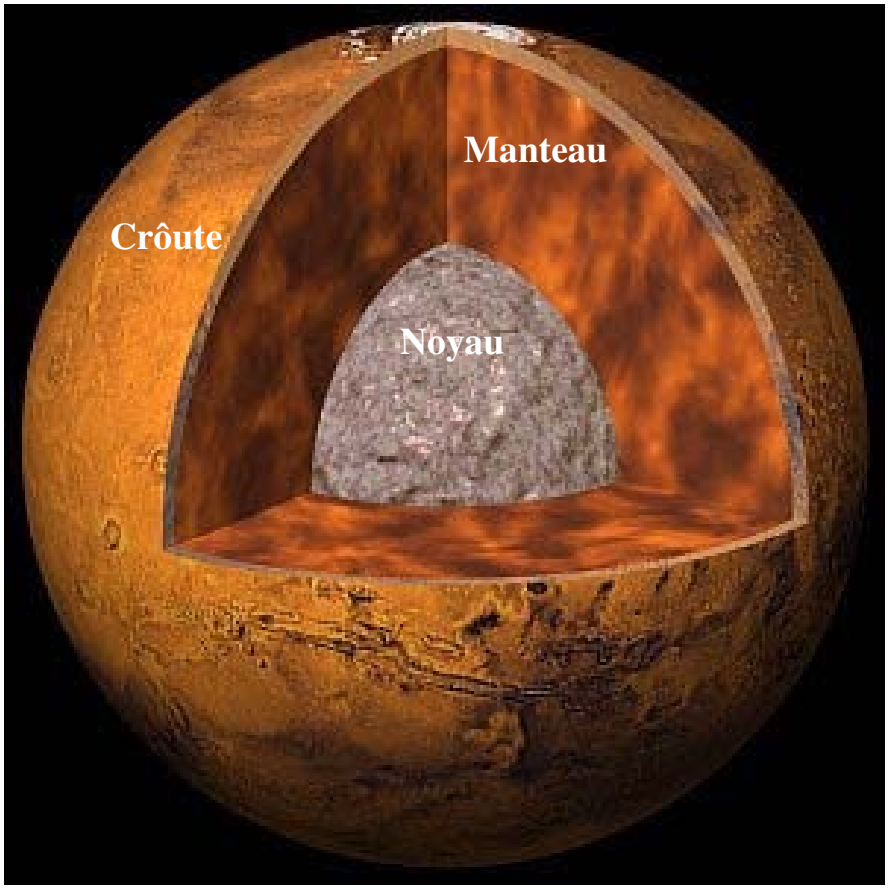

FIG 1.1 – *Structure interne de Mars.*

Mars est une des six planètes facilement observables à l'œil nu et donc connue depuis l'antiquité. Dès 1877, Schiaparelli dessinait des canaux, observés depuis son télescope, mais ne leur attribuait pas une origine spécifique. En revanche, Percival Lowell soutint jusqu'à la fin de sa vie la théorie d'une origine non naturelle de ces canaux.

L'intérêt pour Mars n'a fait que croître lorsque l'on a découvert une surface assez semblable à notre planète. Malgré le fait que Mars soit plus éloignée du Soleil (1,5 UA), que sa taille soit inférieure (6794 km de diamètre) et qu'elle soit moins dense (3,93) que la Terre, elle aurait présenté des conditions environnementales qui auraient pu permettre le développement de la vie, sous certaines conditions.

Malgré une forte ressemblance géologique avec la planète Terre, Mars est géophysiquement très différente. Son rayon équatorial est de 3397 km, sa densité de 3.933 et sa masse de 0.6419 x 10^{24} Kg, ce qui génère une gravité de 3.69 m s^{-2} à l'équateur et une vitesse de libération équatoriale de 5.03 km s^{-1}.

La structure interne de Mars est déduite pour l'instant par des données de gravimétrie. Ainsi, l'épaisseur crustale de l'hémisphère nord serait plus fine (35km) que celle de l'hémisphère sud (80km) [ex. Neumann et al. 2004]. La planète présente un manteau silicaté, (comme celui de la Terre mais plus riche en fer, [Verhoeven et al. 2005] et un noyau métallique solide qui serait composé d'un mélange de fer et de sulfures de fer, et dont le rayon est d'environ 1700 km (Figure 1.1).

L'atmosphère de Mars est constituée essentiellement de dioxyde de carbone (95%), d'azote (moins de 3%) et d'argon (moins de 2%), l'oxygène étant seulement à l'état de trace [Ott, 1991]. Cette atmosphère est très ténue (moins de 1% de la pression atmosphérique sur Terre) mais suffisamment dense pour permettre à des vents violents de créer de vraies tempêtes de sable couvrant presque toute la planète.

La température peut atteindre un maximum de 27 ºC, mais seulement durant la journée et lors de l'été martien. Les températures polaires sont aux alentours de -133 ºC et la moyenne annuelle aux alentours de -55 ºC [Alves, 2003]. Les conditions de pression et température régnant actuellement sur Mars ne permettent pas à l'eau d'être présente à l'état liquide. En fait, la présence de traces de vapeur d'eau dans l'atmosphère martienne a été démontrée. Quant aux calottes polaires, elles sont majoritairement constituées par de la glace de dioxyde de carbone, avec un caractère saisonnier au nord. Enfin, les quantités supposées de glace d'eau restent très incertaines, surtout en ce qui concerne la calotte sud.

Les données de la mission Mars Odyssey (2001) indiquent qu'une grande quantité d'eau à l'état solide serait contenue dans les pores de la subsurface martienne ou comme constituant de la maille des minéraux [Christensen et al. 2000] et cela principalement aux hautes latitudes (supérieures à 60ºN et S), mais aussi dans quelques zones localisées des basses latitudes [Christensen and Ruff, 2004].

Ces quantités d'eau ne sont cependant rien comparées à l'eau qui a façonné les structures anciennes telles que des vallées fluviales, des zones de méandres ou bien des

zones de débâcles. L'eau devait pour cela être présente à l'état liquide. Ainsi, la connaissance de l'évolution des conditions environnementales sur Mars peut nous aider à mieux comprendre l'évolution de notre planète.

Du point de vue géologique, Mars suscite beaucoup d'intérêts et de doutes. Les images globales de la planète révèlent une forte dichotomie avec un hémisphère nord jeune, à faible cratérisation, aux altitudes très basses et un hémisphère sud plus ancien, plus haut et plus cratérisé.

Les différentes mesures de la densité des cratères [ex. Hartmann et Neukum, 2001] ont permis de définir trois grandes périodes pour la datation des surfaces martiennes (voir Figure 1.2) : le Noachian, entre 4,5 Ga et 3,5 Ga très cratérisé (grands cratères), l'Hesperian, jusqu'à 1,8 Ga, dans les hautes zones méridionales, avec beaucoup de petits cratères, et le plus récent, l'Amazonian, dans les plaines septentrionales présentant peu de cratères. Il y a pourtant une large incertitude sur la détermination de ces âges, due surtout au resurfaçage des surfaces [ex. Hartmann et al. 2005] qui aurait oblitéré une quantité de cratères considérable.

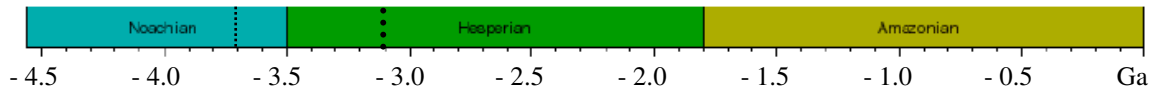

FIG 1.2 – *Echelle de temps géologique de Mars construite à partir de la densité de cratères d'impact [ex. Hartmann and Neukum, 2001]. L'incertitude sur les âges du début et de la fin de l' Hesperian est montrée, respectivement, par les traits pointillés moins et plus épais.*

La dichotomie Nord-Sud s'étend aussi au magnétisme. Mars ne présente plus de champ magnétique dipolaire, comme sur Terre ou sur Mercure. Cependant, la découverte d'une aimantation rémanente dans certaines zones de l'hémisphère sud (roches présentant des polarités alternées) semble indiquer que les débuts de l'histoire martienne furent marqués par la présence d'un champ magnétique.

Les volcans martiens sont, par leurs dimensions, une autre empreinte distinctive de la planète – les plus grands du système solaire. Le plus grand de tous, Olympus Mons, atteint une altitude de 22 km à partir du niveau zéro, ou près de 28 km

à partir du niveau le plus bas. Sa base s'étend sur plus de 800 km de diamètre et est délimitée par un escarpement de 6 km de hauteur. Une des hypothèses sur l'origine d'Olympus Mons est liée à la formation du bassin d'Hellas [Phillips et al. 2001] (gigantesque cratère d'impact, avec plus de 6 km de profondeur et 2000 km de diamètre). Quelques auteurs [ex. Seyfert, 1983] ont proposé qu'une grande quantité d'énergie produite lors de l'impact se soit propagée aux antipodes créant ainsi le plateau de Tharsis, cependant sa formation sera probablement liée à des panaches géants associes aux discontinuités locales [Christensen and Ruff, 2004]. La mise en place de ce plateau gigantesque a généré une fissure tectonique radiale : Valles Marineris, le plus grand système de vallées du système solaire, avec plus de 4000 km d'extension, et 7 km de profondeur.

Plusieurs explications ont été proposées afin d'expliquer l'origine de Tharsis. Ces modèles incluent le support dynamique de la topographie par un géant panache convectif [ex. Hartmann, 1973 ; Carr, 1974], la surrection régionale due au matériel crustal situé en dessous et dérivé de l'hémisphère nord [Wise et al. 1979], ou par surrection due seulement à des anomalies mantéliques (thermiques et/ou compositionnelles) [Sleep and Phillips, 1979]. D'autres explications réfèrent à des épaississements de la croûte provoqués par des intrusions [Phillips et al. 1990] et finalement des charges flexurales dues aux constructions volcaniques [ex. Solomon et Head, 1982; Banerdt et Golombek, 2000; Phillips et al. 1990].

Malgré ses reliefs gigantesques, Mars ne présente apparemment pas de tectonique active. Les analyses in situ de la sonde Mars Pathfinder ont suscité la présence de roches de type andésitique [McSween et al. 1999], associées sur Terre aux zones de subduction et donc à la géotectonique. Néanmoins, la présence d'andésites sur Mars n'est pas bien contrainte du fait de l'absence de mesures de la quantité et de la nature des feldspaths trouvés. Aussi, il n'y a pas d'évidences de subduction, même si cette dernière a été proposée par quelques auteurs (par ex. Sleep, [2000]). Tous ces arguments rendent donc fort improbable l'existence actuelle d'une tectonique active, au moins à l'échelle globale.

Ainsi, malgré les connaissances acquises grâce aux différentes missions, Mars continue à susciter la curiosité de la communauté scientifique.

1.2 Composition de la Planète Mars

Le seul moyen d'obtenir des informations fiables sur la structure interne de Mars est la sismologie. Cependant, la sismologie martienne présente des inconvénients: (1) Cela nécessite la propagation d'ondes mécaniques à travers la planète et donc la présence d'une source sismique (séismes naturels, impacts) [Lognonné et Mosser, 1993]. (2) Il est nécessaire d'installer des sismomètres sur la surface de la planète, ce qui, jusqu'à présent, n'a été réalisé que sur la Terre, sur la Lune (avec succès par les missions Apollo) et sur Mars (sans succès avec les missions Viking).

Malgré ces difficultés, il est possible d'estimer la distribution de densité à l'intérieur d'une planète à partir de sa gravité et de sa rotation, ce qui permet d'estimer les moments principaux d'inertie, et par comparaison avec la gravité et le coefficient J_2, d'estimer la déviation par rapport à l'hydrostaticité.

Ainsi, selon Folkner et al. [1997] et avec les mesures de rotation de Pathfinder, la composition interne théorique d'une planète est obtenue (1) à travers la mesure de sa densité moyenne, (2) à l'aide du moment d'inertie (I), une valeur adimensionnelle qui est égale au moment d'inertie du corps, I, divisé par sa masse et par le carré de son rayon, MR^2 , (ce moment d'inertie est relié à la distribution des masses à l'intérieur du corps. I = 0.4 pour un corps non différencié - de densité homogène). Plus la masse est concentrée au centre du corps étudié, plus la valeur de I/MR^2 est inférieure à 0.4. Cette composition interne peut être aussi déduite (3) de l'étude de la vitesse de propagation des ondes sismiques à l'intérieur de la planète, ou bien (4) pour celle du manteau supérieur, de la composition des roches formées à partir de processus de fusion partielle à l'intérieur de la planète. Les SNC apportent ainsi d'autres contraintes sur la structure interne, en particulier lorsque des hypothèses sur la composition des planetesimaux est faite (Longhi et al. 1992).

Mars a une faible densité moyenne (3.933 g/cm^3) et un rapport du moment d'inertie élevé comparé à celui de la Terre (I/MR^2_{mars} = 0.366). La densité moyenne et le moment d'inertie sont les rares réelles contraintes géophysiques sur la planète. Mais les détails des variations de densité avec la profondeur, en raison de la méconnaissance des gradients de pression et thermique de la planète, ne sont pas contraints directement. La

densité non-comprimée est de 3.75 g/cm^3 pour Mars [Taylor et Norman, 1992] et 4 g/cm^3 pour la Terre [Bertka et Fei, 1998].

Le rapport du moment d'inertie mesuré pour la Terre est de 0.3315. La comparaison entre les moments d'inertie des deux planètes indique que la concentration des masses dans le noyau martien est moins importante que celle du noyau terrestre.

La dimension du noyau terrestre a été déterminée grâce à des études sismiques qui, comme nous l'avons vu précédemment, sont encore impossibles sur Mars. Néanmoins, selon les modèles d'évolution cosmochimique du système solaire [Morgan et Anders, 1979], le noyau martien contient plus d'éléments légers (qui restent cependant minoritaires) que les planètes plus proches du Soleil (Mercure, Vénus, la Terre). Les températures plus basses loin du Soleil permettraient une réaction plus favorable du soufre avec le fer et donc la formation de FeS, entrant dans la composition du noyau. En effet, si le contenu en fer du noyau était plus important, il y aurait eu formation de silicates ferreux ayant pour résultat une densité non-homogène du manteau, créant ainsi un gradient de densité croissante.

1.2.1 Les Météorites SNC

L'association de Mars aux météorites SNC [McSween, 1984 ; Bogard et al. 1984 ; Becker et Pepin, 1984 ; Schubert et al. 1992] a profondément changé notre vision de l'évolution de cette planète.

Nous savons que les météorites sont des fragments de matière de trois types : rocheux, métalliques, ou bien la combinaison des deux. Elles sont issues de la matière résiduelle qui n'a pas été accrétée lors de la formation des planètes du système solaire. La plupart des météorites proviennent de la ceinture d'astéroïdes située entre Mars et Jupiter. Ces fragments d'astéroïdes sont parfois éjectés de leur orbite grâce à des phénomènes de résonance ou de collision et peuvent croiser la trajectoire d'autres corps célestes, notamment les planètes.

Selon Righter [2004], jusqu'à présent, 27 météorites connues seraient d'origine martienne. Celles-ci ont été découvertes sur tous les continents excepté l'Australie. Quatre d'entre elles ont été observées lors de leur chute dans les régions de Shergotty, Nahkla, Chassigny (SNC) et Zagami entre 1815 et 1862.

Righter [2004] invoque plusieurs raisons pour justifier l'appartenance des météorites SNC à la planète Mars :

(1) Les météorites de type SNC sont relativement jeunes (< 1300 Ma), comparées aux autres météorites du Système Solaire (~ 4500 Ma).

(2) Les minéraux composant ces météorites montrent une composition isotopique en oxygène différente de ceux présents sur Terre et sur la Lune.

3) Des inclusions fluides (gaz), dans au moins une des météorites, présentent la même composition chimique et isotopique que l'atmosphère martienne analysée par les modules d'atterrissage Viking en 1976.

4) Toutes les météorites martiennes se sont formées à partir de roches ignées (roches issues de la fusion de silicates dans une planète tellurique ou dans une de leurs lunes). Vénus pourrait aussi être la source de ces météorites. Cependant, l'atmosphère vénusienne étant très dense, la chaleur de friction va provoquer une vaporisation immédiate du matériel éjecté lors de l'impact. Ainsi, seule la planète Mars est la candidate la plus probable pour l'origine de ces fragments éjectés.

(5) Elles sont toutes de type achondrite, formées par différenciation du magma parent, contrairement aux chondrites primitives, formées par accrétion de chondrules de la nébuleuse solaire initiale.

(6) Les météorites martiennes présentent des similitudes avec quelques types d'achondrites telles que les eucrites, les diogénites ou bien les howardites, formées par le mélange des deux précédentes.

Les 27 météorites retrouvées pèsent entre 12 g et 18 kg, les plus petites provenant majoritairement de l'Antarctique. Les météorites martiennes étant des roches ignées, il est parfois difficile de les distinguer des autres roches semblables sur Terre.

Il existe 5 types de roches ignées distinctes, dans la famille des météorites martiennes :

- Les Shergotites qui sont divisées entre les basaltes pyroxèno-plagioclasiques et les lherzolites pyroxèno-oliviniques.
- Les Nakhlites qui sont des cumulats clinopyroxèniques.

- Les Chassignites qui sont des cumulats oliviniques (péridotite de 90 à 100% d'olivine).
- Les ALH84001 qui sont des cumulats orthopyroxèniques.

Les deux premiers types sont représentés par plusieurs échantillons, en revanche, les deux derniers types ne sont représentés que par un échantillon. [Righter, 2004].

La météorite l'ALH84001 semble être la plus ancienne et représente donc l'ancienne croûte martienne. Ces basaltes, pétrologiquement variés, sont pour la plupart des cumulats, mais ils présentent des caractéristiques géochimiques et des isotopes radiogéniques qui suggèrent une formation par recristallisation du même magma parent à des temps différents [McSween, 1994].

L'étude des météorites martiennes permet d'obtenir les informations suivantes :

1) La différenciation de la planète se serait déroulée vers -4.5Ga, probablement en même temps que l'accrétion.

2) Le manteau martien contient en quantité modérée des volatiles et des éléments sidérophiles (qui ont une affinité pour la phase métallique Fe), et présente un enrichissement en fer par rapport à la Terre (implications sur la minéralogie et sur la densité).

3) La composition hypothétique du noyau révèle une plus grande abondance en Soufre près de la plate-forme de solidification du noyau intérieur (Chevrier [2005] révèle la présence de S dans les météorites Martiennes).

4) L'existence d'une magnétisation rémanente dans les météorites SNC, particulièrement dans l'ALH84001 semble indiquer que lors de la formation de ces roches, Mars avait un champ magnétique principal produit par une dynamo interne et que les minéraux ont acquis la magnétisation du champ existant.

5) La minéralogie des unités de la surface martienne (déduite grâce aux instruments TES et OMEGA par exemple) est identique à celle des shergotites basaltiques.

6) Les propriétés rhéologiques des magmas martiens et l'évolution de leur flux de chaleur, ont été mieux comprises grâce à l'étude de ces météorites parce que celles-ci ont permis d'obtenir des donnés de radioactivité.

7) Les estimations de l'abondance d'eau planétaire sont contradictoires avec l'évolution de l'échappement de l'eau. Les mesures d'isotopes stables indiquent que l'hydrosphère martienne n'a effectué des échanges que très limités avec la lithosphère. Cependant, ce processus s'effectue dans un équilibre isotopique avec l'atmosphère et se produit depuis 1,3 Ga [McSween, 1994].

8) Les produits d'altération contenus dans les météorites SNC supportent l'idée de l'existence d'une altération limitée de la lithosphère par l'eau saline et carbonique [McSween, 1994].

9) La composition de l'atmosphère, ainsi que son évolution, sont mieux perçues grâce à la connaissance des gaz nobles dans ces météorites.

1.3 L'Epaisseur de la croûte

Comme nous l'avons vu précédemment, l'hémisphère nord de Mars est moins accidenté et moins cratérisé que l'hémisphère sud. La différence d'altitude entre les deux hémisphères est de 5km. [Frey et al. 1998]. Cette différence est illustrée par la carte d'altimétrie (Figure 1.3) produite à partir des données MOLA. La surface très lisse des basses plaines du nord est attribuée à la présence de matériel volcanique majoritaire mais aussi à celle de matériau sédimentaire.

Une grande quantité de canaux, formés grâce aux agents érosifs présents sur Mars (eau liquide ou solide), relient les plateaux du sud aux basses plaines du nord, impliquant le recouvrement des terres du Nord par un matériau d'origine sédimentaire [Phillips et al. 2001].

Les données de topographie et de gravité obtenues par MGS permettent d'évaluer l'épaisseur de la croûte martienne [Zuber et al. 2000].

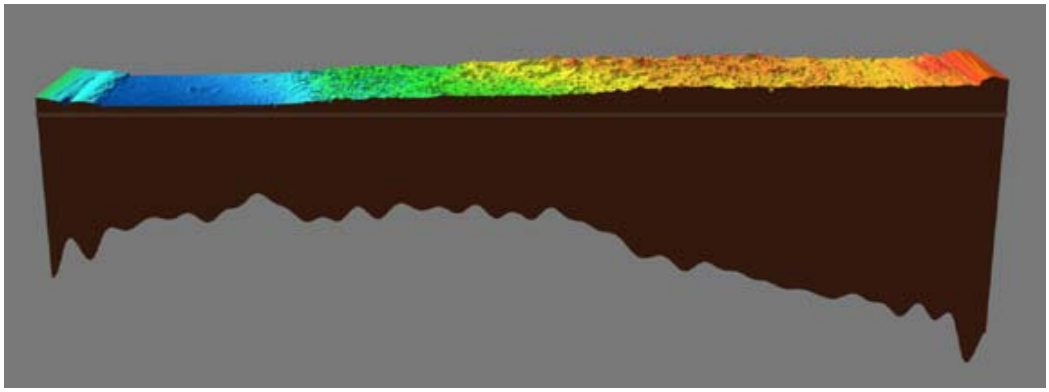

FIG. 1.3 - *Coupe de la structure crustale de Mars centrée sur 0ºE de longitude [Zuber et al., 2000] obtenue à partir des données de gravité et de topographie de la sonde MGS (Mars Global Surveyor). Le Pôle nord se situe à gauche de la figure. Pour une meilleure visualisation, l'échelle verticale est exagérée (40 km d'épaisseur au-dessous de l'hémisphère Nord et 70 km au-dessous de l'hémisphère sud).*

En observant les Figures 1.3 et 1.4, deux terrains distincts apparaissent : les plateaux accidentés du sud et les basses plaines du nord. La zone où est située la transition de la dichotomie Nord/Sud ne semble pas correspondre à celle de l'épaisseur crustale, mais à d'autres phénomènes. Pour Zuber et al. [2000] cette zone de transition semble être reliée à des processus externes, tels que la distribution de cratères et la distribution du champ magnétique, et non à des processus internes.

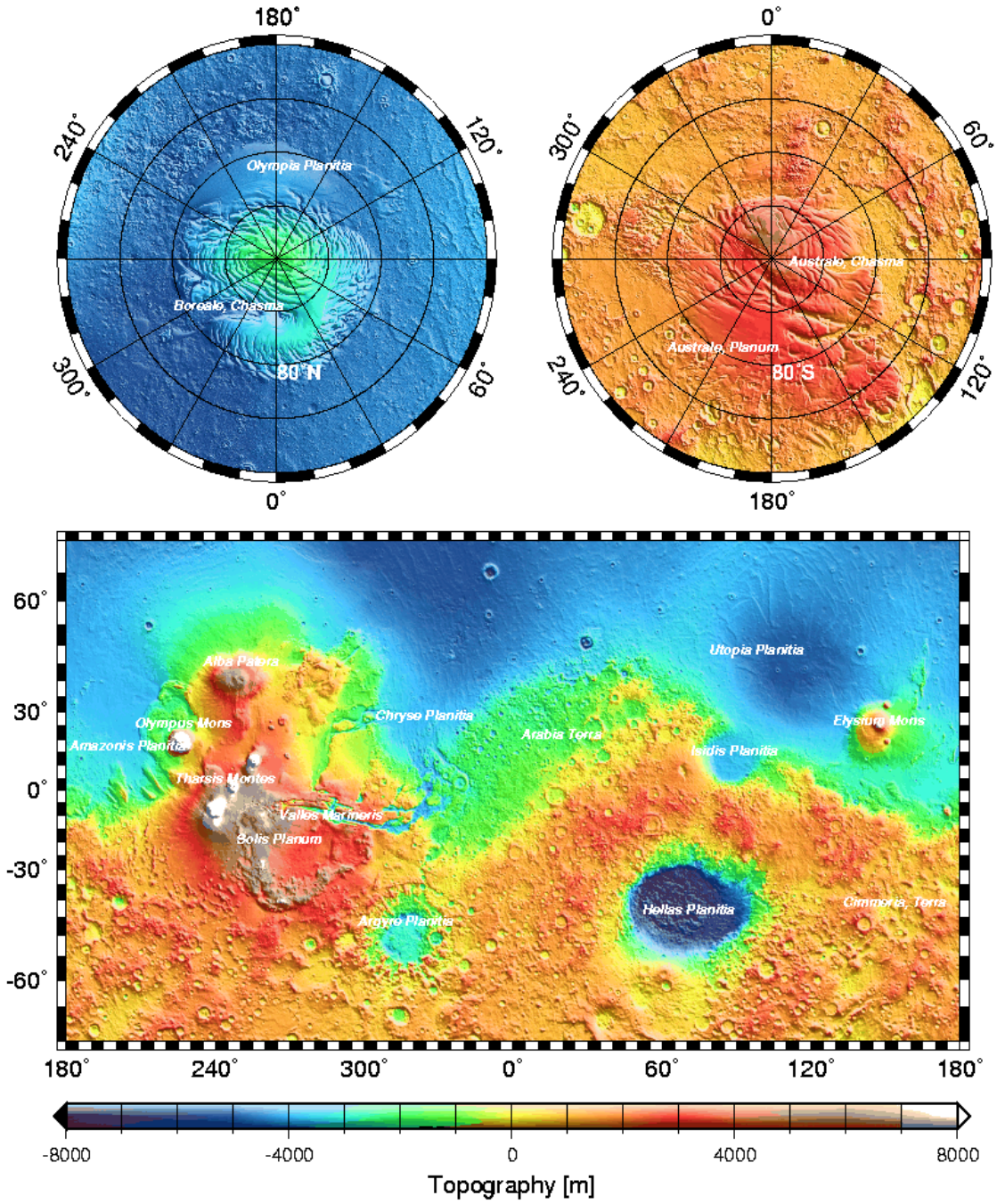

FIG.1.4 – *La dichotomie nord sud est très visible sur cette carte altimétrique. Le relief très lisse des terres du nord (à l'exception de la zone Tharsis, qui présente les 4 plus grands volcans de Mars, parmi lesquels Olympus Mons, le plus grand du système solaire) contraste avec les terres hautes accidentées du Sud (à l'exception d'énormes cratères d'impact, comme c'est le cas d'Hellas). Image MOLA.*

1.4 Isotopes Radioactifs à l'intérieur de Mars - Géothermométrie

Une analyse complémentaire de la topographie et de la gravité indique que, dans le passé, les basses plaines du Nord ont présenté un flux thermique élevé qui résulte d'une convection vigoureuse à l'intérieur de Mars. Par ailleurs, les anomalies gravimétriques importantes dans ces zones révèlent des lacunes dans la compréhension de la topographie [ex. Belleguic, 2005].

Par conséquent, les anomalies gravimétriques observées dans certaines zones de l'hémisphère nord telles que la partie nord de Tharsis et Utopia Planitia reflètent la présence d'un ancien flux thermique élevé [Zuber et al. 2000]. Belleguic et al [2005] notent aussi des valeurs très faibles des lithosphères élastiques pour Alba Patéra et Elyséum. Ce flux important de chaleur pouvait être lié à un volcanisme important et ainsi à un dégazage important de l'intérieur de la planète vers l'atmosphère. Là se trouve peut-être l'origine de l'eau qui a contribué au climat plus humide et moins hostile que le climat actuel [Zuber, 2001], il y a plus de 3 milliards d'années. Ce chauffage aurait été assez important pour faciliter la déformation crustale, qui se serait donc adaptée à la topographie par équilibre isostatique. En revanche, l'hémisphère sud culmine à 5 km au dessus de l'hémisphère nord (en moyenne), ce qui semble indiquer que la croûte des hauts plateaux était trop froide pour pouvoir fluer.

En effet, si, lors de la formation de la planète, le matériel composant la croûte de l'hémisphère sud était également chaud, alors certains grands cratères d'impact comme Hellas (présentant une forte dépression topographique) n'auraient jamais été préservés (notons cependant que ces cratères sont associés à une remontée du manteau supérieur sous les cratères).

Ainsi, plus le flux de chaleur est important (et par là, la teneur en éléments radioactifs dans la croûte importante), plus l'épaisseur de la lithosphère est faible. McLennan [2001] a étudié ce phénomène par comparaison avec la Terre, comme le montre le graphique de la Figure 1.5. Ainsi, McLennan [2001] démontrent que les résultats de d'évaluation de l'épaisseur de la croûte ne sont pas en contradiction avec la théorie de la tectonique des plaques pour cette planète.

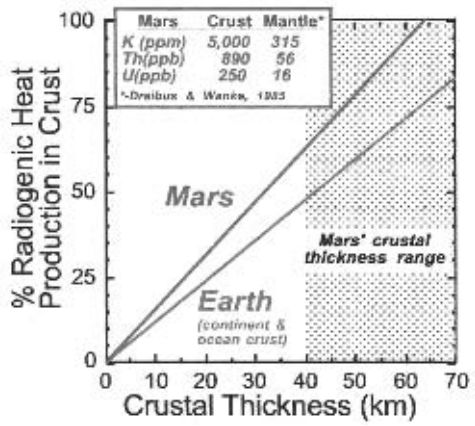

FIG 1.5. *Une forte production de chaleur radiogénique (comme exemple de Mars par rapport à la Terre) génère un amincissement de la croûte. [McLennan, 2001].*

1.5 Le Flux Volcanique

Le volcanisme est l'un des facteurs les plus importants dans la modification de la surface martienne en raison du nombre et de la variété des structures et des constructions volcaniques sur Mars. L'activité volcanique semble s'être surtout développée dans l'hémisphère nord. La province volcanique la plus étendue se situe sur le dôme de Tharsis et est de composition basaltique. Cette province est dominée par 4 grands volcans : Olympus, Arsia, Ascraeus et Pavonis Mons. A environ 1000 km au Nord-Est d'Olympus Mons, la zone volcanique d'Alba Patera exhibe des zones de dépôts pyroclastiques et des zones caractéristiques d'écoulement de lave effusive. Il existe d'autres grandes formations volcaniques telles qu'Elysium Planitia, ou sur les hauts plateaux de l'hémisphère sud non loin du cratère d'impact Hellas, ou bien encore le long de la frontière entre les zones accidentées de l'hémisphère sud et les plaines lisses du nord.

Les données topographiques et les images haute résolution fournies par la caméra HRSC (High Resolution Stereo Camera) semblent indiquer que le volcanisme fut encore actif récemment (< 100 millions d'années) (ex. Hartmann, [2000] ; Werner, [2005]). La datation relative déduite de la stratigraphie et de la superposition de cratères est assez bien connue sur Mars. Toutefois la chronologie relative qui prend en compte le

flux d'impacts et le rapport de la taille de l'objet impacteur sur le diamètre du cratère, permet une datation approximative des surfaces martiennes.

Ainsi, comme le rapportent Schubert et al. [1992], la variation du flux volcanique à travers le temps constitue une contrainte importante pour l'évolution thermique globale de la planète Mars. Selon la littérature, les grands pics d'activité volcanique ont eu lieu au début de l'Hesperian (ex. Tanaka et al. [1986] ; Greeley, [1987]), avec une décroissance du flux volcanique vers ~ 3 à 3.5 Ga.

Le magmatisme est à l'origine de la formation de la croûte et de la migration des éléments radiogéniques producteurs de chaleur du manteau vers la croûte, comme évoqué dans le chapitre 1.4. La migration des sources de chaleur va entraîner un épuisement en éléments radioactifs et une diminution du chauffage, réduisant d'autant la convection et accentuant, dans la partie superficielle, le rôle de la conduction. Ce phénomène aura donc pour conséquence une augmentation de l'épaisseur de la lithosphère, et une réduction du volcanisme à la surface [Schubert et al. 1992]. Le début de l'histoire de Mars est caractérisé par des températures internes élevées, un manteau avec une convection vigoureuse, des flux de chaleur et des transferts de magma vers la surface élevés. Cela s'explique par le fait que la chaleur d'accrétion et la formation du noyau sont contemporaines de la formation planétaire. Le dégazage a ensuite contribué à la formation précoce d'une atmosphère. Par ailleurs, le magmatisme vigoureux a pu contribuer à la libération instantanée d'une grande quantité d'eau de la subsurface, créant ainsi des inondations catastrophiques à grande échelle, comme en résulte la construction de Valles Marineris [ex. Carr, 1996]. Ces périodes cataclysmiques ont été suivies par de longues périodes d'érosion éolienne [Carr, 1996].

1.6 Le Magnétisme

1.6.1 Les Sources du Champ Magnétique

Sur Mars, les mesures du champ magnétique effectuées entre environ 150 km et 400 km d'altitude par l'instrument MAG-ER (à bord de la Mission Mars Global Surveyor) [Acuña et al. 1999] révèlent que la planète ne possède pas actuellement de

champ magnétique interne, à l'échelle globale. Néanmoins, malgré l'absence d'un champ généré par une dynamo interne, il a été mesuré des anomalies magnétiques crustales induites par un champ magnétique rémanent [ex. Purucker et al. 2000 ; Rochette, 2006]. La magnétisation crustale rémanente résulte de la magnétisation des minéraux générée par un champ magnétique global lors de la formation des roches [Acuña et al. 1999].

1.6.2 Les minéraux responsables de l'existence de magnétisation rémanente

La surface de Mars est composée de roches ignées recouvertes de produits très oxydés qui constituent les poussières et les sols relativement clairs. La couleur rouge de la surface de Mars est due à la présence de minéraux ferriques dans la couche superficielle oxydée. [Sherman, 1982].

Les propriétés magnétiques des roches crustales dépendent essentiellement de leur composition chimique en fer révélatrice des conditions qui régnaient dans la croûte lors de la formation de ces roches ou de leur modification [Stevenson, 2001]. Néanmoins, les propriétés magnétiques des roches dépendent aussi de la température de ces roches [Rochette, 2006]. Les zones crustales qui présentent un fort champ rémanent contiennent beaucoup de fer. La forte magnétisation rémanente crustale révèle qu'une grande partie du matériel présentant une magnétisation pourrait provenir du manteau et avoir été ultérieurement modifiée par assimilation des composants aqueux à l'intérieur de la croûte. Ce phénomène conduit à la formation d'une couche plus oxydée dans la partie crustale supérieure. Cet état oxydé est le résultat de la cristallisation d'oxydes de fer magnétiques, tels la titanomagnétite ou la titanohématite [Connerney et al. 2001]. La magnétite et la pyrrhotite (cette dernière dans une moindre mesure) ont la capacité d'acquérir une forte magnétisation rémanente lors de leur cristallisation dans un champ magnétique global semblable à celui de la Terre. Ces minéraux, caractéristiques des météorites (supposées martiennes - Cisowski [1986]) Shergottites, Nakhlites, et Chassignites (SNC) (voir chapitre 1.2), ont un fort champ coercitif et sont très stables.

1.6.3. La Distribution du Champ Magnétique

Comme nous l'avons vu précédemment, le satellite Mars Global Surveyor (MGS) a acquis des données de la distribution globale du champ magnétique, grâce au magnétomètre MAG-ER, lors de la phase d'aérofreinage (afin d'abaisser l'apoastre du satellite en utilisant la force de frottement avec l'atmosphère) entre mars 1999 et août 2000.

Purucker et al. [2000] ont développé une technique de compression et d'analyse des données du champ magnétique terrestre obtenues par satellite, afin de mieux comprendre les observations du champ magnétique faites sur Mars par MGS. Les valeurs de la distribution globale de la composante radiale du champ magnétique sur Mars (Br) sont inversées à partir de la distribution de la source de magnétisation équivalente. Ces valeurs ont été utilisées pour construire une carte (Figure 1.6) normalisée à 200 km d'altitude, et en supposant une zone crustale magnétisée de 40 km d'épaisseur. La corrélation entre les 40546 observations directes du Br et le Br calculé aux mêmes endroits que les observations grâce à l'inversion, est de 0.978, donc très bonne. De plus, Purucker [2000] indique que les bandes magnétiques qui apparaissent tronquées dans quelques lieux, se rapporteraient à des évènements tectoniques. Ces figures magnétiques semblent être liées au système de failles associé aux régions de Valles Marineris et de Ganges Chasma, suggérant une importante modification des propriétés crustales associées à la fracturation.

La Figure 1.6 permet d'identifier une nouvelle zone dans l'hémisphère sud, (où les bandes sont plus denses et plus intenses : > 500 nT à l'altitude de la sonde), comme étant la plus ancienne croûte observée sur Mars [Acuña et al. 1999]. Néanmoins, bien qu'un fort champ magnétique rémanent soit relié à la croûte ancienne de l'hémisphère sud et qu'un plus faible champ soit associé à celle de l'hémisphère nord, il subsiste des exceptions [ex. Langlais et al. 2004].

Connerney et al. [2001] ont affirmé que la magnétisation crustale, ainsi que d'autres paramètres géomorphologiques (comme abordés dans le chapitre 1.1) révèlent là encore une distribution dichotomique, sur Mars : la croûte apparaît fortement magnétisée dans l'hémisphère Sud et dans la zone de transition entre les deux hémisphères, surtout dans les zones de Terre Cimmeria et Terra Sirenum (distribution

qui concorde avec la dichotomie topographique Nord/Sud). Les régions présentant un volcanisme étendu (ex. Olympus Mons et Tharsis Montes) sont des zones non-magnétiques. Il en est de même pour les régions voisines des vastes cratères d'impact de Hellas et d'Argyre.

Certaines régions de l'hémisphère sud sont supposées d'âge identique selon les modèles basés sur la densité de cratères. Cependant, les bandes magnétiques alternées permettent de conclure que des zones, connues pour être de même âge, présentent une magnétisation rémanente différente (elles se sont donc refroidies dans des conditions de champ magnétique différentes) et leur âge pourrait alors diverger d'environ 100 Ma. Concernant l'hémisphère nord, une croûte plus ancienne et donc magnétisée a été recouverte par des couches de lave plus récentes (formation postérieure à l'arrêt de la dynamo) ne présentant pas de magnétisation rémanente [Stevenson, 2001]. Dans la région d'Hellas (hémisphère Sud), les valeurs du champ magnétique sont très basses (voir inexistantes). L'impact a provoqué un amincissement de l'épaisseur crustale et une remontée isostatique du matériel mantellique. Ce cratère permet donc de dater l'arrêt de la dynamo martienne vers 4Ga selon Mitchell [2000].

Une étude postérieure du champ magnétique de Mars (avec des données issues de la phase d'aérofreinage) a été réalisée par Mitchell et al. [2005]. La plus grande résolution apportée par cette nouvelle carte, montre que la magnétisation crustale rémanente s'observe au-delà des terrains anciens du Noachian. De plus, la même structure géométrique E-W observée sur les hauts plateaux du Sud fortement magnétisés se vérifie avec cette nouvelle étude. Néanmoins, un paradoxe subsiste. En effet, les grands cratères situés dans l'hémisphère sud ne présentent pas de magnétisation rémanente alors que les hauts plateaux ainsi que la ceinture hémisphérique sont fortement magnétisés. Cependant, une magnétisation rémanente est observable dans plusieurs cratères de moindre dimension. Enfin, les larges provinces volcaniques (Tharsis, Olympus Mons, Elysium) quant à elles, ne présentent pas de magnétisme rémanent ce qui signifie que les laves qui les composent se sont épanchées après l'arrêt de la dynamo martienne.

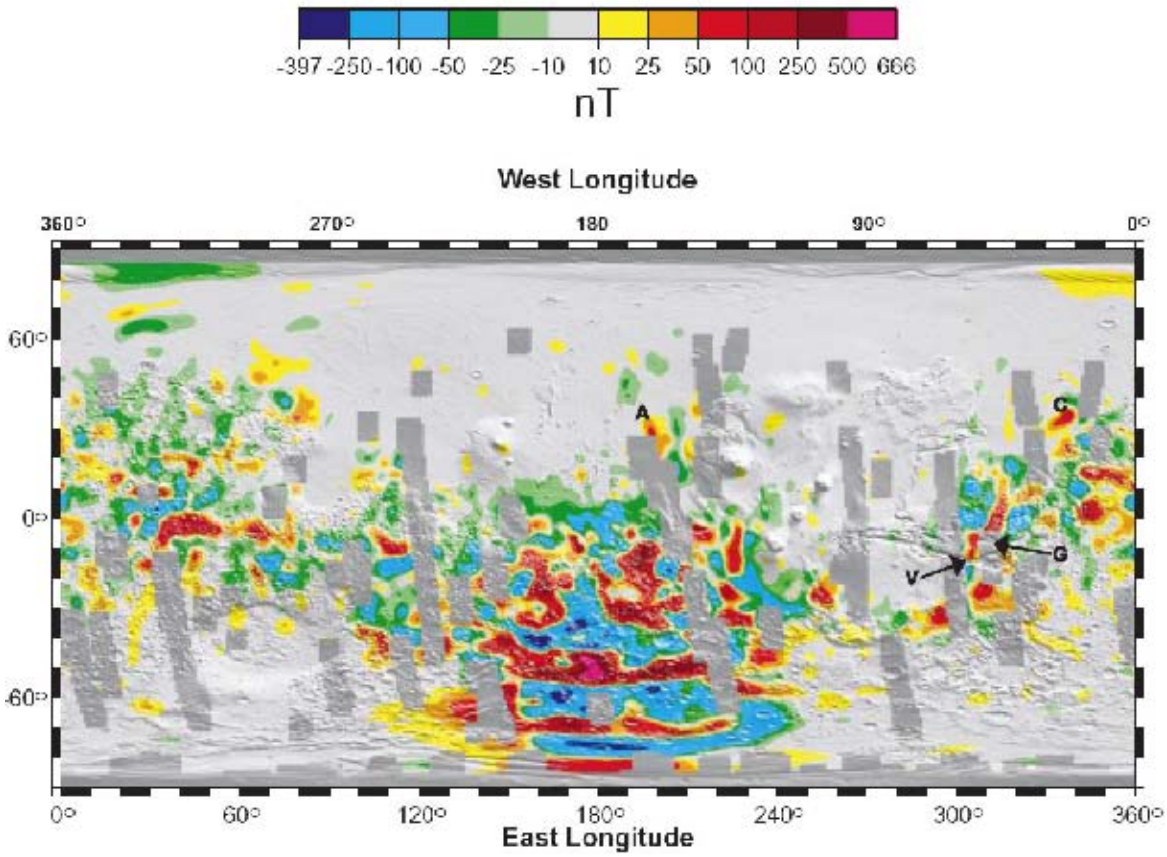

FIG 1.6 - *Champ magnétique radial (Br) normalisé à 200 km d'altitude. Les bandes en gris-foncé sont des zones non couvertes par MGS. « V » indique la localisation de Valles Marineris et « G » indique celle de Ganges Chasma, où la magnétisation apparaît tronquée. « A » et « C » indiquent des figures magnétiques dans des terrains récents à l'ouest d'Olympus Mons (a) et à l'est de Chryse Planitia (c). Fond constitué des données topographiques MOLA [Purucker et al. 2000].*

2. Mars Topography deduced by Satellites

Au cours de cette deuxième partie, nous allons décrire tout d'abord le jeu des données utilisées dans cette étude. Nous présentons les images dans le domaine du visible, obtenues par le satellite Mars Express (à travers la caméra HRSC) ainsi que les données de topographie prises pendant la mission Mars Global Surveyor (par l'altimètre MOLA). Enfin ont été exploitées les données d'albedo de la mission Mars Odyssey (par le THEMIS – spectromètre dans le domaine des infrarouges). La mosaïque des images de HRSC et THEMIS, ajoutée à des modèles numériques de terrain obtenus à partir du MOLA, ont permis d' identifier, de tracer et d'extraire des paramètres géomorphologiques de plusieurs figures volcaniques, ce qui est rapporté dans le chapitre 3. Les données IR-jour et IR-nuit nous donnent les températures de brillance de la surface, ce qui permet de discuter des propriétés des roches de la surface. L'altimétrie a permis de déterminer la forme géométrique quantitative et en conséquence la rhéologie des volcans boucliers ainsi que celle des coulées de lave. Des données d'altimétrie ont été également employées pour établir des modèles thermiques tridimensionnels et paramétrés de la croûte. Ces modèles de volcanisme martien ont été utilisés afin d'étudier l'influence de plusieurs paramètres géophysiques sur le développement du volcanisme dans la province de Tharsis, comme cela sera décrit dans le chapitre 4.

Nous nous focalisons ensuite sur l'étude de la topographie martienne en raison de son rôle extrêmement important sur tous les résultats obtenus dans notre travail. La topographie de Mars est probablement l'un des paramètres les plus connus, suivi de la gravité, connu assez précisément pour identifier les anomalies de gravité de Tharsis. Ces anomalies gravimétriques révèlent d'abord la formation particulière de Tharsis, mais inhibent aussi la compréhension exacte des compensations topographiques

martiennes. Ainsi, les anomalies gravimétriques de Tharsis constituent une importante énigme pour les modèles crustaux et thermiques utilisés pour modéliser le volcanisme martien et donc l'évolution de Tharsis.

Cette analyse nous permettra par la suite de voir comment la formation et notamment la topographie de Tharsis peuvent influencer nos modèles volcaniques et les écoulements volcaniques présentés dans cette dissertation.

In this work chapter, it is first described the data set used during this thesis. Satellite data from Mars Global Surveyor Mission (MOLA topography data), Mars Odyssey (THEMIS albedo data) or Mars Express (HRSC visible imagery data) were processed. The mosaic of images from HRSC, THEMIS and the digital elevation models obtained from MOLA, allowed us to identify, map, and extract morphometric parameters of several volcanic features. The IR day and IR night data give the surface brightness temperature, which is relevant to the discussion of surface rock properties. The altimetry allowed us to determine the quantitative geometric shape of the shield volcanoes and lava flows. Altimetry data was also used to build tridimensional crustal models used to apply thermal parameterized models of Martian volcanism, in order to study the influence of several geophysical parameters on the development of the volcanism in Tharsis. Due to the main role of the Tharsis topography on the results interpretation of this work, we show here the implications and the constraints used to determine the Martian topography. The topography of Mars is probably one of the best known parameters on this planet. Although, strong free-air gravity anomalies on Tharsis - revealing its particular formation - still constitute an important enigma if one uses crustal thermochemical parameterized models to study the volcanism on Mars. The used constraints have extremely important implications for the evolution of Tharsis. So, we set on this fact to present here how the Tharsis bulge formation may have influenced our volcanic models and volcanic flows presented in this dissertation.

2.1 Data Used in this Dissertation

We used high-resolution images acquired by the HRSC camera (orbits 2021, 2032, and 2054), orthorectified in a sinusoidal projection centered at 100ºW longitude, with a resolution of 15 m/pixel. We mosaicked them to cover the region of Syria Planum, where a particular swarm of shield volcanoes is observed (Chapter 3). In addition, we used visible and thermal infrared (IR) images (mosaic of images I17865001, I17290014, I17552023, and I16953015) acquired by the spectrometer Thermal Emission Imaging System (THEMIS) during day or night with a spatial resolution of 100 m/pixel [Christensen, 2003]. Mosaics of IR day images were coregistered with the HRSC image coverage to observe the field of lava flows southwest of the shield volcanoes. All these data allowed us to identify, map, and define the morphology, geometry, and age of the volcanic features of Syria Planum to propose a volcanic scenario in relation to the Tharsis region.

We also used MOLA (Mars Orbiter Laser Altimeter) data, which consists of measurements of the planetary radius at ~ 600 million locations, at a resolution of 128 pixel/degree, about 500 m at the equator [Smith et al., 2001], and a vertical precision around 35 cm [Zuber et al., 1998]. These data have been rectified in the same projection as HRSC images to obtain altimetry, and DEM models were built, on the Tharsis Province (Chapter 3).

MOLA data was also used to build 3D-parameterized models of heat flow on Mars (Chapter 6). For this propose, it was used both MOLA single shots (PEDR) (downloaded at http://pds-geosciences.wustl.edu/missions/mgs/pedr.html), which result from the single points recorded at the passage of the satellite along its orbit, and MEGDR, that result from the application of a Digital Elevation Model (DEM) and are characterized by their spatial resolution and the accuracy of elevations.

The PEDR's profiles of latitude/longitude were extracted using the software pedr2tab(http://pds-geosciences.wustl.edu/geo/mgs-m-mola-3-pedr-l1a-v1/mgsl_21xx/software/) and were then imported to a shape file using ARCGIS.

The binned MOLA radius ''megr90n000eb. img'' - MEGDR - (downloaded at http://pds-geosciences.wustl.edu/missions/mgs/megdr.html) files contain coefficients and related data for a spherical harmonic model of the shape of Mars [Smith et al.,

2003]. In this work it was used the DEM with 32pix/deg. The coordinate system is IAU 1991 [Davies et al., 1992] areocentric, with longitudes measured positively toward east. When evaluated, the model gives absolute radius from Mars center of mass in meters. The model is a numerical transform of planetary radius values from the MOLA 0.5-degree gridded data set into spherical harmonics using Simpson's Rule quadrature [Smith et al., 2003].

2.2 MOLA Data and its application on Martian Topography

The shape of Mars is unique among planets. Topographic data permits to constrain the geological evolution of the planet [e.g. Zuber et al., 1992; Smith et al., 1999].

From the planet's center of mass, its surface is known globally at meter-level accuracy [Neumann et al., 2001]. Cartographers describe positions on Mars with reference to an ellipsoid with mean equatorial and polar radius of 3396.2 km and 3376.2 km respectively [e.g. Alves, 2003]. Geophysicists, however, often adopt a spherical datum of radius R = 3396 km for modeling the gravitational attraction of surface relief. Although, more properly termed, the planetary shape [Neumann et al., 2004] refers to the deviations *h* of planetary radius from this sphere, named as topography. The mean planetary radius R_{mean} = 3389.500 km represents the equivalent spherical planetary volume and is significantly less than the equatorial radius [Neumann et al., 2004].

To reduce dynamic range and to discuss topographic loading, planetary elevations may also be referenced to an equipotential surface, or a geoid, areoid for Mars. So, the term ''topography'' will be used for elevations about an areoid whose mean radius at the equator is 3396 km. This areoid is determined by satellite tracking and departs by up to 2 km from an ellipsoid of revolution [Neumann et al., 2004].

For lithospheric scale tectonic applications such as the crust or elastic lithospheric thickness estimation, as used in Chapter 4 of this work, a resolution around a few kilometers is enough [Zuber et al., 2000] and even hectometric spatial resolution with hectometer vertical accuracy can be used. Although, when used for large impact craters or volcanic structures, as in Chapter 3, a Digital Elevation Model (DEM) with a

spatial resolution ranging from 2 to 10 km with a decametric vertical accuracy is therefore needed [McEwen et al., 1999; Smith et al., 1999 ; Delacour et al., 2003].

2.3 DEM Technique

The techniques to produce digital elevation models (DEM) have been improved from the last few decades. Delacour et al. [2003], describe the first, using CO_2 pressure measurements realized by the Viking probes [Soffen, 1977] that were used to derive a 10-km scale DEM of the entire planet with a poor kilometric precision. Then, some attempts were achieved to produce DEMs with photogrammetric techniques on Viking images [e.g. Thornhill et al., 1993]. These methods were then improved by Baratoux et al. [2001] to produce DEMs with high spatial resolution close to the resolution of stereoscopic pairs of images. The third method of DEMs calculation uses the Mars Orbital Laser Altimeter (MOLA) launched in the frame of the Mars Global Surveyor mission in 1997, which acquired more than 600 million topographic measurements. The precision of the altimeter was specified to be around 35 cm [Zuber et al., 1998]. The laser measures the elevation over a spot of 130 m, although the final, vertical, absolute precision rests between 3 and 5 m, due to uncertainties in orbit determination. The altimeter registered topographic data along the orbit of the satellite with one point of measure each 300 m. The topography was then measured along profiles separated by 2 km near the equator, and by some hundreds meters at high latitudes due to the near-polar orbit of the satellite [Delacour et al., 2003]. Though, despite its high vertical accuracy, the main limitation of this technique appears when topographic maps are needed. To create a DEM or a topographic map, an interpolation on individual MOLA measurements on regular grids is required [Delacour et al., 2003]. The best resolutions of released DEMs produced by the MOLA team are up to 1/128th degrees, equivalent to ~ 0.5 km at the equator. The final DEM can then be used with an accompanying header file that describes the data format.

2.3.1 DEM Processing

The binned MOLA – MEGDR - data are downloaded at http://pds-geosciences.wustl.edu/missions/mgs/megdr.html. For a given area, topographic data are distributed over several files. So, for the a specific area the topographic information for DEM processing need to be extracted: geographic coordinates of each point, local radius of the planet, and elevation, which is the local difference with the geoid given by gravity models of Mars [e.g. Smith et al., 1999]. Then, the extracted points are classed by area. All of the MOLA points for a given area are then grouped into a file. After the request of a DEM computation on a selected area with a given resolution, the points belonging to this area are extracted. Then, ancillary files are created, including a file containing all of the MOLA points used during the interpolation process and an image file in tiff format, which is a color-coded topographic map of the area. MOLA DEMs and HRSC data, used in Chapter 3 were processed with the help of V. Ansan at IDES Orsay.

2.4. The Martian Geoid calculation

Gravity and topography are the only observations available which relate directly to the structure and state of Mars' interior, given the present lack of surface-based seismic and heat flow measurements. Topography provides a direct measure of the surface contribution to the gravity field. The gravity and topography reveals the internal structure. The admittance and other joint analysis of the gravity and topography provide information of the past lithosphere thickness, when the lithosphere was formed [Belleguic et al., 2005].

The geodetic parameters provide the only remotely accessible information on the internal distribution of mass in the planet. It is thus frequently convenient to describe the topography and the gravity in terms of their spherical harmonics coefficients [Alonso and Finn, 2000]. The choice of the most convenient solution degree depends on the measurement noise.

To evaluate the degree needed we'll interpret the meaning of the potential expansion in spherical harmonics [Alves, 2003]; For the gravity, we imagine that we

observe Mars at a distance *r*, much bigger than its radius, knowing that the differences between our sphere (the closest to the Mars's shape that includes all its mass) and the real shape of the planet are negligible. This way it is possible to assimilate the Planet to a punctual mass concentrated at its gravity centre (which is allowed by the Gauss theorem [see on Alonso and Finn, 2000]); the first potential is then given by an expression in 1/r (the first harmonic). When we get closer to *O* (the centre of mass) the differences between the sphere and the planet start to become sensitive. At an observation point P, in addition to the referred term in 1/r, it will appear one term in $1/r^2$ (it's generally null once the referential center corresponds to the center of mass of the planet). The next coefficient that affect the term in $1/r^3$ depends on the angle θ between the observation direction and the direction of *O*. This coefficient is given by the Legendre polynomial associated to the second harmonics and is related to the gravitational ellipticity (including the J_2 coefficient). As we are getting closer to Mars, these terms, which describe the planet gravity ellipsoide and associated polar flattening, are insufficient to fully describe the gravity. It is then necessary to introduce terms in $1/r^4$, $1/r^5$, ..., successively, respectively associated to degree 3, 4, etc.. For more details, see Wieczorek [2007].

The same development in spherical harmonics can be done for the radius and topography, with however a l=1 term, associated to the dichotomy and difference between the center of mass and center of figure. The l=2 coefficients are associated to the ellipticity of the planet. The difference between the ellipsoid and the sphere indicates a polar flattening of 1/176.875, which for Mars gives an equatorial radius of 3396.2 km and a polar radius of 3376.2 km [Alves, 2003]. These values are those of an ellipsoid with a shape the closest to the Martian shape. The coefficient associated to l=1 gives the fact that Mars is not symmetric in relation to the equator: the southern hemisphere is more voluminous, as described by Zuber [2000]. The l=3 and l=4 terms are associated almost entirely with the Tharsis bulge [Esposito et al., 1992], which contributes also to the l=1 and l=2 terms. The Tharsis bulge must therefore be corrected from the low order terms, if a better value of the planetary ellipticity is requested [Zuber and Smith, 1997].

So, regarding Esposito et al. [1992], the gravitational potential U and the topographic heights T with respect to some reference surface are expanded in normalized spherical harmonics as:

$$U(r,\phi,\lambda)=\frac{GM}{r}\sum_{1}^{1}\left(\frac{R}{r}\right)^{1}\sum_{m=0}^{1}\left(\overline{C}_{lm}\cos m\lambda+\overline{S}_{lm}\sin m\lambda\right)\overline{P}_{lm}(\sin\phi) \tag{2.4-1}$$

$$T(\phi,\lambda)=R\left[1+\sum_{l\rangle 0}\sum_{m=0}^{1}\left(\overline{A}_{lm}\cos m\lambda+\overline{B}_{lm}\sin m\lambda\right)\overline{P}_{lm}(\sin\phi)\right] \tag{2.4-2}$$

Where r, ϕ, λ, = radial distance from the centre of planet, latitude and east longitude; $\overline{P}_{lm}(\sin\phi)$ = Legendre polinomials (m=0) and associated functions of first kind (m>0), fully normalized; $\overline{C}_{lm}$, $\overline{S}_{lm}$ = normalized harmonic coefficients of *U*, of degree l and order m; $\overline{A}_{lm}$, $\overline{B}_{lm}$ = normalized harmonic coefficients of *T,* of degree l and order m; and *R* is the reference mean radius of Mars and *GM* = planetary gravitational constant. In addition it is defined the spectral components, for the potential:

$$S_l(U,U)=\sum_{m=0}^{l}\left(\overline{C}_{lm}^{2}+\overline{S}_{lm}^{2}\right) \tag{2.4-3}$$

And similarly for the topography:

$$S_l(T,T)=\sum_{m=0}^{l}\left(\overline{A}_{lm}^{2}+\overline{B}_{lm}^{2}\right) \tag{2.4-4}$$

The cross-spectrum components are also defined as

$$S_l(U,T)=\sum_{m=0}^{l}\left(\overline{C}_{lm}\overline{A}_{lm}+\overline{S}_{lm}\overline{B}_{lm}\right) \tag{2.4-5}$$

The series are limited to the common maximum degree l_{max} [Esposito et al., 1992] to which the coefficients are available in order to investigate correlative properties.

Martian topography is then given by Equation (2.4-2) with respect to the geoid surface.

The geoid is the appropriate reference surface to use for geologic and geophysical applications, as departures from an equipotential surface, which provide the

forces involved in dynamic processes such as water or lava flow and lithospheric flexure [Esposito et al., 1992]. Although the geoid is somewhat smoother than topography, the correlation between gravity and topography at long wavelengths can be easily seen. On Mars, this correlation is particularly strong for the Tharsis rise (e.g. Zuber 2000), that has the largest long-wavelength gravity anomaly. More subdued gravity signatures can be identified for the Hellas and Argyre basins, the Syrtis Major and Chryse Planitiae and the Elysium Rise.

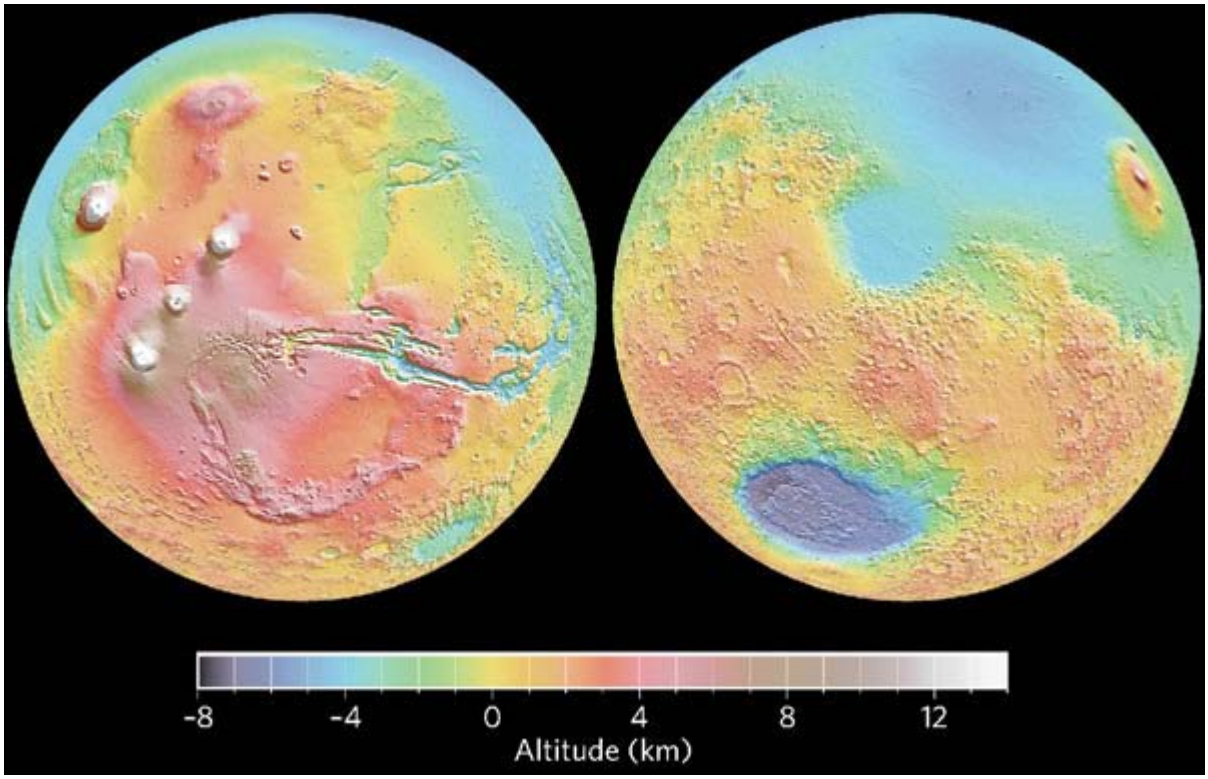

FIG. 2.1 – *Martian topography with respect to the reference ellipsoide*

2.5. The implication of Tharsis on the Geoids' calculation

In chapter 2.4 it was denoted the close relation between gravity and topography.

Even having had in consideration the gravity anomalies and the effect of the topography in the geoids' determination (Figure 2.1), it is observed for Mars that the experimental values of *g* are lower than previewed on the mountains (see Tharsis province). This effect may be related to the fact that the crust may have variable densities and/or thicknesses, as verified on Earth, where the oceanic crust density is higher than the continental crust density, and the oceanic crust thickness is smaller than the continental crust.

According to the Airy's isostasy Principle [Alonso and Finn, 2000] (Figure 2.2) the Earth's crust is more rigid and floats above a more dense mantle. The mechanism of compensation (the isostasy) would be reached in a way that under a mountain chain the crustal thickness would be higher than under big depressions. The mantle-crust boundary would be therefore anticorrelated to the topographic surface, and the pressure of the crustal edifice and upper mantle material will be constant at the level of the compensation depth, located at the base of the elastic lithosphere.

If the cooling of the planet is such that isostasy is lost, or if processes are faster than the time scale for isosatic equlibrium, this very simple principle is not valid anymore: erosion processes would lead to roots with bigger mass than the exposed part – overcompensation. And after recent constructive processes like lava flows, the roots of volcanoes may not have enough mass to compensate a topography that was over-elevated.

This simple principle permitted however to Zuber et al., [2000], as example, to explain why the Olympus Mons and the Tharsis Montes have all similar highs (approximately 20 km above zero surface). Zuber's crustal model was however constructed by using only the gravity and topography data, and by assuming that the entire gravity signal was related to crustal thickness variations.

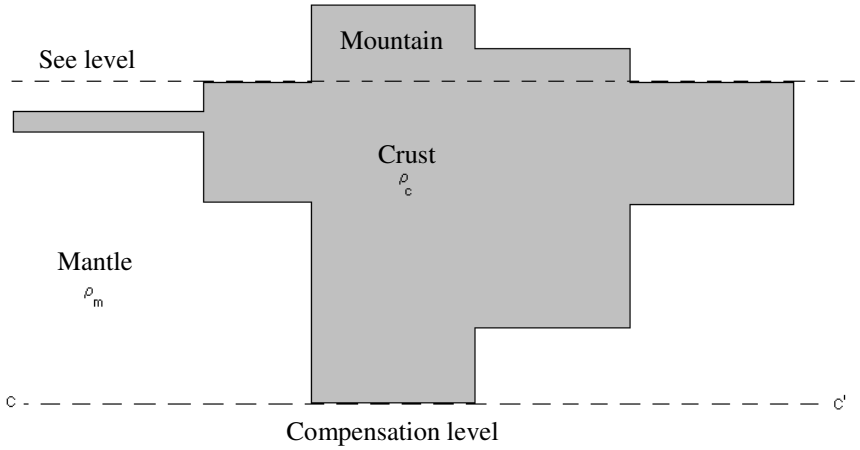

FIG. 2.2 – *Airy Compensation Model (from Alves, 2003).*

However it is difficult to explain the relative amplitude of Martian gravity anomalies, when compared to the topography, in terms of a single, simple global compensation mechanism. Esposito et al., [1992] found that the second and third harmonics (almost entirely associated with Tharsis, as it was said) require much deeper compensation. Despite the rest of the planet, which appears to be compensated at a depth from 100km – 200km [Phillips and Saunders, 1975; Phillips and Lambeck, 1980], Tharsis seems to be supported by some other mechanism. Stated plainly, there is a large excess of gravity at long wavelengths relative to that which can be explained by simple compensation models.

Several isostatic-based models [e.g. Banerdt et al., 1982; Willemann and Turcotte, 1982; Sleep and Phillips, 1985; Banerdt et al., 2000] were applied to explain the large free-air anomaly on Tharsis, and require a close fit to the topography/gravity boundary conditions (see Chapter 3.1). These mechanisms reduce the amount of compensating mass required in the lithosphere, resulting in large net gravity signature as required by observations. However, they have extremely different implications for the evolution of Tharsis. For some models [e.g. Richards and Hagger, 1984] (which invoke a non-concentrated means of support, either statically by elastic flexure or dynamically by mantle convection) the topography is formed primarily by uplift of the surface. These models would imply the presence of a single immense plume beneath Tharsis that

feeds it, and that it has not moved significantly with respect to the lithosphere since the Noachian. For a flexural case (isostatic-compensated based models) the highlands are formed by a combination of extrusive and intrusive volcanism, resulting in a crust that is about 30-km thick than the planetary mean. This would make the formation of Tharsis a significant event in the differentiation of the Martian mantle [Esposito, et al., 1992]. This also requires an elastic lithosphere at least 100 km thick that is capable to support stresses on the order of several hundred MPa, which also places a constraint on the thermal structure of the interior.

Finally, it is therefore evident that the relation between the gravity and the topography are essential tools for the determination of the crust thickness or the elastic lithosphere thickness, which are related to the formation and thermal history of a planet. These assumptions are debated on chapters 3 and 4 of this dissertation. In order to show the correlation between topography and gravity on Mars, Figure 2.3 plots the coherence for some gravity models developed in spherical harmonics [e.g. Neumann et al., 2004; Belleguic et al., 2005]. The coherence approaches to one when the gravity anomalies are mainly due to topography. It is observed (Figure 2.3) a good correlation between gravity and topography till the degree 60, approximately. Beyond degree 60, for jgm85h02, even if the coherence is decreasing it continues to be important, which means that the gravity anomaly is still due to the topography.

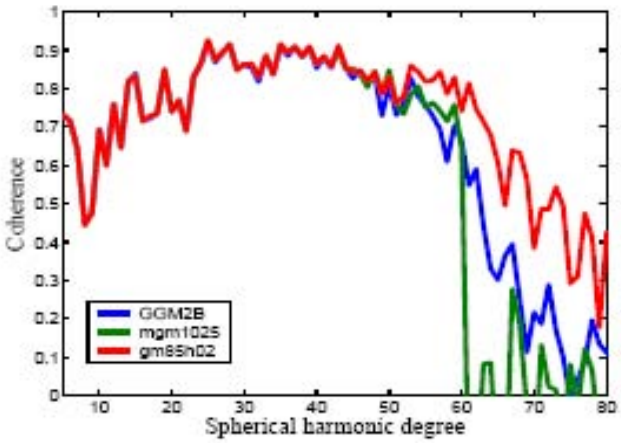

FIG. 2.3 – *Correlation of gravity fields with topography referenced to a spherical datum [Belleguic et al., 2005].*

Part II – the role of Syria Planum on the Tharsis Volcanism

3. The Syria Planum Formation and its role on the Tharsis Volcanism

3. The Syria Planum Formation and its role on the Tharsis Volcanism

Dans le chapitre actuel il est d'abord décrit l'histoire volcano-tectonique de la province de Tharsis. Le premier but est de comprendre comment cette formation a été affectée, à un certain moment de son passé géologique, par l'histoire volcanique de Syria Planum.

Dans le chapitre 3, il est décrit le travail effectué sur Syria Planum. L'étude de Syria Planum a commencé parce que jusqu'aux missions les plus récentes, les différentes données et notamment les images connues, (fournies par la Mariner 9 ou par la navette spatiale Viking [par exemple, Carr, 1973, 1974 ; Mouginis-Mark et al. 1992] étaient tout à fait pauvres. En utilisant de nouvelles images de plus haute résolution et des données d'altimétrie, à partir des missions MGS et MO) il a été détecté une multitude de formes volcaniques [e.x., Tanaka and Dohm, 1989; Davis and Tanaka, 1993; Webb et al., 2001; Hauber and Kronberg, 2001; Plescia, 2003; Sakimoto et al., 2003; Sakimoto, 2003; Vaucher et al., 2006; Bleacher et al., 2007; Hauber et al., 2007]. Dans ce travail il est réalisé une amélioration de leurs observations, en utilisant notamment les images stéréo de haute résolution de la caméra HRSC. Ces données associées à celles d'altimétrie MOLA ont permis d'identifier, de caractériser, et de tracer une suite de formes de relief volcanique sui-generis dans la région de Syria Planum. Cette dernière est une région de plaine volcanique où l'identification de ces formes de relief a été limitée en détail, comme cela a été décrit, lors des données précédentes.

Un important point de départ à l'étude de Syria Planum est le fait qu'elle est placée sur la partie la plus élevée de Tharsis (représentant une étape importante du développement volcano-tectonique de Tharsis), en sachant que Syria n'a pas été considérée comme centre volcanique principal, en raison de l'absence de volcans géants dans cet endroit.

Dans ce chapitre, il est donc identifié et analysé des volcans boucliers accolés, qui, en tenant compte de leurs caractéristiques morphologiques ne sont pas connus ailleurs sur Mars. Il est ainsi réalisé une étude détaillée de leur forme, de leurs contacts aux frontières, de leurs pentes, de leur rhéologie, de leur âge, de leur morphologie et de leur relation par rapport au modèle de tectonique régionale. En plus de ces volcans boucliers, Syra a été aussi dominée par un plus grand édifice volcanique singulier qui est la source de longues coulées de lave. Ces coulées de lave sont en contact avec les volcans boucliers et en diffèrent en âge, rhéologie et morphologie. Dans ce chapitre, il est aussi présenté une étude approfondie de la rhéologie de ces coulées de lave.

A la suite de ces observations plusieurs questions ont dû être résolues ; (1) les essaims de petits volcans boucliers accolés ne sont pas habituels dans la région de Tharsis. Quel type de phase volcanique indiquent-ils ? Comment se sont-ils reliés aux longs écoulements de lave placés autour d'eux ? (2) Ce présent travail a permis de démontrer que le volcanisme sur Syria Planum s'est achevé pendant l'Hesperian. Pourquoi a-t-il fini tandis que dans les zones du nord et de l'ouest de la région de Tharsis l'activité volcanique a probablement continué pendant les 3 milliards d'années suivantes ? Cette réponse sera traitée dans le chapitre 4 de ce travail.

In the present Chapter it is first presented the volcano-tectonic history of the Tharsis Province. One first aim is to understand how this formation was somehow affected in a certain moment in its geological past by the history of Syria Planum itself. In Chapter 3.2 and follows, we describe the work done on Syria Planum. We have started working in Syria Planum once till the most recent

missions, the imagery that we had from this place, from Mariner 9 or Viking Orbiter [e.g., Carr, 1973, 1974; Mouginis-Mark et al., 1992] was quite poor. Using new imagery and altimetry data from the recent missions Mars Global Surveyor (MGS) and Mars Odyssey (MO), many small volcanic features were detected here [e.g., Tanaka and Dohm, 1989; Davis and Tanaka, 1993; Webb et al., 2001; Hauber and Kronberg, 2001; Plescia, 2003; Sakimoto et al., 2003; Sakimoto, 2003; Vaucher et al., 2006; Bleacher et al., 2007; Hauber et al., 2007]. In this work, we try to improve these volcanoes observations using high resolution stereo images from HRSC camera, associated to MOLA altimetry data, which allow us to identify, characterize, and map a suite of sui-generis volcanic landforms in the Syria Planum region; a plain-style volcanic region where the identification of these landforms was limited in detail with previous imagery. An important beginning-point for the study of Syria Planum is the fact that it is placed at the uppermost part of Tharsis (representing an important stage of the Tharsis volcano-tectonic development) although Syria has not been considered as a main volcanic center mainly due to the lack of giant volcanoes. We identified and described a pattern of coalesced shield volcanoes, which, taking into account their morphological characteristics, are not known anywhere else on Mars. It was done a detailed study of its shape, border contacts, slopes, rheology, age, morphology and relation to the main tectonic pattern. These small shields are in contact with extensive long and lobate shape lava flows that differ in relative age, rheology and morphology from the shield volcanoes. Syria Planum was dominated by both swarms of small shields, and a single larger edifice as the source of long lava flows, that were also studied in detail in this dissertation. From our observations several questions needed to be solved; (1) swarms of coalesced small shield volcanoes are not usual in the Tharsis region. What kind of volcanic phase do they indicate? How are they related to the long lava flows placed around them? (2) Our work showed that the volcanism in this area ended during the Hesperian epoch. Why did it end whereas the northern and western parts of the Tharsis region

continued to display volcanic activity throughout the next 3 Ga? This answer will be treated on Chapter 4 of this work.

3.1 Introduction to Tharsis Volcanism

3.1.1 Volcano - Tectonic description of Tharsis

Tharsis is the most extensive basaltic volcanic province on Mars, and is dominated by five major volcanoes; Alba Patera, the Olympus Mons, the Tharsis Montes Group (Arsia, Ascraeus and Pavonis), and also by small shields (on Syria Planum and Tharsis Montes flanks) and vent fissures, Tholi and small Paterae.

Tharsis dominates the western hemisphere of Mars, with heights that may reach 10 km above the Mars datum [U.S.G.S. 1989]. It is intensely fractured by long and narrow grabens that extend radially hundreds of km beyond the rise and is surrounded by compressional wrinkle ridges that formed over 2000 km from the center of the rise. The Tharsis region experienced a long and extensive history of tectonics, often associated to volcanism, once the most important tectonic centers are often associated to magmatic centers [Anderson, et al., 2001].

Alba Patera

Alba Patera is unique on Mars. The all complex extends by more than 1600 km diameter, has a central caldera that doesn't overpass 6 km high, flank slopes of about 1º, and one of the largest calderas found on Mars [diameter of about 120 km]. It might have been formed by several flow events, much more intense and prolonged than known anywhere else [Greeley and Spudis, 1981; Mouginis-Mark et al., 1992; Cattermole, 1990; McGovern et al., 2001]. The summit region has a caldera complex, extensive lava flows and local dendritic valleys on the flanks that have been interpreted to indicate a pyroclastic phase of the eruptive history [Mouginis-Mark et al., 1992].

From Scott and Tanaka [1986], the lower member (unit Hal) is Hesperian in age and corresponds to a broad area of lava flows surrounding the main construction of Alba Patera from the west, north, and east (Figure 3.1). The middle member (unit Aam), early Amazonian in age, coincides with the main

construct of Alba Patera and the upper member (unit Aau), also early Amazonian in age, occupies the central portion (summit) of the main construct between Alba Fossae and Tantalus Fossae.

Olympus Mons

Olympus Mons is the largest and most prominent Martian shield volcano [e.g. Scott and Tanaka, 1998], which has a relief of about 21 km and a basal extent of about 840 km by 640 km, measuring the edges that surround the main edifice. The width is extended over many hundreds of kilometers northeastward into the lowland units in the aureole deposits. The slopes are about 5º and up to 30º at the scarp, confirming its asymmetric shape. The steepest slopes [up to 20–30º] are observed on the caldera walls or on portions of the basal scarp that are not covered by lavas. The caldera of Olympus Mons consists of at least six coalescing depressions [Mouginis-Mark, 1981; Zuber and Mouginis-Market al., 1992; Plescia, 2004] and suggests a sequence of at least six episodes of caldera collapse. Both of the smallest calderas and larger ones appear very smooth in their floor morphology and are covered by volcanic flows from effusive fissure, resurfacing most of the caldera floors [Mouginis-Mark, 1981]. In the vicinity of the caldera it is observed superimposed lava flows, which represent the latest active phases.

From Scott and Tanaka [1986] the main geological units from Olympus Mons are: (Aos) that represent young shield lavas. (Aoa1-4) that constitutes the Aureole Member formed by gravity spreading of materials forming a larger, earlier Olympus Mons; alternatively, could be ash or lava flows. (Aop): Long Lava Flows extruded from fissures.

The Tharsis Montes

From southwest to northeast Arsia Mons, Pavonis Mons, and Ascraeus Mons form the Tharsis Montes. Plescia and Saunders [1982] and Neukum and Hiller [1981] determined average surface ages which increase to the southwest, giving Arsia as the first volcano formed on the chain.

From Scott and Tanaka [1986] the main geological units are: (At6) – Fresh appearing lava flows form smooth, fan-shaped arrays on flanks of Arsia, Pavonis and Ascraeus Montes. This Member also includes most recent fill within central calderas of Tharsis Montes. (At5) Member 5 – it forms elongate, light-colored flow lobes with abundant dark wind streaks. It is cut by few faults. (At4) Member 4 - Consists of overlapping light flows with dark wind streaks similar to those of Member 5; their flows elongate on steep upper slopes, and broad on gentler lower slopes. High resolution images show pressure ridges concentric with lobate flow fronts; they present minor faulting. (AHt3) Member 3 - Makes up central shields of Arsia, Pavonis, and Ascraeus Montes.

Arsia Mons

Its summit elevation is at about 18 km and has a height of about 11 km if compared to the surrounding plains. It has a single caldera, the largest on Mars with a diameter of about 120 km [Crumpler and Aubele, 1978] that is bounded by concentric normal faults [e.g. Crumpler and Aubele, 1978]. The main edifice has a width of about 400 km and is composed of by a central shield and two aprons, one on the northeast and a second on the southwest, originated about 5 – 7 km below the summit [Werner, 2005].

Arguments concerning its morphology, slope steepness and caldera complexity [a broad feature with low slopes and a large simple caldera] favoured Arsia to be the oldest Tharsis Mons [Plescia, 2004], previous to 3.55 Ga ago, when the last shield formation may have ended [Werner, 2005]. Many episodes of surface modification, which covered the edifice by many layers of lava flows may have then occurred, as prove the existence of several vent fissures and low shields on the Montes flanks [e.g. Bleacher et al., 2007], indicative of very recent geological time volcanism, although the presumably extinct large shields. Moreover, the caldera floor has surface ages of about 200-100 Ma [Neukum et al., 2004] confirming later stages of volcanic eruptions at the summit and flank of the volcano. Plescia [2004] attests this dating describing the temporal succession of

geological events on Arsia Mons; building of the main edifice, the development of the flanking aprons, filling of the caldera and the later volcanic phase with the construction of low shields on the caldera floor.

Pavonis Mons

Pavonis Mons has the lowest summit altitude of the Tharsis Montes [about 14 km high], although it has a 10 km relief comparing to the surrounding plains and only reveals a slight asymmetry once the eastern flank is 4.6º steep vs. 4.1º for the western flank. The two visible caldera depressions occupy an area of about 100 km in diameter and indicate the latest periods of summit activity. Based on crater counts [Neukum et al., 2004] determined that the larger caldera floor formation ended about 370 Ma ago and the smaller caldera floor at about 80 Ma ago.

After the initial shield-building phase ended at Pavonis Mons, debris aprons of the northwest flank were formed. This was followed by the development of the volcanic aprons on the flanks where the southermost flanks are carved by prominent lava channels and smaller alcoves and occupied by small low–shield volcanoes [e.g. Bleacher et al., 2007]. These regions are associated with the youngest parts of the Pavonis Mons, with ages between about 800 Ma and about 100 Ma [Werner, 2005].

Ascraeus Mons

Ascraeus Mons is the northernmost volcano and the tallest of the Tharis Montes [approximately 18 km high]. Like Pavonis, it reveals marginal lava aprons extending northeast and southwest at the flanks, although it exhibits smaller aureole deposits at the northwestern flank segment. The flanks have slopes of about 7 º and exhibit terraces as the flanks of Olympus Mons [Plescia, 2004]. Flank terraces have been suggested to be both thrust faults [Thomas et al., 1990] and normal faults [Montesi, 2001; Cipa et al., 1996].

The summit caldera is complex compared to the other shield calderas. Werner [2005] obtained ages from about 3.6 Ga ago, time at when the main edifice was already emplaced, to as recent as 100 Ma [Neukum et al., 2004]. Plescia [2004] reveals a complex history of flank eruption and apron formation; the apron extending from the northeast flank is comparatively larger than those aprons found on the other Tharsis Montes, beginning at an elevation of 6.0 km and where flow lobes cover the plains to the north and northeast. Lava flows from the younger apron extend down slope and along the eastern margin of the volcano burying the distal eastern flows of the northern apron.

Similar to Pavonis Mons, Ascraeus Mons has a long volcanic history with the development of the shield and multiple summit calderas. Low shield volcanoes, fissure vents and other volcanic activity are observed following the overall northeast–southwest trend as already observed at Arsia and Pavonis Montes.

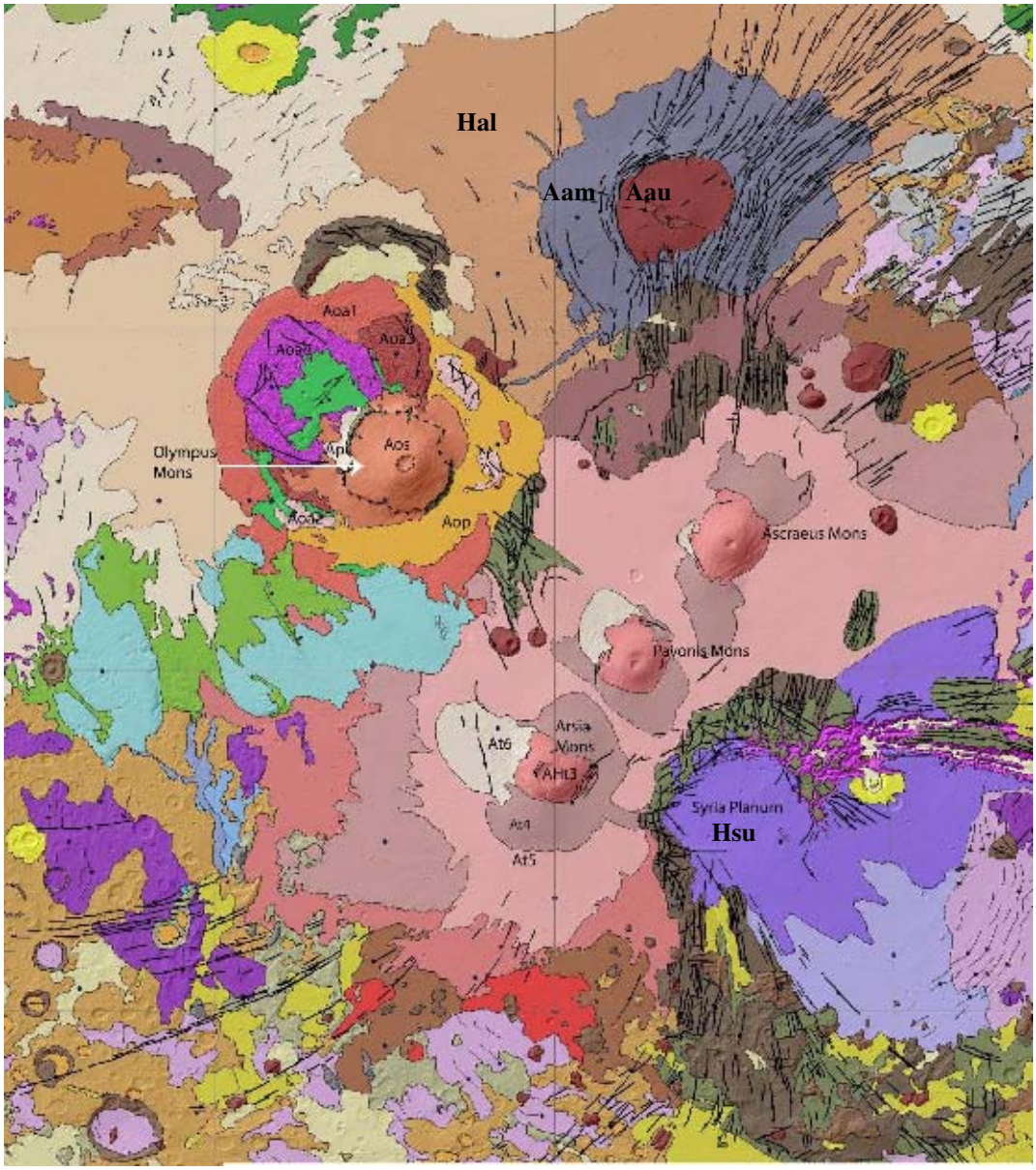

FIG 3.1 – *Geologic map of the Tharsis Rise region superposed on a MOLA shaded relief map. Figure modified from Scott and Tanaka [1986] in simple cylindrical projection. Units described in Scott and Tanaka [1986].*

3.1.2 Volcano-tectonic origin of Tharsis

Magmatism and tectonism have mostly contributed to the geological evolution of Mars [e.g. Scott and Tanaka, 1998; Anderson et al., 2004]. This is particularly evident on the Tharsis region.

There are several hypotheses for the formation of this *sui generis* planetary feature; some of these hypotheses are mostly based on tectonic aspects, others centered on volcanic aspects.

Tectonics-centered hypotheses are: (1) Several authors refer the existence of a mantle plume developed in an area of convecting upwelling to produce uplift and volcanism [e.g. Hartmann, 1973; Carr 1974; Schubert et al., 1990; Wise et al., 1979], or even (2) that material eroded from the base of the early crust in the northern plains was redeposited and intruded into the crust below the site of Tharsis, resulting in isostatic uplift [Wise et al., 1979]. Schultz [1984] by his turn, (3) proposed basin rings surrounding Syria Planum that aligned with the Tharsis Montes, suggesting the volcanism was concentrated along pre-existing basin structures.

Moreover, according to Banerdt et al. [1992], (4) the mechanisms for the origin of Tharsis can be divided into three general hypotheses: external loading, uplift and isostatic. The stress patterns as well as the subsurface structures that result from each of these scenarios would be quite different; (a) Due to external loading, the downward displacement of the lithosphere beneath Tharsis should produce generally radial compression within the Tharsis rise and concentric extension farther out. In this case, it would imply a crust significantly thicker beneath Tharsis (60-75 km thick lithosphere) due primarily to the great thickness of extrusives required; (b) The uplift scenario (doming) that is caused by support applied to the base of the lithosphere produces stresses with the same orientations but with the opposite sign, with inner extension and outer compression; (c) For isostasy, radial compression appears outside Tharsis, with concentric extension being developed out in the flanks [Banerdt et al., 1992]. It is although commonly

accepted that more than one mechanism of lithospheric deformation is needed to produce the enormous extent of concentric extensional stresses required to form the radial grabens. In particular, concentric extensional stresses on the top of the Tharsis rise are only produced by isostatic models [Banerdt et al., 1992], which show compressional stresses off of the rise. On the other hand, only flexural loading produces concentric extensional stresses off of the rise [Banerdt et al., 1992]. However it is still not clear how to form such extensive radial features in a single event, when the stress models seem to require two distinct events. It should be first solved the link between these stress systems and the evolution of the lithosphere and astenosphere on the Tharsis region. The strongest constraint still comes from the gravity measurements which indicate a very large free-air anomaly [e.g. Belleguic et al., 2005]. Isostatic models with reasonable compensation depths can be constructed by "burying" part of the load [Sleep and Phillips, 1979] by thinning the crust or requiring its density to be higher beneath Tharsis [Belleguic et al., 2005]. Banerdt et al., [1992] propose a scenario in which Tharsis is partially supported by the elastic strength of the lithosphere, with the remainder of its support derived from the buoyancy of a crustal root at a depth of about 50 to 100 Km. This would imply an excess crustal thickness of about 25 to 30 km, suggesting a scenario of a transient mode of support (thermally or chemically induced density deficit in the upper mantle, or a convective plume) early in the story of the Tharsis thick lithosphere formation. Also, the fault and rift systems of varying extent and relative age of formation, including the vast canyon systems of Valles Marineris are interpreted to be the site of a lithospheric zone of weakness and consequent vertical uplift presumably related to plume manifestation [Anderson et al., 2004]. Right on the vicinity of this canyon, the crustal thickness increases drastically, about 40 kilometers (see Chapter 4).

Scott and Tanaka [1980], using Viking images, indicated that (5) most of the Tharsis faulting developed in association with three major centers of uplift; Syria Planum, Alba Patera and Tharsis Montes. According to these authors, the main and global tectonic history of Tharsis may be resumed by six important

events of ridges and grabens: (I) Pre-Tharsis faulting in the Thaumasia region and at Acheron Fossae; (II) Syria centered radial faulting; (III) Wrinkle ridges concentric to the Tharsis swell; (IV) Pavonis centered radial faulting; (V) faulting at alba Patera, Tempe Terra and Tharsis Montes; (VI) radial and concentric grabens surrounding the Tharsis Montes.

The radial grabens that surround Tharsis show north and northeast trends, which Carr [1979] (6) attributed to one main event of uplift in Syria Planum, and variations in fracture density to the irregular shape of the dome itself. By another side, (7) [Plescia and Saunders, 1982] divided the development of main radial fractures system into three episodes taking Syria and Pavonis as centers. Another detailed study (9) by Anderson [2001] reveals five main tectonic center: 1 - On the Noachian; Acheron Fossae, Claritas Fossae, Warrego, Thaumasia; 2 - Late Noachian to Early Hesperian; Sirenum Fossae, Syria Planum, Valles Marineris, Memnonia Fossae, Ceranius Fossae; 3 - Hesperian; Lunae Planum, Tempe Terra Noctis Labyrinthus; 4 - Late Hesperian to Early Amazonian; Tharsis Montes, Alba; 5 – Mid to Late Amazonian; Tharsis Montes.

Volcanic-centered hypotheses are: (1) Many authors have suggested that the development of Tharsis resulted by plume-driven activity [Mège and Masson, 1996; Kiefer, 2003], or even by (2) superplume activity [Baker et al., 2002; Dohm et al., 2000], similar in many respects to putative superplumes of Earth [e.g. Li et al., 2003]. Plescia and Saunders [1982] (3) suggested that Tharsis originated and grew till its present size by an extended period of regional volcanism on a massive scale.

Representative of the intense magmatic activity in Tharsis are the volcanic constructs of diverse sizes and shapes and extensive lava flow fields or large igneous plateaus. Also, early explosive activity that evaluated into more concentrated and effusive activity, small shield volcanoes and fissure-fed eruptions.

Besides all these different proposed models and this permanent controversy concerning for the Tharsis formation, a central concept is important to be kept in mind: The Tharsis formation is mainly due to this strict cause/effect relation of the Magmatic-Tectonic events, with a most probable origin due to mantelic giant plumes. Precisely, the magmatic-driven activity includes the deformation of crustal materials, dike emplacement and the emplacement of lavas to form volcanoes, shield fields and lava flow fields [Mege and Masson, 1996; Dohm et al., 2001; Baker et al., 2002; Komatsu et al., 2004].

As also Wilson and Head [2002] demonstrated with their magmatic models, Tharsis grabens are formed from stresses associated with plume and reservoir over-pressurization with lateral propagation of magma-filled cracks. Thus the grabens are associated primarily with magmatic history and can form then at any time throughout the history of the plumes. Moreover these grabens are likely to present a wide range of ages, revealing an associated long-life of volcanic events, studied then in this chapter.

As described, the vast tectonic signature is given by vast canyon systems, systems of radial faults and circumferential systems of wrinkle ridges and fold belts centered at the centers of magmatic-driven activity, and catastrophic outflow channels or early basins formation [e.g. Scott and Tanaka, 1998; Anderson, 2001].

3.1.3 Longstanding Volcanism

The recent volcanic activity on Mars, especially on the Tharsis region have been commonly accepted [Hartmann et al., 1999; Weizman et al., 2001; Schumacher and Breuer, 2006] and demonstrated by crater counting [Neukum et al., 2004]. Namely, recent evidence from the Mars Global Surveyor (MGS) suggests the latest activity at the Tharsis area to be no older than 40–100 Myr [Hartmann et al. 2000].

From the Geophysics we know that volcanism is possible in regions where the mantle temperature is higher than the solidus temperature of the mantle

material. As long as a global partial melt zone is located underneath the stagnant lid, this melt zone could be the source region for volcanism on Mars [e.g. Schumacher and Breuer, 2006].

For Mars, in particular for the Tharsis and Elysium regions, it has been suggested that plume volcanism is necessary to explain its long-standing and recent volcanism [e.g., Redmond and King, 2004]. Although, the apparent misfit between Martian topography and geoid (see Chapter 2) and used in models of thermal convection [Harder, 2000] have also been pointed as sufficient reasons to argue against the deep mantle plumes being in the origin of long-lived volcanism in the Tharsis region [Phillips et al., 2001]. Moreover, Schumacher and Breuer [2006] demonstrated with thermochemical parameterized models that a plume-fedded longstanding volcanism is unlikely to occur. This process may have been in the origin of Tharsis and Elysium during their early stages of formation, although another mechanism is more likely to explain its long duration or reactivation. For instance, the presence of a global partial melt zone during most of the planet's evolution and in particular the influence of lateral variations in crustal thickness on the temperature distribution may be responsible for the recent volcanism [Schumacher and Breuer, 2006; Chapter 6] on Tharsis. Moreover, as already stated by Zuber [2001], underneath these large volcanic regions with comparatively thick and low conducting crust, higher temperatures than average are likely. It has also been suggested that the crust underneath Tharsis is about 20 to 40 km thicker than in its surroundings [Neumann et al., 2004] and it's shown on Chapter 6.

The appearance of water-generated landforms on Mars within the last 10 Ma would also require an increased heat flow [Baker, 2002], which some authors attribute to the existence of volcanic intrusions. If the existence of a geologically recent volcanism seems well constrained [e.g., Neukum et al., 2004; Schott et al., 2001; Schumacher and Breuer, 2007], the factors of its longstanding duration are still not understood. The difficulty on its understanding is particularly due to the Mars' small size compared to the Earth, which suggests rapid cooling of the

planet as predicted by one-dimensional models of parameterized thermal convection [e.g. Weizman et al., 2001]. The description of long lived Martian volcanism by Wilson [2001] raised a new explanation for the melt necessary to generate volcanic activity and the formation of a depleted layer preventing the planet from rapid cooling. On Mars the depleted layer is especially thick, because of the low lithostatic pressure compared to the Earth [Schott et al., 2001].

3.1.4 Small shield Volcanoes – The interest of its study

A small shield volcano is a term for a small constructional feature formed by the eruption of lava flows from a central vent [Greeley, 1982].

Shield volcanoes have been mapped, in addition to fissure vents in the vicinity of the bases, or within the floor of caldera of the Tharsis Montes [Bleacher et al., 2007], namely on the flanks of Ascraeus Mons, Pavonis Mons and Arsia Mons, as it was explained in chapter 3.1. In particular, the small-vent fields of the eastern Tharsis province (Figure 3.2) are the result of late Amazonian volcanism associated more or less directly with the Tharsis Montes [Bleacher et al., 2007]. To the north of the Tharsis dome, shield volcanoes also occur within the terrain of Tempe Terra [Davis et al., 1993] dated from Hesperian [Moore et al., 2001; Skinner et al., 2006]. This region shows a variety of volcanic landforms that range in size from 10 km to 150 km. The volcanoes are aligned along the dominant northern and northeastern trending faults in this region, and many volcanoes occur on grabens.

The low shields detected on Pavonis and Ascraeus flanks [Plescia, 2004; Bleacher et al., 2007] are typically 200 m high and several tens kilometers wide. Most of them are located on the south-trending aprons that extend from the flanks of both volcanoes. In addition, low shields occur on the plains east of the Pavonis Mons and north of Noctis Labyrinthus. There does not appear to be any particular structural control of the location or orientation of the low shields on the aprons, although their preferred northeast orientation on the plains [Plescia, 2004]. The graben of Noctis Labyrinthus, which presumably lie at depth below the younger

volcanic plains, have northnortheast trends. The low shields have a northeast structural control suggesting that the older tectonic features are no longer exerting influence.

Tharsis magmatism, especially the one responsible for the previous extensive Tharsis Montes production, is likely to have resulted from single or multiple mantle plumes, as mentioned on chapter 3.2 [e.g. Wilson and Head, 2002]. Some authors [e.g. Sakimoto, 2008] state that dikes swarms and plains volcanism around Tharsis thus reflect multiple intrusions, consistent with prolonged magmatism concentrated along zones of weakness in the crust.

Moreover, small shield volcanoes in Syria Planum (e.g. Figure 3.3) indicate later volcano-tectonic driven reactivation of magmatism, as it will be demonstrated during this chapter.

Though, small shield volcanoes represent a later volcanic event during Tharsis history, thus resulting from the reactivation of ancient faults, from where the lava floods. Their study and comprehension permit the understanding of the most recent episodes of volcanism around Tharsis. They represent a geological evidence for the recent volcanism in the Tharsis Province. To understand its formation on the highest plateau of Tharsis, on Syria Planum, we made a detailed study that is described during this chapter.

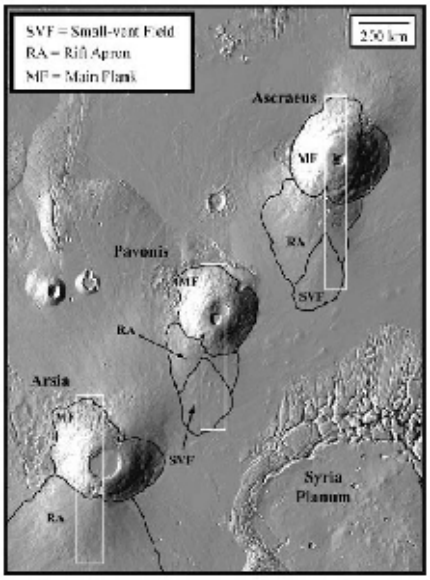

FIG. 3.2 – *A MOLA shaded relief image (from Bleacher et al. [2007]) showing the Tharsis Montes and the part of Syria Planum. The main flanks (MF) of the three Tharsis Montes, rift aprons (RA), and small-vent fields (SVF) (the same area where small shields were also detected) are outlined. The white boundaries of each shield correspond to HRSC coverage. Although rift aprons are also located to the northeast of each shield [Crumpler and Aubele, 1978]. Map zone boundaries were inferred from a combination of mapping and past geologic maps [Bleacher et al., 2007].*

3.2 Syria Planum Volcanism and Tectonics

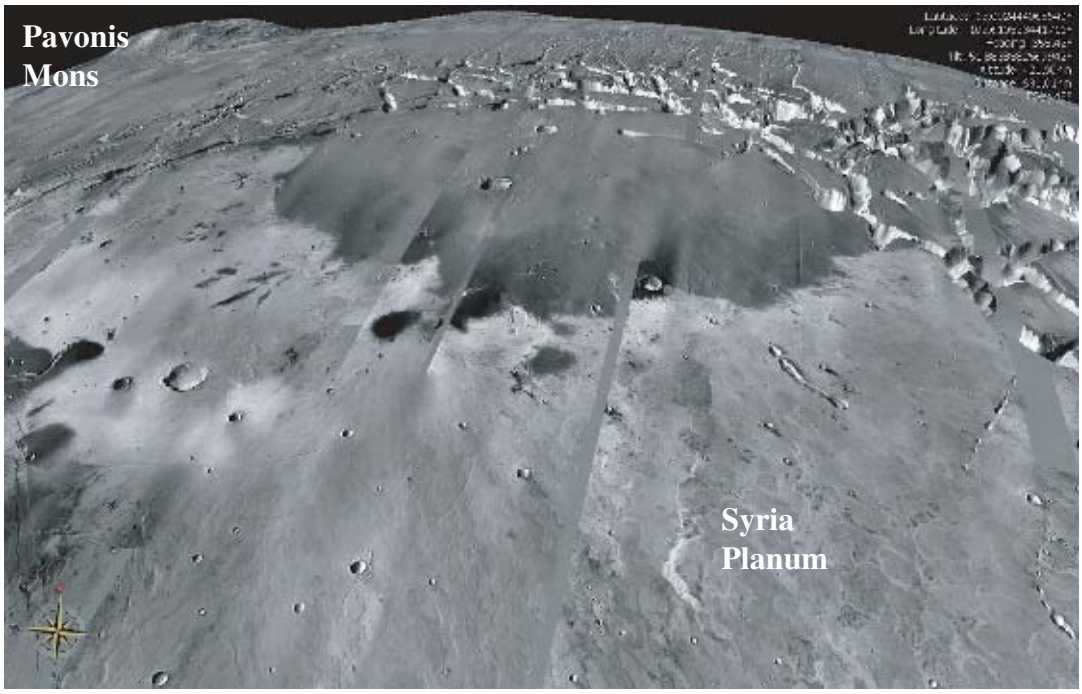

FIG. 3.3 – *THEMIS Mosaic image of Syria Planum. Credits: NASA World Wind.*

Syria Planum is a broad volcanic plateau located at the summit of the Tharsis rise (> 6 km high above MOLA datum). Plescia and Saunders [1982] first recognized Syria as a center of tectonic activity.

The plateau of Syria Planum is about 450 by 700 km wide, and is centered at 12ºS; 104ºW (Figures 3.3 and 3.4). It is separated from the Tharsis Montes volcanoes by Noctis Labyrinthus to the north and Claritas Fossae to the West [Masson et al., 1980, Tanaka and Davis, 1988, Head et al., 2000]. Based on Viking images, Syria Planum has been mapped as a volcanic plain of Hesperian age, with lava flows interpreted to originate from both the summit area and the flanks of a topographic elevation in northern Syria Planum and Noctis Labyrinthus [Tanaka and Davis, 1988; Scott and Tanaka, 1998]. Syria Planum also displays radial volcanic flow patterns [e.g., Tanaka and Davis, 1988] and volcanic eruptions along tube and vent-fed flows [e.g., Chadwick et al., 2004; Webb, 2001]. Within this tectono-volcanic province, small volcanic edifices were

locally found using Viking images [Hodges and Moore, 1994]. These edifices stand at elevations >6 km and are several tens of kilometers in diameter and several hundreds of meters high.

Now, in this work, new data allowed us to better characterize the landforms observed in Syria Planum.

Figure 3.4 shows mosaics of MOLA, THEMIS and HRSC images and a simplified geomorphic map drawn from these mosaics. We detail hereafter the three main morpho-structural units deduced from these data and mapped in the simplified geomorphic map: (1) in the northern and eastern regions, a group of conical features that resemble small volcanoes and correspond to the protuberances seen on MOLA data; (2) in the western and central regions, extensive lobate shaped lava flows; (3) in the southern region, a highly fractured terrain displaying graben-like structures.

In the NE region of Syria Planum, HRSC and THEMIS images show a group of 10 to 60 km diameter, relatively circular features, corresponding to the topographic protuberances seen in the MOLA map (Figure 3.4a). This swarm of protuberances displays a distinct pattern of coalesced landforms, as seen on Figures 3.4b, c and d (between 12-21ºS; 96-100ºW). A total of 30 individual protuberances are identified on these images (Tab. 1). They stand at the highest elevations on the plateau (>7 km). Some of protuberances (e.g., # 1 and 5) located to the northern edge of the swarm have a higher albedo, interpreted as a dust cover, as confirmed by the low brightness in THEMIS IR-night images (Figure 3.4c). Using the MOLA slope map expressed in percentage (Figure 3.4d), we observe that these protuberances have a central axis-symmetry slope less than 3%, indicating shallow slope cones. Some protuberances display a central vent or radial fractures (Figures 3.4f and 3.5). The combination of topography and imagery suggests that these topographic protuberances correspond to small volcanic edifices. We studied these landforms, and discuss in the next section how our results evidence this volcanic interpretation.

Table 1. Morphometric Parameters of Some Small Volcanoes in Syria Planum[a]

Volcano	W-E Width (km)	Mean Slope (°)	Altitude (m)	Mean Relief (m)	Area (km^2)	Mean Volume (km^3)	Vent	Eccentricity
1	41	0,7	6965	133	1081	55,7	yes	0,7
2	40,9	1,0	7264	248	794	103,6	yes	0,4
3	28	0,5	7060	117	637	22,8	yes	0,4
4	32	0,6	7053	195	836	49,9	yes	0,5
5	50,4	0,7	7085	241	1431	152,7	yes	0,5
6	16,2	0,7	6933	81	139	5,3	no	0,4
7	28	0,6	6999	105	704	20,5	yes	0,5
8	19	0,7	7208	151	459	13,6	yes	0,5
9	31,4	0,8	6999	202	839	49,8	no	0,5
10	16,5	0,7	7208	110	318	7,5	no	0,4
11	32	0,5	6955	70	686	17,9	yes	0,8
12	29,5	0,4	6901	105	638	22,9	no	0,4
13	29	0,5	7113	118	927	24,8	yes	0,8
14	14	0,3	7051	30	157	1,5	no	
15	14	0,7	7059	87	630	4,3	yes	
16	9	0,4	7002	29	78	0,6	yes	0,4
17	22,4	0,4	6977	77	363	9,6	yes	
18	10,4	0,3	6920	36	131	1,0	no	
19	9,6	0,7	6961	94	118	2,2	yes	
20	23	0,6	6901	117	600	15,5	yes	0,7
21	59	0,2	6858	50	444	43,5	no	
22	26,4	0,3	6788	27	570	4,7	yes	
23	10	0,5	6712	59	120	1,5	yes	0,6
24	10	0,5	6657	40	264	1,0	yes	0,6
25	7	0,3	7045	31	161	0,4	no	
26	10	0,1	6737	10	112	0,2	yes	
27	11	0,5	6763	57	270	1,7	yes	0,8
28	14,5	0,4	6703	90	346	4,7	yes	0,9
29	8,5	0,3	6628	67	82	1,2	no	
30	8,7	0,2	6421	9	158	0,2	no	

[a]Averaged values of slope, relief, and volume were determined considering separately the northern, southern, western, and eastern flanks. In some cases, not all of the four orientations were measured. For the volcanoes 14, 17, 18, 21, 26, 28, 29, and 20 the northern slope and relief values were not considered for the mean slope average. Also, the eastern values of volcanoes 15, 19, 21, and 29 were not considered. The difficulty in measuring some of the flanks is due to the superposition of lavas from adjacent volcanoes, which obviously hides the real contours of each volcano. The volumes were calculated using $V = 1/3 \times \pi r^2 h$, where h is the average relief and r is half of the W-E width. Topographic data and images were used to determine the contact between the shields and the plains and the shape of this contact was then used to determine the eccentricity.

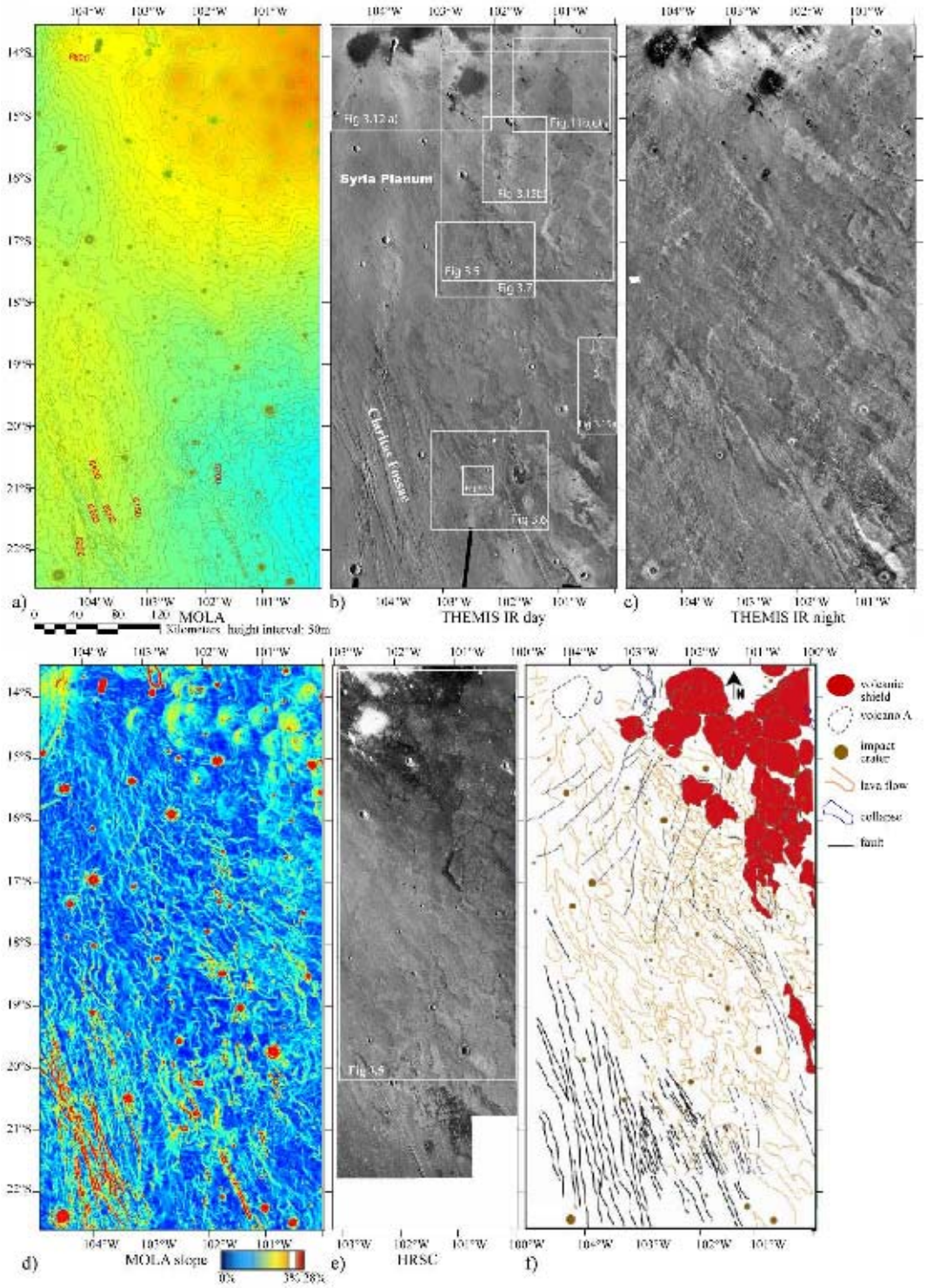
Syria Planum
Fig. 3.12 a)
Fig. 3.13 a)
Fig. 3.13 b)
Fig. 3.5
Fig. 3.7
Fig. 3.6
Fig. 3.8
Claritas Fossae
a) MOLA
Kilometers; height interval: 50m
b) THEMIS IR day
c) THEMIS IR night
d) MOLA slope
0°
35.28°
e) HRSC
f)
volcanic shield
volcano A
impact crater
lava flow
collapse
fault

FIG. 3.4 – *(a) MOLA altimetry with height contour intervals of 50 m. Regionally, the topography decreases from the north to the south and from the east to the west. (b) THEMIS IR day images (I17865001, I17290014, I17552023, and I16953015) where the white rectangles place and localize the figures shown in this work. (c) THEMIS IR night images. (d) MOLA slope expressed in percent. Some ruptures of slope are observed on the northwest and southwest, evidence for the presence of oriented fractures. The axisymmetrical protuberances on the northeast show higher dip mainly on their western flanks. Note the 20 km diameter protuberances on the higher (from about 6.8 to 7.5 km altitude) lands of Syria Planum. (e) Mosaic of HRSC images (orbits 2021, 2032 and 2054). (f) Geomorphologic map of Syria Planum. The axisymmetrical protuberances (morphostructure 1) are in red with impact craters in brown. The lava flows (morphostructure 2) that follow the regional slope are represented in orange. These formations are dissected by two families of lineations in black. On the southern part, these lineations become wider (morphostructure 3). In blue, at the top, we can distinguish some features that are the result of collapsed terrain. In gray are represented possible contours for the top of the volcano A.*

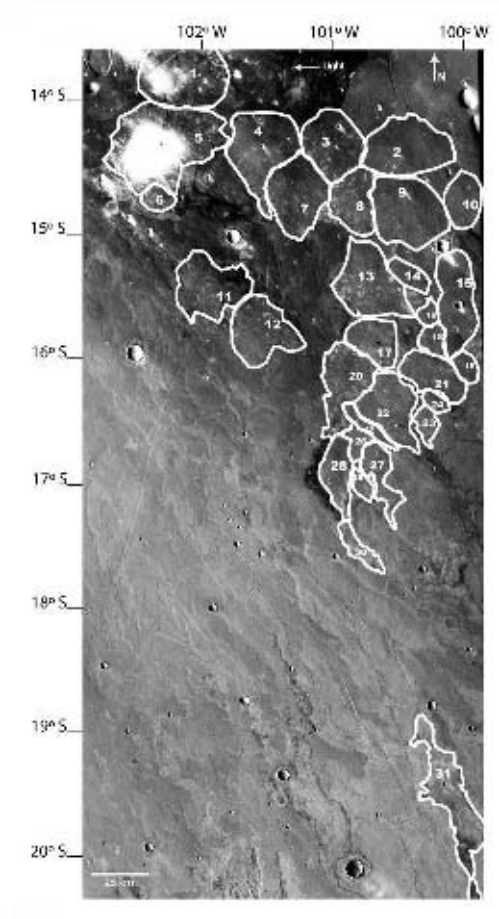

FIG 3.5 - *HRSC mosaic of the Syria Planum studied region. The context of this area is shown on Figure 3.4e. The higher albedo surfaces show areas highly covered by dust, while the lower albedo surfaces reveal contours of some circular features (on the East), extensive lava flows (coming from the Northwest), and two families of faults, more visible on the southern terrains. Several impact craters are also distinguished. Each single circular protuberance is circumscribed by a white contour and numbered (see Table 1).*

In the central part of the HRSC image mosaic, we observe an intermediate albedo feature, ~10 km wide and > 100 km long, with elongated shapes bounded by lobate fronts and scarps, covering a widespread area oriented NW-SE. In THEMIS day-IR, these landforms are characterized by an intermediate albedo with lobate shapes. These landforms are interpreted as lava flows that erupted

from the NW of Syria Planum, and flowed to the SE as indicated by the location of their lobate fronts. Their NW-SE trend is parallel to the SE regional topographic slope of 0.5% in this part of Syria Planum (Figure 3.4a and d). These lava flows stand between 5.4 and 6.8 km in altitude. They are poorly cratered and crosscut by tens of km long, 2.5 km wide, N-S trending linear fractures (Figure 3.6).

On the southernmost part of the HRSC image mosaic (Figure 3.5 and 3.7), below altitudes of 5.4 km on the MOLA map, the lava flows are crosscut by a widespread field of NW-SE-trending grabens. In contrast to their smooth surface at the HRSC image scale, the darkest areas located eastward in Figure 3.7 correspond to rough bedrock that lava flows did not cover.

In addition to these three main units, we observe that a few grabens cross both the protuberances (inferred small shields) and the lava flows. Ovoid depressions, apparently resulting from a collapsed surface, exist on the top west and east at the external margins of the plateau. A large number of impact craters are also visible from a few tens of meters to ~10 km diameter.

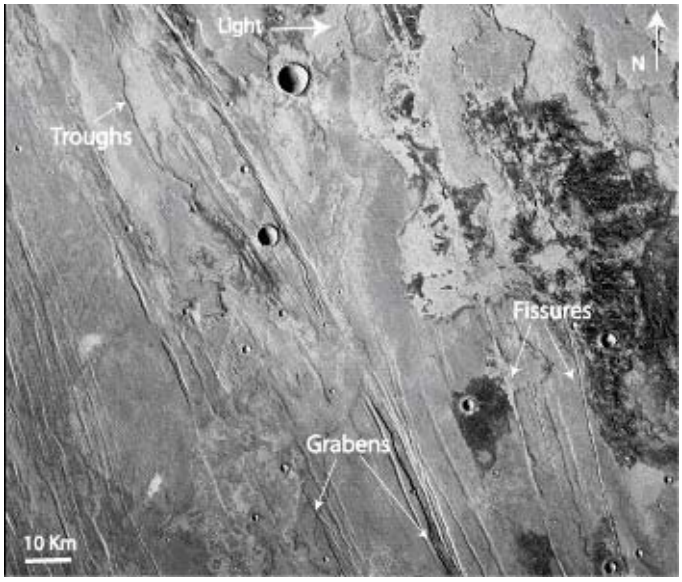

FIG. 3.6 - *HRSC mosaic showing lava flow contours displayed in orange on Figure 3.4f. These lavas have a lobate and elongated shape, mainly oriented from NW to SE. Some of these flows are intersected by several lineations or faults. Illumination comes from the East. The image is centered at approximately 18.5ºS; 102.7ºW. See context on Figure 3.4.*

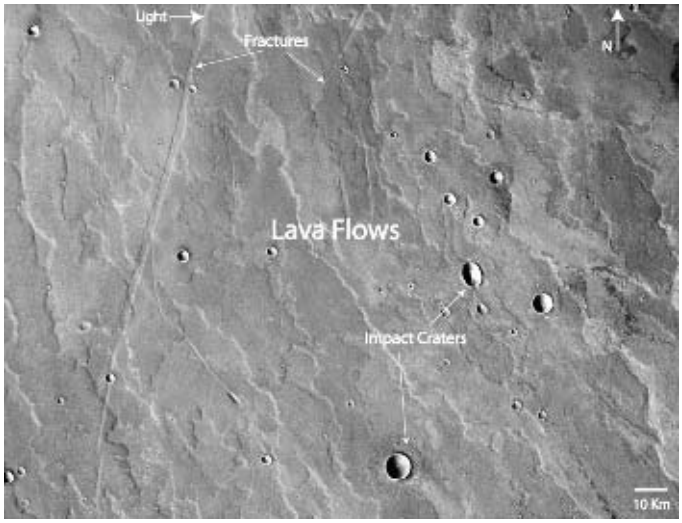

FIG. 3.7 - *HRSC mosaic image showing several fractured lavas. Troughs are observed to be surrounded or filled-in by lava. These fractured lava terrains show grabens of about 4 km width and several fissures that may be the result of ancient faults activated by volcanism. The image is centered at approximately 20.5ºS; 101.5ºW. See context on Figure 3.4.*

3.2.1 Analysis of Syria Planum Small Shield Volcanoes

The swarm of protuberances covers an area of about 250 km (NS) by 150 km (EW) (Figure 3.5). It is likely that other cones might exist east of the studied region, because similar structures are observed with THEMIS and MOLA data. However, we limit our characterization to the features observed in HRSC images.

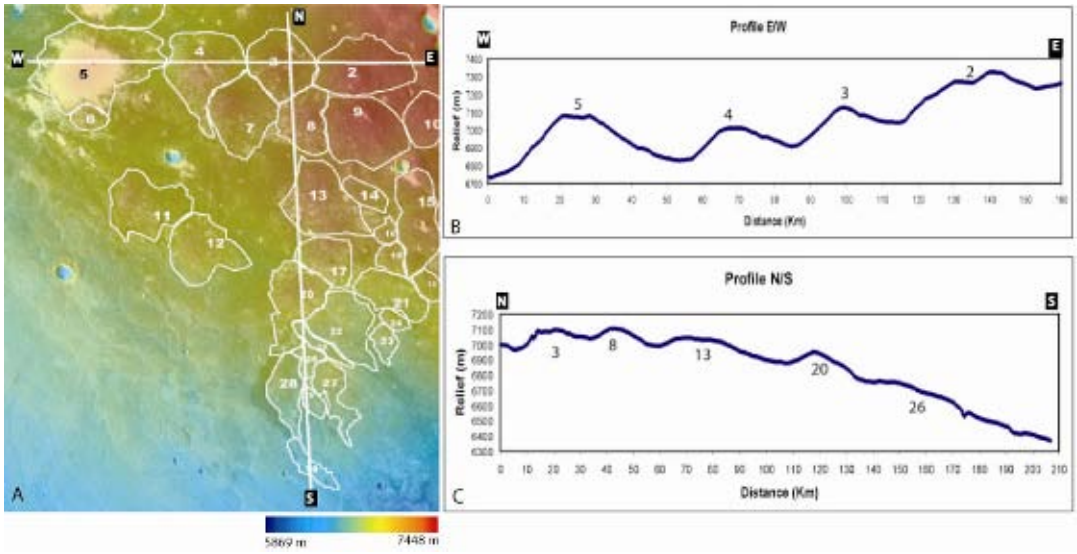

FIG 3.8. *Image A – HRSC image superimposed on MOLA data. The white contours limit the swarm of Syria Planum small shield volcanoes, numbered from 1 to 31. The center of the image is approximately 15.40ºS; 101.1ºW. Images B and C– Profiles E-W and N-S, respectively, obtained from MOLA DTMs and located in image A. From North to South, the small shield volcanoes assume a more elongated shape, following the decreasing topography.*

The HRSC images outline the extent of each axi-symmetrical landform, showing their individual shapes (Figure 3.5 and 3.8). The topographic profile of each protuberance observed in the MOLA data coincides with the imagery, except for some protuberances located at the northern edge of this area that are covered by dust (numbers 5 and 1 on Figure 3.5). A predominant central fissure is also present on most of these landforms (for example number 3 and 27 on Figure 3.8).

This fissure is inferred to be a vent, similar to those observed on terrestrial volcanoes.

These protuberances have flat conical shapes with basal diameters from 7 to ~60 km and individual heights from 10 to 250 m (measured using MOLA data on Figure 3.4). The flank slopes of the individual features are between 0.2º and 1.0º, with a median slope at 0.5º. The volume of the small shields (V) was calculated, assuming a conical shape, using their average relief (h) and their W–E basal width (2r): $V = 1/3\ p\ r^2\ h$. The volume of volcanic edifices ranges from 0.2 to 152.7 km^3. These values should be considered lower bounds on the volume because many of the volcanoes may be embayed by younger materials such as lavas from the adjacent volcanoes and any loading phenomena would have compressed the volcanic material. Although, another study demonstrated (see chapter 3.8) that these volcanoes are not considerably embayed by other lavas.

It is also observe that these shield volcanoes tend to have elongated shapes with the decrease in the regional topography and, consequently, the increased regional slope below 6.5 km.

Although these volcanoes usually have a conical shape, there are some exceptions. Some of them (e.g., #20 and #27, in Figure 3.9) display slightly asymmetrical E-W topographic profiles, with the steeper side often on the west. These steeper slopes occur at the intersection with the lava flows, as observed on our map of slopes (Figure 3.4d), whereas the volcanoes that are surrounded by other volcanoes tend to have a rounder shape and no preferential higher flank dip. Second, the volcanoes tend to be circular north of 15ºS (Figure 3.9), but the shape can be N-S elongated, following the regional topography (e.g., #20 on Figure 3.8). We observe that these volcanoes tend to have elongate shapes with the decrease in the regional topography, and consequently the increased regional slope, below 6.5 km. To support these observations, we tested the circularity of each volcano. The assessment of the circularity can be done using the eccentricity, a parameter of the distortion of a circle into an ellipse, which corresponds to the ratio of the linear eccentricity (square root of the difference between the square of the semi-major

axis and the square of the semi-minor axis) to the semi-major axis. To compute this, we extracted the altitude values of the largest closed contour (contours spaced of 20 m) of each volcanic feature from the MOLA contour data. The results are shown in Table 1. The absence of results for volcanoes 14, 15, 17-19, 21, 22, 25, 26, 29 and 30 is due to their flatter surface; the limited vertical resolution of MOLA data does not permit the isolation of their contours.

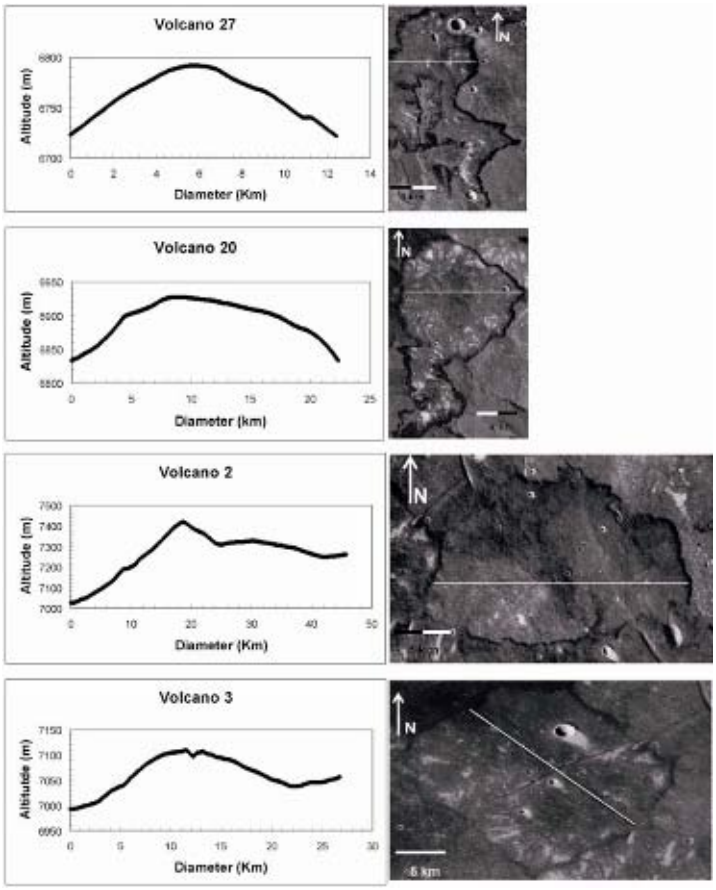

FIG. 3.9 – *Detail of some shield volcanoes on Syria Planum as seen by HRSC, and their correspondent profile West-East (illumination from West). From the top to the bottom we can see that volcanoes 27 and 20 show a NS elongated shape, and volcano 2 shows different flank slopes from West to East. Volcano 3 shows a vent on its summit, which crosses its section NE/SW.*

Based on these calculations, we observe that the northern volcanoes (e.g., #2-10) are rounder (eccentricity between 0.4 and 0.5) than the southern ones (e.g., #13, 20, 23, 24, 27, 28), which tend to be more elongated (eccentricity between 0.6 and 0.9).

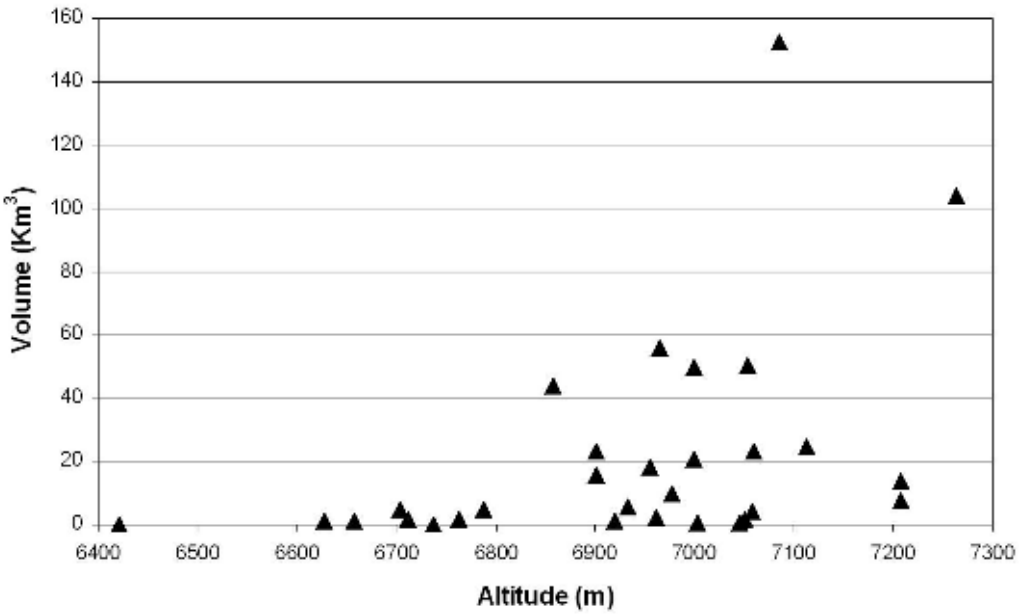

FIG. 3.10 - *Distribution of Syria Planum small shield volcanoes volumes according to their summit altitudes. It is observed a general tendency for the volcanoes with higher volumes of lava to concentrate at higher altitudes.*

Each volcano increases in slope in the E-W direction (as shown on the profiles of Figure 3.9). Over all Syria Planum, the volcanoes increase in volume in the S-N direction, consistent with the increase in altitude (Figures 3.7-3.9). The slope increase to the west occurs closer to the units of large lava flows (e.g., #5, Figure 3.4 or Figure 3.9). The volume decrease to the south is correlated to a decrease of elevation and an increase of the slope (Figures 3.8-3.10). This might be due to the fact that the slope impedes the development of a (well developed) circular volcano creating more elongated edifices. As a consequence, the volcanoes with higher volumes and more circular shapes occur in the northern

region where the terrains are flatter and the elevation reaches a maximum (e.g., # 2 and 3, Figures 3.8 and 3.9).

The protuberances have a significant variability in their size, shape, volume, and the existence of an observable vent, but they have the mean shape of a flat cone that can be interpreted as being formed by the progressive accumulation of lavas, similar to terrestrial small shield volcanoes. We test this hypotheses through comparison with other Martian volcanoes and analogues on Earth, on chapters 3.6 and 3.7, respectively.

3.2.2 Dating Syria Planum Small Shield Volcanoes – Crater counts Method

Craters larger than 250 m in diameter were counted and classified over a surface of 7,760 km^2 corresponding to the small shield volcanoes, and over 20,945 km^2 on the lava flows. For the volcanoes, the craters were first counted for each isolated volcano and then summed over the entire surface, in order to be able to date them both individually and as a whole.

The cumulative number of impact craters with diameter ≥ 1 km is:

$$N(1) = \frac{N}{S} \pm \frac{\sqrt{N}}{S} \tag{3.4-1}$$

where N is the number of craters per surface S. We determined 0.0029 ± 0.0006 craters/km^2 for the small shields and 0.0025 ± 0.0003 craters/km^2 for the lava flows. These counts correspond to ages of 3.5 - 3.6 Gy for small shields and approximately 3.6 Gy for the lava flows from volcano A [Hartmann and Neukum, 2001]. According to error bars, the ages are not significantly different, suggesting that the period of time between the formation of volcano A and the small shields was limited.

For a more accurate estimation, we plotted ages in increments of $\sqrt{2}$, as in the model of Hartmann and Neukum [2001]. The isochrones plotted on Figure

3.11 correspond to the density of craters that should be observable on a surface preserved from erosion and deposition since its formation.

The model takes into account the crater production function of the Moon, adapted for Mars, which fixes the slope of craters smaller than 1 km and is adapted to show turndowns and variations of populations that could be interpreted in terms of obliteration, erosion or deposition [Hartmann et al., 2000]. On Figure 3.11, one can observe the frequency of each interval of crater size, for the volcanoes (in dots) and for the lava flows (in stars). Both units follow isochrones of the Hesperian period with small shields appearing slightly younger than the lavas. The more recent ages for craters <500 m correspond, therefore, to surface degradation due to resurfacing since the formation of lava.

We next tried to individually date each volcano, although statistically this estimate is not valid once recent resurfacing processes obliterate the smaller craters. The smaller-sized craters may be a good indicator of resurfacing and erosion periods, whereas, to date bedrock (not surface) processes, the bigger sizes (up to 250-350 m) are better.

The dating of these volcanoes, as well as their topographic analyses, confirm previous propositions [Plescia, 2004] of the fact that they might have occurred during a geologically short period of time, probably not more than some tens of millions of years. From this work, and using HRSC images and MOLA data on crater-counting, we assume that these events may have lasted from the Early Hesperian to the middle of the Hesperian, which means that the main volcanic activity in Syria Planum occurred during this period.

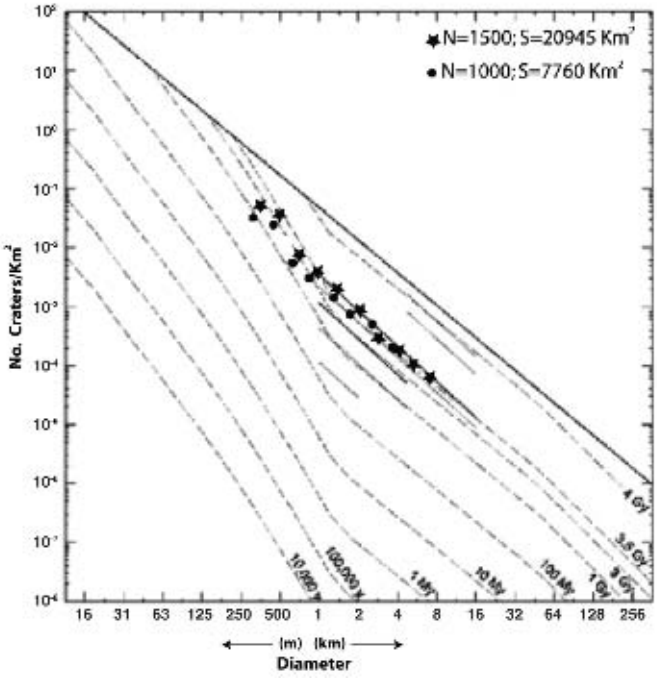

FIG 3.11 - *Crater distribution over the studied Syria Planum lava flows and shield volcanoes. Isochrones are plotted according Hartmann et al. (2000). We used only craters >250m diameter for this study. The ages associated with the isochrones are given by the lunar rates modulated by a ratio of R=1.6 corresponding to the ratio between the crater production function on Mars and the same rate on the Moon. However, these could all correspond to Hesperian ages. Dots correspond to volcanoes ages, associated with a surface of 7760 km².*

3.2.3 Characterization of the lava flow's unit

3.2.3.1 Morphology and lavas origin

The extensive field of lava flows, identified between approximately 15º-19ºS and 105º- 102ºW, covers an area of approximately 100,000 km^2 (Figure 3.4). Through the study of HRSC images and THEMIS IR-day and IR-night images, we can identify elongated and lobate shapes for these flows with preferential orientation NW to SE, following the regional slope.

Using THEMIS and MOLA data, we observe that these lava flows erupted from an isolated volcano – hereafter named Volcano A - on the northeast of Syria

Planum (Figure 3.12, represented on the geomorphic map on Figure 3.4f). The summit cone of volcano A is about 40 km in diameter, and it lies at an elevation of approximately 6.700m. This volcano is located outside of the HRSC mosaic, although a new HIRISE image enables its study (Figure 3.12). On Figure 3.12 we show a MOLA profile from "a" to "b". From the center of the volcano to the side "a", the slope is about 1.4º while from the center to the side "b" the slope decreases to 0.7º, to the side where the lava flows extend.

We can observe the presence of post-flow tectonic deformation. In Figure 3.12 it is of note that the flanks facing east are considerably smoother than the western flanks, where the slope is more accentuated. On the southern part of Syria Planum, and from an extension of some hundreds of kilometers SE of the volcano A, we observe that the lava flows partially cover a field of grabens (Figure 3.13). We detail the fault system and its relationship with lava flows in point 3.4.4.

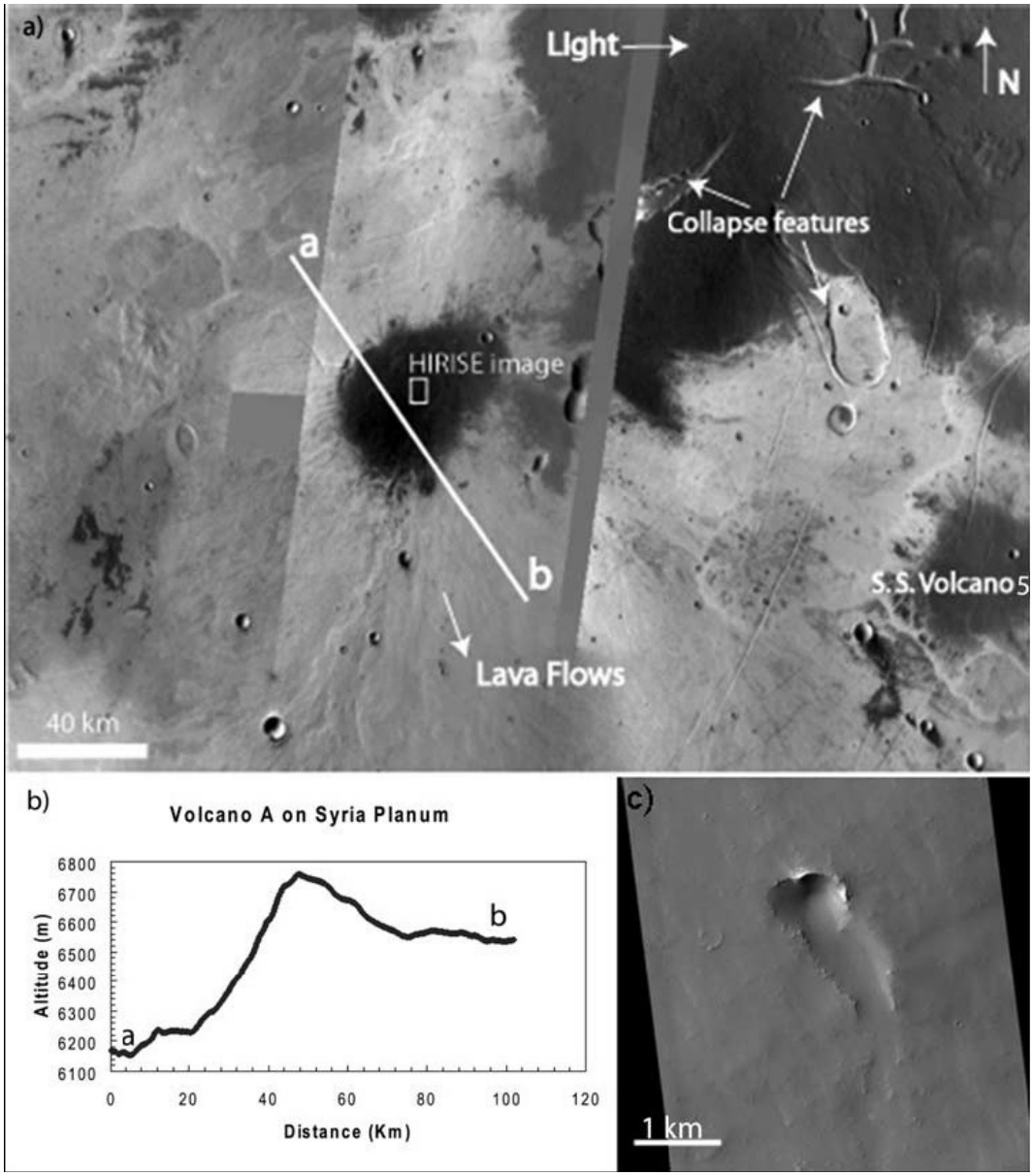

FIG. 3.12 - *a) at the center of this image it can be observed volcano A, which is the eruption center of the described lava flows. The caldera is about 40 km wide. On the bottom right of the image the shield volcano 5 is visible. On the top right several collapse features are noted. The profile a-b is shown on image b). c) HIRISE image (PSP_001840_1660) showing a volcanic vent, with about 700 m width, on the top of volcano A.*

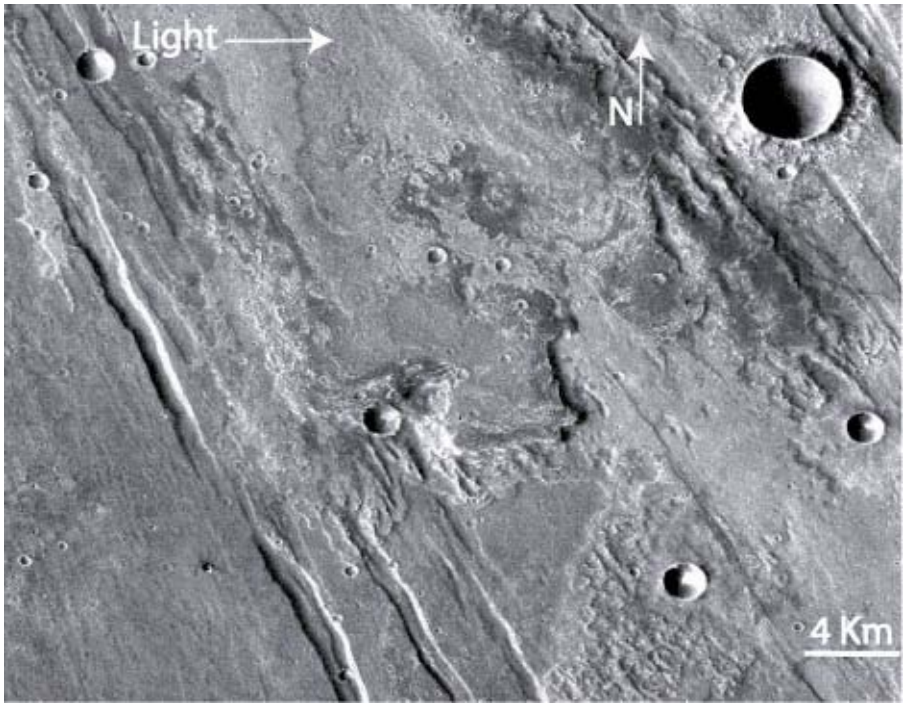

FIG. 3.13 - *HRSC image centered at 20.5ºS; 102.3ºW, where some NW/SE - oriented grabens are covered by lavas with the same orientation.*

3.2.3.2 Lava Flows Rheology

Using HRSC images, THEMIS IR-day and MOLA data, we studied several lobate lava flows on Syria Planum. The results from its geometry and rheology are shown on Table 2. It is largely known that Martian volcanic edifices can produce several features such as lava tubes and channels [e.g., Carr, 1973, 1974; Greeley, 1973; Greeley and Spudis, 1981; Cattermole, 1987, 1990; Sakimoto et al., 1997]. In terrestrial volcanology, there exists a link between tube flows and a more steady flow rate, and conversely the connection between channels and unsteady flow rates [e.g., Sakimoto et al., 1997].

Table 2. Geometric and Rheologic Parameters Measured From Topographic Data From Profiles on 10 Lava Flows

	Length (m)	Thickness (m)	Width (m)	Slope (°)	Effusion Rate (m^3 s^{-1})	Viscosity (Pa s)	Yield Stress (Pa)
Minimum	45×10^3	15	5×10^3	0.15	990	6.89×10^5	–
Maximum	200×10^3	70	15×10^3	1	6,075	4.23×10^6	–
Mean	150×10^3	34.5	9.4×10^3	0.2	3,300	–	1.2×10^{3a}

[a]Lengths between 100 and 200 km and thicknesses between 15 and 70 m were used. The mean value for the smaller size lavas is 7.9×10^2 and 1.7×10^7 for the larger ones.

We infer that Syria Planum lava channels are predominantly the result of constructional processes (flow confined by building of levees), often roofing over to form tube-flows. The lava channels occur in the area immediately south of the Syria Planum shield volcanoes (Figure 3.14), an area where several periods of intensive fracturing are recognized (as described in point 3.4.4).

The techniques described below consider alternatively the lava flows as Newtonian fluids (which allows the determination of the flow rate and viscosity), or as Bingham flows characterized by a yield stress. These techniques are useful in providing a comparison between terrestrial flows (of known composition) and Martian lava flows [e.g., Hulme, 1976]. However, given the fact that these rheological models are mutually inconsistent, the computed absolute values should be viewed with extreme caution.

Lava Flows Dimensions

We isolated 10 lava flows, where channel - or tube - flows are mostly present and their rheology was studied using MOLA DTM data. The size of the observed lava flows varies from a few hundred meters to about 200 km, with the mean length of about 150 km. Their width varies from 5 km to 15 km, with the mean value of 9.4 km. The levees on the lava flow have a mean width of 5 km. Thicknesses of the lava flow vary from 15 m to 70 m, with a mean value of 34.5 m. The average slopes of the studied flows are approximately to 0.2º, although in a few cases (in places with superposition of lavas) it can exceed 1º. This results in volumes of individual lava flows ranging from an average of 40 km^3 to a maximum of 200 km^3.

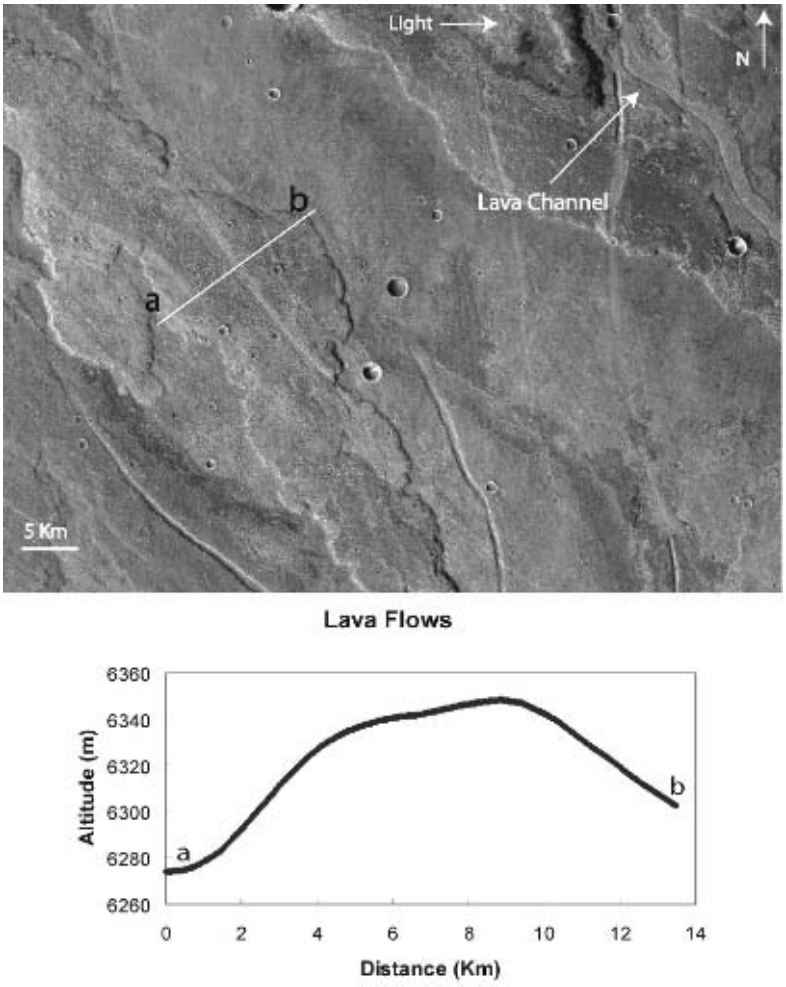

FIG. 3.14 - *Image centered at 17.3ºS, 100ºW. Lava channels are visible on the described lava flows. The channel on the top right displays lava levees on its sides. The profile a – b is shown on the bottom graphic.*

Effusion Rate

The effusion rate of this system, or its volume flow rate (Q, $m^3\ s^{-1}$), can be determined using the Graetz dimensionless number (Gz) [e.g., Knudson and Katz, 1979; Pinkerton and Wilson, 1994; Warner and Gregg, 2003; Hiesinger et al. 2005]:

$$Q = \frac{G_z kxw}{b} \qquad (3.4\text{-}2)$$

The Graetz number that is related to the cooling of a warm fluid moving through a cold pipe [Hulme and Fielder, 1977; Wilson and Head, 1983; Zimbelman, 1985] assumes laminar flow and relates the heat lost by diffusion in a flow to the heat lost by advection along its length [Warner and Gregg, 2003], in which k is the thermal diffusivity (3.0 x 10^{-7} m^2 s^{-1}, a similar value for both Martian and terrestrial lavas) [e.g., Gregg and Fink 1996; Warner and Gregg, 2003], x is the flow length (m), w is the width of the flow (m) and b is the thickness of the flow (m). In analogy to terrestrial lava flows we assumed a value of 300 for the Graetz number (e.g., Hiesinger et al., 2005). As a result, we find that effusion rates range from 990 m^3s^{-1} to 6,075 m^3s^{-1}, and the mean value is 3,300 m^3s^{-1}. These values are the same order of magnitude as the ones determined for Arsia Mons [Warner and Gregg, 2003], although they are of some orders of magnitude superior to those found on Ascraeus Mons (18-60 m^3s^{-1} and a mean value of 35 m^3s^{-1}, from Zimbelman [1985]) or on Olympus Mons (400 m^3s^{-1}, from Zimbelman [1985]). Regarding the effusion rates and determining the volumes of individual lava flows, we calculated that the time necessary to emplace these flows is 140 days in average, with a maximum of 700 days.

Viscosity

The viscosity can be determined using a model obtained from a steady laminar isothermal gravity-driven Newtonian flow, with no slip at the base and no shear stress at the top surface [Sakimoto et al., 1997]. This flow system can be resolved in a rectangular flow solution - equation (3.4-3) - where flow depth and flow width are comparable. The surface velocity is independent of the cross-flow direction, likewise because there are no channel walls [Sakimoto et al., 1997]. So, the flow rate per unit width is given by:

$$\frac{Q}{w} = \frac{b^3 \rho g' \sin(\theta)}{3\mu} \qquad (3.4\text{-}3)$$

Here, Q is the volume flow rate (i.e., eruption rate), w is full flow width (in sheet flow), b is the flow depth in a Newtonian channel and sheet flow, g' is the adjustment made for the acceleration of gravity on Mars (3.73 ms^{-2}), θ is the slope, μ the viscosity and ρ is the density (we assumed 2800 kg m^{-3}, knowing that this value can change by 30-50% in the presence of bubbles/vesicles in lavas).

Our estimate of the viscosity ranges from a minimum of 6.89 x 10^5 Pa.s to a maximum of 4.23 x 10^6 Pa.s (depending on the previous determined values of effusion rate). These values are in agreement with several other viscosities determined for Martian lavas [e.g., Hiesinger et al., 2005; Warner and Gregg, 2003]. On Earth, terrestrial basalts and andesites have viscosities from 1.4 x 10^2 to 1.4 x 10^7 Pa.s [e.g., Hiesinger et al., 2005; Wilson, 2001]. So, the Syria Planum lava flows are in the range of relatively viscous basalt to andesite. Also, Fink and Zimbelman [1986], assembling different methods, determined values from approximately 0.8 x 10^6 to 8 x 10^6 Pa.s, for the Kilauea lava flows.

Yield stress

Alternatively, we consider below that the lava flows can be approximated using Bingham fluids, which differ from Newtonian fluids by the existence of yield strength in addition to the viscosity.

The yield stress may be estimated from the combination of three parameters: b, the flow depth, θ, the slope, and w, the width of the flow, and also by assuming a density flow value equivalent to terrestrial basalt (2800 kg m^{-3}) [e.g., Hiesinger et al., 2005].

$$\sigma_s = \rho g b^2 / w \tag{3.4-4}$$

$$\sigma_s = \rho g b \sin\theta \tag{3.4-5}$$

Using equations (3.4-4) and (3.4-5), for 10 lava channels of Syria Planum, with lengths between 100 and 200 km and thickness between 15 and 70 m, we obtain mean values between 7.9 x 10^2 Pa (for the smaller sizes) and 1.7 x 10^3 Pa (for the larger sizes) and the overall mean value is 1.2 x 10^3 Pa. These values are

consistent with terrestrial basaltic to andesitic lava flows and also with the Arsia Mons lavas (see Moore et al., 1978). Also, Zimbelman, [1985] determined similar values for Arsia Mons ($1.0 \pm 0.8 \times 10^3$ Pa) and larger values for Ascraeus Mons ($2.1 \pm 1.8 \times 10^4$ Pa) and Olympus Mons ($2.0 \pm 0.3 \times 10^4$ Pa). Fink and Zimbelman [1986] determined different values of viscosity depending on the place that the measurements were made along the lava flow; higher with the increasing distance to the lava source. These authors analyzed lavas from the Kilauea volcano, which lengths are always inferior to 3 km, so some orders inferior to the Martian ones, and obtained values from approximately 4×10^3 to 40×10^3 Pa.

Overall, rheologic parameters from Hawaiian and Arsia Mons flows are about the same order of magnitudes of those determined in Syria Planum.

3.2.4 Syria Planum Tectonics

In this studied area, we identify at least 4 tectonic episodes distinguishable from their different directions and patterns.

First, using MOLA and HRSC data, we observe NW-SE faults typically a few kilometers wide and hundreds of kilometers long, as seen at the bottom of the studied images (Figure 3.4, Figure 3.13). These fractures exhibit a very dense network of faults defining many small grabens, which are covered by lava flows related to volcano A in the Northwest. These grabens might correspond to the most primitive tectonic pattern that affected the bedrock previously to the discussed volcanic events. Syria Planum was the center of tectonic activity before the emplacement of the volcanic plains at the surface. Those older faults are observed in Claritas Fossae and north of Noctis Labyrinthus. Presumably those faults underlie the present surface and can exhibit control on the area's volcanism.

Second, the lava flows of volcano A have been intersected by faults, mainly oriented NE/SW, in the northern region of Syria Planum (Figure 3.15, right). We determine that these fractures are hundreds of km long and approximately some tens of meters in depth. They are much more scattered and less densely distributed than the NW-SE-oriented faults found to the south.

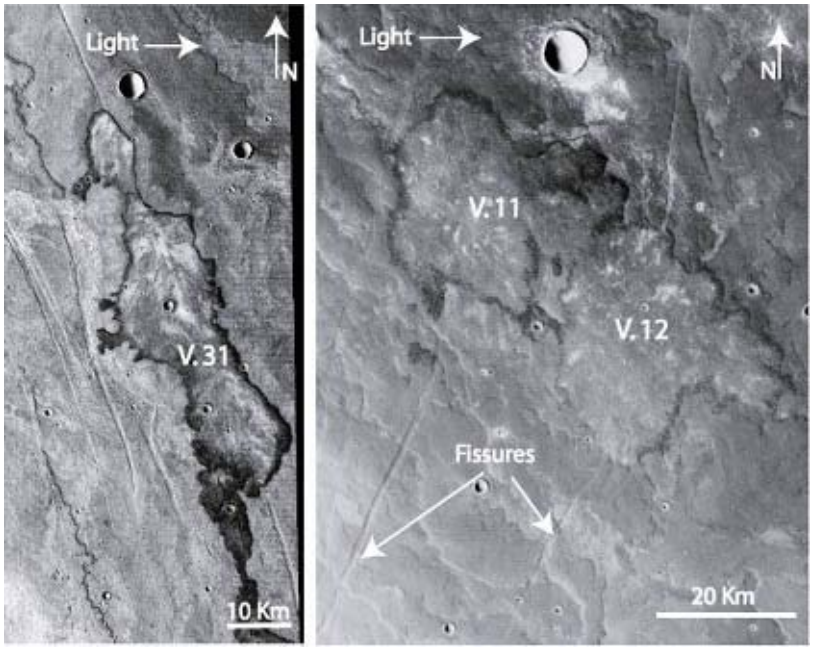

FIG 3.15 - *Left: HRSC image centered approximately at 19.8ºS; 100.9ºW, showing the volcano 31, a fissure some tens of kilometers long from which lavas erupted. Its borders, which have a clearly darker tone, define well its shape. Right: HRSC image centered at 15.4ºS; 101.5ºW, where volcanoes 11 and 12 superimpose lavas that were intersected by fissures oriented NE/SW.*

Third, in the southern and eastern regions of Syria Planum (Figure 3.15, left), next to the NW-SE oriented grabens, there are fissures some hundreds of meters wide. Volcano 31 appears to have been created by such NW-SE reactivation. This activity thus clearly postdates the lava flows of volcano A, and therefore the NW-SE faults that are buried beneath the lava flows. We interpret these faults and related activity to have resulted from a reactivation of the ancient NW-SE fractures possibly as a consequence of volcanic activity. It can be seen from the chronological relationships that the overall NW-SE features were formed earlier (without relation to this volcanic episode) and buried beneath lava flows from volcano A, whereas individual faults in same direction found over the lava flows formed later, probably in relation to the formation of the small shields.

Finally, it can also be identified several collapsed features (represented in blue on the geomorphologic map of Figure 3.4f) in the proximity of the isolated volcano A (Figure 3.5), and structural depressions that extend laterally to volcano 2 (e.g., Figure 3.5). These collapse features postdate all the different terrains of Syria Planum, affecting the small shields at their northern boundary.

These four types of tectonic patterns can result from different volcano-tectonic activities [e.g., Masson, 1980]. Faults with NW/SE preferential orientation correspond to the Noachian-Hesperian graben construction [e.g., Plescia and Saunders, 1982; Tanaka and Davis, 1988]. This activity is related to the first episode of faulting to the south, corresponding to a major stress field that crossed most of the Tharsis region. Faults with a NE-SW trend are more scattered, resembling individual fissures rather than a main tectonic episode. It has been shown that such features can be produced by near-surface stress fields associated with intrusive magma, which can fill-in the existing fractures and sometimes increase their dimensions [e.g., Wilson and Head, 1981 and Tanaka and Davis, 1988]. Due to the proximity of the small shield volcanoes, these faults might be interpreted as dikes from which several volcanic edifices were created. The ancient NW-SE fault direction might have been reactivated, possibly at the same time as the NE-SW faults formed, to localize the emplacement of the elongated volcanoes such as number 31. The collapse features that crosscut all units might be related to the period of main collapse of the Noctis Labyrinthus region north of Syria Planum.

Chronologically, the sequence of tectonic and volcanic activity is very clear from relative stratigraphy. If we interpret the collapse features to have formed during the Noctis Labyrinthus event, then the age of these collapses would correspond to approximately the end of the Late Hesperian and beginning of the Early Amazonian [Tanaka and Davis, 1988]. This suggests that the volcanoes were all formed prior to that period. In the next section, we test this possibility by dating the volcanoes using crater counts.

3.2.5 Chronology of volcanic and tectonic episodes on Syria Planum

Our study of the HRSC images suggests that a much more complex geologic history of Syria Planum exists than was previously expected, especially in light of the identification of a unique swarm of small shield volcanoes that occur in the most elevated part of the region (Figure 3.16). Southwest of these edifices, ~200 km long lava flows erupted from a volcano also not previously identified. Both volcanic systems have embayed the highly faulted crust that is only visible in the southern part of the region (example on Figure 3.16).

The geological episodes that existed in this location can be chronologically described as follows (see also Figure 3.17):

Phase 1: Formation of the grabens, with a few on the order of 4 kilometers width, which is dated to the Late Noachian to Early Hesperian epoch [Tanaka and Davis, 1988].

Phase 2: Formation of volcano A in the Early Hesperian, which partially covers the grabens of phase 1 (Figures 12 to 15), but are not cut by these grabens.

Phase 3: Lava flows from Volcano A are cut by NE-SW faulting event of Early Hesperian age. In some areas the faults may serve as conduits for magma eruptions that postdate the lava flows from volcano A. In that case phase 3 and 4 are almost contemporaneous.

Phase 4: A swarm of shield volcanoes (formed during the Hesperian period) are superimposed on these lava flows (Figure 3.15). Also, at least three volcanic shields are clearly superimposed on lava flows from volcano A (see volcano 5 on Figure 3.5, or volcanoes 11 and 12 on Figure 3.15).

Phase 5: A few depressions formed by collapse might signify the last episode of activity, perhaps generated by the Noctis Labyrinthus opening in, or after, the Late Hesperian. (Figure 3.12).

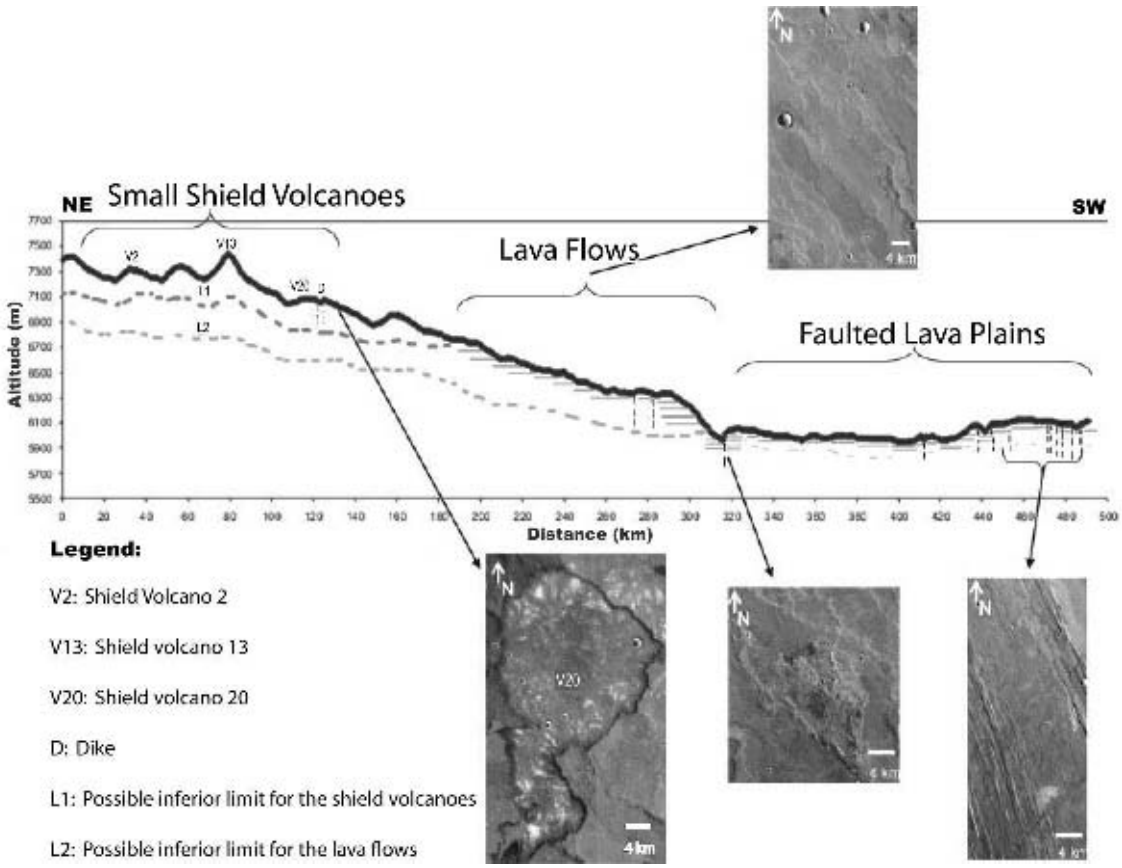

FIG. 3.16 - *Profile NE–SW from Syria Planum. From highest to lowest altitudes we can observe the succession of the low shield volcanoes, the lava flows intersected by predominantly NE–SW fissures, and the highly faulted lava terrains. As it is observed by the profile, the thick crust in Syria is clearly not due to the accumulation of Hesperian lava flows, which we can limit to 1-2 km (Lava Flows Unit). These terrains could have been tilted by the bulge beneath the Syria Planum unit (dot lines) which in that case would limit the thickness of Hesperian lavas below 1 km.*

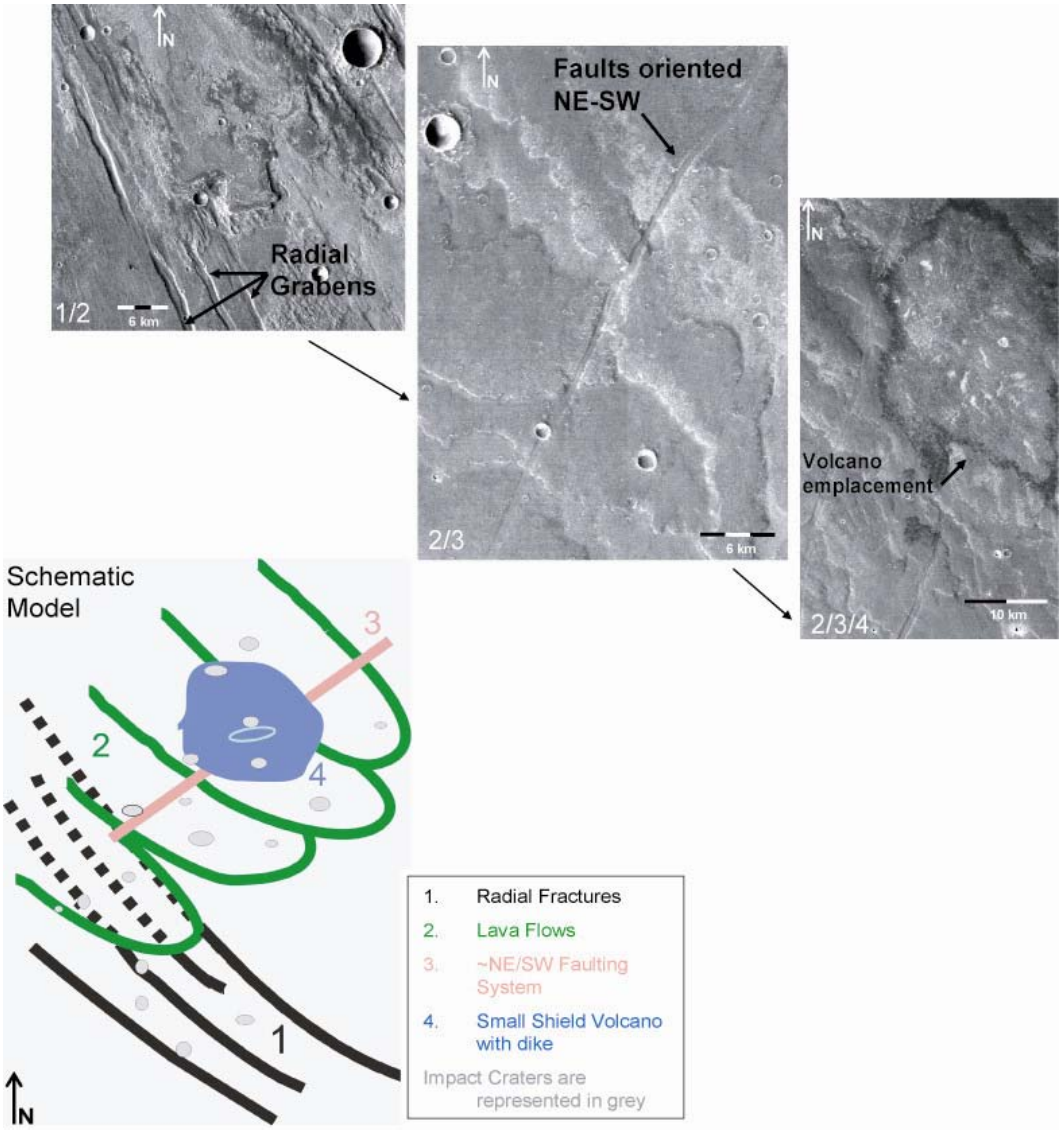

FIG. 3.17 - *Chronologic relationship between the 4 magmato-tectonic phases from the early to the late Hesperian period in Syria Planum and described in in this work. Phase 1: extensional field stress that produced grabens; Phase 2: eruption of volcano A resulting in lavas that spread all over Syria Planum; Phase 3: tectonic deformation of the emplaced lava flows by the formation of several fractured patterns such as NE–SW en echelon faults, troughs, and adjacent grabens; and Phase 4: new episodes of volcanic activity, forming the coalesced small shield swarms that bury preexisting faults. Preliminary crater counts show ages from the Hesperian period.*

The schematic cross section in Figure 3.16 also shows that the total unit of Hesperian-aged volcanic landforms does not have a large thickness. From the relationship with the fault system to the south, it is likely that the total thickness of this material does not exceed 2 km, although it is difficult to estimate a boundary that depends on preexisting terrains (now completely buried). This remark is important because it shows that the elevation acquired by Syria Planum predates the age of the visible surface, at least to the elevation of about 6 km over Mars datum, suggesting the Noachian rise of the bulge reached this minimum value of 6 km.

3.3 The importance of Syria Planum on the volcanic context of Tharsis

Concerning to Syria Planum, a mainly tectonically driven activity is proposed [Scott and Tanaka, 1998; this work], which peaked early and then decreased. The intensive magmatic activity is thought to have been localized in time, and have decreased early in the Martian history. The intense surface deformation, marked by fresh radial grabens, wrinkle ridges, collapsed features and several fault patterns without apparent resurfacing since approximately 3.2 Ga (Chapter 3.4) implies that the mechanical properties of the lithosphere did not change with progressing age [Anderson et al., 2001]. This seems to be consistent with the fact that the lithosphere and deplected layer forms early and does not undergo further significant alteration [Schott et al., 2001]. Also Zuber et al. [2001] refers that the main part of the elastic lithosphere was formed during the first Ga of the planet's formation.

The suite of volcano-tectonic episodes identified in Syria Planum has two specific characteristics that require a few comments. First, swarms of coalesced small shield volcanoes are not usual in the Tharsis region. What kind of volcanic phase do they indicate? How are they related to volcano A? Second, our work shows that the volcanism in this area ended during the Hesperian epoch. Why did

it end whereas the northern and western parts of the Tharsis region continued to display volcanic activity throughout the next three billion years?

To answer the first question, we first note that both earlier studies of Martian volcanism [e.g., Greeley and Crown, 1990; Crown and Greeley, 1993] and more recent works [e.g., Plescia, 2004], proposed that the older volcanoes have smaller volumes and dimensions than the younger giant shields. Syria Planum small shield volcanoes are of a relative age older than the Tharsis shield volcanoes, (at least to their current surfaces). Nevertheless, volcano A has many characteristics similar to the Tharsis Montes, such as the effusion rates, except that it did not grow as high as the Tharsis Montes. In addition, isolated small shield volcanoes were already observed in the flanks of Pavonis Mons and in the caldera of Arsia Mons, as well as an extensive field of small vents on Ascraeus Mons [e.g., Greeley and Spudis, 1981; Hodges and Moore, 1994, Bleacher et al., 2007]. Greeley [1977, 1982] characterizes it as a plains-style volcanic field area, where lava flows between the low shields and fissures were emplaced via a combination of lava tubes and extensive sheets. As they are distal to the caldera, or to the last volcanic episodes on the flanks, they might be a sign of late activity in the region of the large Tharsis Montes [Bleacher et al., 2007], probably from the Late Amazonian - an age much younger than the Syria Planum volcanoes. Syria Planum was dominated both by swarms of coalesced small shields and a single larger edifice (volcano A) as the source of long lava flows. The small shield volcanoes might signify late-stage activity that once began with the emplacement of volcano A, identified by long lava flows and a lava viscosity similar to the Tharsis Montes. This volcano A might never have reached the stage to enable the construction of a larger volcano at this location.

This style of multi-staged volcanic activity with different stages suggests that there is a need to examine the role of the local lithospheric structure. It is of note that the heights of volcanoes may provide significant constraints on the lithospheric thickness for terrestrial planets [e.g., Blasius and Cutts, 1976]. Assuming that the heights of the shield volcanoes are hydrostatically limited,

there is a simple relationship between the height of the volcano and the base of the lithosphere considered to be the source of the magma. The region of Syria Planum is characterized by a thick crust (more than 80 km, from Neumann et al., [2004]) and the highest altitude of the Tharsis region [Neumann et al., 2004]. Furthermore, according to Neumann et al. [2004], the deepest mantle, or the deepest Mars-equivalent Moho interface, occurs in southern Tharsis, near Syria and Solis Planum. Considering that the crust has a lower thermal conductivity (~2.5 W/K/m) than the mantle (~4 W/K/m) [Schumacher and Breuer, 2006], this fact implies that the present lithosphere is thinner below this region. The elastic thickness of the lithosphere (Te) at the time of loading has been estimated independently from gravity/topography admittances [McGovern et al., 2000]. Below Solis Planum, a region having a thick crust in the immediate vicinity of Syria Planum, Te ranges from about 40 – 60 km corresponding to 10 – 15 K/km, whereas Te has been estimated at twice this value below the Tharsis Montes. It is thus possible that the structure below Syria Planum is characterized by a thick crust associated with a thin lithosphere at the time of the magmatic activity, which has resulted in shallower magma sources in Syria Planum. As a consequence, the maximum height for the possible volcanic constructs in this region was more limited than in the other regions of the Tharsis plateau. As it was suggested in Baptista et al., [2008] the cessation of activity of a large volcano on Syria Planum might signify the presence of a thicker crust in that part of the bulge. The development of this thicker crust may explain the incomplete development of the larger volcano at this location by the end of the volcanism, early in the geologic history of the Tharsis region.

In previous works [e.g., Anderson et al., 2004; Scott and Wilson, 2003] it was suggested that the thickened crust under Syria Planum is a result of the formation of the Syria plain volcanism itself. In our study, the thick crust is clearly not due to the accumulation of Hesperian lava flows, which we can limit to 1-2 km (Figure 3.15). Indeed, Noachian age terrain with faulted outcrops are observed at elevations of 5700-5900 m. Assuming that this terrain was flat below

Syria, this implies a thickness of 1.5 km for the Hesperian lava flows. A possibility is that these terrains could have been tilted by the bulge beneath the Syria Planum unit (as shown by dot lines on Figure 3.15); in that case the thickness of Hesperian lavas can be lower (< 1 km). Nevertheless, the lack of Noachian crater rim outcrops in Syria Planum suggests the first hypothese (1-2 km) is more likely. This also implies that Syria Planum was already an area at a high elevation at the end of the Noachian, in agreement with our proposed timing for the Tharsis bulge formation.

3.4 Comparison of Syria Planum with other volcanoes on Mars

Figure 3.18 displays a graph of height versus slope for the main Martian volcanoes and the small volcanoes of Syria Planum. The small volcanoes observed in Syria Planum are different from the three main classes of volcanoes on Mars [e.g., Plescia, 2004]. The Tharsis Montes, which display a higher relief (>10 km), are characterized by moderate slopes (3-10°) and broad collapse calderas at their summits [Malin, 1977]. Close to their flanks, low thickness shields with few kilometers in diameter can also be observed [e.g., Greeley, 1977; 1982; Hodges and Moore, 1994, Bleacher et al., 2007]. Tholii are smaller (1-10 km) than the Montes but they have steeper flank slopes (7-12°), much steeper than the Syria Planum volcanoes [e.g., Mouginis-Mark et al., 1992]. Highland Paterae have gentle slopes (<5°) with shallow relief (1-8 km) [e.g., Greeley and Crown, 1990]. By comparison, the Syria Planum small edifices have a distinct shape from the three main classes of Martian volcanoes. While they have slopes similar to those of the Paterae (but much smaller in size], they are unlikely to be similar in terms of spatial extent and temporal activity. Syria Planum edifices therefore correspond to a distinct class of volcano that we may compare to small edifices found in Cerberus or Tempe Terra [e.g., Hauber et al., 2007].

Comparing the volume of erupted magma, Plescia [2004] determined values for the large Tharsis shields, like Olympus Mons (2.4 x 10^6 km^3), Alba

Patera (1.8 x 10^6 km^3) and Ascraeus Mons (1.1 x 10^6 km^3). The other volcanoes are all in the order between 10^3 – 10^5 km^3, with the exception of the Jovis Tholus (10^2 km^3), the minimum determined value. These volume amounts contrast with the Syria Planum small shields that are normally below 10^2 km^3 (see Table 1).

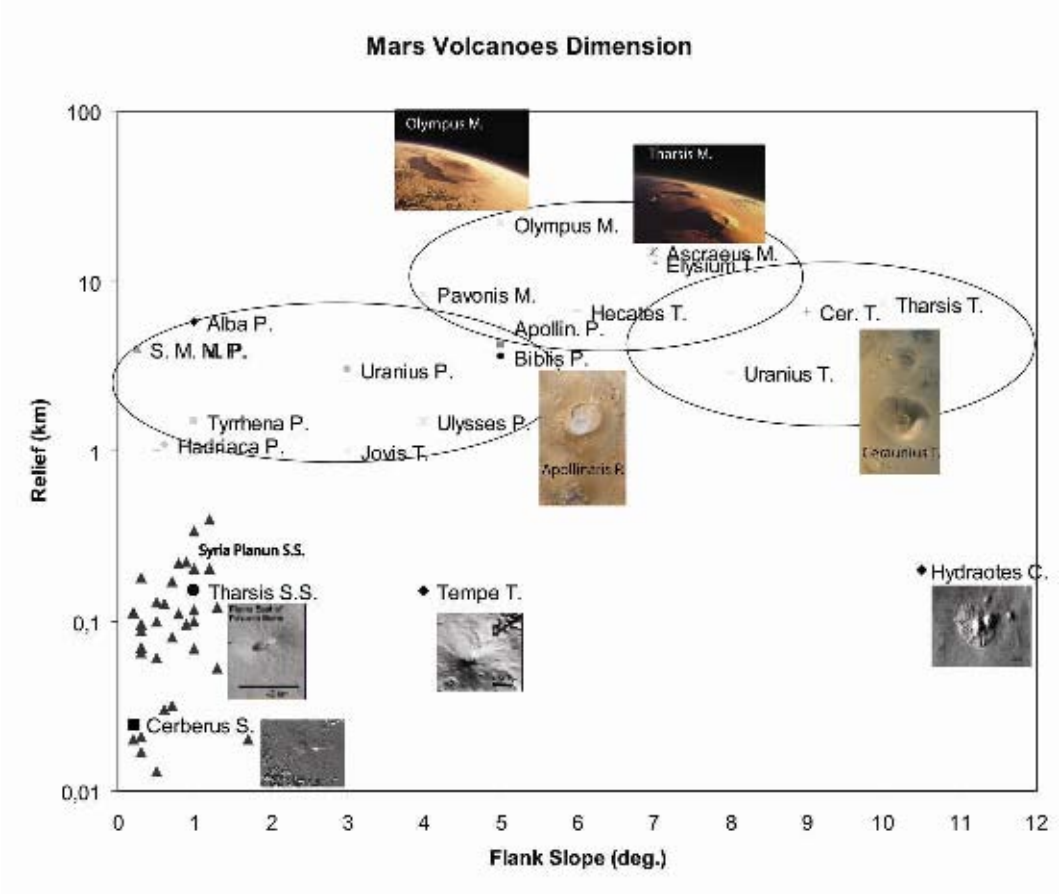

FIG. 3.18 – *Size of Martian volcanoes. The highest topographies are dominated by the Tharsis Montes, while the Highland Paterae are characterized by their flatness [Plescia, 2004]. The highest volcano flank dip exists on the Tholii [Plescia, 2004] and on the little cones of Hydraotes Chaos [Meresse et al., 2008]. The Cerberus shields (symbolized by a square) represent the smallest shield volcanoes observed on Mars [Plescia, 2003] while those observed in Tempe Terra have higher thicknesses [Davis and Tanaka, 1993]. The Syria Planum small shield volcanoes (represented by the bigger triangles) are also flat and of low relief, similar to those shields observed close to the Tharsis Montes (the Tharsis Small Shields are symbolized by a small circle) [Bleacher et al., 2007].*

3.5 Comparison of Syria Planum with other volcanoes on the Earth

On Earth, similarly shaped small shield volcanoes are found in locations such as Iceland. Rossi (1996) presented a study of 24 basaltic post-glacial shield volcanoes in Iceland. He found a median slope of 2.7° (from 0.6° to 8°), a median height of 60 m (from 12 m to 520 m) and a median diameter of 3.6 km (from 500 m to 11 km). The shallow shape of these shields is due to the fluid lavas coming out of rift regions.

Syria Planum cones can be compared to some of the Icelandic cones (Figure 3.19). A comparison is proposed with the Eldborgir shield volcano (also called Lambahraun), which formed 6000 years ago from a single long-duration eruption (Figure 3.20). The 10 km-diameter volcano has a mean slope of 2° with a summit vent. Its shape is not purely conical, as it formed over pre-existing, non-flat topography. Several Icelandic cones have slopes smaller than 2°, or even 1°, such as Strandarheiði with a slope of 0.6° [Rossi, 1996], comparable to those of Syria Planum edifices. On average, the small edifices of Syria Planum have a median slope of 0.5º, thus 5 times smaller than in Iceland. A possible explanation of this difference is that it might come from a difference in viscosity of lavas, slightly more fluid on Mars.

.

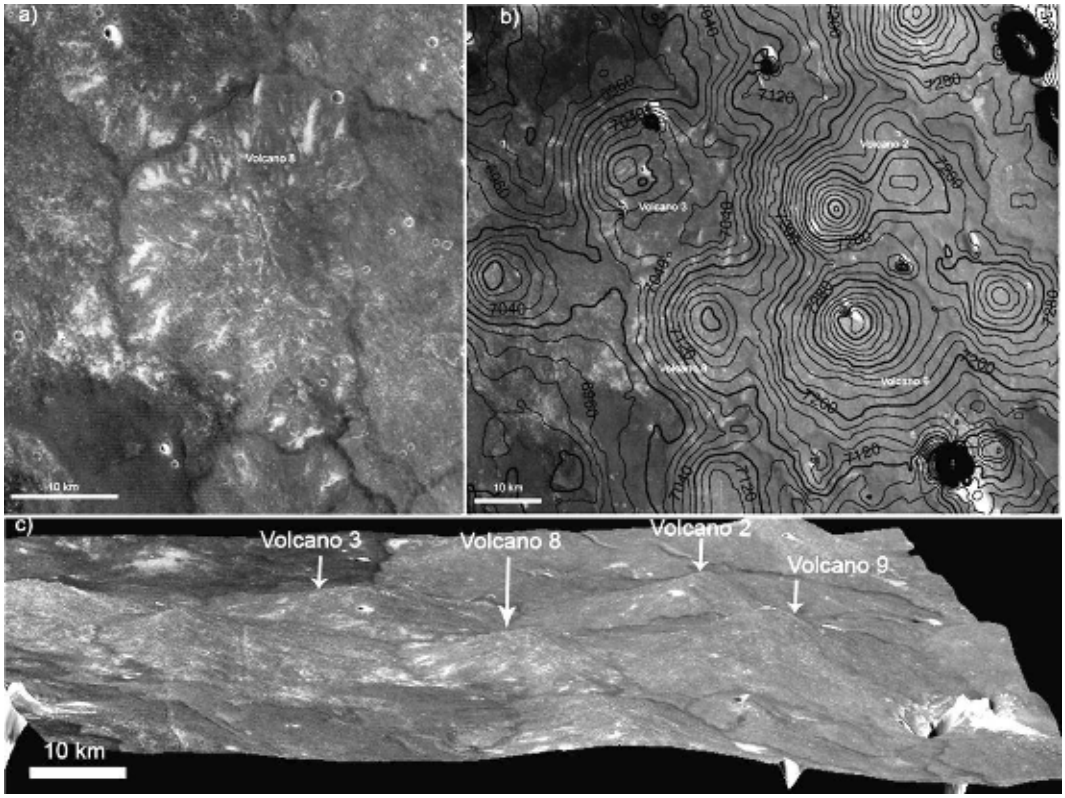

FIG.3.19 - *a) Shield volcano 8 seen by HRSC, where a small vent is visible on the top. b) HRSC image superimposed on MOLA data where the contour lines (spaced of 20 m) delineate each volcanic shield. The field of coalesced shield volcanoes is represented in a 3D picture, with 10X vertical exaggeration. c) The volcanoes 2, 3, 8 and 9 elevation is shown on images b) and c).*

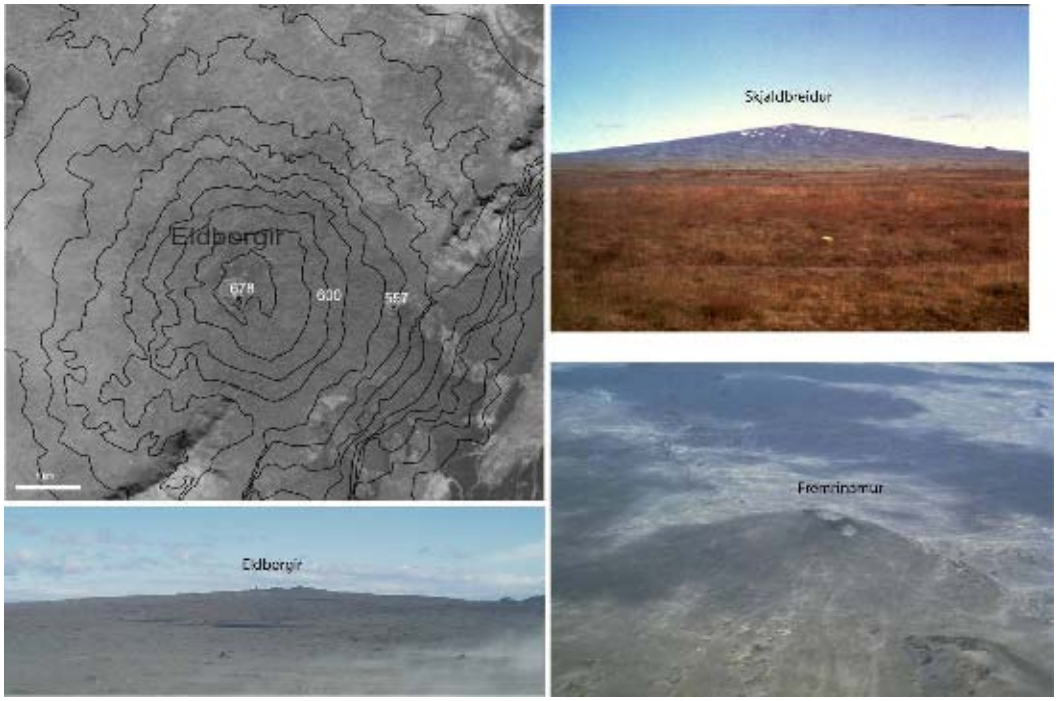

FIG. 3.20 - *Icelandic small shield volcanoes. On the left is Eldborgir (top) SPOT 5 satellite image with 20 m height contour intervals; (bottom) photography, with a summit high of 200 m and a diameter of ~1000 m. Eldborgir is located in the south of Iceland in a periglacial cold desert area. On the right side are Skjaldbreidur and Fremrinamur.*

3.6 Darcy's law equation applied to determine small shields rheology

Baratoux et al., [2008 *Submitted*] developed a method, which consists in approaching theoretically the shape of small shield volcanoes using a Turcotte and Schubert's [2002] method with the Darcy's law equations. This method is based on the porous flow of an unconfined aquifer and allows the derivation of flow rates by viscosity products ($Q\mu$), being then applied to the Martian objects. $Q\mu$ estimates are homogeneous within a given volcanic region, although viscosities change considerably from one region to another [e.g., Vaucher et al., 2007].

In Baratoux et al., [2008 *submitted*] they compared the shape, volume, effusion rate and emplacement times of 31 shield volcanoes of small to

intermediate sizes (few tens of kilometers in diameter) in different places on Tempe Terra, Syria Planum, Pavonis Mons, Arsia Mons and Cerberus. For each shield volcano, it was then obtained several topographic profiles using High-Resolution Stereo Camera and Mars Orbiter Laser Altimeter (MOLA, onboard Mars Global Surveyor) Digital Elevation Models (DEM). These profiles were fitted to ideal small shields' profiles obtained by Turcotte and Schubert's referred approximation.

The results from Baratoux et al. [2008 *Submitted*] indicated that the product effusion rate x viscosity is larger for Syria Planum than for Cerberus (which can be consistent with the higher viscosity of Syria volcanoes). Deduced from the volumes, the emplacement time are quite short (< 1 year), which is in agreement with what was stated in chapter 3. Also, from the fit of the profiles in Baratoux et al., [2008 *Submitted*] the Syria Planum shield volcanoes are not buried below other lavas but emplaced on top of the terrain, as also demonstrated on Chapter 3.4.1, by the superposition of these volcanoes on other rheological type lava flows.

A good adjustment of the profiles in Baratoux et al., [2008 *Submitted*] reveals other important issues; the Syria volcanoes suggest a lower degree of erosion (than the terrestrial analyzed analogues, for instance) even for volcanoes dated with more than 3 Gyrs (see Chapter 3.4.2). It is in agreement with what is shown in this work concerning the existence of some tens meters of thick leveed lava flows. Also, it is found that all the volcanoes in Syria Planum are entirely observed suggesting that they all postdate the terrain on which they formed, as it is also in agreement with what is found in Chapter 3.4.2. Another important issue taken from Baratoux et al. [2008 *Submitted*] is that larger volcanoes may essentially result from longer eruption history than from higher averaged total effusion rates from individual volcanic eruptions, which states a good agreement with the long duration Tharsis Montes large shields and the temporal localized eruptions proposed to Syria Planum in this thesis work.

3.7 Summary and Discussion

HRSC images combined with MOLA and THEMIS data enable a better understanding of some geophysical processes and structures in the Syria Planum region of Mars. The conclusions taken from this work include:

(1) The Syria Planum region reveals an original pattern of volcanic features distinct from the other areas over the Tharsis bulge:

a) Syria Planum contains a swarm of small shield volcanoes centered in the northeast. Each volcano has a small height (<0.3 km) and relatively moderate diameter (10-60 km), with a small slope (<2°), compared to most other Martian volcanoes. Their origin may be related to fissure-fed eruptions, that ceased in the early Hesperian.

b) A larger volcano (volcano A) is identified west of the small shield swarm. It displays long lava flows (>200 km) resulting from high effusion rates. On the basis of our investigation, we conclude that these lava flows are likely to be basaltic to andesitic in composition, similar to Montes lava flows.

c) The small shield volcanoes and the extensive lava flows of volcano A appear to be structurally different and chronologically distinct, despite no precise timescale can be proposed. In comparison with the elongated lava flows, the small shield volcanoes imply a lower volcanic eruption volume that was subsequent to the flows from volcano A.

d) We can constrain the formation of Syria Planum to successive magmatic and tectonic events, from the Early to the Late Hesperian period: I) extensional field stress that produced grabens; II) eruption of volcano A resulting in lavas that spread all over Syria Planum; III) tectonic deformation of the emplaced lava flows by the formation of several fractured patterns such as NE-SW en-echelon faults, troughs and adjacent grabens; IV) new episodes of volcanic activity, forming the coalesced small shield swarms that bury preexisting faults.

In the present chapter we interpreted the formation of small shield volcanoes on Mars, and its role on Martian volcanism, namely on the Tharsis Region, where small shields were formed after the Noachian/early Hesperian

principal extensive volcanism, representing later stages of magmatism originated on zones of weakness.

As it was referred, Tharsis dominates the western hemisphere of Mars. It's an elongated area centered on Syria Planum. The Tharsis region experienced a long and extensive history of tectonics, often associated to volcanism, once the most important tectonic centers are often associated to magmatic centers. In this work we proposed a strong influence of Syria Planum on the long-live volcanism with successive tectonic periods (as described on Chapters 3.1-3.5). The Tharsis Montes and Olympus Mons flanks are mostly covered by tube fed-flows, small shields and other effusive features, revealing a permanence of volcanism much later than the Hesperian, unlike Syria Planum.

The structure below Syria Planum is characterized by a thick crust associated with a thin lithosphere at the time of the magmatic activity, which possibly has resulted in shallower magma sources in Syria Planum. As a consequence, the maximum height for the possible volcanic constructs in this region was more limited than in the other regions of the Tharsis plateau. As it was suggested in chapter 3.5, the cessation of activity of a large volcano on Syria Planum might signify the presence of a thicker crust in that part of the bulge. The development of this thicker crust may explain the incomplete development of the larger volcano at this location by the end of the volcanism, early in the geologic history of the Tharsis region.

Summarizing, we can conclude that Syria Planum shield volcanoes played an important role in the primordial Tharsis Province volcanism and that their activity ceased in the Hesperian, early in the geologic history of this region. The progressive cessation of activity might be due to the enhanced crustal thickness in the magmatic processes of this region. The highest crustal thickness beneath Syria Planum led us to focus on its principal role in the origin, but also the decline, of volcanism in this area and its continuation on the northwestern side of Tharsis, leading to the formation of the present Tharsis Montes. Moreover, analysis by

Neukum et al. [2004] on Tharsis, leads to the conclusion that some of these flows are very recent, about 2 Ma. Although the evidence for recent volcanism namely in the Tharsis province is assumed by the several authors [e.g. Neukum et al., 2004; Schumacher and Breuer, 2006], the mechanism which causes the on-going volcanic activity is still not well understood on Mars. The influence of this thick crust on the stall of a giant volcano on Syria, and on the volcanism continuation beneath the Tharsis Montes and Olympus Mons, are analyzed in Chapter 4.

Part III – Heat flux conductive model of the Tharsis crust

4. Steady-state analysis of conductive heat flux within a thick crust

4. Steady-state Analysis of Conductive Heat Transfer within a Thick Crust

Afin de mieux comprendre le comportement mécanique d'une planète nous devons comprendre sa structure thermique.

Le comportement des roches proches de la surface est principalement élastique, tandis que les roches plus profondes montrent un comportement fluide, sur un temps géologique, afin de relaxer les efforts [Turcotte and Schubert, 2002]. La rhéologie des roches du manteau est directement liée à la température en fonction de la profondeur. Celle-ci est dépendante du flux de chaleur de l'intérieur vers la surface.

Il y a trois mécanismes de transfert de chaleur dans une planète : conduction, convection et rayonnement.

La distribution de la température dans la croûte et la lithosphère de Mars est gouvernée principalement par la perte de chaleur par conduction vers la surface. Cette chaleur est produite (1) intérieurement par la décroissance des isotopes radioactifs dans les roches, et (2) par la chaleur transmise à la base de la lithosphère, issue du manteau et du noyau.

Dans ce chapitre, nous décrivons rapidement l'équation de la loi de Fourier, qui permet de calculer les températures dans la lithosphère planétaire thermique. Ceci s'obtient par l'intégration de l'équation de flux de chaleur à toutes les profondeurs. Les températures effectives trouvées pour la lithosphère de Mars, notamment dans le cas de Tharsis, serons alors montrées et comparées dans ce chapitre.

De plus, nous examinons l'effet de la topographie dans la détermination des températures de surface et subsurface. Nous montrons comment la présence/absence

d'une chaîne de montagnes peut affecter les températures déterminées. Concernant la planète Mars, et en particulier pour les objectifs de ce travail, cet effet est important

Dans le chapitre 3, nous avions analysé le rôle possible des volcans boucliers de Syria Planum sur la permanence du volcanisme dans l'ouest de Tharsis. Nous avions alors supposé que la fin progressive de l'activité volcanique de Syria Planum était reliée à un épaississement crustal associé aux processus magmatiques de cette région.

L'épaisseur crustale la plus élevée sous Syria Planum nous a permis de remarquer son important rôle dans l'origine mais aussi dans le déclin du volcanisme de cette région. Néanmoins, le volcanisme a poursuivi son activité dans la partie nord-ouest de Tharsis, en conduisant à la formation des Montes Tharsis jusqu'à l'époque actuelle. Les analyses des données d'imagerie d'HRSC/MarsExpress menées par Neukum et al. [2004] sur Tharsis, montrent que Tharsis présente des coulées de lave récentes, âgées de 2 Ma. Ce volcanisme récent sur Tharsis est expliqué par des modèles de convexion thermique du manteau [par ex. Schumacher and Breuer, 2006]. Cependant, les détails du maintien de ce volcanisme sont encore méconnus.

Pour mieux comprendre la persistance du volcanisme sur la province de Tharsis, nous avons donc réalisé une modélisation 3D du flux de chaleur dans la partie conductive de sa lithosphère.

La topographie MOLA et l'épaisseur de la croûte dérivées de la gravimétrie, ont été employées pour déterminer la géométrie 3D du plateau de Tharsis. Aussitôt, l'équation de transfert thermique a été résolue pour cette région, en un état d'équilibre pour la croûte et le manteau supérieur.

L'influence de la topographie a été le premier paramètre analysé. Ceci nous permet de mieux comprendre et comparer les différents modèles thermiques sur Tharsis, et de mettre en évidence ceux qui auraient contraint le volcanisme à se prolonger jusqu'à l'Amazonian sur Tharsis.

Nous avons étudié en détail les frontières comportant des variations d'épaisseur de croûte, notamment celles associées à des racines crustales, ainsi que leur rôle sur l'élévation locale des températures et leur influence sur la durée du volcanisme.

In order to understand the volcanism and evolution of the Tharsis region, we must understand its thermal structure and evolution.

The thermal structure of Mars, in Tharsis as well as in the other geological areas, can be modeled by a possibly convective mantle and a thermal lithosphere. Part of the thermal lithosphere is located in the upper mantle, and the remaining part is the crust. We refer to textbook [e.g. Turcotte and Schubert, 2002]. for a detailed description of the processes in thermal transfer and will only summarize the later in this introduction There are three mechanisms for the transfer of heat: conduction, convection and radiation.

The temperature distribution in the Martian crust and thermal lithosphere is governed mainly by the conductive heat flux toward the surface. In the lithosphere (in all this section, we will focus on the thermal lithosphere, even when not précised), this heat is generated (1) internally by the decay of radioactive isotopes in the rocks, and (2) by the heat that flows upward from the upper mantle. The later is also related to the radioactive decay of mantle materials, but also to the accretion heat.

Here it is presented a brief description of the Fourier's law Equation, which permits to calculate the temperatures along a planetary lithosphere, by the integration of the heat flux equation at any depth. We will use and solve this equation in this section, in order to model the temperatures found for the Martian lithosphere, taking into account both the topography effect and crustal thickness variations on the temperatures determination. We will focus our analyze on how the presence/absence of a mountain range may affect the determined temperatures. For the case of Mars, and for this work's purpose, these effects have a relevant importance.

On chapter 3 it was invoked the role of Syria Planum shield volcanoes on the possible long-standing volcanism on the western of Tharsis. It was hypothesized that the progressive cessation of volcanic activity on Syria Planum might have been due to the enhanced crustal thickness in the magmatic processes of this region. The highest crustal thickness beneath Syria Planum led us to think on its principal role on the origin but also on the decline of the volcanism in this area, and it's continuation on the northwestern side of Tharsis, leading to the formation of the present Tharsis Montes. Furthermore, analysis by Neukum et al. [2004] on Tharsis, leads to the conclusion that

some of these flows are very recent, about 2 Ma. The evidence for recent volcanism namely in the Tharsis province is already assumed by the several authors [e.g. Neukum et al., 2004] and Schumacher and Breuer [2006], have already shown the importance of a large crustal thickness in the explanation of the most recent volcanism . Realistic crustal models have however not been yet used, and the mechanism which causes the longstanding volcanic activity is therefore still not completely understood.

To test the hypothesis of the long-standing volcanism on the Tharsis province, we have therefore realized a numerical simulation of the heat transfer within the conductive part of the lithosphere of the Tharsis Plateau. The MOLA topography and the crust thickness derived from gravimetry were used to determine several 3D blocks of the Tharsis Plateau for which the heat transfer equation was solved first in a steady state case for the crust and upper mantle.

The influence of the topography was the first analyzed parameter, as a constraint for the thermal and heat conductive conditions that would have led the volcanism to extend till the Amazonian on Tharsis. Also, we analyzed boundary zones where there are crustal thickness variations, crustal roots, and their role on local temperatures elevation and its influence on the volcanism duration.

4.1. Heat transfer

There are three mechanisms for the transfer of heat through a planet: conduction, convection and radiation.

Depending on the depth, they play different roles; Radiation plays the major role for the surface temperature, and is dependent on the energy balance between sun heating and surface re-emission. Radiative equilibrium generally defines the surface temperature, especially on planets like Mars where the heat capacity of the atmosphere is too weak to have a role in the surface temperature. Conduction describes the heat processes in the thermal lithosphere. Heat is conducted through a medium where there is a spatial variation in the temperature. On the Earth, the internal heat loss through the oceanic crust and lithosphere is also controlled by convective effects of circulating groundwater, but these effects will be neglected in our application devoted to Mars; Convection plays finally the dominant role in the transport of heat from the planet's deep mantle and in controlling the temperature on its interior. We will not model the thermal transfert in the Martian mantle and will only assue in our study a heat flow at the base of our model, associated to the mantle. We invite the reader to refer to recent papers on mantle convection simulation.

4.1.2. The Fourier's Law of Heat

As it was said, the main heat transport process in the crust is done by conduction. The conduction is the transfer of energy through the collisions and vibrations of molecules and atoms [Lowrie, 1997], and the temperature of molecules or atoms are related to their velocity.

The Fourier's law describes the conductive heat transport, and states that the heat flux q, or the flow of heat per unit area and per unit time, at a point in a medium is directly proportional to the temperature gradient at the point:

$$q \sim dT/dy \tag{4.1}$$

and can be expressed, in 3 dimensions, as:

$$\vec{q} = -k \vec{\nabla} T \tag{4.2}$$

where k is the thermal conductivity (units of $Wm^{-1}K^{-1}$) and T is the temperature field (K). This relationship is defined in a conductive medium. The negative sign indicates that the heat is flowing from the hot to cold.

The mathematical model of finite element analysis for heat transfer by conduction is the heat equation:

$$\rho C \frac{\partial T}{\partial t} - \vec{\nabla}.(k\vec{\nabla}T) = Q \tag{4.3}$$

Where T is the temperature, ρ is the density, C is the heat capacity per mass unit (at constant pressure), k is thermal conductivity, Q is the volumetric heat source. For a steady-state model, temperature does not change with time, and the first term containing ρ and C vanishes.

4.1.3. Energy Balance

The Enthalpy (hereafter called heat content) can be expressed as $\rho C_p \Delta T$, where ρ is the density, C_p is the specific heat (J kg^{-1} K^{-1}). (The specific heat is the amount of energy required to raise the temperature of 1 kg of material by 1 degree Kelvin, and it is a property of the material.)

$$C_p = \frac{dH}{dT} \tag{4.4}$$

Where H is the Enthalpy per unit of mass and the subscript 'p' denotes that the derivative is taken with pressure kept constant.

The rate of change in heat content over a time interval Δt is given by:

$$\rho C_p \frac{\Delta T}{\Delta t} \rightarrow \rho C_p \frac{\partial T}{\partial t} \tag{4.5}$$

where we use a partial derivative because T depends on space as well as time.

4.1.4. Steady Two- and Three-Dimensional Heat Conduction

Taking the energy conservation equation, and knowing that the heat can be conducted in both x and y directions (taking for example the previous slab geometry), the heat flux in the direction x is q_x and in the direction y is q_y. The rate at which the

heat flows into the element in the y direction is $q_y(y)\delta xl$, where l is an arbitrary length on the third dimension (in two-dimensional heat conduction it is assumed that nothing varies in the third dimension) [Turcotte and Schubert, 2002]. Similarly happens in the x direction at the rate $q_x(x)\delta yl$.

In steady-state it's assumed that heat is produced internally in the slab element.

Thus, if we have heat conduction in 3 dimensions, the heat flow rate generation is then given by

$$\frac{\partial q_x}{\partial x} + \frac{\partial q_y}{\partial y} + \frac{\partial q_z}{\partial z} = \rho H \tag{4.6}$$

Fourier law of heat conduction relates the heat flow in any direction to the temperature gradient in that direction. If we assume that the thermal conductivity of the rock is isotropic, that is, rock conducts heat equally readily in any direction, Fourier's law of heat conduction can be written:

$$q_x = -k\frac{\partial T}{\partial x} \tag{4.7}$$

$$q_y = -k\frac{\partial T}{\partial y} \tag{4.8}$$

Generalizing to the three-dimensional heat conduction, gives in a homogeneous model

$$-k\left(\frac{\partial^2 T}{\partial x^2} + \frac{\partial^2 T}{\partial y^2} + \frac{\partial^2 T}{\partial z^2}\right) = \rho H \tag{4.9}$$

4.1.5. Heat sources of a planet

There are several sources of heat within a planet:

1. Original heat of accretion.
2. Conversion of gravitational potential energy (e.g., core formation)
3. Exothermic phase or compositional changes.
4. Decay of radiogenic isotopes.
5. Mechanical heat dissipation.

The original heat of accretion arises from the conversion of gravitational potential energy associated with the infall of material forming the planet. On the Earth,

about 20% of the heat is associated to this original heat. Smaller the terrestrial-sized planets are, larger the loss of this original heat is. On the other hand, the giant planets have not lost this heat.

Another source of primordial heat is associated to the conversion of gravitational potential energy during the core formation. The formation of the solid inner core at the expense of the molten outer core also produces heat and helps maintain the geodynamo. In the late 70^{th}, these effects were considered as important in the thermal evolution of ars (e.g. Solomon, 1979). The most recent analysis of SNCs have however shown that this is not the case:: very likely, the core was formed very early [e.g. Halliday et al., 1996] and no evidence for inner core has been recorded.

A last source of primordial heat is the Decay of short-lived isotopes (e.g., $^{26}Al \rightarrow {}^{26}Mg$). They are responsible for differentiating the meteorite parent bodies and may have contributed to early heat of Mars. Their contribution, if any, will be integrated in our boundary conditions.

Finally, the largest source of heat in the terrestrial planets with Mars size appears to be the decay of long- lived radiogenic isotopes [Lowrie, 1997]. This will be the first source of heat taken in our study, which will be developed hereafter.

4.1.6. Heat Generation by the Decay of Radiogenic isotopes

This radioactive process is manifested in the emission of particles or electromagnetic radiation. The two major types of emissions are α particles (charged helium nucleus), β particles (electrons) and γ particles. These types of particles are brought to rest in a rock within a few mm of where they are emitted. When this happens, their kinetic energy is converted to heat, although in fewer scale concerning the γ particles.

Radioactive heating of the mantle and crust arises from the decay of isotopes ^{238}U, ^{235}U, ^{232}Th, and ^{40}K. The contribution of each isotope individually depends on its intrinsic heat generation and initial abundance and half-life (or, alternatively, its present abundance) [Turcotte and Schubert, 2002]. The Table 4.1 is elucidative: the total heat production has dropped by about a factor of three over the last 4 Gyr. The isotopes ^{238}U and ^{232}Th dominate heat production today, but in the past ^{235}U and ^{40}K were the

dominant isotopes because of their shorter half-lives. The concentrations of radioactive isotopes for the Earth's interior are shown in Table 4.1.

For Mars, no information on the present heat flow at the surface is available, in contrary to the Earth and Moon. The composition of the SNCs is however well known and provides key information on the content of radioactive material in the crust. The concentration in the heat-producing elements in surface rocks varies however considerably and is the results of partial melting which depletes mantle rock of incompatible elements such as uranium, thorium and potassium. These incompatible elements are concentrated in the basaltic partial melt fraction. As a result, these rocks (like the oceanic crust on the Earth or about 1/3 of the Martian crust –see chapter 5) are enriched in these elements by a factor of about 4-6 relatively to the fertile mantle [Turcotte and Schubert, 2002]. We note however that the values shown in Table 4.1 correspond to peridotites and Table 4.2 corresponds to basaltic meteorites and clinopyroxenites. As our work will focus on the Tharsis area we will use the content of basaltic SNCs.

TAB 4.1 *List of isotopes and their Heat production, Half-life and Concentration of Radioactive isotopes on the Earth's interior.*

Isotope	Heat Production* W kg^{-1} x 10^5	Half-life Gyr	Concentration* kg kg^{-1} x 10^9
^{238}U	9.37	4.47	25.5
^{235}U	56.9	0.704	0.185
^{232}Th	2.69	14.0	103
^{40}K	2.79	1.25	32.9

*Heat production per element, which multiplied by the concentration (column 4), gives the heat value on the Earth's mantle.

TAB 4.2 *List of average concentrations in Shergotty and Nakhla Martian meteorites (from Dreibus and Wanke [1982] and Lodders [1998], respectively).*

Rock Type	Th (ppb)	^{40}K (ppb)	U (ppb)	^{235}U (ppb)	^{238}U (ppb)
SNC (Shergotites)	390	0.901	116	0.835	115.16
SNC (Nakla)	198	0.714	52	0.374	51.62

Assuming the content of the Martian core, we can therefore extrapolate the past heat generation. The total present-day production H_0 is related to the heat generation rates of the individual radioactive elements by

$$H_0 = C_0^U \left(H^U + \frac{C_0^{Th}}{C_0^U} H^{Th} + \frac{C_0^K}{C_0^U} H^K \right) \tag{4.10}$$

The mean heat production rate of the mantle in the past can be related to the present heat production rate using the half-lives of the radioactive isotopes. The concentration C of a radioactive isotope at time t measured backward from the present is related to the present concentration C_0 and the half life of the isotope $\tau_{1/2}$ by

$$C = C_0 \exp\left(\frac{t \ln 2}{\tau_{1/2}} \right) \tag{4.11}$$

Therefore, the past mean mantle heat production rate is given by

$$H_0 = 0.9928 C_0^U H^{U^{238}} \exp\left(\frac{t \ln 2}{\tau_{1/2}^{U^{238}}} \right) + 0.0071 C_0^U H^{U^{235}} \exp\left(\frac{t \ln 2}{\tau_{1/2}^{U^{235}}} \right)$$

$$+ C_0^{Th} H^{Th} \exp\left(\frac{t \ln 2}{\tau_{1/2}^{Th}} \right) + 1.19 \times 10^{-4} C_0^K H^{K^{40}} \exp\left(\frac{t \ln 2}{\tau_{1/2}^{K^{40}}} \right) \tag{4.12}$$

The rate of mean mantle heat production based on Equation 4.12 and parameter concentrations in Table 4.2 and half-life values in Table 4.1 is plotted in Figure 4.1 as a function of time from the present till the initial Martian crustal formation.

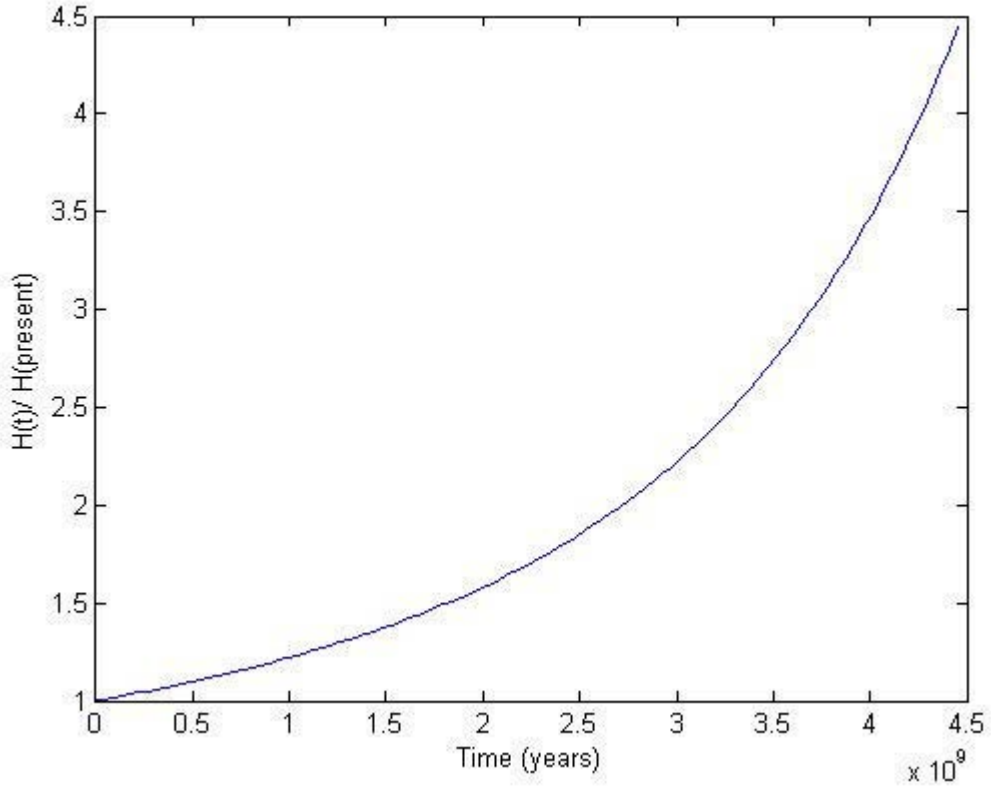

FIG 4.1 – *Mean total Martian mantle heat production rate due to the decay of the radioactive isotopes of U, Th and K as function of time, from the present till 4.5 Gy, based on Shergotites' composition.*

4.2 Conductive Heat Flow Problem for Mars

In the absence of direct measurements of heat flow, the elastic lithosphere thickness *Te* is one of the few clues we have to determine the (paleo) surface heat flow of a planet, enabling to reconstruct its thermal history. Since the thermal flux significantly influences tectonic, magmatic and geological processes present on the surface, properly dated and measured heat flux estimates are extremely important. Many authors have already constrained *Te* for various regions on Mars. [e.g. Comer et al. 1985; Schultz and Watters, 2001; McGovern et al. 2004; Belleguic et al. 2005; Grott et al. 2005].

To study the thermal behavior of a planet, it is necessary to understand how interior heat is transported from the deep interior to the surface. This heat is generated

inside a planet by radioactive heat sources, and was accumulated during the planet's formation. In the mantle, convection is the primary heat transport mechanism by which hot buoyant material rises to colder regions and heats them whereas cold material sinks and cools the surroundings [Turcotte and Schubert, 2002]. The heat conduction in the thermal lithosphere plays an important role in particular in one-plate planets like Mars. The loss of the planet's internal heat through the upper layer, consisting of a large part of the upper mantle and crust, is mainly controlled by conduction; mantle convection and the associated heat transport take place underneath the nonconvecting upper lithosphere layer [Breuer and Spohn, 2006].

Mars is a differentiated planet with a solid mantle and, most likely, a fluid core [Lognonné and Mosser, 1993; Yoder et al. 2003] in which a dynamo produced an early magnetic field [Connerney et al. 2001] (see chapter 1 for more detail concerning the Martian magnetic field). In general, the intensity of Mars interior activity decreased over time with the decay of radioactive heat sources and loss of the primary accretion heat, leading to the cooling of mantle and core. This statement was proposed by Connerney et al. [2001] as an explanation for the rapid cessation of the dynamo [Schubert et al. 2000; Stevenson, 2001]. Moreover, the outermost layer of this one-plate planet formed a stagnant lid that has grown in thickness over time [e.g., Zuber et al., 2000; Weizman et al., 2001; Hauck and Phillips, 2002; Breuer and Spohn, 2006]. The models presented by these authors predicted that most of the crust formed in the first billion years with the cessation of the crustal production some few billion years ago and a present-day thickness of some tens of kilometers [e.g., Zuber et al., 2000; Hauck and Phillips, 2002] to about 100 km [Breuer and Spohn, 2006] and 200 km [Weizman et al., 2001] depending on the assumed thermochemical parameters (such as the initial mantle temperature, the content of volatiles in the mantle associated with mantle viscosity, and the concentration of radioactive elements). Hauck and Phillips [2002] compared a dry and wet mantle rheology for Mars, and favor a wet Martian mantle necessary to fit the observations of early crustal formation.

Moreover, other models [Solomon et al., 2005; Nimmo and Tanaka, 2005] tend to justify a continuous decline of global volcanism and crustal growth since the Noachian, with a major part of the crust being formed during the Noachian. However,

not much care has been taken whether these models can also explain the observed recent volcanic activity in the large volcanic provinces of Tharsis and Elysium [e.g., Hartmann et al., 1999; Neukum et al., 2004; Werner, 2006]. In this work, we take the recent volcanic activity on Tharsis as a statement, situation that was also described by other authors [e.g. Neukum et al., 2004; Schumacher and Breuer, 2007] and which our findings support.

4.3 Method Description in 3D

4.3.1 Application Variables

The conduction application was done to a 3D geometric model where the dependent variable is the temperature, *T*. It was then solved a three dimensional heat equation with a 3-D finite elements code, using COMSOL Multiphysics, for the temperature distribution in the lithosphere for present-day Tharsis conditions.

The variables used for domain equations, boundary equations and postprocessing purposes are shown in Table 4.3.

TAB. 4.3 – *Application variables used in the models*

NAME	DOMAIN/TYPE	DESCRIPTION	EXPRESSION
T	S/B	Temperature	T
flux	S	Heat flux	q
nflux_T	B	Normal heat flux	nq
rho	S	Density	ρ
C	S	Heat capacity	C_p
k, kx*ixj*	S	Thermal conductivity	k, k_{ij}
Q	S	Heat source	Q
T0	B	Prescribed temperture	T_0

Note: B refers to the boundary condition and S to the subdomain.

4.3.2 Subdomain Settings

The subdomain quantities are shown in Table 4.4.

TAB. 4.4 – *Subdomain quantities used in the models*

QUANTITY	VARIABLE	DESCRIPTION
ρ	rho	Density (Kgm^{-3})
Cp	C	Heat capacity ($JKg^{-1}K^{-1}$)
k	k	Thermal conductivity ($Wm^{-1}K^{-1}$)
Q_H	Q	General Heat source (Wm^{-3})
H	H	Radiogenic heating per mass (Wkg^{-1})
T	T_0	Initial temperature (K)

Density

It specifies the rocks' density.

Heat capacity

The heat capacity C describes the amount of heat energy required to produce a unit temperature change in a unit mass.

Thermal conductivity

The thermal conductivity k describes the relationship between the heat flux vector q and the temperature gradient ∇T as in *Fourier's* Equation *of heat conduction* (4.2). This quantity represents the power per length and temperature.

Heat source

The heat source describes heat generation within the domain. Express heating and cooling with positive and negative values, respectively. This quantity Q represents a unit power per unit volume.

4.3.3 Boundary Conditions

The boundary conditions are shown in Table 4.5.

TAB. 4.5 – *Boundary conditions used in the models*

BOUNDARY CONDITION	DESCRIPTION
Equation 4.2	Heat flux
$(k\nabla T) = 0$	Insulation
$T = T_0$	Prescribed temperature

Heat Flux

The application interprets the heat flux q_0 in the direction of the inward normal. We specify q_0 to represent a heat flux that enters the domain, which geometry was previous defined. The quantity q_0 is expressed as unit power per unit area (W/m^2 using SI units) and is directly applicable to the 3D domain.

For a steady-state model, temperature does not change with time, and as we said, the heat transfer is done by conduction only, so, q is determined by Equation (4.2). Therefore, the expressions for the radiation heat transfer with the surrounding environment and for the convective heat transfer appear zero.

Insulation or Symmetry

This condition specifies where the domain is well insulated, or it reduces model size by taking advantage of symmetry. Intuitively this equation says that the gradient across the boundary must be zero. For this to be true, the temperature on one side of the boundary must equal the temperature on the other side. Because there is no temperature difference across the boundary, heat cannot transfer across it. This condition applies to the lateral vertical borders.

Prescribed Temperature

This boundary prescribes the temperature at the surface.

4.3.4 Method description

The models of conductive heat transfer were calculated using the parameters described on chapter 4.3.1-3 and then their variation was explored. It was investigated the effect of the temperature at the base of the elastic lithosphere, the different thermal conductivity values on the crust and mantle, the general heat (affected by the radiogenic decaying) and the presence of a stagnant lid, on the temperatures variation.

For each model, we obtained temperature profiles for the surface and along the crustal depth. Then it was determined the associated heat flux variations (models M1-M7 and MSL – model with a stagnant lid at 300 km depth).

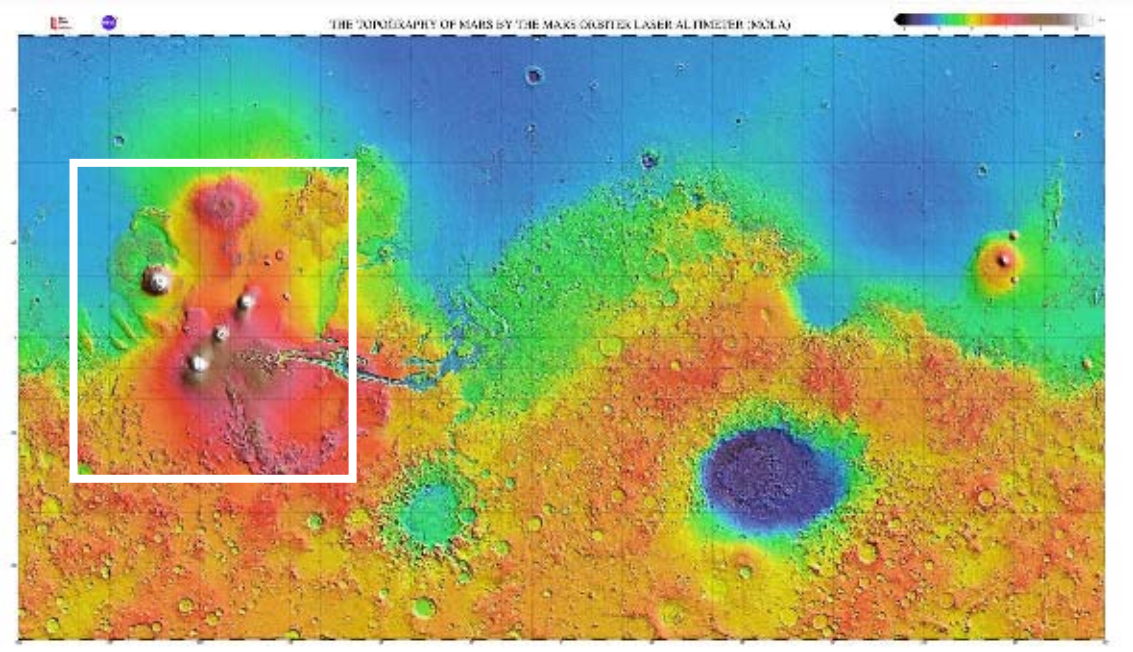

FIG. 4.2 – *MOLA shaded relief map of Mars where in white is shown the studied area - Tharsis.*

It was built a 3D Geometrical block with the dimensions of the Tharsis region crust (Figures 4.2 to 4.4). For the upper limit, it was used MOLA altimetry shot points that were obtained by the Mars Orbiter Laser Altimeter (MOLA) [Zuber et al., 1998; Smith et al., 2001; Smith et al., 2003]. These measurements were made through the

determination of the planetary radius at ~600 million locations. For the Moho altimetry it was used data given by gravimetric corrected topographic models [e.g. Smith et al., 2003; Neumann et al., 2004] downloadable at http://pds-geosciences.wustl.edu/missions/mgs/mola.html, assuming therefore a homogeneous structure for the crust.

Taking into account the limitations given by the MOLA topographic data (discussed on Chapter 2) and the thermal isolation conditions given by the model itself, we represented the area of Tharsis, till a depth of -150 km, for Models M1-M6 and till -300 km for Model MSL. These depths correspond, as it was said, to a 1073 K isotherm at -150 km, and at -300 km to the base of the stagnant lid, both in the upper Martian mantle.

Looking at the topographic map (Figure 4.2) we can realize how the Tharsis volcanoes (Olympus, Arsia, Pavonis and Ascraeus Montes) are enough far to each other, in opposition to those of Syria Planum that appear coalesced (see chapter 3), so the size of the net used for the model should be chosen with careful. It was used a maximum of 60 km in distance between two horizontal measured points and 15 km between two vertical measured points.

In summary, the present chapter will examine the influence of the topography on the thermal conditions in the present-state evolution of Mars. Some other parameters such as the thermal conductivity, the density, the radioactive heat flow, or the presence of a stagnant lid are also evaluated. The models are tested over some assumptions stated for the observed crustal and elastic lithosphere evolution: (1) first, assumes present-day crustal models – for the Moho determination [e.g., Zuber et al., 2000; Smith et al., 1996]; (2) also, it is assumed a continuous decline of global volcanism and crustal growth since the Noachian, with a major part of the crust being formed during the Noachian [e.g., Nimmo and Tanaka, 2005]; (3) it is also presupposed recent volcanism in the large volcanic provinces, Tharsis and Elysium [e.g., Hartmann et al., 1999; Neukum et al., 2004; Schumacher and Breuer, 2006]; (4) the estimates of the elastic lithosphere are formed at the age of the lithospheric load at the Hesperian [e.g., McKenzie et al., 2002; McGovern et al., 2002]; (5) we assume the isotherm of 1073 K

for a depth of -150 km (Models M1-M4), or a constant heat flux at the elastic lithosphere (Model M5 and M6), or even a stagnant-lid at -300 km for Model MSL.

All Models use the parameterization of conductive heat transport in the elastic part of the Martian lithosphere, or at the stagnant lid.

4.3.5 Geometry and Mesh Discretization

We solve a three dimensional steady-state heat conduction equation with a 3-D finite elements code for the temperature distribution in crust and upper-mantle for present day Mars conditions. Boundary conditions are constant surface temperatures or constant heat flux, as surface temperature is in radiative equilibrium and we neglect therefore the variation of albedo. Also, it's assumed constant mantle heat flow (whose value is given by 1-D parameterized mantle convection models) as well as thermal insulation for the left and right boundary. The width of the models was chosen in a way that the temperature distribution close to the sidewise boundaries of each volcano is not influenced by the absence of crust on the limits of the block.

Models with a constant crustal thickness consist of an approximately 6000 km per 5000 km wide and a crustal thickness which is delimited by an upper part given by MOLA altimetry records data (PEDRs) and a lower limit (composing the crustal roots) given by the topographic model developed in spherical harmonics (MEGDRs) [e.g. Smith et al., 1996; Neumann et al., 2004] (see Figures 4.3 and 4.4). The crust is underlain by a conducting upper mantle (which extends till 150 km - the elastic lithosphere - which is the part of the lithosphere marked by a 1073K isotherm, or extends till the base of the stagnant lid).

In the present investigation, we considered the finite element approach as the most appropriate. A mesh was done with 142538 elements for Models M1-M6 and 290547 elements for Model MSL. Sensitivity runs showed that higher refinement of the finite element chosen mesh did not significantly change the solution ($\Delta T < 10^{-3}$ K). In particular, the finite element method reveals that the 3-D effects become more pronounced at greater depth, where the mesh gets larger.

After building the referred geometry, the several models run a mesh that has been defined with an increasing vertical refinement from 250 m at 30000 m depth to

~25 m near the surface. The vertical discretization was conditioned by COMSOL, once the discontinuities altitude is assumed by the software. Moreover, such used discretization in space yields a maximum temperature difference of less than 10^{-1} K compared to the 1-D solution, which can be considered sufficient for the present set of calculations.

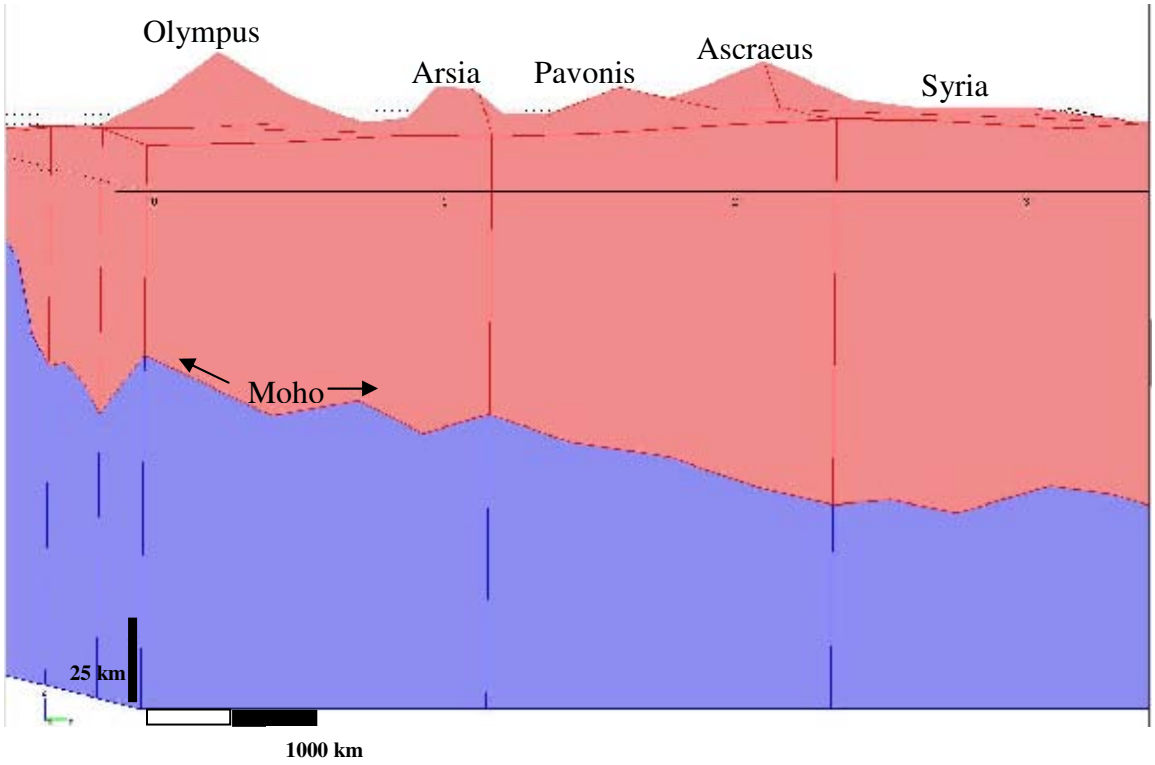

FIG. 4.3 – *3D block from the Tharsis region, represented with 15 times vertical exaggeration* x=*4000Km; y=6000Km; z=150km from the z=0 level. The surface altitudes are given by the MOLA data records (PEDRs). The Moho altitudes are given by the model obtained from gravity corrections with MOLA data [e.g. Neumann et al., 2004].*

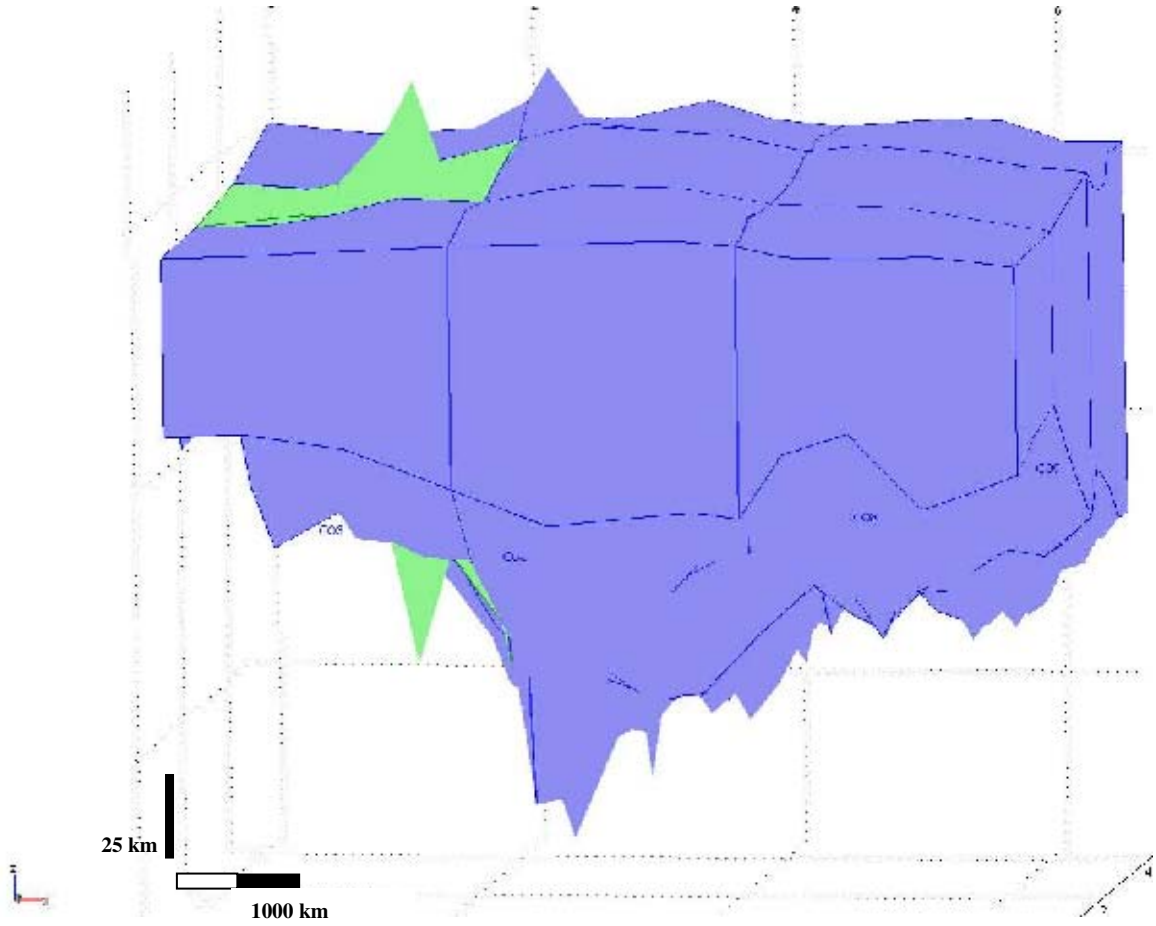

FIG. 4.4 - *3D geometric block of the Tharsis crust (represented in pink in Figure 4.3) with 15 times exaggeration in z, and respective crustal thickening. In green is highlighted the Olympus Mons, where its crustal root is visible. The biggest visible root corresponds to Arsia Mons, and the largest thick area (right side of the block) corresponds to Syria Planum. This block is referred to an area between approximately 50º N-40ºS; 50ºW-140ºW on Mars.*

4.3.6 Choice of Parameters Values

Heat capacity

The chosen value, 1000 ($JKg^{-1}K^{-1}$), corresponds to the one of a basalt on Earth [Turcotte and Schubert, 2002], as the Martian crust is believed to be mostly composed of basalt [e.g., Christensen et al., 2000], andesite or andesitic basalt [Nimmo and Tanaka, 2005].

Thermal conductivity

Most thermal evolution models assume a constant thermal conductivity in mantle and crust of 4 $Wm^{-1}K^{-1}$ [e.g. Hauck and Phillips, 2002; Schumacher and Breuer, 2007] although, Schumacher and Breuer [2006] have shown that different thermal conductivities in crust and mantle due to compositional, temperature and pressure variations should be considered. Although, the value of the crustal conductivity for basaltic material is about 2 $Wm^{-1}K^{-1}$ [e.g., Clifford and Fanale, 1985] and that the thermal conductivity depends on various factors like temperature, pressure, composition, and texture of the material.

Moreover, as the Martian crust is believed to be mostly composed of basalt [e.g., Christensen et al., 2000], with an average thickness between 40 to 120 km [e.g., Zuber et al., 2000; Zuber, 2001; Nimmo and Stevenson, 2001; McGovern et al., 2002; Turcotte et al., 2002; Wieczorek and Zuber, 2004], the thermal conductivity of the majority of compact volcanic materials ranges between 1.5 and 3.5 $Wm^{-1}K^{-1}$ at ambient temperatures [e.g., Clifford and Fanale, 1985] but decreases with temperature like for mantle material [e.g., Seipold, 1998]. For example, the thermal conductivity of typical compact basalt decreases from about 2 $Wm^{-1}K^{-1}$ at 270 K to about 1.5 $Wm^{-1}K^{-1}$ at 800 K [e.g., Seipold, 1998]. In addition to the temperature effects on the thermal conductivity, the structure of the material can also change significantly the thermal conductivity. Fractured and porous material has a reduced thermal conductivity in comparison to compact material. The upper Martian crust has been fractured due to impact processes, in particular in the early period of heavy bombardment (e.g.

Hartmann et al., [1999]). These impacts resulted in the production of a porous megaregolith that extends to considerable depths, possibly to about 10 km [Clifford, 1993]. Given the range of possible variations in the composition of the regolith and the compact crust, the porosity, the filling materials, and the influence of the temperature on the thermal conductivity, a column-averaged thermal conductivity of about 2 ± 1 $Wm^{-1}K^{-1}$ can be assumed for the entire Martian crust [Clifford and Fanale, 1985; Turcotte and Schubert, 2002].

In the presented models, we used values of 3 $Wm^{-1}K^{-1}$ for both mantle and crust and made it vary on Model M3, M5, M6, M7 and MSL from $3Wm^{-1}K^{-1}$ to 1.5 $Wm^{-1}K^{-1}$for the crust.

Constant temperatures

The mean surface temperature on Mars is globally at 220 K (from TES instrument measurements) [Christensen, et al., 2004].

At -150 km, the base of the elastic lithosphere is defined by an isotherm. We have chosen an isotherm of 1073 K, which can be derived for mantle material dominated by olivine using the rheology parameters of Karato et al. [1986] for olivine. This isotherm defines the maximum thickness of the elastic lithosphere as the thickness of the effective elastic lithosphere decreases with its deflection. As it was already said, the elastic lithosphere thickness, which were derived from the analysis of the gravity and topography data, suggest a rapid growth during the Noachian and a slower subsequent growth [e.g., Zuber et al., 2000; McGovern et al., 2004].

Density

The mean density of Mars is 3930 kg m^{-3} [Smith et al., 1999], considerably less than the terrestrial, although the Martian mantle and crust are more iron-rich and consequently denser than Earth's. We assume ρ_m = 3500 kg m^{-3} for an olivine upper mantle based on SNC geochemistry [Sohl and Spohn, 1997]. For the crust, McGovern et al. [2002] found that ρ_c = 2900 kg m^{-3} provided the best fit to localized admittance over much of the planet Mars, if one allows in some places the presence of subcrustal

loading. McGovern et al. [2002, 2004] suggested that the Tharsis Montes are denser than the average 2900 kg m^{-3} crustal density, although their analyses represented averages over a broader region than a single volcano. Belleguic et al. [2005] found a range of bulk crustal densities from 2700 to 3100 kg m^{-3}. On our Model M4 and M7, when we make vary the crust and mantle densities, we assume a crustal density of 3100 kg m^{-3}.

Roots effect related to density

The values assumed for crustal and mantle densities, which are higher than those assumed to build the topography model from Neumann at al. [2004], have an effect on the observed roots' size. The gravity models have been done by assuming that the gravity signal is directly related to the crust variation. Assuming that the crustal variation leads, in a surface approximation, to a surface density given by

$$\sigma = h_T \rho_c + h_o \rho_c + h_r (\rho_c - \rho_m) \tag{4.13}$$

where *hT*, *ho* and *hr* are the topographic variation, mean crustal variation and root topography respectively.

Considering now two models with different crustal densities; we must have the same surface density, so that

$$h_T \rho_c^{'} + h_o^{'} \rho_c^{'} + h_r^{'} (\rho_c^{'} - \rho_m) = h_T \rho_c + h_o \rho_c + h_r (\rho_c - \rho_m) \tag{4.14}$$

We assume here that the mean gravity is the same for the two models, and therefore that

$$h_o^{'} \rho_c^{'} = h_o \rho_c \tag{4.15}$$

Consequently, this leads to the following expression for the root's topography:

$$h_r^{'} = h_T \frac{\rho_c - \rho_c^{'}}{\rho_c^{'} - \rho_m} + h_r \frac{\rho_c - \rho_m}{\rho_c^{'} - \rho_m} = h_r + (h_r + h_T) \frac{\rho_c - \rho_c^{'}}{\rho_c^{'} - \rho_m} \tag{4.16}$$

This gives the crustal thickness expression for one model with respect to the other as

$$H^{'} = h_T + h_o^{'} + h_r^{'} = h_T + h_o^{'} + h_r + (h_r + h_T) \frac{\rho_c - \rho_c^{'}}{\rho_c^{'} - \rho_m} =$$

$$h_T + h_o \frac{\rho_c}{\rho_c'} + h_r + (h_r + h_T)\frac{\rho_c - \rho_c'}{\rho_c' - \rho_m} \tag{4.17}$$

which finally comes

$$H' = H + (h_r + h_T)\frac{\rho_c - \rho_c'}{\rho_c' - \rho_m} + h_o \frac{\rho_c - \rho_c'}{\rho_c'} = H + H\frac{\rho_c - \rho_c'}{\rho_c' - \rho_m} + h_o\left(\frac{\rho_c - \rho_c'}{\rho_c'} - \frac{\rho_c - \rho_c'}{\rho_c' - \rho_m}\right) \tag{4.18}$$

if we have ρ_m=3500 kg m^{-3} , $\rho_{c'}$=3100 kg m^{-3}, ρ_c=2900 kg m^{-3}, this leads to

$$H' = H + \frac{H}{2} - h_o \frac{35}{62} = H + \frac{H - h_o}{2} - h_o \frac{2}{31} \tag{4.19}$$

This expression shows that a higher value than 2900 kg m^{-3} (assumed by Neumann et al. [2004]) for the crust, will reflect a deeper crustal root. Therefore, using a density of 3100 kg m^{-3} would imply a crust, where we have large roots, 16.5% thicker than the one determined with the values used to build the model.

Under the southern region of Tharsis (Syria and Solis Planum) the mean crustal thickness is ~80km [Neumann, et al, 2004] so, a crustal density of 3100 kg m^{-3} would imply a crust (80-45)/2-45*2/31 = 17.5 – 2.9 = 14.6 km thicker. Therefore, we built the model M7 with a mean crustal thickness of ~94.6 km, which means ~18% thicker than the other models.

General Heat source

We used values for the concentration of radioactive heat sources in the present primitive mantle of 1.38 × 10^{-8} W m^{-3} [Treiman et al., 1986, see also chapter 4.5.1 the value obtained for the elements concentrations], which these authors estimated from the concentration of incompatible elements in SNC-meteorites [e.g., Dreibus and Wanke, 1982; Treiman et al., 1986]. For a density of 3500 kg/m3, this give about 3.94 10^{-8} W kg^{-3}.

As it was described in chapter 1, and because of the generally young crystallization ages of the Martian meteorites, they are believed to have originated in either the Tharsis plateau or Elysium rise [McSween, 1994]. From the known half-lives and the rates of heat release of these elements [see Chapter 4.5.1], an initial heat production density of the primitive mantle of Q_0 = 1.385 x 10^{-8} W/m^3 is obtained.

The crust is also homogeneously enriched in radioactive elements compared to the primitive mantle by an enrichment factor, Λ equal 5, on our Models M2, M3, M6 and M7. As seen in Table 4.6, the corresponding enrichment factors of the crust are varying indeed from 2.7 to about 5.53 for the SNCs.

			Earth	Shergotite	Nakhla
	Heat production		Concentration		
U238	9,37E-05		2,55E-08	1,15E-07	5,16E-08
U235	5,69E-04		1,85E-10	8,35E-10	3,74E-10
Th232	2,69E-05		1,03E-07	3,90E-07	7,14E-10
K40	2,79E-05		3,29E-08	9,01E-10	1,98E-07
			6,18E-12	2,18E-11	1,06E-11
Ratio with respect to Earth				3,52E+00	1,71E+00
Ratio with respect to "Mars mantle"				5,53E+00	2,69E+00
3,94E-12					

TAB 4.6 - *Heating values of the SNCs.*

The basis for this enrichment comes from the fact that the heat source density in the mantle Q_m decreases with time due to the decay of radioactive elements and as a consequence of the irreversible transfer of mantle heat sources to the crust. The crustal enrichment factor is assumed to be constant. The silicate mantle of Mars is thought to be peridotitic in composition, similar to the Earth's mantle [e.g., Basaltic Volcanism Study Project (BVSP), 1981; Sohl and Spohn, 1997]. The first liquid formed upon melting is basaltic, which is enriched in radiogenic elements with respect to the primitive mantle [e.g., BVSP, 1981]. By further melting, the mantle becomes depleted in this component [Breuer and Spohn, 2006].

The actual crustal enrichment factor for present-day Martian conditions will be indeed due to the initial general heat source from radioactive elements contribution accresced to its heat decaying factor along time (see Figure 4.1) related to an assumed mean crust and mantle densities.

Heat flux

We used a constant mantle heat flux q of 0.012 Wm^{-2} [Treiman et al., 1986] at the base of the elastic lithosphere, on Models M6 and M7, instead of a constant

temperature value of 1073 K, for the same depth. On Model MSL we also used q of 0.012 Wm^{-2}.

4.3.7. Subdomain and Boundary settings for Models M1-M7 and MSL

In the Model M1 (Table 4.7), the control model, there's no crustal enrichment. In M2 (Table 4.8) there's crustal enrichment, Λ=5, due to partial melting, and the value for heating is the present value. In M3 (Table 4.9) there's crustal enrichment and a radiogenic heating are 10% higher (correspondent to ~550 Ma ago, as shown on the graphic of Figure 4.1). M4 (Table 4.10) assumes the same as M1 however the radiogenic heating is dependant of the assumed mass density. In M5 (Table 4.11) there's no crustal enrichment but the crustal conductivity is reduced. Therefore, M1-M5 models allow identifying the effect of the different variables. M6 and M7 (Table 4.112) assemble all the effects for 550 Ma ago and takes into account the crust and mantle densities. Finally, MSL (Table 4.113) corresponds to a model assuming a stagnant-lid till 300 km deep. Temperatures' maps obtained for each parameter variation (Models M2-M7 and MSL), at several depths, are shown in Figures 4.5-4.12.

TAB. 4.7 – *Subdomain and boundary settings used in the model M1*

PARAMETER	DESCRIPTION	VALUE
C_p	Heat capacity ($JKg^{-1}K^{-1}$)	1000
k	Thermal conductivity ($Wm^{-1}K^{-1}$)	k_c=3* K_m=3*
Q_H	General Heat source (Wm^{-3})	$1.378e^{-8}$
T	Temperature at -150 km (K)	1073
T_0	Temperature at the surface (K)	220

TAB. 4.8 – *Subdomain and boundary settings used in the model M2*

PARAMETER	DESCRIPTION	VALUE
C_p	Heat capacity ($JKg^{-1}K^{-1}$)	1000
k	Thermal conductivity ($Wm^{-1}K^{-1}$)	k_c=3* K_m=3*
Q_H	General Heat source (Wm^{-3})	Crust = $5*1.378e^{-8}$ Mantle = $1.378e^{-8}$
T	Temperature at -150 km (K)	1073
T_0	Temperature at the surface (K)	220

TAB. 4.9 – *Subdomain and boundary settings used in the model M3*

PARAMETER	DESCRIPTION	VALUE
C_p	Heat capacity ($JKg^{-1}K^{-1}$)	1000
k	Thermal conductivity ($Wm^{-1}K^{-1}$)	k_c=3* K_m=3*
Q_H	General Heat source (Wm^{-3})	Crust = $5*1.378e^{-8}*1.1$ Mantle = $1.378e^{-8}*1.1$
T	Temperature at -150 km (K)	1073
T_0	Temperature at the surface (K)	220

TAB. 4.10 – *Subdomain and boundary settings used in the model M4*

PARAMETER	DESCRIPTION	VALUE
C_p	Heat capacity ($JKg^{-1}K^{-1}$)	1000
k	Thermal conductivity ($Wm^{-1}K^{-1}$)	k_c=3* K_m=3*
Q_H	General Heat source (Wm^{-3})	$1.378e^{-8}$
H	Radiogenic heating per mass (Wkg^{-1})	Crust: $4.4e^{-12}$ Mantle: $3.94e^{-12}$
T	Temperature at -150 km (K)	1073
T_0	Temperature at the surface (K)	220

TAB. 4.11 – *Subdomain and boundary settings used in the model M5*

PARAMETER	DESCRIPTION	VALUE
C_p	Heat capacity ($JKg^{-1}K^{-1}$)	1000
k	Thermal conductivity ($Wm^{-1}K^{-1}$)	k_c=1.5 K_m=4
Q_H	General Heat source (Wm^{-3})	$1.378e^{-8}$
T	Temperature at -150 km (K)	1073
T_0	Temperature at the surface (K)	220

TAB. 4.112 – *Subdomain and boundary settings used in models M6 and M7*

PARAMETER	DESCRIPTION	VALUE
C_p	Heat capacity ($JKg^{-1}K^{-1}$)	1000
k	Thermal conductivity ($Wm^{-1}K^{-1}$)	$k_c=2$ $K_m=4$
Q_H	General Heat source (Wm^{-3})	Crust = $5*1.378e^{-8}*1.1$ Mantle = $1.378e^{-8}*1.1$
H	Radiogenic heating per mass (Wkg^{-1})	Crust: $5*4.4e^{-12}$ Mantle: $3.94e^{-12}$
q	Constant Heat Flux at -300 km (Wm^{-2})	0.012
T_0	Temperature at the surface (K)	220

TAB. 4.13 – *Subdomain and boundary settings used in the model MSL*

PARAMETER	DESCRIPTION	VALUE
C_p	Heat capacity ($JKg^{-1}K^{-1}$)	1000
k	Thermal conductivity ($Wm^{-1}K^{-1}$)	$k_c=3$ $K_m=3$
Q_H	General Heat source (Wm^{-3})	$1.378e^{-8}$
H	Radiogenic heating per mass (Wkg^{-1})	Crust: $4.64e^{-12}$ Mantle: $3.94e^{-12}$
q	Constant Heat Flux at -300 km (Wm^{-2})	0.012
T_0	Temperature at the surface (K)	220

4.4 Data Analysis

For each of our presented Models (M1-M7 and MSL) it a comparative study of temperature differences between models is done. This allows us to study the effect of parameters variations such as the crustal enrichment in relation to the mantle, conductivity of the mantle, heat production rate, temperature at -150 km, and the presence of a stagnant lid.

Here we specifically calculate the contributions of heat conduction to the overall heat transfer rate through the lithosphere and assume for simplicity that the volcanic heat is completely lost to the surface [e.g., Breuer and Spohn, 2003].

4.4.1 Crustal Thickness Variations

Unlike the Earth, for the Martian crust there are no direct measurements of its thickness, so this interface depth must be assumed, based on several different models, as already said. Sohl and Spohn [1997], using geochemical arguments, estimated mean crustal thicknesses in the range of 100–250 km. Viscous relaxation arguments [Zuber, 2000; Nimmo and Stevenson, 2001] suggest that 50–100 km is the maximum thickness that could maintain hemispheric crustal variations against channel flow over Martian history. Wieczorek and Zuber [2004] suggest a 50 ± 12-km average thickness on the basis of a combination of several geophysical and geochemical studies. Turcotte et al. [2002] found higher (>90 km) crustal thickness surrounding the Hellas basin, but used a Cartesian approximation not referenced to the center-of-mass and neglected the non-Airy flexural signature of Tharsis. Following Zuber et al., [2000] it is thus assumed that the crust is basaltic, with a mean thickness of 45 km, consistent with global density models of large impact basins. We assumed this model to build the Moho altimetry, when changing the crustal density.

Moreover, and according to Wieczorek and Zuber [2004], a more “enriched” primary crust is likely to have been formed during the first ~30 Ma, leaving a more depleted mantle. This situation is likely to have occurred in about one third of the planet. Subsequent partial melting in areas of relatively recent volcanism, would

originate a secondary crust composed of these ancient "enriched" materials. This situation is likely to explain the present-day Tharsis crust.

The crustal thickness geometry, used in the presented Models M1-M6, varies from ~ 40–120 km, with the smallest values near the southwestern floor of Olympus Mons. As previously stated, the global mean thickness is about 43.5 km [Zuber et al., 2000] for the entire globe, although, for the Tharsis rise separately, it ascends the 50 km.

The crustal dichotomy is visible in our model by a local minimum at ~ 40 km, southwestern of Olympus (Figure 4.3). The Syria Planum region contribute with the largest deepest surface, with nearly all the crust thicker than 60 km, although, concerning isolated crustal roots, the biggest is under Arsia Mons (~110 km), followed by Ascraeus and Olympus Mons, both ~ 70 km, and Alba Patera with ~ 50 km. As also stated by Neumann et al. [2004], the southern highlands have a relatively uniform thickness, while the northern lowlands show a latitudinal dependent crustal thickness structure. The crust thickens effectively eastward of Olympus Mons, with the thickest crust corresponding to the Syria Planum and Claritas Fossae (western of Syria) structures on the Tharsis rise (Figures 4.3 and 4.4).

The transitions in crustal thickness between each of the major volcanoes of Tharsis are abrupt, while elsewhere the crust thickens more gradually. Figures 4.3 and 4.4 show that southwestern of Olympus the dichotomy boundary is compensated by a crustal thickness variation, with more pronounced relief along the Moho than at the surface.

Tharsis is surrounded by a roughly circular bulge ~6000 km in diameter straddling the equator and covering more than 1/6 of the planet [Zuber and Smith, 1997]. This province includes Alba Patera, Tempe Terra, Lunae Planum and the Olympus Mons aureoles in the north, and the Tharsis Montes, Daedalia, Syria, Sinai, Solis, and Icarius Planae in the south. Restricting to this circular region, the volume of this province is 1.5×10^9 km^3, of which 0.36×109 km^3 was required to form the Tharsis rise beyond that of the southern highlands [Neumann et al., 2004]. This volume places an upper bound on the amount of volcanic material emplaced by Tharsis formation [Phillips et al., 2001].

As referred by Anderson and Grimm [1998], occurrences of thin crust into the Tharsis region have a linear character which suggests tectonic control of these channeled regions.

4.4.2 Moho Depth Variations

Figures 4.3 and 4.4 show the Moho depth.

The depth from crust to mantle increases from the northwest of Olympus to the southeast of Syria (Figure 4.3). The deepest mantle occurs in southern Tharsis near Syria, reaching values close to 80 km, while the shallowest Moho lays southwestern of Olympus.

From Neumann et al. [2004], on his crustal model, neither Olympus nor Ascraeus or Pavonis Montes exhibit local compensation by deepening of the mantle. Their surface expressions were explicitly modeled as having denser surface composition; otherwise, they would exhibit crustal thinning. Their interiors may indeed be denser than the authors have assumed.

The broad Arsia and Alba volcanic features, or "domal rises", are supported mainly by depression of the crust-mantle boundary, and therefore did not require very thick lithospheric or dynamic support, unlike the Olympus Mons edifice [McGovern et al., 2002]. On the basis of surficial distribution of tectonic features, McGovern et al. [2002, 2004] suggested that these features were formed via intrusive sills with superposed volcanism.

4.4.3 Temperature Variations

The results of conductive heat models within the elastic crust of Mars are first presented for initial conditions similar to the crust and mantle (Model 1) (Figure 4.5 and Tables 4.14 – 4.17). The temperature graphics for each of the Models M2-M7 and MSL are shown in Figures 4.5 -4.12.

On Tables 4.14-17 it is given the maximum temperature at the centre of each Tharsis Mons and at the geometric centre of a considered single volcano in Syria Planum. From each of the studied models (M1-M7 and MSL) it is given the determined

temperature value at 10 km high, at z = 0 km, at -10 km, at -80 km and at -120 km. Also, it is given the temperatures variation, between 10 km and zero elevation, and between zero level and -80 km.

In general, there are only small differences, of less than 25 K in the mantle temperature between the various models.

A significant temperature increase below regions with thickened crust roots can be observed, although the location of the temperature maximum strongly depends on the parameters that we considered.

Temperatures in and below the crustal root are higher than in the surrounding regions (see graphics on Figure 4.13), although a vast area of crustal thickness does not imply higher temperatures, like we observe on Syria Planum.

An increase of few km of the crustal root thickness results in a temperature increase of some tens K, as it's observed on Figure 4.5 B, and on Table 4.15, above Arsia Mons, which root is the biggest of all Tharsis Montes. Thus, minor local crustal variations may have a significant effect on the local temperature distribution.

An important fact is that for smaller diameters of thickened crust, the largest temperature difference is located right at the base of the thickened crust (see Figure 4.5 for Arsia Mons).

Along Valles Marineris over a narrow portion of Coprates Chasma, temperature changes are easily observable, even if the chasm itself is considerably narrow (easternmost side trend on Figure 4.5).

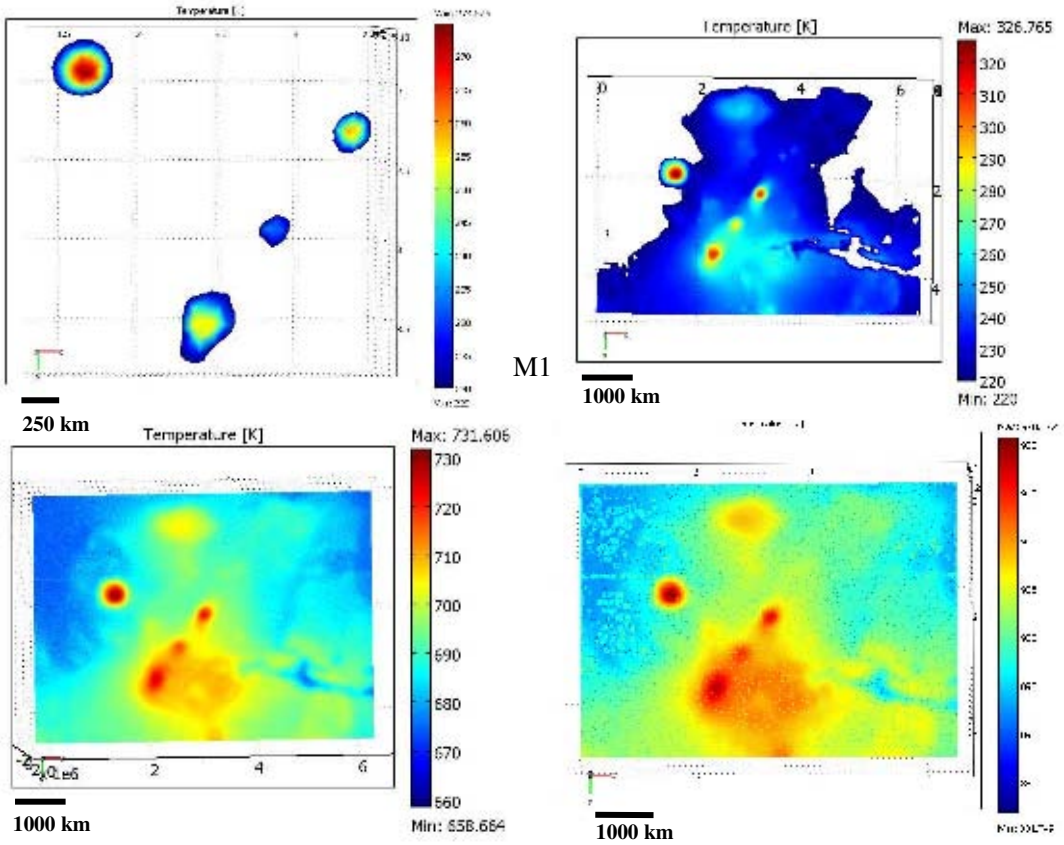

FIG 4.5 – *Calculated temperatures using Model M1 (with no parameters variation between crust and mantle). On the top left, temperatures are taken at 10 km high; top right at z=0 km; bottom left at -80 km; bottom right at -120 km.*

The influence of radioactive elements distribution between mantle and crust (the enrichment factor, i.e., the ratio of crustal heat sources and of heat sources in the primitive mantle) on the temperatures distribution is shown in Model 2 (Figure 4.6), for present/day conditions and on Model M3 for 550 Ma ago. With a total enrichment factor of approximately 5, obtained from SNC's composition, which is also representative for basaltic like material, the temperatures obtained in relation to the control model M1, increase of about 20-80 K for Model M2 and ~100 K with Model M3 (Tables 4.14-4.17).

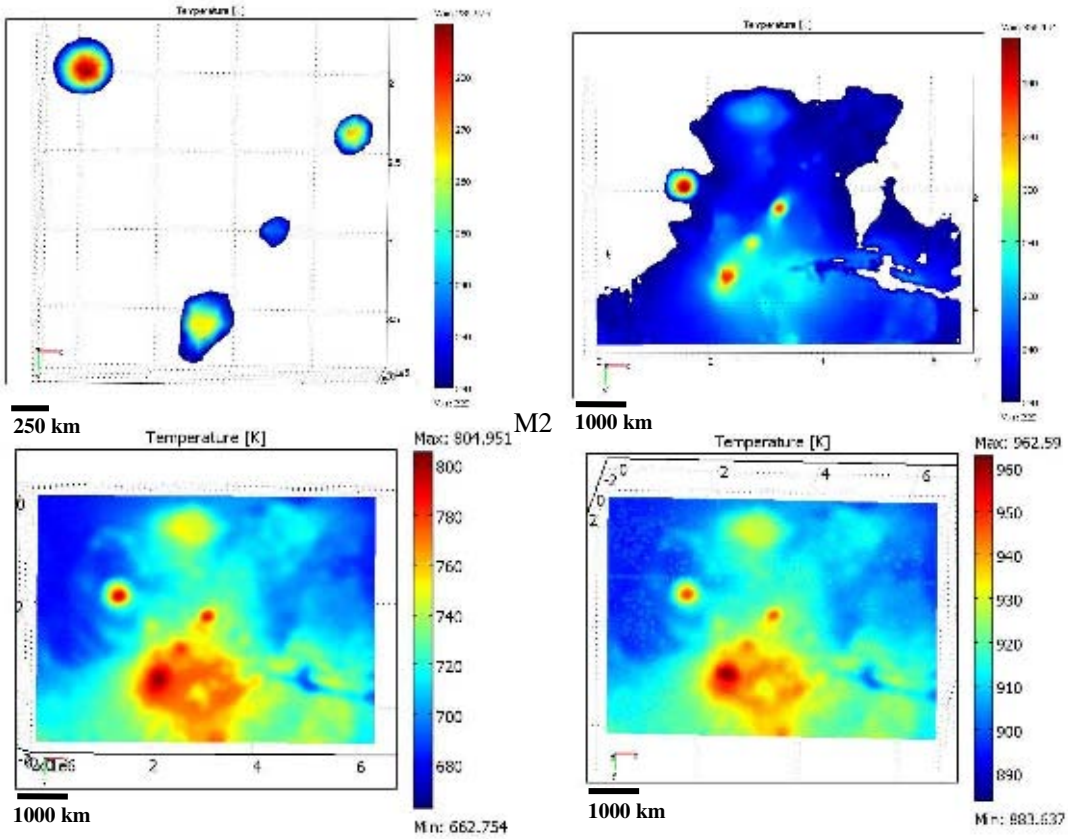

FIG 4.6 – *Calculated temperatures using Model M2 (with total crustal enrichment Λ~5, given by SNC's, at a present heat production).On the top left temperatures are taken at 10 km high; top right: at z=0 km; bottom left at -80 km; bottom right at -120 km.*

Assuming a crustal thermal conductivity lower than that of the mantle (Model M5), a variation of about 40 to 150 K is likely underneath thick crustal roots as observed for the Tharsis Montes (Tables 4.14-4.17). One can thus say that a big percentage of increasing temperature is due to thermal conductivity only.

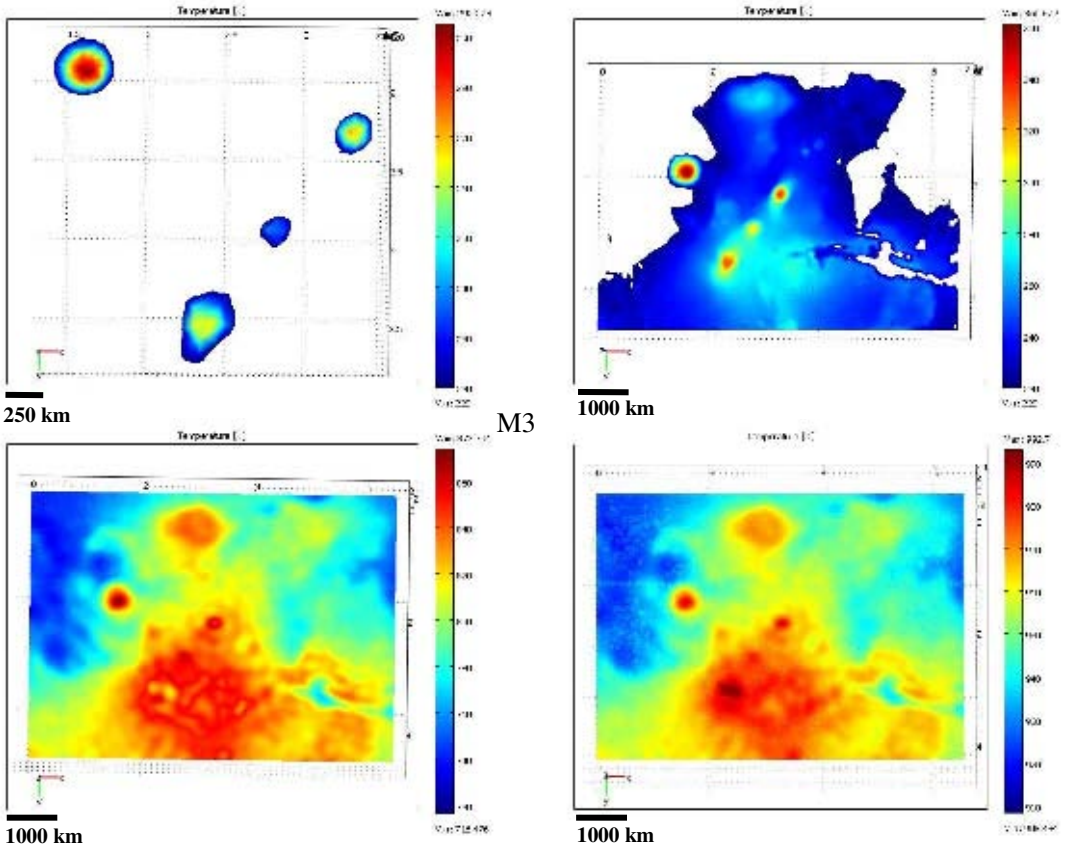

FIG 4.7 – *Calculated temperatures using Model M3 (with total crustal enrichment Λ~5, given by SNC's, and a heat production from ~550 Ma ago).On the top left temperatures are taken at 10 km high; top right: at z=0 km; bottom left at -80 km; bottom right at -120 km.*

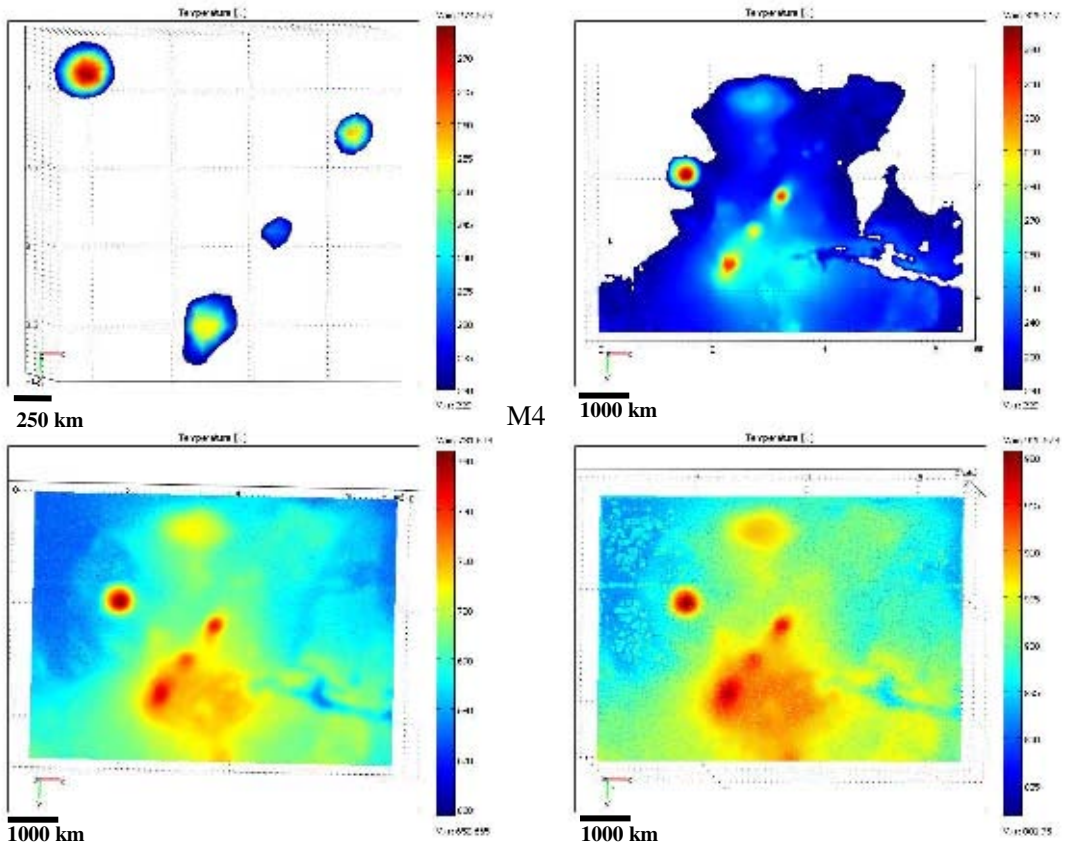

FIG 4.8 – *Calculated temperatures using Model M4 (with crustal enrichment concerning rocks density).On the top left temperatures are taken at 10 km high; top right: at z=0 km; bottom left at -80 km; bottom right at -120 km.*

The isotherm of 1073 K at -150 km represents the temperature of dominant mantle material, i.e. olivine, and provides, as mentioned above, an upper limit for the elastic lithosphere thickness. If the temperature at the base of the crust is equal or higher than 1073 K (like observed with Model MSL), the mantle below is ductile and does not contribute to the strength of the upper layer [Schumacher and Breuer, 2006]. Thus the rheologic behavior of the crust determines the elastic strength envelope, which is defined by a lower isotherm as compared to the mantle material. With Model MSL (Figure 4.10) we tested the temperatures increasing using a heat flux of 0.0012 W/m^2, at the base of the stagnant lid. It was obtained temperatures increasing of several tens K.

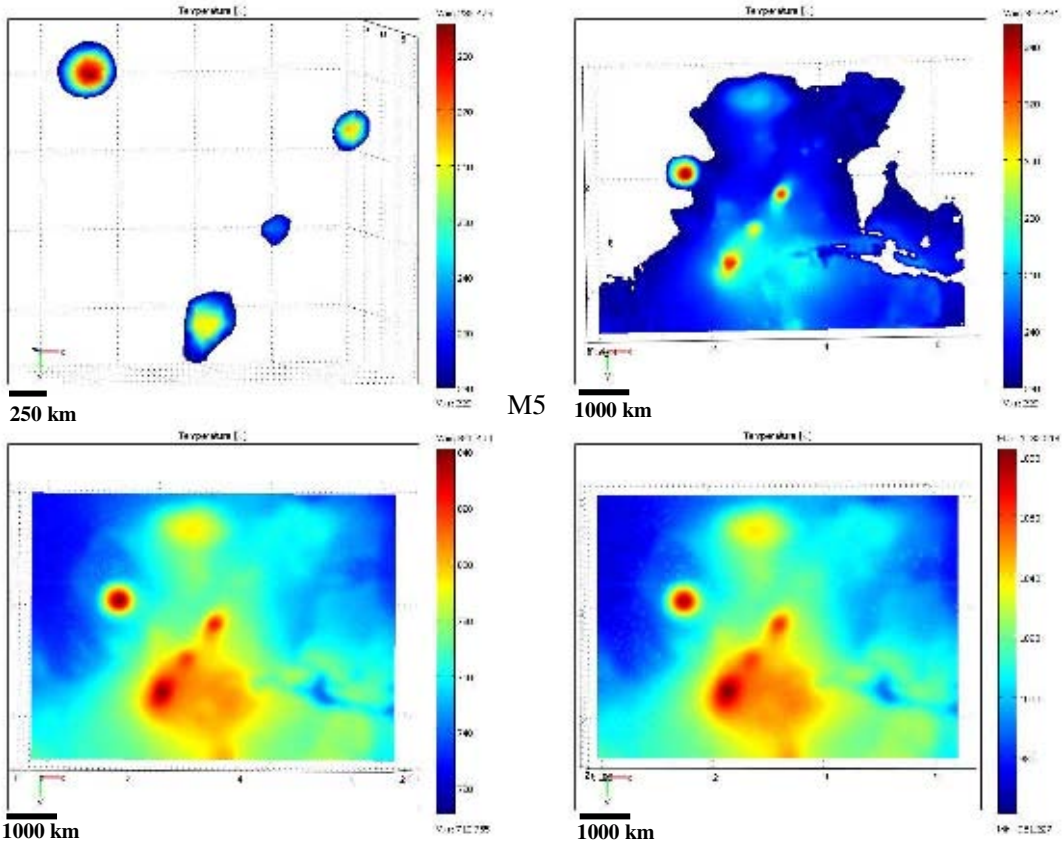

FIG 4.9 – *Calculated temperatures using Model M5 (with a less conductive crust, in relation to the mantle). On the top left temperatures are taken at 10 km high; top right: at z=0 km; bottom left at -80 km; bottom right at -120 km.*

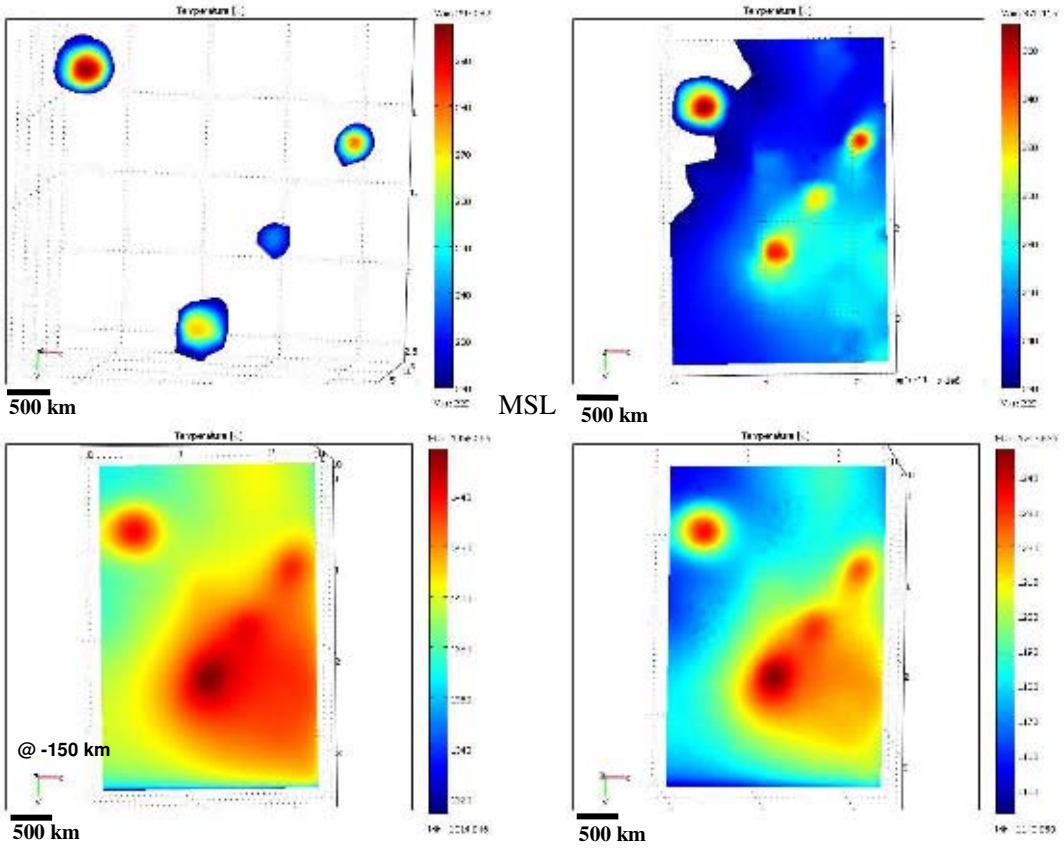

FIG 4.10 – *Calculated temperatures using Model MSL (with a stagnant lid).On the top left temperatures are taken at 10 km high; top right: at z=0 km; bottom left at -150 km; bottom right at -120 km.*

With Model M6 we integer all effects. An increased crustal thermal conductivity in relation to the mantle with an enrichment factor Λ=5 for the crust, for the conditions at ~500 Ma ago, resulted in temperatures increasing always up to 200 K (see Figure 4.11).

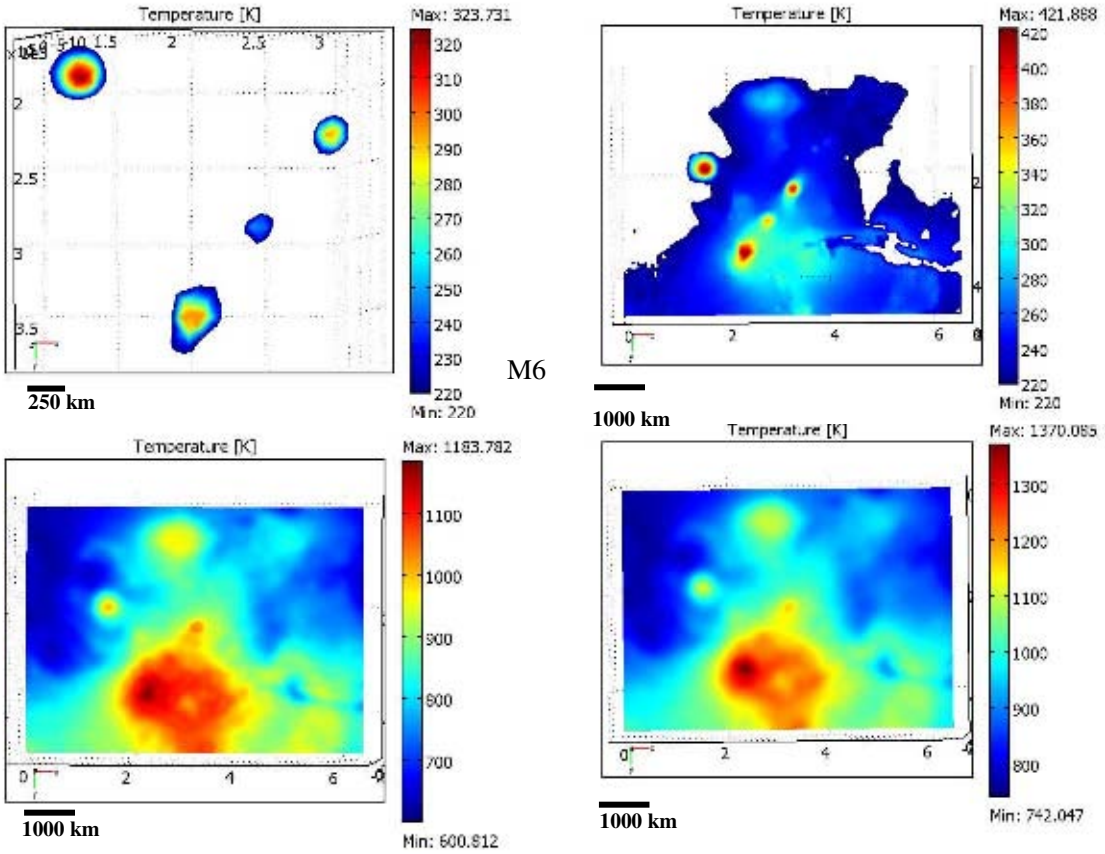

FIG 4.11 – *Calculated temperatures using Model 6 (with decreased thermal conduction, enrichment fact of Λ=5 on the crust and present heat production). On the top left temperatures are taken at 10 km high; top right: at z=0 km; bottom left at -80 km; bottom right at -120 km.*

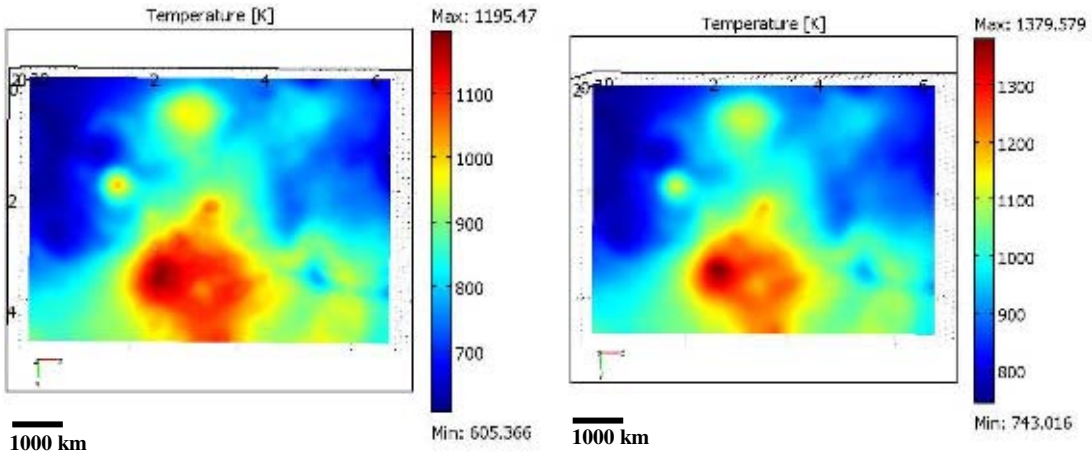

FIG 4.12 – *Calculated temperatures using Model 7 (using M6 parameters but ρ_c=3100* kg m^{-3}*). On the top left temperatures are taken at 10 km high; top right: at z=0 km; bottom left at -80 km; bottom right at -120 km.*

In the Tharsis Province, it can also be observed that the centre of Olympus Mons is warmer than the centre of the other volcanoes (Table 4.14). At z = -10 km, the warmest surfaces are on Olympus Mons.

Although, if we analyze the temperature increasing from -80 km to the surface (Tables 4.14 - 4.17), the highest increase is verified with Models M3 and M6, mostly in Olympus Mons, favoring the fact that its geometry is favorable of a good heat conductor.

As observed in Figures 4.5 - 4.11, the highest temperatures on Olympus Mons are located closer to the surface, if we compare with the other volcanoes, such as with Arsia Mons.

At – 80 km is at Syria Planum that the temperatures decrease the most (Table 4.17). So, the roots alone, like for the Tharsis Montes case are capable to originate more heat than the thick crust of Syria. By another way, at the surface z = 0, Syria Planum has the coldest surface.

The most significant factors for temperatures increase are: i) a topographic high, as represented by the higher temperatures around Olympus Mons, although; ii) the crustal roots thickness are an important factor of temperature variations on the lithosphere, for two reasons: first, it's around the Tharsis Montes Olympus roots that the

temperatures are significantly higher; second, as observed in Arsia Mons, the variation of temperatures between the surface and -80 km are higher than in the rest of the Tharsis bulge, which is implied by a deeper root; third, a deeper but also thick root, as observed on Syria, doesn't provide higher temperatures increasing iv) the lower thermal conductivity on the crust in comparison to the mantle has a significant influence on the temperatures increasing (Model M5), which accresced with a crustal enrichment in radiogenic sources (M6) favors the highest temperatures at the lithosphere of Tharsis. A most pronounced variation between crust and mantle thermal conductivities (k_c=1.5 and k_m=4) provides temperatures increasing of about 100 K, at -120 km (Figure 4.14). We note also in the figure that the Curie temperature is reached after depth of about 40 km below the zero altitude of MOLA, which is about half of the crust for Arsia Mons. As these volcanoes have been probably built by the superposition of lava flows and as very little thermal anomalies have been found in Tharsis, this thermal constraint shows indicate that about half of the Tharsis material were deposited after the cessation of the dynamo.

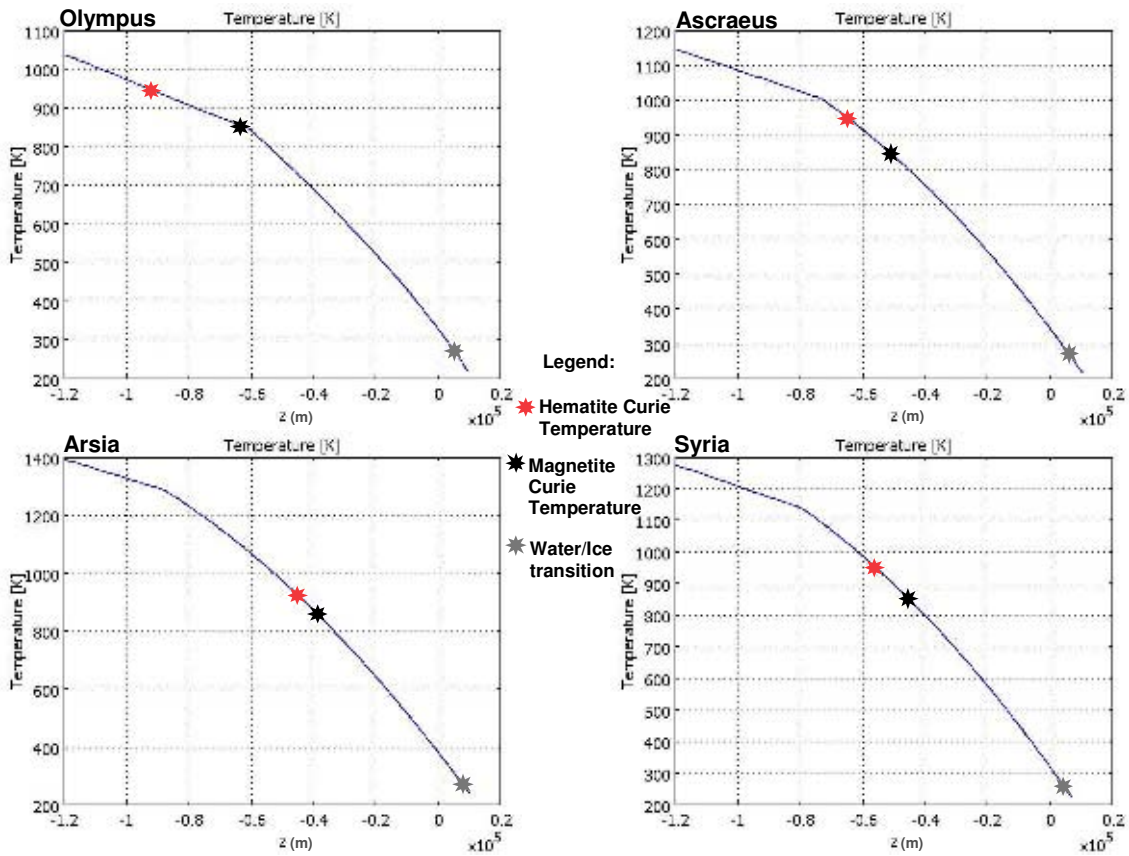

FIG. 4.13 – *Vertical Temperature profile along the Tharsis Volcanoes and Olympus Crustal roots. It is also shown the Curie temperatures corresponding to a single-domain magnetite (853 K) and to the hematite (943 K). In grey it's shown the depth for the transition ice-water. The brake in the profiles seems to correspond to the depth where there's the passage between a thicker crust and a crustal root.*

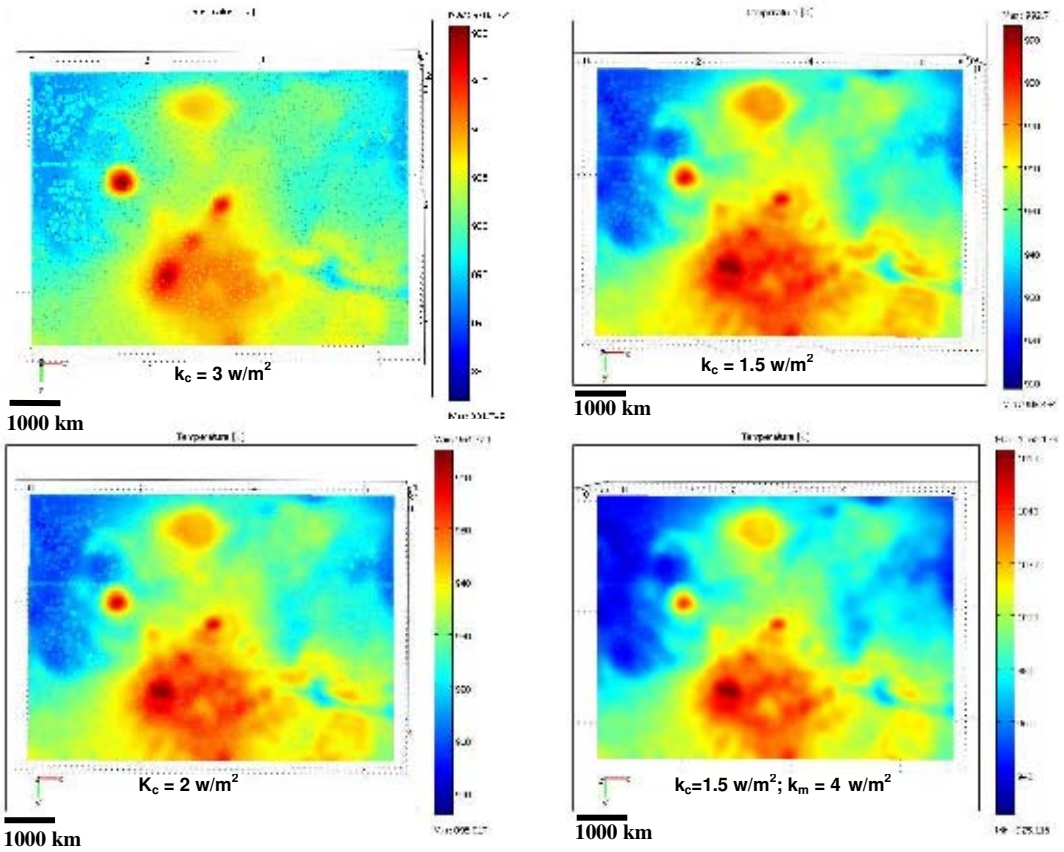

FIG 4.14 – *Temperature measurements between models with different Crustal thermal conductivities in relation to the mantle, at -120 km.*

TAB. 4.14 – *Maximum temperatures (K) measured at the centre of the Olympus Mons volcano, using Models M1-M6 and MSL (Model with stagnant-lid). Temperature differences at 0 km (difference between maximum temperatures at 10 km and 0 km) and -80 km (difference between maximum temperatures at 0 km and -80 km) are shown.*

Olympus	M1	M2	M3	M4	M5	M6	MSL
At 10 km	275	290	292	275	285	327	297
At 0 km	327	356	361	326	347	400	370
At -80 km	732	805	874	732	840	1100	980
At -120 km	951	963	993	921	1082	1250	1240
ΔT at 0 km	52	66	69	51	62	102	73
ΔT at -80 km	405	449	513	406	493	700	610
q at the base (W/m^2)	0.0129	0.011	0.010	0.0129	0.008	0.012	0.012

TAB. 4.15 - *Maximum temperatures (K) measured at the centre of the Arsia Mons volcano, using Models M1-M6 and MSL (Model with stagnant-lid). Temperature differences at 0 km (difference between maximum temperatures at 10 km and 0 km) and -80 km (difference between maximum temperatures at 0 km and -80 km) are shown.*

Arsia	M1	M2	M3	M4	M5	M6	MSL
At 10 km	255	265	265	255	260	290	270
At 0 km	310	340	350	305	325	420	350
At -80 km	725	787	860	725	840	1180	988
At -120 km	918	955	990	918	1080	1374	1248
ΔT at 0 km	55	75	75	50	65	90	80
ΔT at -80 km	415	447	520	420	515	760	638
q at the base (W/m2)	0.0131	0.010	0.009	0.0130	0.007	0.012	0.012

TAB. 4.16 - *Maximum temperatures (K) measured at the centre of the Ascraeus Mons volcano, using Models M1-M6 and MSL (Model with stagnant-lid). Temperature differences at 0 km (difference between maximum temperatures at 10 km and 0 km) and -80 km (difference between maximum temperatures at 0 km and -80 km) are shown.*

Ascraeus	M1	M2	M3	M4	M5	M6	MSL
At 10 km	270	270	270	260	265	300	280
At 0 km	312	342	342	310	327	400	355
At -80 km	720	780	860	720	825	1110	980
At -120 km	915	945	980	915	1065	1300	1230
ΔT at 0 km	42	72	72	50	62	90	75
ΔT at -80 km	408	438	518	410	498	710	625
q at the base (W/m2)	0.0132	0.011	0.010	0.0131	0.008	0.012	0.012

TAB. 4.17 - *Maximum temperatures (K) measured at the centre of the Syria Planum volcanic region, using Models M1-M6 and MSL (Model with stagnant-lid). Temperature differences at 0 km (difference between maximum temperatures at 10 km and 0 km) and -80 km (difference between maximum temperatures at 0 km and -80 km) are shown.*

Syria	M1	M2	M3	M4	M5	M6	MSL
At 10 km	-	-	-	-	-	-	-
At 0 km	260	270	270	265	270	300	280
At -80 km	705	760	855	710	805	1000	870
At -120 km	910	940	980	910	1045	1150	1215
ΔT at 0 km	-	-	-	-	-	-	-
ΔT at -80 km	445	490	585	445	535	700	590
q at the base (W/m2)	0.0136	0.015	0.011	0.0136	0.009	0.012	0.012

4.4.4 Heat Flow Variations

The estimated thermal gradients may be converted to heat fluxes using Fourier's law (Equation 4.2).

The results from the 3D models (Figures 4.15 and 4.16 for the Model M1) show that the heat flow beneath regions with higher crustal thickness is not diminished, but equal or even slightly enhanced compared to surrounding areas, like we observe in the Tharsis Montes.

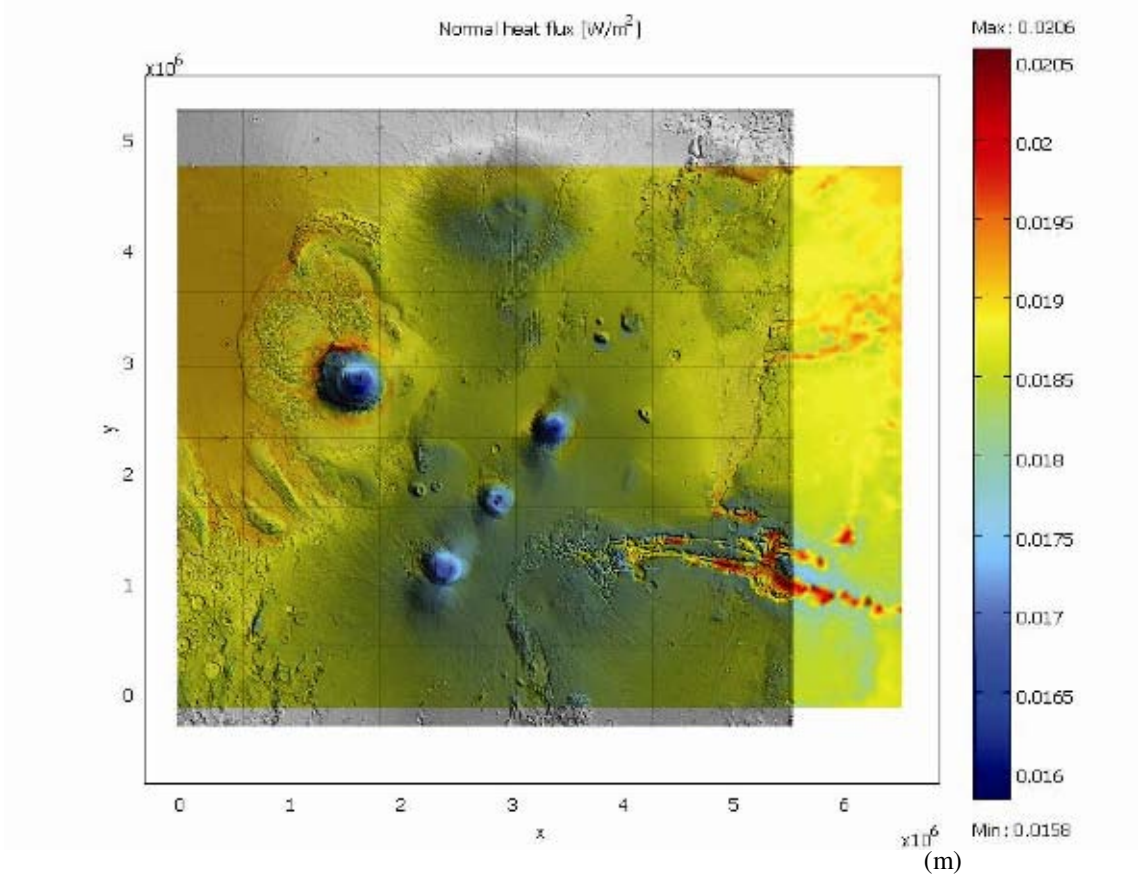

FIG. 4.15 - *Normal heat flux calculated at the Tharsis volcanoes' surface using Model M1.*

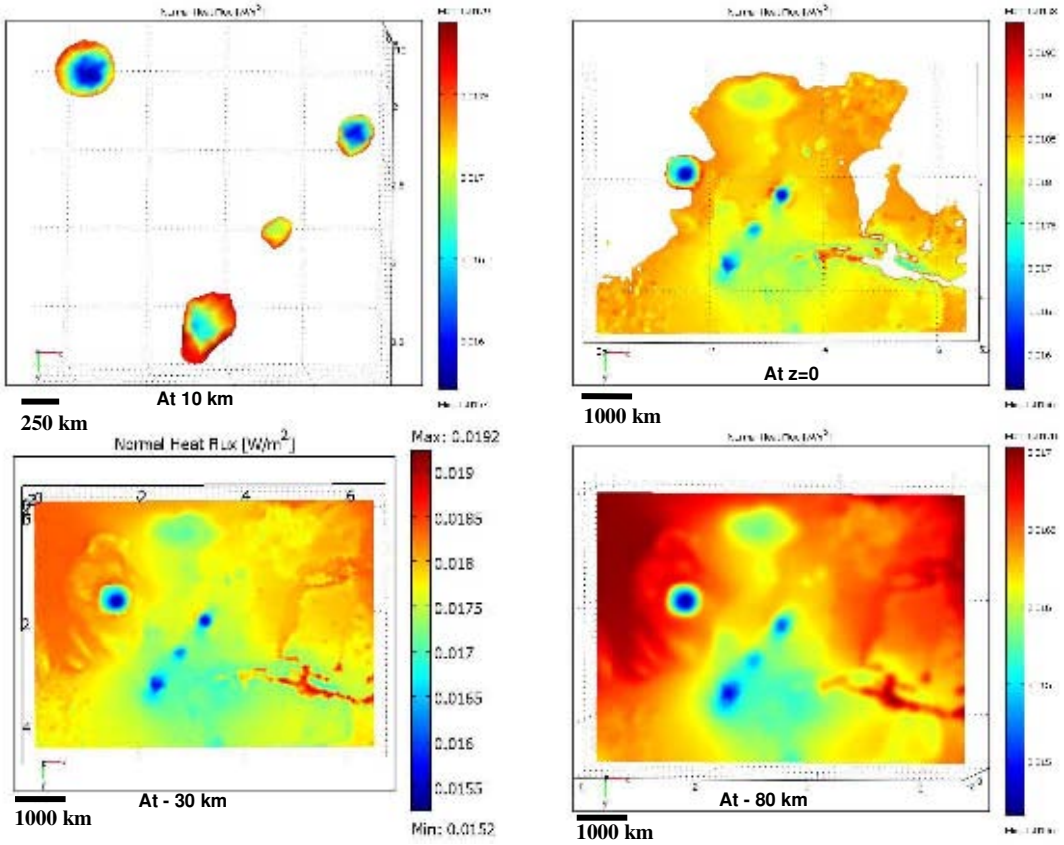

FIG. 4.16 - *Normal heat flux calculated for four different depths on the Tharsis lithosphere, using Model M1.*

Although, as also observed during this chapter, even with about the same size of crustal thickness, at the surroundings of Olympus or at the surroundings of Arsia, Ascraeus or Syria, the heat distribution is rather different. It is around the Olympus main volcano that one can find the highest heat elevation. One can say that lateral heat propagation between a big crustal root and a thinner crust is possible, as confirms Olympus Mons studies.

In order to evaluate the effective heat flow inside or outside the given volcanoes, it was checked the ratio *R* of the heat flow at the centre of the volcano to the heat flow at the borders' volcano surface, which is equal to:

$$R = \frac{\phi_{centre}}{\phi_{borders}} = \frac{h-r}{c} \cdot \frac{k_c(d-c)+k_m c}{k_c(r-d)+k_m(h-r)} \tag{4.20}$$

where k_c is the conductivity of the crust; k_m the conductivity of the mantle; d the depth of the elastic lithosphere ($d < 0$ following the orientation of the z-axis); r the depth of the root of the volcano ($r < 0$); c the depth of the crust without the root ($c < 0$); h the elevation of the volcano ($h > 0$).

Using Equation (4-20) we verify that by the volcanoes' geometry we wait that the heat flow at the centre of Tharsis volcanoes should vary from 79 - 98 % (from Olympus to Syria, respectively) (see Table 4.18) of the heat flow outside of it (so the heat flow at the centre of the volcano should be 79 - 98 % of the heat flow outside of it). This is also the right explanation for the fewer heat flow at the centre of the volcanoes.

Moreover, and using Model M6, the expected heat inside the volcano will be 73% for the Olympus Mons or 85% and 75% for Arsia and Ascraeus Montes, respectively, revealing a big percentage of heat at the surface of Olympus, unlike Syria Planum, that would keep inside about the same heat as when using the Model 1 (97%).

TAB. 4.18 – *Determination of R - Percentage of heat flow at the centre of the volcano, for z = 0 (equation 4.1) using Model M1 and comparing with the heat flow using Model M6.*

	Olympus	Arsia	Ascraeus	Syria
d (km)	-150	-150	-150	-150
r (km)	-70	-110	-70	-80
c (km)	-40	-70	-60	-80
h (km)	22	18	18	6
R using M1	79%	92%	81%	98%
R using M6	73%	85%	75%	97%

TAB. 4.19 – *Percentage of heat flow at the centre of the volcano (in relation to its surroundings) using Model 1 at four different depths.*

M1	Olympus	Arsia	Ascraeus	Syria
at 10 km	90%	94%	93%	-
at 0 km	79%	92%	81%	98%
at -30km	79%	92%	82%	98%
at -80 km	86%	94%	90%	98%

In Table 4.19 the heat flow variations of *R* only depend on the topography of the feature (as it is used Model 1). One can say that in an elevated high (at 10 km) the heat is almost the same inside and outside of the volcano (90-94%), reaching a maximum with the proximity of the highest point of the volcano, which seems obvious.

Although what seems interesting is that at the surface level (at 0 km), the highest single volcano is capable to keep a certain temperature gradient around it, which proves the highest heat flux around the surface of Olympus, Ascraeus or Arsia, for example. Also, in depth (at -30 km), the heat differences are remarked; higher heat variations in depth for higher volcanoes. For Syria Planum, which has a mean maximum of 6 kilometers high, no remarkable heat flux differences are noted on the surface or beneath the volcano (the amount of heat is almost the same inside and outside the volcano).

Finally, and as has been suggested and demonstrated in this work, the surface heat flux is relatively smaller at the top of the volcanoes. Moreover, as has been already discussed and shown by Neukum et al., [2004] or Schumacher and Breuer [2007], geologically recent lavas may have erupted at the Tharsis province around its main volcanoes and near Olympus Mons. The cooling rate of these lavas should provide a heat flux that would increase the one calculated during this work. The emplacement of surface lava flows heats the underlying crust till a certain depth, which can be determined by the Curie temperatures of the magnetic minerals [Johnson and Philipps, 2005]. The Curie isotherm (see Figure 4.13) may linearly correspond to the most recent flow thickness. With the conditions given by Model 7, the graphics in Figure 4.13 predict a depth to the Curie isotherm at ~60 km from the top centre of the Olympus

Mons, ~ 40 km for Arsia Mons, ~ 50 km for Ascraeus Mons and ~ 45 km for the Syria Planum geometric center. These depths may correspond to the base of a geologically more recent crustal layer. The Curie temperatures used here correspond to single domain magnetite (Curie temperature at 853 K [Johnson and Philipps, 2005]) and to hematite (Curie temperature at 943 K [Johnson and Philipps, 2005]). The results reveal a thicker recent volcanic layer when it's used hematite.

4.5 Topographic Correction to the Heat Flux

The results of conductive heat models within the elastic crust of Mars were first presented for initial conditions similar to the crust and mantle (Model 1), so with this model we can test the effect of the topography only.

To measure the effect of the present Tharsis topography on the heat flow determination, a topographic correction is then needed, i.e. to evaluate the presence/absence of a topographic high on the surface heat determination.

The perturbation of a vertical heat flow field induced by topography has been an important issue in interpretations of geothermal data [e.g. Jeffreys, 1983; Kohl, 1999; Turcotte and Schubert, 2002].

We used the method developed by Turcotte and Schubert [2002] in order to evaluate its impact on the Tharsis province of Mars.

As stated by Turcotte and Schubert [2002] have presented an analytical treatment for a sinusoidal topography, which may be a good approach to the Tharsis topography, which demonstrates the influence of different parameters to the subsurface temperature distribution.

Assuming a flat rectangle with a sinusoidal surface temperature variation calculated from the true sinusoidal topography, Turcotte and Schubert [2002] showed that the amplitude of the perturbation is reduced exponentially with depth. In the case of an isothermal surface, whose surface altitude variation has wavelength λ (the rectilinear distance from the beginning of a high till the end of a valley), the temperature variation at depth z is proportional to the factor $\exp(-2\pi z/\lambda)$, i.e. a topographical variation at surface with an amplitude A = 1.5 km and λ = 20 km would have been reduced to an

approximately 0.12 K amplitude in 30 km depth. (With heat flow at z = 0 of 0.012 Wm^{-2} and k = 3 Wm^{-1} K^{-1}). The correspondent heat flow that would have existed at 30 km depth if there was no topography will be of ~ 0.01 mWm^{-2}.

As expected, for a given depth, the influence of the topography on the temperature is much more significant for larger-wavelength or larger topographical amplitudes. Turcotte and Schubert [2002] predict an exponential decrease of the depth range of a topographical perturbation with decreasing wavelength.

It is essential to note that the depth at which the topographically induced temperature perturbation disappears is determined by the amplitude of the valley height (minimum elevation) and not by the mean topographical altitude [Kohl, 1999]. One can effectively observe (see Tables 4.14-4.17) that the temperatures difference from the highest top of Syria Planum (that is an uniform volcanic high plateau) till the base of its crustal root (at ~ - 80 km) vary less then at the same highs for volcanoes Olympus, Arsia or Ascraeus. It means that an isolated high would interfere more in the heat flow than several coupled highs. This is an important conclusion that we take from this work; the temperature contribution of isolated highs like Olympus Mons, Arsia Mons or Ascraeus Mons is more important than the contribution of several "coalesced" highs, like those on Syria Planum, for lateral variation in the temperature.

The difference in heat flow profiles taken in the plains (e.g. in Syria Planum or the plains between Olympus and the Tharsis Montes) (Figure 4.15 and 4.16), are in the range of 0.05 to 0.1 mW m^{-2} (using the Model M1).

On the other hand, if we measure the heat flux between a minimum and a maximum elevation (at the volcanoes' surface and at z = 0) (Table 4.20), which represent the topographic influence, we can observe that in steeper topographies, (like Olympus Mons, or the Tharsis Montes) the heat flow variations will increase much more, from 0.4 to 1.5 mWm^{-2} (using the control Model M1, or 1.6 to 3.1 mWm^{-2} using Model M6) (Table 4.20 and Figures 4.17-4.18, respectively).

Moreover, the difference between heat flow measurements taken at maximum and minimum elevation increases at surface but decreases quickly below that depth (see *q* at -30 km on Table 4.20). These observations also show a decrease of the temperatures range with depth, of a topographical perturbation, with decreasing

wavelength (see on Table 4.18 that the heat flux under and above the zero level on Syria Planum keeps the same, in comparison to Olympus Mons that shows wider rages of heat).

TAB. 4.20 - *Heat flow determination (W/m^2) using M1, at 3 different depths.*

M1	Olympus	Arsia	Ascraeus	Syria
q at surface	0.0159	0.0166	0.0160	0.0182
q at 0 km	0.0156	0.0161	0.0156	0.0177
q at -30 km	0.0152	0.0160	0.0153	0.0172
q at -80 km	0.0146	0.0150	0.0152	0.0157

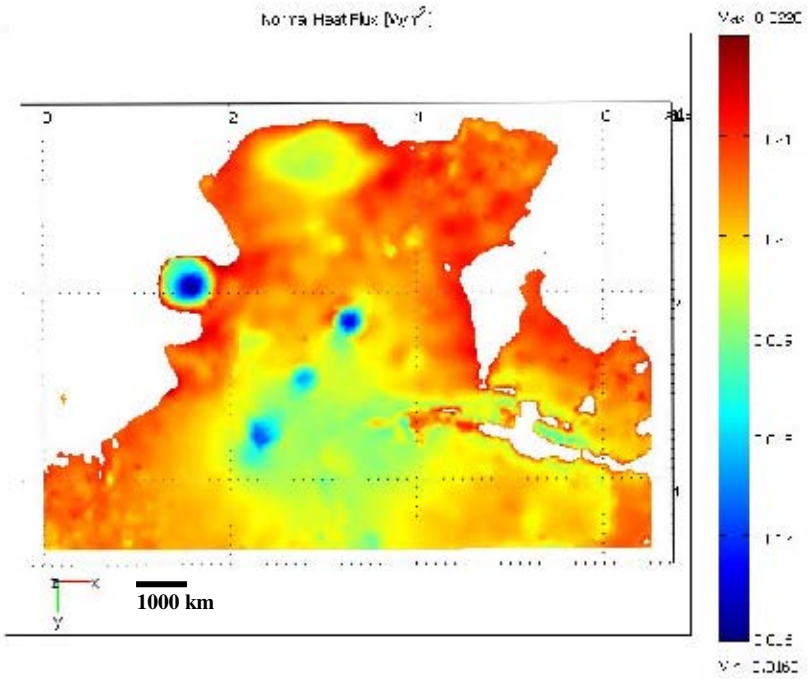

FIG. 4.17 – *Normal heat flux calculated at z = 0 using Model M6.*

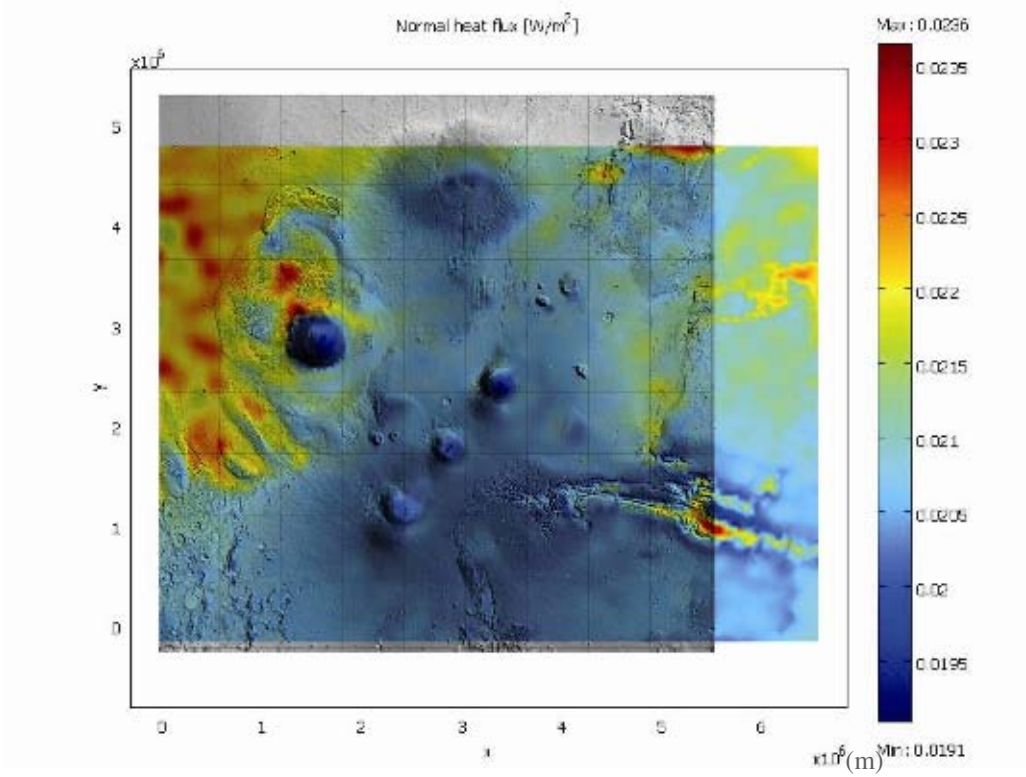

FIG. 4.18 – *Normal heat flux calculated at the Tharsis volcanoes' surface using Model M6.*

4.6 Discussion of the obtained Results

Estimates of the temperatures may be obtained by applying the conductive heat flow model on the elastic lithosphere of the Tharsis region on Mars.

It should be first underlined that the steady state regime doesn't take into account the heat lost due to the cooling of the planet (see development of Equations 4.2 - 4.4). Therefore, the temperatures obtained by the presented models are only minimum temperatures, once they are only associated to the steady state regime. According to topography and gravimetry data from Zuber et al., [2000] and taking into account the presence of a global magnetic field in the early Mars [Connerney et al., 2004] it is accepted by some authors [e.g. McEwen et al., 1999; Head et al., 2001; Zuber, 2001; Frey et al., 2002; Frey et al., 2002; Solomon et al., 2005; Breuer and Spohn, 2006] that the bulk of the crust (primordial and secondary) formed during the Noachian with possibly widespread volcanic activity also from the Hesperian [Head et al., 2002] or

even till a recent geological past [Neukum et al., 2004]. Before reaching a steady-state (thermal equilibrium), Mars initial transient evolution, as stated by Choblet and Sotin [2001], include the referred initial stage with intensive volcanism, resulting in the depletion of the upper mantle and consequent radiogenic enrichment of the crust, followed by a cooling stage and a transient convective stage. This effect would imply a mean global cooling that can be measured by an instantaneous cooling of a semi-infinite half-space equation [Turcotte and Schubert, 2002]. This solution maybe obtained by Equation 4.2, where it is applied a semi-infinite half space defined by y>0, and whose surface experienced an instantaneous change in temperature. Initially at t = 0, the half-space has a temperature T_1; for t>0, the surface y = 0 is maintained at a constant temperature T_0. As a result, heat is transferred into the half-space if $T_0>T_1$, and the temperature increases. If $T_1>T_0$, the half-space cools, and its temperature decreases. So, the temperatures distribution is the solution of Equation 4.2 subject to the conditions

$T=T_1$ @ t=0, y>0

$T=T_0$ @ y=0, t>0

$T\rightarrow T_1$ as $y\rightarrow\infty$, t>0

Resolving the problem in the way that

$$-\nabla(k\nabla T_0) = Q(t) \tag{4.21}$$

$$-\nabla(k\nabla T_1) = Q(t)\rho C\frac{\partial T_0}{\partial t} \tag{4.22}$$

$$-\nabla(k\nabla T_2) = Q(t)\rho C\frac{\partial T_1}{\partial t} \tag{4.23}$$

(…)

$$\text{So that } T_n \rightarrow T_{n-1},\ \frac{T_{n+1}-T_n}{T_n} \rightarrow 0 \tag{4.24}$$

Considering, as it was said, that Mars underwent a major change of thermal state 4 Ga before present, this would imply a mean global cooling of ~100 K (considering model M1 parameters conditions, and temporal heating described in chapter 4.2). So, Mars would now have cooled by an average of ~100 K from its former peak. This heat should though be considered as a factor for our underestimated heat results. Moreover,

Choblet and Sotin [2001] demonstrated that the transient periods may have been longer on Mars, which would have signified more input in our heat values.

We can then estimate the cooling effect contribution (term $-\rho C\frac{T_1 - T_2}{t_1 - t_2}$ on the Equation 4.2) to a period for example between 500 Ma (t_1), (see Figure 1 in annexes) and 600 Ma (t_2) (see Figure 1 in annexes), where, ρ=3100 kgm^{-3}, C=1000 JKg^{-1}K^{-1}, and T_1=1379.046 K, T_2=1381.245 K. So, the resulting heat due to the cooling effect is 4.80 x10^{-9} Wm^{-3}, which, considering the general heat source for the steady-state regime Q=1.38x10^{-8} Wm^{-3}, confirms the fact that the obtained heat values are indeed minimum estimations. Hence, these results show that the heat due to the radioactive decay effect is ~34% of the general heat, for this period of time. So, taking into account the cooling effect of the planet, we applied the procedure described in Equation 4.9 - 4.10. Figure 2, in annexes, shows the temperatures field of Model 7, for 500 Ma and for 600 Ma, accounting with the cooling effect. For the same time frame, and if it's taken into account the cooling effect on the general heat Q, this would result in temperatures increase (comparing to Model M7 without cooling effect) of about 40 K. Continuing with the procedure till the present-time (see details in annexes), we'll obtain a temperatures field that will permit partial melt at ~1.3 GPa. This situation is represented by Model Mc in Figure 4.19. In order to validate the cooling effect on the general heat, it was evaluated the convergence of the calculated temperatures for Arsia Mons on the last 1000 Ma. The radiogenic heating for each period of time was obtained from Figure 4.1. In annexes, it is shown the Table 1 where it can be observed that after some iterations the temperatures variation $T_{n+1} - T_n$ is less than 5 K, which verifies the convergence.

As it was already stated, for the steady state case, the estimated thermal gradients may be converted to heat fluxes using Fourier's law. However, care should be taken due to the uncertainties connected to the choice of parameters. Namely, the value of the thermal conductivity *k,* that strongly depends on material properties like porosity and water content, mostly at the surface. Taking into account thermochemical models [e.g. Breuer and Spohn, 2006; Schumacher and Breuer, 2007] and the presence of a top

layer of poorly conducting megaregolith [Clifford, 1993; Squyres et al., 1994] we adopted a column of crustal thermal conductivity of k = 3 W m^{-1} K^{-1}, for the base model. We made then it varies for Models M5, M6 and M7.

We then discuss the parameters that most influence an increasing temperature on the lithosphere and surface of Mars. We then made vary the several parameters and analyzed how the temperature difference evolves with the thickness of the crustal roots, with the conductivity differences, with the radiogenic heating and with the thickness of the lithosphere. Also, the same can be made with constant bottom heat flow rather than constant bottom temperature. This procedure made us build the 3D-models M1-M7, shown on chapter 4.3. The procedure can also serve as a guide to decide which 3-D numerical simulation could be relevant. The proposed 3D-Model M6 is the result, which was then used to justify the observable surface morphologies around Tharsis volcanoes.

It is clear that the temperature determined at the zero elevation in the volcano will be higher than the surface temperature (at the zero elevation) outside the volcano. This lateral thermal gradient will induce a heat flow in the horizontal direction, and then an increase of the temperature in the normal section of the crust in the vicinity of the volcano. As a result, an increase of the heat flow in the vicinity of the volcano can be expected.

As it can be observed by our results: (1) there are weak temperature variations where there are no lateral variations of crustal thickness, although the existence of a crustal thickness root is the principal factor of temperature variations on the lithosphere (see Tables 4.14 – 4.17 where in Arsia, the temperatures variation at the surface and at -80 km is higher than in the rest of the Tharsis bulge). A thick crust alone is not able to contribute to higher temperatures elevation (as observed for Syria Planum; (2) a lower crustal thermal conductivity compared to the mantle seems to have more influence in the temperatures increasing at the surroundings of the Tharsis and Olympus Volcanoes (temperatures obtained with Model M5); (3) in addition to a lower crustal thermal conductivity compared to the mantle, another parameter which influences a temperature increase is the higher concentration of radioactive heat sources (Model M3), although with less influence than the thermal conductivity; (4) as demonstrated by topographical

corrections, the depth at which the increase of temperature induced by a topographic high is noted, is given by the amplitude of the valley height and not by the mean topographical altitude. This situation gives arguments for the importance of crustal peaks for the temperatures increase. One can effectively observe that at 120 km depth, the increase due to the larger crustal root of Arsia is larger than the topography effect of Olympus. It means that an isolated high would interfere more in the heat increase than several coupled highs. This is an important conclusion that we take from this work; the contribution for a temperature increase of isolated highs like Olympus Mons, Arsia Mons or Ascraeus Mons is more important than the contribution of several "coalesced" highs, like those on Syria Planum, for the local temperatures increasing.

With our Models M1-M7 and MSL, we find a temperature increase of several tens K below the volcanic peaks when compared to the surroundings. Knowing that the rate of crust growth is a function of temperature, which must be above the solidus in the upper mantle, this lateral temperature variation maybe sufficient to produce locally partial melt in-between the elastic part of the lithosphere, in the case of a wet mantle conditions (see Schumacher and Breuer, [2006] or Medard and Grove, [2006] for mantle solidus curves) on present day thermal conditions. Although, this statement needs some further discussion: Assuming the maximum depth of our models (-150 km), with Models M1-M5, the maximum temperature reached at -120 km is ~ 800ºC, so under the solidus curve for the Martian mantle (see Figure 4.19), and consequently under any melt possibility. Even though, the melting processes are probable to occur in the upper part of the mantle at 500 Ma ago if we consider Model M6 and at the present considering a model with a stagnant lid (Model MSL). Once with the Model M6 we can reach temperatures of ~1100ºC at ~1.3 GPa, the solidus curve can then be reached for these conditions (see graphic of Figure 4.19). Moreover, with Model MSL (Figure 4.10) the solidus curve can also be reached at -120 km deep. With M7 melting temperatures are also attended. However, care should be taken considering the models M6, M7 and MSL, once these models overpass the isotherm of 1073 K at -150 km, in several places of Tharsis, namely on Olympus or Arsia Montes. Considering a constant mantle heat flux of 0.012 Wm^{-2}, the observed temperature values must be taken with precaution. An

explanation for this fact is that the thickness of the stagnant lid limits somehow the depth from which the melt rises toward the surface. The melt content below the large volcanic regions but also the temperatures in crust and upper mantle in these regions are enhanced compared to surrounding areas in Model MSL, with a stagnant lid, making it thus significantly easier for melt to rise to the surface.

Using a one-dimensional steady state heat conduction equation, we can determine the temperature variation as a function of the crustal thickness variations. An increase in crustal thickness by 20 to 30 km compared to an average crustal thickness of 50 km can thus cause a temperature increase of about 100 to 150 K, at the base of the stagnant lid (Model MSL) or even at pressures around 1.3 GPa (Models M6 and M7). For the first case (Model MSL) assuming a constant heat flow from the mantle at the base of the stagnant lid, and for the second case (M6), assuming a basaltic crust enriched in radioactive elements and a less thermal conductive crust, in relation to the mantle, which is likely to occur (e.g. Clifford and Fanale, 1985; Schumacher and Breuer, 2006).

The cases of Olympus Mons and Arsia Mons flanks recent volcanism sets in this situation. At the level of the elastic lithosphere isotherm, the temperature increase is already some tens K. As a consequence, partial melt can be generated locally underneath the thickened, low conducting crust. Moreover, Schumacher and Breuer [2006] confirm that the melt transported toward the surface may be refill by material from the convecting part of the mantle which may melt and rise again and that allows a continuous generation of melt underneath these volcanic regions. This situation may explain the longstanding and recent volcanism in Tharsis without the need of a giant plume underneath, for the present Martian conditions. As also observed, the highest temperatures on Olympus Mons are located closer to the surface, if we compare with the other volcanoes, like with Arsia Mons. This supports also the possibility of existing several small magmatic chambers close to surface of Olympus, and the intense volcanic activity on the slopes of Olympus Mons [e.g. Neukum et al., 2005; Bleacher et al., 2007]. This situation accords with the determined depths of the Curie temperature; it's in Olympus that a thicker more recent volcanic layer exists (~ 60 km of flow thickness). Moreover, and according to Figure 4.12, the passage from water to ice is attempted at

lower altitudes (closer to the zero surface) in Olympus than in any other studied volcanoes. Furthermore, the higher elevation of Olympus Mons, in comparison with the Tharsis Montes or Syria Planum, induces more favorable conditions for important daily thermal amplitudes around the volcano.

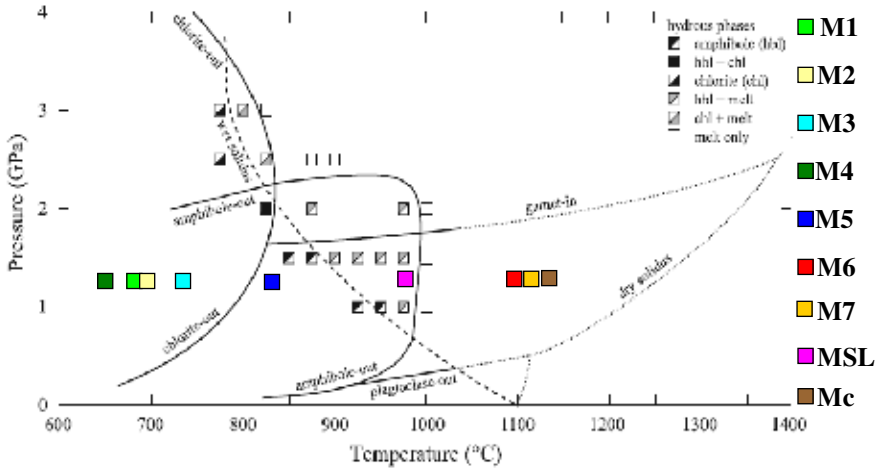

FIG. 4.19 – *Experimental water-phase relation for a primitive mantle + crust Martian composition, from Medard and Grove [2006]. Dry solidus is from Bertka and Holloway [1994], garnet-in curve is from Koga [2000], and low-pressure amphibole-out curve is from Lykins and Jenkins [1992]. The shape of the chlorite-out reaction has been modified by Medard and Grove [2006] from Jenkins and Chernosky [1986] and Pawley [2003]. The solidus is reached, at ~120 km (~ 1.3 GPa), for present-day conditions considering a conductive heat flow model with a stagnant lid (MSL) and for approximately 550 Ma ago considering models M6 and M7. Mc is the model, for the present-day, in which the cooling effect is taken into account on the general heat calculation.*

Another important assumption that can be taken from these simulations concerns the thermal gradients on rifts. The thermal gradient in the Noachian period has been previously constrained for rift terrains, namely in Thaumasia, by Schultz and Watters [2001] and McGovern et al. [2004]. These authors obtained dT/dz = 14 – 20 and >20 K km^{-1}, respectively. The discrepancy to the lower value of dT/dz = 5 – 15 K km^{-1} found for the Claritas Fossae, located between Syria Planum and the Tharsis Montes, may be

attributed, at least partly, to the later (Hesperian to Amazonian ?) resurfacing of the Tharsis volcanic surfaces, or even to possible recent volcanism. This situation also evidences later volcanism in the Tharsis area.

4.7 Conclusions

As observed during this chapter, the surface heat distribution is rather different in the surroundings of Olympus Mons, Ascraeus, Arsia Montes or Syria Planum, even if they have about the same crustal size. It is around Olympus Mons volcano that one can find the highest heat elevations.

It can be assumed that lateral heat propagation between a big crustal root and a thinner crust is possible, as confirmed by these studies, and observed on Olympus Mons, for instance. However, the heat propagation it's rather more difficult beneath a large uniform thick crust, like the one in Syria Planum. Despite the early existence of plume-fed flows beneath the Tharsis region, the lateral heat flow between two different thickened crusts may explain the surface features around volcanoes like Olympus Mons, at the present-day Martian conditions.

This lateral heat flow is enhanced by a changing of materials properties, namely between crust and mantle. The lower thermal conductivity of crustal material in comparison to mantle material is supported by several thermochemical models [e.g. Breuer and Spohn, 2006; Schumacher and Breuer, 2007]. We observed that the thermal conductivity of the crust, accresced with a radiogenic crustal enrichment, is of great importance for the crustal formation of Mars. It may also helps to explain the observed recent volcanism and/or the existence of features related to temperature increases underneath and close to the surface of large volcanic regions like Olympus Mons, or the Tharsis Montes. It maybe responsible to produce sufficient large temperature variations in combination with lateral variations in crustal thickness (existence of roots) which then may allow melt production underneath a thicker than average crust in contact with a more thermal conductive mantle.

4.8 Summary

Using 3D parameterized models of the heat conduction on the lithosphere of Tharsis, we may assume that the parameters that most influence the heat elevation on volcanic provinces are (1) a lower thermal conductive crust in relation to the mantle, (2) topographic highs, and fewer, (3) radioactive heat sources. Although the thermal conductive parameter has the most influence on the heat elevation, it is also constraint by the shape of the crust. A temperature increase is inhibited by a large thick crust, rather than by thin crustal roots. The first case is observed on Syria Planum and the second on Olympus and Tharsis Montes where a higher heat is observed on the surrounding of their crustal roots, particularly closer to the surface. The observed temperatures increasing were sufficient to permit a longstanding volcanic activity, as it is evidenced on the surface by fissure-fed flows or small shield volcanoes on the flanks of the Tharsis Montes (see chapter 3).

This study permitted to understand and give arguments in favor to the origin of a longstanding volcanic activity on the Tharsis Montes and Olympus Province, and moreover, to understand why Syria Planum volcanic region lost its capacity of keeping volcanic activity once it is formed by a great assemblage of significant volcanoes (see chapter 3), placed on the highest top of Tharsis.

Part IV – Discussion and Conclusions

5. Global Discussion from the Work developed during the PhD

Previous Viking and THEMIS studies have measured the physical characteristics of lava flows as a way to estimate parameters such as rheology and effusion rates on Mars [e.g. Zimbelman, 1998]. These studies are important for understanding the types and styles of volcanic eruptions that have occurred through time. However, with high spatial and spectral resolution data, particularly HRSC, MOC or HIRISE, we can now identify and analyze individual lava flows and small volcanic structures many of which have never been identified before. Such data make it possible to understand the geologic history of some volcanic terrains on Mars at the same spatial scale as many volcanic terrains on Earth. It also requires that we develop a variety of new techniques and refine some existing ones, which I did during my PhD thesis.

As part of my PhD I have deconvolved the complex volcanic history of Syria Planum on Mars by extracting topographic information from high-resolution stereo pairs obtained from HRSC. I used THEMIS, HIRISE and MOC images to help map the extent of major lava flows, identify source vents, and characterize the stratigraphy of an extremely active but short-lived volcanic episode. I identified and described a pattern of coalesced shield volcanoes, which, taking into account their morphological characteristics, have not been seen anywhere else on Mars. My analyses provided detailed information regarding the shape, geologic contacts, slopes, rheology, age, and morphology of the volcanic features in this area and placed this information into context with the surrounding tectonic pattern. The volcanic edifices in this region are in contact with extensive long and lobate lava flows and differ in relative age, rheology and morphology from the larger shield volcanoes. I demonstrated the fact that Syria Planum

was dominated by both swarms of small shields, and that a single, larger edifice was the source for the long lava flows.

Based on crater age dates and superposition relations, the volcanic activity in Syria Planum appears to have ceased early in Martian geologic history and subsequently moved northwest towards Tharsis. I speculated that a possible reason for this shift in volcanism may have been due to the high crustal thickness of the Syria Planum region. To test this hypothesis, I modeled the internal heat on the Tharsis Plateau and how it may have changed over time. This was accomplished by simulating the Martian crust in MATLAB creating several three-dimensional blocks that were based upon available MOLA topographic data and estimates of the crustal thickness [Zuber et al., 2000; Neumann et al., 2005]. The blocks were then subjected to a 3D steady-state conductive model to simulate the thermal conditions on Tharsis crust and upper mantle, with the use of COMSOL.

The first parameter I analyzed was the influence of topography and how it may have controlled the thermal and heat conditions through time. I also analyzed locations where there may have been variations in the crustal thickness and how this may have affected temperature and volcanic duration. It was observed that the volcanism ceased, during the early Hesperian in Syria Planum, probably due to a thicker than average crust. Therefore, secondary and less intense volcanic episodes may have possibly continued around the Tharsis "peaks". The causes for this longstanding volcanism on the Tharsis region are mainly due to differences in parameters' conditions between the Martian crust and mantle.

6. Conclusions

As shown in this work, Olympus Mons and the Tharsis Montes are big topographic highs compensated by deep crustal roots. Moreover, under the also high volcanic Syria Planum, the crust is therefore largely thick.

As stated by most of the thermochemical models for the Martian lithosphere, the crust is less conductive than the mantle, so impeding a preferential ascension of magma. Consequently, according to our observations, it's on the present northwestern flank of Olympus Mons, where there's a passage from a crustal root to a thin crust (with the consequent surface proximity of the mantle), that we observe the highest temperatures.

As demonstrated in this work, on Syria Planum, there were detected several particular assembled volcanic features, such as coalesced shield volcanoes in contact with long lobate shape lava flows. These volcanic eruptions may have stopped in the early Hesperian. From then on, on the surface of Syria Planum, there are no evidences for other secondary volcanic manifestations or for surface features related to local heat-increasing, such as those found on Olympus or Tharsis Montes. Furthermore, the thick less conductive crust under Syria may have conditioned the stall of volcanism in that zone. Underneath the Syria crust, the existing melt may have diffused on the lithosphere to the adjacent more conductive mantle, reaching closer the surface. These surfaces are located on the surroundings of the main Tharsis Montes and Olympus Mons.

6. Conclusions

Comme il a été présenté dans ce travail, Olympus Mons et les Tharsis Montes sont de grandes hauteurs topographiques, compensées par une croûte aux racines profondes. Sous la haute province volcanique de Syrie Planum, la croûte est également largement épaisse. De plus, comme indiqué par la plupart des modèles thermochimiques de la lithosphère de Mars, la croûte est moins conductrice que le manteau, empêchant ainsi une ascension préférentielle du magma. En conséquence, et selon nos observations, c'est sur le flanc nord-ouest de l'actuel Olympus Mons que nous observons les températures les plus élevées, au niveau du passage d'une racine de croûte à une croûte mince (avec en conséquence la proximité du manteau à la surface). Comme démontré dans ce travail, sur Syria Planum ont été détectées plusieurs figures volcaniques assemblées, telles que les volcans boucliers accolés en contact avec les longues coulées de laves de formes lobaires. Ces éruptions volcaniques se sont arrêtées dans le début de l'Hesperian. Depuis, sur la surface de Syria Planum, il n'y a eu aucune évidence d'autres manifestations volcaniques secondaires ou de la formation de formes liées à une augmentation locale de la chaleur, comme celles trouvées sur Olympus Mons ou Tharsis Montes. En outre, la croûte épaisse moins conductrice sous Syria a pu contribuer à la cessation du volcanisme dans cette zone. En-dessous de la croûte de Syria, le magma existant a pu se répandre à la lithosphère adjacente où le manteau est plus conducteur, et est arrivé près de la surface. Ces surfaces sont situées sur les environs des Tharsis Montes et d'Olympus Mons.

7. Work Perspectives based on the acquired knowledge during the PhD

As part of my post-doctoral fellowship at the Smithsonian Institution, I will conduct terrestrial analogue studies of small shield volcanoes found in Hawaii as a way of testing some of the hypotheses I put forward in my dissertation. There are two main objectives in which I would like to focus my work:

(I). Terrestrial Analogues Studies of Small Shield Volcanoes in Hawaii:

As part of my study, I would like to conduct analyses of some of the parasitic shield volcanoes located on Kilauea Volcano, Hawaii. I intended to use published historical observations, modern day field observations, analyses of remote sensing data, topographic analyses from 30-m Digital Elevation Models and measurements taken from Differential GPS instruments to characterize the textural and morphologic variability of flow fields and emplacement history associated with Mauna Iki and Mauna Ulu. These edifices are morphologically similar to low shield volcanoes found in Syria Planum and Tharsis Montes on Mars [Baptista et al., 2008; Bleacher et al., 2007]. Parasitic shield eruptions have contributed significantly to the growth of Kilauea, and they are closely associated with lava tube systems and long duration eruptions [Rowland and Munro, 1992].

From this information, I would attempt to map the surface and subsurface lava flows to better understand the evolution of these features and place their development into context with regional faulting patterns. The use of multiple remote sensing datasets and precise topographic and positional information, such as local emplacement processes, topographic controls, changes with distance from the eruptive vent, and local

superposition relationship, are important for interpreting flow fields construction and evolution. A comparative study of analogous volcanic systems is required for both Mars and Earth.

(II). Model of regional supply and recharge centers and processes for outflow.

Lava flow construction and lateral dike emplacement are the primary contributors to the subsurface structure of Hawaiian shield volcanoes and influence the locations of local groundwater systems [Buttner and Huenges, 2003]. Groundwater and geothermal gradient of Hawaii can also be characterized by:

(1.a) The Big Island is composed of five large volcanoes that create orographic effects resulting in dramatic microclimatic variations. For example, Kilauea is approximately 1400 m high, and receives approximately 175 cm of rain on the eastern flank and only about 15 cm on the western flank.

(1.b) Because it is surrounded by an ocean, salt water infiltrates into the fresh groundwater system. The effectiveness of this infiltration is influenced by local topography and climate.

(1.c) The presence of dikes, radial and circumferential to the main volcanic centers induces important changes in local porosity.

(2.) Numeric thermal models presented by Ribe and Christensen [1994, 1999] suggested there is no anomalous heat flow from the Hawaii mantle plume at the surface. However, drill holes near the center of the mantle plume [Buttner and Huenges, 2003] with conduction-dominated temperature measurements provided indications of heat flow anomalies associated with the larger volcanoes. Accurate modeling of the heat flow is required to better understand the thermal fields of the Island and describe its thermo-hydraulic field.

The scientific questions that are posed in this issue are:

(1) What are the heat flow anomalies on the surrounding of a high Hawaiian Mount like the Kilauea?

(2) What are the mechanisms for charging the groundwater system on the surrounding of this volcano and/or evidences for runoff?

(3) The relation between Kilauea's topography, heat flow and associated hydraulic system.

The methods I propose to use are:

(1) Knowing the heat properties of the subsurface Kilauea volcano, build a 3D model of heat conduction capable to explain its origin.

(2) Model the hydraulic system around the Kilauea volcano.

(3) Model for the circulation of water in the porous and permeable system.

The expected results are:

(1.) The influence of the topography in the hydraulic system close to a volcano; close to higher altitudes it is expected to find important groundwater-sapping systems and next to lower altitudes the materials transport at the surface is supposedly more important.

(2.) The heat flow generated on the base of a high-altitude volcano may have an important role on the water flow and sediments transport on its surroundings.

The knowledge I acquired doing models (1D to 3D) of heat flow conduction of the Martian lithosphere permits me to apply them now in a good Martian analogue. The study of the associated morphological surfaces is then the necessary tool used to justify the previewed modeling.

References

Acuña, M. H.; J. E. P. Connerney; P. J. Wasilewski; N. F. Ness; H. Reme; C. Mazelle; D. Vignes; R. P. Lin; D. L. Mitchell; P. A. Cloutier (1999). Global distribution of crustal magnetism discovered by the Mars Global Surveyor MAG-ER Experiment. *Science*. *284*, 790-793.

Alonso, M., e Finn, E. J. (2000) – *Física: um Curso Universitário*. Ed. Bras. Blücher, São Paulo.

Alves, E. I. (2003) – *Atlas do Sistema Solar*. http://www.uc.pt/iguc/did_planets.htm.

Anderson, S., and R. E. Grimm (1998), Rift processes at the Valles Marineris, Mars: Constraints from gravity on necking and rate-dependent strength evolution, *J. Geophys. Res.*, *103*(E5), 11,113–11,124.

Anderson, R. C., J. M.Dohm; M. P.Golombeck, A. F. C.Haldemann, B. J. Franklin, K. L.Tanaka, J. Lias and B.Peer (2001), Primary centers and secondary concentrations of tectonic activity through time in the western hemisphere of Mars, *J. Geophys. Res., 106* (E9), 20563-20586.

Anderson, R. C., J. M. Dohm, A. F. C .Haldemann, T. M. Hare and V. R. Baker (2004), Tectonic histories between Alba Patera and Syria Planum, Mars, *Icarus*, *171*, Issue 1, p. 31-38.

Andrews-Hanna, J. C., M. T. Zuber, and S. A. Hauck II (2008), Strike-slip faults on Mars: Observations and implications for global tectonics and geodynamics, *J. Geophys. Res.*, *113*, E08002.

Baker V. R. ; R. G Strom; V. C. Gulick; J. S. Kargel; G. Komatsu and V. S. Kale. (1991), Ancient oceans, ice sheets and the hydrological cycle on Mars. *Nature*, Volume *354*, Issue 6348, pp. 86-87.

Baker V. R. (2002), *Mars: Water and the Martian Landscape*. Encyclopedia of Astronomy and Astrophysics, Edited by Paul Murdin, article 5428. Bristol: Institute of Physics Publishing.

Banerdt, W. B.; Golombek, M. P.; Tanaka, Kenneth L. (1992), Stress and tectonics on Mars. *Mars*. p. 249-297.

Banerdt, J.W. Head; C.L. Johnson; F.G. Lemoine; P.J. McGovern; G.A. Neumann; D.D. Rowlands; S.J. Zhong (2000), Internal structure and early thermal evolution of Mars from Mars Global Surveyor topography and gravity. *Science*. *287*, 1788-1793.

Barabash, Stas; Fedorov, A.; Lundin, , R.; Sauvaud, J. (2007), Martian Atmospheric Erosion Rates, *Science*, *315*, Issue 5811, pp. 50.

Baratoux, D., C. Delacourt, and P. Allemand (2001) Digital Elevation Models derived from Viking images: Method and comparison to MOLA data, *J. Geophys. Res., 106*, 32,927-32,941.

Baratoux, D.; P. Pinet; M.J. Toplis; N. Mangold; A.R. Baptista (2008), Shape, rheology and emplacement times of small martian shield volcanoes. *Icarus (submitted)*.

Becker, R. H.; Pepin, R. O. (1984), The case for a Martian origin of the shergottites - Nitrogen and noble gases in EETA 79001 *Earth and Planetary Science Letters*. *69*, no. 2, Aug., p. 225-242.

Belleguic, V., P. Lognonné, and M. Wieczorek (2005), Constraints on the Martian lithosphere from gravity and topography data, *J. Geophys. Res.*, *110*, E11005.

Bertka, C. M. e F. Yingwei (1998). Implications of Mars Pathfinder Data for the Accretion History of the Terrestrial Planets. *Science*. *281*, 1838-1840.

Bertka, C. M., and J. R. Holloway (1993), Pigeonite at Solidus Temperatures: Implications for Partial Melting, *J. Geophys. Res.*, *98*(B11), 19,755–19,766.

Bleacher, J.E., R. Greeley, D.A. Williams, G. Neukum (2007), Morphometric characterization and comparison among the Tharsis Montes-related low shield and fissure vent fields, *38th Lunar Planet. Sci. Conf.*, abstract 1314.

Blasius, K.R. and J.A.Cutts (1976), Shield volcanism and lithospheric structure beneath the Tharsis plateau, Mars, *Lunar Science Conference, 7th*, Proceedings. Volume 3.

Bogard, D. D.; Nyquist, L. E.; Johnson, P. (1984), Noble gas contents of shergottites and implications for the Martian origin of SNC meteorites. *Geochimica et Cosmochimica Acta*, *48*, Sept., p. 1723-1739.

Breuer, D.; Yuen, D.A.; Spohn, T. (1997), Phase transitions in the Martian mantle: Implications for partially layered convection, *Earth and Planetary Science Letters, 148, Issues 3-4*, May, Pages 457-469, ISSN 0012-821X.

Breuer, D., and T. Spohn (2003), Early plate tectonics versus single-plate tectonics on Mars: Evidence from magnetic field history and crust evolution, *J. Geophys. Res.*, *108*(E7), 5072.

Breuer, D.; Spohn, T. (2006), Viscosity of the Martian mantle and its initial temperature: Constraints from crust formation history and the evolution of the magnetic field. Planetary and Space Science, Volume *54*, Issue 2, p. 153-169.

Carr, M. H. (1973), Volcanism on Mars, *J. Geophys. Res*., *78*, 4049-4062.

Carr, M.H. (1974), Tectonism and volcanism of the Tharsis region of Mars. *J. Geophys. Res.*, *79*, 3943-3949.

Carr, M. H. (1975), The Volcanoes of Mars. *Scientific American*, 234, 32-43.

Carr, M. H. (1979). Formation of Martian flood features by release of water from confined aquifers. *J. Geophys. Res.*, *84*, 2995-3007.

Carr, M. H. (1981), *The Surface of Mars*. Yale University Press, New Haven. Chapter *7*, pp. 87-113.

Carr, M. H. (1996), *Water on Mars*, Oxford University Press.

Carr, M. H., and J. W. Head III (2003), Basal melting of snow on early Mars: A possible origin of some valley networks, *Geophys. Res. Lett.*, *30*(24), 2245.

Cattermole, P. (1987), Sequence, rheological properties, and effusion rates of volcanic flows at Alba Patera, Mars, *J. Geophys. Res*., *92*(B4), E553-E560x.33.

Cattermole, P. (1990), Volcanic flow development at Alba Patera, Mars, *Icarus*, *83*, 453-493.

Chadwick , D. J., S. S.Hughes and S. E. H. Sakimoto (2004), Deflections In Lava Flow Directions Relative To Topography In The Tharsis Region Of Mars: Indications of Post-Flow Tectonic Motion, *Second Conference on Early Mars*.

Chevrier, V.; Rochette, P.; Mathé, P.; Grauby, O. (2004), Weathering of iron-rich phases in simulated Martian atmospheres. *Geology*, vol. *32*, Issue 12, p.1033.

Christensen P. R.; J.L.Bandfield; R.N.Clark; K.S.Edgett; V.E.Hamilton; T.Hoefen; H.H.Kieffer; R.O.Kuzmin; M.D.Lane; M.C.Malin; R.V.Morris; J.C.Pearl;

R.Pearson; T. L.Roush; Ruff, S. W. e M. D.Smith (2000). Detection of crystalline hematite mineralization on Mars by the Thermal Emission Spectrometer: Evidence for near-surface water. *JGR*. *105*, 9623-9642.

Christensen, P.R. (2003), Evidence for recent climate fluctuations on Mars - from cold to colder, *American Geophysical Union, Fall Meeting*, #P32B-01.

Christensen, P. R., and S. W. Ruff (2004), Formation of the hematite-bearing unit in Meridiani Planum: Evidence for deposition in standing water, *J. Geophys. Res.*, *109*, E08003.

Choblet, G. and C. Sotin (2001), Early Transient Cooling of Mars, *Geophys. Res. Lett.*, *28*(15), 3035–3038.

Cipa, A.; Bebien, J.; Bonin, B.; Brousse, .R.; Masson, P. (1996), Control of the basement structure of the Olympus Mons volcano morphology on Mars. Academie des Sciences (Paris), Comptes Rendus, Serie II - Mecanique, Physique, Chimie, Sciences de la Terre et de l'Univers, vol. *315*, no. 7, p. 801-806.

Cisowski, S.M. (1986). Magnetic studies on Shergotty and other SNC meteorites. *Geochimica et Cosmochimica Acta* (ISSN 0016-7037). *50*, June, p. 1043-1048.

Clifford, S. M.; Fanale, F. P. (1985), The Thermal Conductivity of the Martian Crust. *LPSC XVI*, PP. 144-145. Abstract.

Clifford, S. M. (1993), A Model for the Hydrologic and Climatic Behavior of Water on Mars, *J. Geophys. Res.*, *98*(E6), 10,973–11,016.

Comer, R. P., S. C. Solomon, and J. W. Head (1985), Mars: Thickness of the Lithosphere from the Tectonic Response to Volcanic Loads, *Rev. Geophys.*, *23*(1), 61–92.

Connerney, J. E. P.; M. H. Acuña; P. J. Wasilewski; G. Kletetschka; N. F. Ness; H. Rème; R. P. Lin e D. L. Mitchell (2001). The Global Magnetic Field of Mars and Implications for Crustal Evolution. *Geophysical Research Letters*. *28*, Issue 21, pp. 4015-4018.

Crown, D. A. and R. Greeley (1993), Volcanic geology of Hadriaca Patera and the eastern Hellas region of Mars, *J. Geophys. Res*, *98* (E2), 3431-3451.

Crumpler, L. S.; Aubele, J. C. (1978), Structural evolution of Arsia Mons, Pavonis Mons, and Ascreus Mons Tharsis region of Mars. *Icarus*, *34*, June , p. 496-511.

Davis, P.A. and K.L. Tanaka (1993), Small volcanoes in Tempe Terra, Mars: Their detailed morphometry and inferred geologic significance. *In Lunar and Planetary Inst., Twenty-fourth Lunar and Planetary Science Conference*. Part 1: A-F p 379-380.

Davies et al., (1992) *Celestial Mechanics and Dynamical Astronomy*, *53*, 377-397.

Davies, Geoffrey F. (1999). *Dynamic Earth*. Cambridge University Press.

Delacour, C.; N. Gros ; P. Allemand and D. Baratoux (2003) Online Mars Digital Elevation Model Derived from MOLA Profiles, *EOS*, *84*, No. 52

Dreibus, G.; H. Wanke (1982). Parent body of the SNC meteorites: chemistry, size and formation. *Meteoritics*. *17*, p.207.

Dohm, J.M.; R.C. Anderson; V.R. Baker; J.C. Ferris; R.G. Strom; J.W. Rice Jr.; D.H.Scott (2000). NorthwEstern Tharsis latent outflow activity Mars. *Mars Polar Science 2000*.

Dohm, J.M., K.L Tanaka and T.M. Hare (2001), Geologic map of the Thaumasia region of Mars. USGS Misc. Inv. Ser. Map I-2650 (scale 1:5,000,000).

Esposito, P. B.; Banerdt, W. B.; Lindal, G. F.; Sjogren, W. L.; Slade, M. A.; Bills, B. G.; Smith, D. E.; Balmino, G. (1992), Topography and Gravity. *Mars*. p. 209-248.

Fassett, C. I.; Head, J. W. (2006), Hesperian-aged Valleys on Martian Volcanoes: Snowmelt, Drainage, and Erosion on Ceraunius Tholus. *AGU Fall Meeting 2006*, abstract #P13D-03.

Fairén, Alberto G.; Dohm, James M.; Baker, Victor R.; de Pablo, Miguel A.; Ruiz, Javier; Ferris, Justin C.; Anderson, Robert C.Episodic flood inundations of the northern plains of Mars (2003), *Icarus*, Volume *165*, Issue 1, p. 53-67.

Fink, Jonathan H., James R. Zimbelman (1986), Rheology of the 1983 Royal Gardens basalt flows, Kilauea Volcano, Hawaii, *Bulletin of Volcanology*, *48*, p. 87-96.

Folkner, W. M.; C. F. Yoder; D.N. Yuan; E.M. Standish; R.A. Preston (1997). Interior structure and seasonal mass redistribution of Mars from radio tracking of Mars Pathfinder. *Science*. *278*: 1749-1752.

Forget, F.; Levrard, B.; Montmessin, F.; Haberle, R. M.; Head, J. W. (2005), Glaciers, ice mantling, gullies and polar caps on Mars: a model-based scenario for the Amazonian climates and geology. *AGU*. abstract #P34A-08.

Forget, F.; Haberle, R. M.; Montmessin, F.; Levrard, B.; Head, J. W. (2006), Formation of Glaciers on Mars by Atmospheric Precipitation at High Obliquity. *Science*, Volume *311*, Issue 5759, pp. 368-371.

Frey, H. (1979), Thaumasia - A fossilized early forming Tharsis uplift. *J. Geophys. Res.*, *84*, Mar. 10, p. 1009-1023.

Frey, H. V.; S. E. Sakimoto e J. Roark (1998). The MOLA topographic signature at the crustal dichotomy boundary zone on Mars. *Geophys. Res. Lett. 25***:** 4409-4412.

Greeley, R. (1973), Mariner 9 photographs of small volcanic structures on Mars, *Geology*, *1*, 175-180.

Greeley, R. (1977), Basaltic "plains" volcanism. *Volcanism of the Eastern Snake River Plain, Idaho: A Comparative Planetary Geology Guidebook*, NASA CR-154621, edited by R. Greeley, and J. S. King, pp. 23-44, NASA, Washington, D. C.

Greeley, R. and P. D. Spudis (1981), Volcanism on Mars, *Rev. Geophys. Space Phys., 19*, 13-41.

Greeley, R. (1982), The Snake River Plain, Idaho: Representative of a new category of volcanism. *J. Geophys. Res.*, *87*(B4), 2705-2712.

Greeley, R. and D. Crown (1990), Erratum: ``Volcanic geology of Tyrrhena Patera, Mars", *J. Geophys. Res.*, *95*, 7133-7149.

Gregg, T. K. P. and J. H. Fink (1996), Quantification of extraterrestrial lava flow effusion rates through laboratory simulations, *J. Geophys. Res*, *101*(E7), 16891-16900.

Grott, M. (2005), Late crustal growth on Mars: Evidence from lithospheric extension, *Geophys. Res. Lett.*, *32*, L23201.

Gulick, V. C. (1998), Magmatic intrusions and a hydrothermal origin for fluvial valleys on Mars. *J. Geophys. Res. 103*, Issue E8, p. 19365-19388.

Halliday, A.; Rehkämper, M.; der-Chuen, L.; Wen, Yi (1996), Early evolution of the Earth and Moon: new constraints from Hf-W isotope geochemistry, *Earth and Planetary Science Letters*, *142*, Issue 1-2, p. 75-89.

Harder, H. (1998), Phase transitions and the three-dimensional planform of thermal convection in the Martian mantle, *J. Geophys. Res., 103(E7)*, 16,775–16,797.

Harder, H. (2000), Mantle Convection and the Dynamic Geoid of Mars, *Geophys. Res. Lett.*, *27*(3), 301–304.

Hartmann, W. K (1973), Martian Surface and Crust: Review and Synthesis. *Icarus*, *19*, p.550.

Hartmann, W.K. (1973), Martian cratering: 4. Mariner 9 initial analysis of cratering chronology, *J. Geophys. Res*. *78*, pp. 4096–4116.

Hartmann, W. K.; Malin, Michael; McEwen, Alfred; Carr, Michael; Soderblom, Larry; Thomas, Peter; Danielson, Ed; James, Phillip; Veverka, Joseph. (1999), Evidence for recent volcanism on Mars from crater counts. *Nature*, Volume *397*, Issue 6720, pp. 586-589.

Hartmann, W. K. e D. C. Berman (2000.) Elysium Planitia lava flows: Crater count chronology and geological implications. *J. Geophys. Res. 105,* 15011-15025.

Hartmann, W. K., J. A. Grier, D. C. Berman and G. A. Esquerdo (2000), The Case for Youthful Geological Activity on Mars. American Astronomical Society, DPS Meeting #32, #58.02, *Bulletin of the American Astronomical Society*, *32*, p.1111.

Hartmann, W. K. and G. Neukum (2001), Cratering Chronology and the Evolution of Mars, *Space Science Reviews*, *96*, Issue 1/4, p. 165-194.

Hauber, E. and P. Kronberg (2001), Morphology and Topography of Fretted Terrain at the Dichotomy Boundary in Tempe Terra, Mars: General Characteristics. *J. Geophys. Res.*, *106*(E9), 20,587.

Hauber, E., J. Bleacher; D. Williams and R. Greeley (2007), Plains Volcanism on Mars revisited: The topography and morphology of low shields and associated volcanic landforms. *European Mars Science and Exploration Conference: Mars Express & ExoMars,* ESTEC, Noordwijk, The Netherlands.

Hauck, S. A., II, and R. J. Phillips (2002), Thermal and crustal evolution of Mars, *J. Geophys. Res.*, *107*(E7), 5052.

Head, J. W., III, M. A. Ivanov, H. Hiesinger, M. Kreslavsky, B. Thomson and S. Pratt (2000), Oceans in the Past History of Mars?: Evidence for Recession and Timing from MOLA Data. *31st Annual Lunar and Planetary Science Conference*, Houston, Texas, abstract no. 1750.

Head, James W.; Marchant, David R. (2003), Cold-based mountain glaciers on Mars: Western Arsia Mons. *Geology*, vol. *31*, Issue 7, p.641.

Hiesinger, H., J.W. Head, G. Neukum and HRSC Co-Investigator Team (2005), Rheological Properties of late-stage lava flows on Ascraeus Mons: new evidence from HRSC. *36st Annual Lunar and Planetary Science Conference*, Houston, Texas, abstract no. 1727.

Hiesinger, H.; J. W. Head and G. Neukum, (2007), Young lava flows on the eastern flank of Ascraeus Mons: Rheological properties derived from High Resolution Stereo Camera (HRSC) images and Mars Orbiter Laser Altimeter (MOLA) data. *J. Geophys. Res.*, *112*(E5).

Hodges, C.A. and H.J. Moore (1994), *Atlas of volcanic landforms on Mars*, U.S. Govt. Printing Office.

Hulme, G. (1976), The determination of the rheological properties and effusion rate of an Olympus Mons lava, *Icarus*, *27*, p. 207-213.

Hulme, G. and G. Fielder (1977), Effusion rates and rheology of lunar lavas, Philos. *Trans. R. Soc. London A*, *285*, 227-234.

Jeffreys, Harold (1983), The Disturbance of the Temperature Gradient in the Earth's Crust by Inequalities of Height. *Geophysical Journal International*, vol. *4*, issue s4, pp. 309-312.

Jenkins, D. M., and J. V. Chernosky (1986), Phase equilibria and crystallographic properties of Mg-chlorite, *Am. Mineral.*, *71*, 924–936.

Johnson, C.L. and R. J. Phillips (2005), Evolution of the Tharsis region of Mars: insights from magnetic field observations, *Earth and Planetary Science Letters, 230, Issues 3-4*, 15 February, Pages 241-254.

Karato, S.-I., M. S. Paterson, and J. D. Fitzgerald (1986), Rheology of Synthetic Olivine Aggregates: Influence of Grain Size and Water, *J. Geophys. Res.*, *91*(B8), 8151–8176.

Kiefer, W. S (2003), Melting in the martian mantle: Shergottite formation and implications for present-day mantle convection on Mars. *Meteoritics & Planetary Science*, *38*, Issue 12, Pages 1711-1875.

Knudson, J.G. and D.L. Katz (1979), *Fluid Dynamics and Heat Transfer*, 576 pp., Robert E. Krieger, Huntington, N.Y.

Kohl, T. (1999), Transient thermal effects below complex topographies. *Tectonophysics*, vol. *306*, issue 3-4, pp. 311-324.

Komatsu, G.; Ori, G. Gabriele; Ciarcelluti, P.; Litasov, Y. D. (2004), Interior layered deposits of Valles Marineris, Mars: analogous subice volcanism related to Baikal Rifting, Southern Siberia. *Planetary and Space Science*, v. *52*, iss. 1-3 [SPECIAL ISSUE], p. 167-187.

Koga, K. T. (2000), Kinetic processes of mantle minerals, *Ph.D. thesis*, Mass. Inst. of Technol., Cambridge, Mass.

Langlais, B., M. E. Purucker, and M. Mandea (2004), Crustal magnetic field of Mars, *J. Geophys. Res.*, 109, E02008.

Laskar, J.; Correia, A. C. M.; Gastineau, M.; Joutel, F.; Levrard, B.; Robutel, P. (2004), Long term evolution and chaotic diffusion of the insolation quantities of Mars. *Icarus*, Volume *170*, Issue 2, p. 343-364.

Li, H.; Robinson, M. S. (2003), Investigation of Lobate-Shaped Deposits in Eastern Acheron Fossae, Mars. *AGU Fall Meeting 2003*, abstract #P11B-1041.

Lillis, Robert J.; Herbert V. Frey, Michael Manga, David L. Mitchell, Robert P. Lin, Mario H. Acuna, Stephen W. Bougher (2008), An improved crustal magnetic field map of Mars from electron reflectometry: Highland volcano magmatic history and the end of the martian dynamo, *Icarus, 194, Issue 2*, April, Pages 575-596.

Lodders, K. (1998). A survey of SNC meteorite whole-rock compositions. *Meteoritics*. *33,* supl. pgs. 183-190.

Lognonné, P.; Mosser, B. (1993), Planetary seismology, *Surv. Geophys*., Vol. *14*, No. 3, p. 239 – 302.

Longhi, John; Knittle, Elise; Holloway, John R.; Waenke, Heinrich (1992), The bulk composition, mineralogy and internal structure of Mars. *Mars*, p. 184-208.

Lowrie, William (1997). *Fundamentals of Geophysics*. Cambridge University Press.

Lykins, R. W., and D. M. Jenkins (1992), Experimental determination of pargasite stability relations in the presence of orthopyroxene, *Contrib. Mineral. Petrol., 112*, 403– 413.

Malin, M. C. (1977), Comparison of volcanic features of Elysium (Mars) and Tibesti (Earth), *Geol. Soc. Amer. Bull*., *88*, pp. 908-919.

Masson, P. (1980), Contribution to the structural interpretation of the Valles Marineris-Noctis Labyrinthus-Claritas Fossae regions of Mars, Laboratorio di Astrofisica Spaziale di Frascati, *European Workshop on Planetary Sciences*, Rome, Italy, Apr. 23-27, 1979. Moon and the Planets, *22*, April, p. 211-219. Centre National de la Recherche Scientifique.

McEwen, A. S., M. C. Malin, M. H. Carr, and W. K Hartmann (1999) Voluminous volcanism on early Mars revealed in valles marineris, *Nature, 397*, 584-586,.

McGovern, G.; A.Neumann; D.D. Rowlands; S. Zhong (2000). Internal structure and early thermal evolution of Mars from Mars Global Surveyor topography and gravity, *Science*. *287*, 1788-1793.

McGovern, P. J., S.C. Solomon, D. E. Smith, M. T Zuber, M.Simons, M. A.Wieczorek, R. J. Phillips, G. A Neumann, O. Aharonson, J. W. Head, (2002), Localized gravity/topography admittance and correlation spectra on Mars: Implications for regional and global evolution, *J. Geophys. Res.*, *107*(E12), pp. 19-1

McGovern, P. J., J. R. Smith, J. K. Morgan, and M. H. Bulmer (2004), Olympus Mons aureole deposits: New evidence for a flank failure origin, *J. Geophys. Res.*, *109*, E08008.

McKenzie, Dan; Barnett, David N.; Yuan, Dah-Ning (2002), The relationship between Martian gravity and topography. *Earth and Planetary Science Letters*, Volume *195*, Issue 1-2, p. 1-16.

McLennan, S. M. (2001), Crustal Heat Production and the Thermal Evolution of Mars, *Geophys. Res. Lett.*, 28(21), 4019–4022.

McSween, Harry (1994), What we have learned about Mars from SNC meteorites. *Meteoritics. 29*, 757-779.

Médard, E., and T. L. Grove (2006), Early hydrous melting and degassing of the Martian interior, *J. Geophys. Res.*, *111*, E11003.

Mège, D.; Masson, P. (1996), A plume tectonics model for the Tharsis province, Mars. *Planetary and Space Science*, v. *44*, p. 1499-1546.

Meresse, S., F. Costard, N. Mangold, P. Masson, G. Neukum and the HRSC Co-I team (2008), Formation and evolution of the chaotic terrains by subsidence and magmatism: Hydraotes Chaos, Mars, *Icarus*, *194*, Issue 2, p. 487-500.

Milkovich, Sarah M.; Head, James W. (2003), Olympus Mons Fan Shaped Deposit Morphology: Evidence for Debris Glaciers. *Sixth International Conference on Mars*, July 20-25, Pasadena, California, abstract no.3149.

Milkovich, Sarah M.; Head, James W.; Marchant, David R. (2006), Debris-covered piedmont glaciers along the northwest flank of the Olympus Mons scarp: Evidence for low-latitude ice accumulation during the Late Amazonian of Mars. *Icarus*, Volume *181*, Issue 2, p. 388-407.

Mischna, M. A., M. I. Richardson, R. J. Wilson, and D. J. McCleese (2003), On the orbital forcing of Martian water and CO_2 cycles: A general circulation model study with simplified volatile schemes, *J. Geophys. Res.*, *108*(E6), 5062.

Mitchell, D. L.; R. P. Lin; C. Mazelle; H. Rème; P. A. Cloutier; J. E. P. Connerney; M. H. Acuña e N. F. Ness (2001). Probing Mars' crustal magnetic field and ionosphere with the MGS Electron Reflectometer *JGR. 106*, N. E10, pp. 23,418-23,427.

Mitchell, D. L.; R. J. Lillis; R. P. Lin; J. E. P. Connerney e M. H. Acuña (2005). A Global map of Mars crustal magnetic field based on electron reflectometry, *LPSCXXXVI.*

Montesi, L.; Zuber, M.T. (2001), Crustal Thickness Control on Martian Wrinkle Ridge Spacing. LPSC XXXII. abstract no.1879.

Moore, H. J.; D. W. G. Arthur, G. G. Schaber (1978), Yield Strengths of Flows on the Earth, Moon, and Mars, *9th Lunar Planet. Sci. Conf*., PP. 750/751.

Moore, Jeffrey M.; Wilhelms, Don E. (2001) Hellas as a Possible Site of Ancient Ice-Covered Lakes on Mars. *Icarus*, Volume *154*, Issue 2, pp. 258-276.

Morgan, J. W. e E. Anders (1979). Chemical composition of Mars. *Geochim. Cosmochim. Acta 43*, 1601-1610.

Morris, E.C., Tanaka, K.L., 1994. Geologic maps of the Olympus Mons region of Mars. *U.S. Geol. Surv. Misc. Invest. Ser. Map I-2327*.

Mouginis-Mark, P.J., L. Wilson and M. Zuber (1992), The physical volcanology of Mars. *In Mars,* The University of Arizona Press, pp. 424-452.

Mouginis-Mark, P.J (1981), Late-Stage Summit Activity of Martian Volcanoes, LPSC XII, P. 726-728.

Mutch T. A., R. E. Arvidson, J. W. Head III, K. L. Jones and R. S. Saunders (1976), *The Geology of Mars*. Princeton University Press, Princeton. Chapter 4, pp. 151-201.

Neukum, G., and K. Hiller (1981), Martian Ages, *J. Geophys. Res.*, *86*(B4), 3097–3121.

Neukum, G.; B.Ivanov e W. K.Hartmann (2001). Cratering records in the inner solar system in relation to the lunar reference system. *Space Science Rev*. in press.

Neukum, G.; Jaumann, R.; Hoffmann, H.; Hauber, E.; Head, J. W.; Basilevsky, A. T.; Ivanov, B. A.; Werner, S. C.; van Gasselt, S.; Murray, J. B.; McCord, T.; (2004), Recent and episodic volcanic and glacial activity on Mars revealed by the High Resolution Stereo Camera. *Nature*. *432*, *7020*, pp. 971-979.

Neumann G. A., M. T. Zuber, M. A. Wieczorek, P. J. McGovern, F. G. Lemoine and D. E. Smith (2004), Crustal structure of Mars from gravity and topography, *J. Geophys. Res*., *109*, E08002.

Nimmo, F., and D. J. Stevenson (2001), Estimates of Martian crustal thickness from viscous relaxation of topography, *J. Geophys. Res.*, *106*(E3), 5085–5098.

Nimmo, Francis; Tanaka, Ken (2005), Early Crustal Evolution of Mars. *Annual Review of Earth and Planetary Sciences*, vol. *33*, p.133-161.

Ott, U. (1991), Composition of the Martian atmosphere. *Space Science Reviews*, vol. *56*, April, p. 23-29.

Parsons,R. L. Head, J.W., III (2004), Ascraeus Mons, Mars: Characterisation and Interpretation of the Fan-shaped Deposit on Its Western Flank. *LPSC XXXV*, March 15-19, League City, Texas, abstract no.1776.

Pawley, A. R. (2003), Chlorite stability in mantle peridotite: The reaction clinochlore + enstatite = forsterite + pyrope + H_2O, *Contrib. Mineral. Petrol.*, *144*, 449–456.

Phillips, R. J., and R. S. Saunders (1975), The Isostatic State of Martian Topography, *J. Geophys. Res.*, *80*(20), 2893–2898.

Phillips, R. J., and K. Lambeck (1975), Gravity fields of the terrestrial planets - Long-wavelength anomalies and tectonics. *Reviews of Geophysics and Space Physics*, *18*, Feb., p. 27-76.

Phillips, R.J.; N.H. Sleep and W.B. Banerdt (1990), Permanent uplift in magmatic systems with application to the Tharsis region of Mars, *J. Geophys. Res. 95*, pp. 5089–5100.

Phillips, R. J.; Jakosky, B. M.; Hynek, B. M.; Hanna, J. C. (2001), Understanding the Global Geological History of Mars: The Contributions of Mars Global Surveyor. *AGU Fall Meeting 2001*, abstract #P41A-07.

Phillips, R. J.; M. T. Zuber; S.C. Solomon; M.P. Golombek; B.M. Jakosk; W.B. Banerdt, D.E. Smith; R.M.E. Williams; B.M. Hynek; O. Aharonson e S.A. Hauck (2001). Ancient geodynamics and global-scale hydrology on Mars. *Science. 291*, 2587-2591.

Pinkerton, H. and L. Wilson (1994), Factors controlling the lengths of channel-fed lava flows, *Bulletin of Volcanology*, *56*, Issue 2, pp. 108-120.

Plescia, J.B.(1981), The Tempe volcanic province of Mars and comparisons with the Snake River Plains of Idaho, *Icarus*, *45*, p. 586-601.

Plescia, J.B and S. Saunders (1982), Tectonic history of the Tharsis region, Mars. *J. Geophys. Res., 87*, p. 9775-9791.

Plescia, J.B. (2004), Morphometric properties of Martian volcanoes, *J. Geophys. Res.*, *109*, E03003.

Purucker, M.; D.Ravat; H. Frey; C. Voorhies; C. Sabaka e M. Acuña (2000). An altitude-normalized magnetic map of Mars and its interpretation. *Geophys. Res. Lett. 27*, 2449-2452.

Redmond, H. L., and S. D. King (2004), A numerical study of a mantle plume beneath the Tharsis Rise: Reconciling dynamic uplift and lithospheric support models, *J. Geophys. Res.*, *109*, E09008.

Reese, C. C., V. S. Solomatov, and J. R. Baumgardner (2002), Survival of impact-induced thermal anomalies in the Martian mantle, *J. Geophys. Res., 107(E10)*, 5082.

Righter, K. (2004). Water in Terrestrial Planets: Always an Oxidant?. *Lunar and Planetary Science Conference XXXV*. March 15-19, 2004, League City, Texas, abstract no.1674.

Rochette, P. (2006), Crustal magnetization of Mars controlled by lithology or cooling rate in a reversing dynamo?, *Geophys. Res. Lett.*, 33, L02202.

Rossi, M. J. (1996), Morphology and mechanism of eruption of postglacial shield volcanoes in Iceland, *Bulletin of Volcanology*, *57*, Number 7/April.

Sakimoto, S. E. H., J. Crisp and S. M. Baloga (1997), Eruption constraints on tube-fed planetary lava flows, *J. Geophys. Res.*, *102*(E3), p. 6597-6614.

Sakimoto, S.E.H., T. K. P. Gregg, S. S. Hughes and J. Chadwick (2003), Martian Plains Volcanism in Syria Planum and Tempe Mareotis as Analogs to the Eastern Snake River Plains, Idaho: Similarities and Possible Petrologic Contributions to Topography, *34th Lunar Planet. Sci. Conf.*, abstract 1740.

Sakimoto, S.E.H. (2003), Re-Assessing Plains-style Volcanism on Mars, *6th International Conf. Mars*, abstract 3197.

Schott, B., A. P. van den Berg, and D. A. Yuen (2001), Focussed Time-Dependent Martian Volcanism From Chemical Differentiation Coupled with Variable Thermal Conductivity, *Geophys. Res. Lett.*, *28*(22), 4271–4274.

Schubert, G., and T. Spohn (1990), Thermal History of Mars and the Sulfur Content of Its Core, *J. Geophys. Res.*, *95*(B9), 14,095–14,104.

Schubert, G.; Solomon, S. C.; Turcotte, D. L.; Drake, M. J.; Sleep, N. H. (1992) Origin and thermal evolution of Mars. *Mars*. p. 147-183.

Schubert, G.; Russell, C.T.; Moore, W. B. (2000), Geophysics: Timing of the Martian dynamo, *Nature*, *408*, Issue 6813, pp. 666-667.

Schultz, R. A., and T. R. Watters (2001), Forward Mechanical Modeling of the Amenthes Rupes Thrust Fault on Mars, *Geophys. Res. Lett.*, *28*(24), 4659–4662.

Schumacher, S., D. Breuer (2006), Influence of a variable thermal conductivity on the thermochemical evolution of Mars, *J. Geophys. Res.*, *111*(E2).

Schumacher, S., and D. Breuer (2007), An alternative mechanism for recent volcanism on Mars, *Geophys. Res. Lett.*, *34*, L14202.

Seyfert, C. K. (1983), Impact-Generated Plume Traces on Mars, *LPSC XIV*, P. 688-689. Abstract.

Scott, D. H. and K. L. Tanaka (1998), Geological map of the equatorial region of Mars, *USGS* Misc. Invest. Ser. Map I-1802-A, scale 1:15,000,000.

Scott, E. and L. Wilson (2003), Did the Alba Patera and Syria Planum regions of Mars lose their lithospheric roots in convective overturn events? *J. Geophys. Res.*, *108*(E5), pp. 1-1.

Seipold, U. (1998), Temperature dependence of thermal transport properties of crystalline rocks — a general law. *Tectonophysics*, vol. *291*, issue 1-4, pp. 161-171.

Sherman, D. M.; R. G.Burns; V.Mee Burns (1982). Spectral characteristics of the iron oxides with application to the Martian bright region mineralogy. *J. Geophys. Res, 87*, Nov. 30, 1982, p. 10169-10180.

Shean, D. E., J. W. Head, and D. R. Marchant (2005), Origin and evolution of a cold-based tropical mountain glacier on Mars: The Pavonis Mons fan-shaped deposit, *J. Geophys. Res.*, *110*, E05001.

Skinner, J. A., Jr.; Hare, T. M.; Tanaka, K. L. (2006), Digital Renovation of the Atlas of Mars 1:15,000,000-Scale Global Geologic Series Maps. *LPSC XXXVII*, abstract no.2331.

Sleep, N.H. and R.J. Phillips (1979), An isostatic model for the Tharsis province, *Geophys. Res. Lett. 6*, pp. 803–806.

Sleep, N. H., and R. J. Phillips (1985), Gravity and Lithospheric Stress on the Terrestrial Planets With Reference to the Tharsis Region of Mars, *J. Geophys. Res.*, *90*(B6), 4469–4489.

Sleep, N. H. (2000), Evolution of the mode of convection within terrestrial planets, *J. Geophys. Res., 105(E7)*, 17,563–17,578.

Smith, D.E., M.T. Zuber, H.V. Frey, J.B. Garvin, J.W. Head, D.O. Muhleman, G.H. Pettengill, R.J. Phillips, S.C. Solomon, H.J. Zwally, W.B. Banerdt, T.C. Duxbury, M.P. Golombek, F.G. Lemoine, G.A. Neumann, D.D. Rowlands, O. Aharonson, P.G. Ford, A.B. Ivanov, P.J. McGovern, J.B.Abshire, R.S. Afzal, and X. Sun (1999) The global topography of Mars and implications for surface evolution, *Science, 284*, 1495-1503.

Smith, D.E., M.T. Zuber, H.V. Frey, J.B. Garvin, J.W. Head, D.O. Muhleman, G.H. Pettengill, R.J. Phillips, S.C. Solomon, H.J. Zwally, W.B. Banerdt, T.C. Duxbury, M.P. Golombek, F.G. Lemoine, G.A. Neumann, D.D. Rowlands, O. Aharonson, P.G. Ford, A.B. Ivanov, P.J. McGovern, J.B.Abshire, R.S. Afzal, and X. Sun (2001), Mars Orbiter Laser Altimeter (MOLA): Experiment summary after the first year of global mapping of Mars, *J. Geophys. Res*., *106*, (E10) 23689-23722.

Smith, D. E., and M. T. Zuber (2003) The shape of Mars and the topographic signature of the hemispheric dichotomy, *Science, 271*, 184-188.

Soffen, G. A. (1977), Scientific results of the Viking Project, *Science, 194*, 3959.

Sohl, F., and T. Spohn (1997), The interior structure of Mars: Implications from SNC meteorites, *J. Geophys. Res.*, *102*(E1), 1613–1635.

Solomon, S. C. (1979), Formation, history and energetics of cores in the terrestrial planets, *Physics of the Earth and Planetary Interiors*, *vol. 19*, June, p. 168-182.

Solomon, S. C. and J. W Head (1981), The Evolution of Multi-Ringed Basins: Viscoelastic Relaxation of Topographic Relief. *LPSC XII*, P. 1023-1025. Abstract.

Solomon, S.C. and J.W. Head (1982), Evolution of the Tharsis province of Mars: the importance of heterogeneous lithospheric thickness and volcanic construction, *J. Geophys. Res. 87*, pp. 9755–9774.

Solomon, Sean C.; Aharonson, O.; Aurnou, J.M.; Banerdt, W. B.; Carr, M.H.;Dombard, A.J.; Frey, H. V.; Golombek, M. P.; Hauck, Steven A.; Head, J. W.; Jakosky, B. M.; Johnson, C. L.; McGovern, P. J.;Neumann, G. A.; Phillips, R. J.; Smith, D. E.; Zuber, M. T. (2005), New Perspectives on Ancient Mars. *Science*, Volume *307*, Issue 5713, pp. 1214-1220.

Squyres, S.W e Kasting, J.F. (1994). Early Mars: How warm and how wet? *Science*. *265*,744-748.

Stevenson, D. (2001). Mars core and magnetism. *Nature*. *412*. July.

Tanaka, K. (1986). The stratigraphy of Mars. JGR.(ISSN 0148-0227), *91*, Nov. 30, 1986, p. E139-E158.

Tanaka, K. L. and P. A. Davis (1988), Tectonic History of the Syria Planum Province of Mars, *J. Geophys. Res*., *93*, 14893-14917.

Tanaka, K. L., J. M. Dohm (1989), Volcanotectonic Provinces of the Tharsis Region of Mars: Identification Variations, and Implications, *MEVTV Workshop on Early Tectonic and Volcanic Evolution of Mars.* pp.79.

Taylor, G. J.; Norman, M. D. (1992), Evidence for Magma Oceans on Asteroids, the Moon, and Earth. Workshop on the Physics and Chemistry of Magma Oceans from 1 Bar to 4 Mbar. A Lunar and Planetary Institute Workshop held December 6-8, 1991, at Burlingame, California. Sponsored by LPI, Lunar and Planetary Sample Team (LAPST), and the NASA Johnson Space Center. Edited by Carl B. Agee and John Longhi. LPI Technical Report 92-03, published by Lunar and Planetary Institute, 3303 NASA Road 1, Houston, TX 77058, 1992, p.58.

Thornhill, G. et al., (1993) Topography of Apollinaris Patera and Ma'adim Vallis: Automated extraction of Digital Elevation Model, *J. Geophys. Res., 98*, 581-587.

Thomas, P. J., S. W. Squyres, and M. H. Carr (1990), Flank Tectonics of Martian Volcanoes, *J. Geophys. Res.*, *95*(B9), 14,345–14,355.

Treiman, A. H.; Drake, M. J.; Janssens, M.-J.; Wolf, R.; Ebihara, M. (1986), Core formation in the earth and shergottite parent body (SPB) - Chemical evidence from basalts. *Geochimica et Cosmochimica Acta* , vol. *50*, p. 1071-1091.

Turcotte, Donald L.; Schubert, Gerald (2002), *Geodynamics - 2nd Edition*. Cambridge University Press, Cambridge, pp. 472.

van Thienen, P.; A. Rivoldini, T. Van Hoolst, Ph. Lognonne (2006), A top-down origin for martian mantle plumes, *Icarus*, *185, Issue 1,* November, Pages 197-210.

Vaucher, J., D. Baratoux, P. C. Pinet, N. Mangold, G. Ceuleneer, M. Gregoire, Y. Daydou, S. Chevrel, G. Neukum and HRSC Co-Investigator Team (2006), Cerberus Plains, Mars: Chronology of Volcanic Event and Evidence of Recent Tectonic Activity. *37th Annual Lunar and Planetary Science Conference,* abstract no.1851.

Verhoeven, O.; A. Rivoldini; P. Vacher; A Mocquet; G. Choblet; M. Menvielle; V. Dehant; T. Van Hoolst; J. Sleewaegen; J.-P. Barriot; P. Lognonné (2005), Planetary interiors structure inferred from electromagnetic, geodetic and seismic network science I: Forward problem an the case of Mars, *J. Geophys. Res*., *110,* doi: 10.1029/2004JE002271.

Wang, H.F. and Anderson, M.P. (1982). *Introduction to Groundwater Modeling: Finite Difference and Finite Element Methods*, 237.

Wänke H. e G.Driebus (1988) Chemical composition and accretional history of terrestrial planets. *Phil. Trans. Royal Soc. London A235*, 545-557.

Warner, N. H. and T. K. P. Gregg (2003), Evolved lavas on Mars? Observations from southwest Arsia Mons and Sabancaya volcano, Peru, *J. Geophys. Res.*, *108*(E10), 1-1.

Werner, Stephanie C. (2005), Major Aspects of the Chronostratigraphy and Geologic Evolutionary History of Mars. *PHD thesis*, Fachbereich Geowissenschaften Freie Universität Berlin, 160 pages.

Webb, B., J. W. Head III, B. E. Kortz, S. Pratt (2001), Syria Planum, Mars: A Major Volcanic Construct in the Early History of Tharsis. *32nd Annual Lunar and Planetary Science Conference*, Houston, Texas, abstract no.1145.

Weizman, A.; Stevenson, D. J.; Prialnik, D.; Podolak, M. (2001), Modeling the Volcanism on Mars. *Icarus*, Volume *150*, Issue 2, pp. 195-205.

Wieczorek, M. A., and M. T. Zuber (2004), Thickness of the Martian crust: Improved constraints from geoid-to-topography ratios, *J. Geophys. Res.*, *109*, E01009.

Wieczorek, M. A. (2007), Gravity and topography of the terrestrial planets, *Treatise on Geophysics, 10*, 165-206, doi:10.1016/B978-044452748-6/00156-5.

Willemann, R. J., and D. L. Turcotte (1982), The Role of Lithospheric Stress in the Support of the Tharsis Rise, *J. Geophys. Res.*, *87*(B12), 9793–9801.

Wilson, L. and J. W. Head (1981), Volcanic Eruption Mechanisms on Mars: Some Theoretical Constraints. *12th Annual Lunar and Planetary Science Conference*, Houston, Texas, P. 1194-1196 abstract.

Wilson, L. and J. W. Head (1983), A comparison of volcanic eruption processes on Earth, Moon, Mars, Io and Venus, *Nature*, *302*, 663-669.

Wilson, L. and J. W. Head III (1994), Mars: Review and analysis of volcanic eruption theory and relationships to observed landforms. *Reviews of Geophysics* (ISSN 8755-1209), *32*, no. 3, p. 221-263.

Wilson, L. (2001), Evidence for episodicity in the magma supply to the large Tharsis volcanoes. *J. Geophys. Res., 106*(E1), 1423-1434.

Wilson, L. e J. W.Head III (2002). Tharsis radial graben systems as the surface manifestation of plume-related dike intrusion complexes: Models and implications. *J. Geophys. Res., 107*, E8, 10.

Wise, D. U., M. P. Golombek, and G. E. McGill (1979), Tectonic Evolution of Mars, *J. Geophys. Res.*, *84*(B14), 7934–7939.

Wise, D.U., M.P. Golombek and G.E. McGill (1979), Tharsis province of Mars: geologic sequence, geometry and a deformation mechanism, *Icarus 38*, pp. 456–472.

Yoder C. F. ; A. S. Konopliv ; D. N. Yuan ; E. M. Standish; W. M. Folkner (2003), Fluid Core Size of Mars from Detection of the Solar Tide, *Science 300*, 299.

Zimbelman, J.R. (1985), Estimates of Rheologic Properties for Flows on the Martian Volcano Ascraeus Mons, *J. Geophys. Res., 90 Supplement*, D-157-D162.

Zhong S. (2008), Differential Rotation of Lithosphere for One-plate Planets and its Implications for the Tharsis Rise on Mars, American Geophysical Union, Fall Meeting, abstract #P43C-1408.

Zuber, M. T. et al., (1992) The Mars Orbiter laser altimeter investigation, *J. Geophys. Res., 97*, 7781-7797.

Zuber, M. T. and Mouginis-Mark, P.J. (1992), Caldera subsidence and magma chamber depth of the Olympus Mons volcano, Mars. *J. Geophys. Res., 97*, no. E11, p. 18,295-18,307

Zuber, M. T., and D. E. Smith (1997), Mars without Tharsis, *J. Geophys. Res.*, *102*(E12), 28,673–28,685.

Zuber, M. T.; D. E. Smith, R.J. Phillips, S.C. Solomon, W. B. Banerdt, G. A. Neumann and O. Aharonson (1998), Shape of the northern hemisphere of Mars from the Mars Orbiter Laser Altimeter (MOLA), *Geophysical Research Letters*, *25*(24), p. 4393-4396.

Zuber, M. T. Solomon, Sean C.; Phillips, Roger J.; Smith, David E.; Tyler, G. Leonard; Aharonson, Oded; Balmino, Georges; Banerdt, W. Bruce; Head, James W.; Johnson, Catherine L.; Lemoine, Frank G.; McGovern, Patrick J.; Neumann, Gregory A.; Rowlands, David D.; Zhong, Shijie (2000), Internal structure and early thermal evolution of Mars from Mars Global Surveyor topography and gravity, *Science, 287*, 1788-1793.

Zuber, M. T. (2001), The crust and mantle of Mars, *Nature, 412,* 12 July.

Zuber, M. T.; S. C. Solomon; R.J. Phillips; D.E. Smith; G.L. Tyler; O. Aharonson e G. Balmino (2001), Evidence for pigmentary hematite on Mars based on optical, magnetic, and Mössbauer studies of superparamagnetic (nanocrystalline hematite), *J. Geophys. Res., 94*, 2760-2778.

Annexes

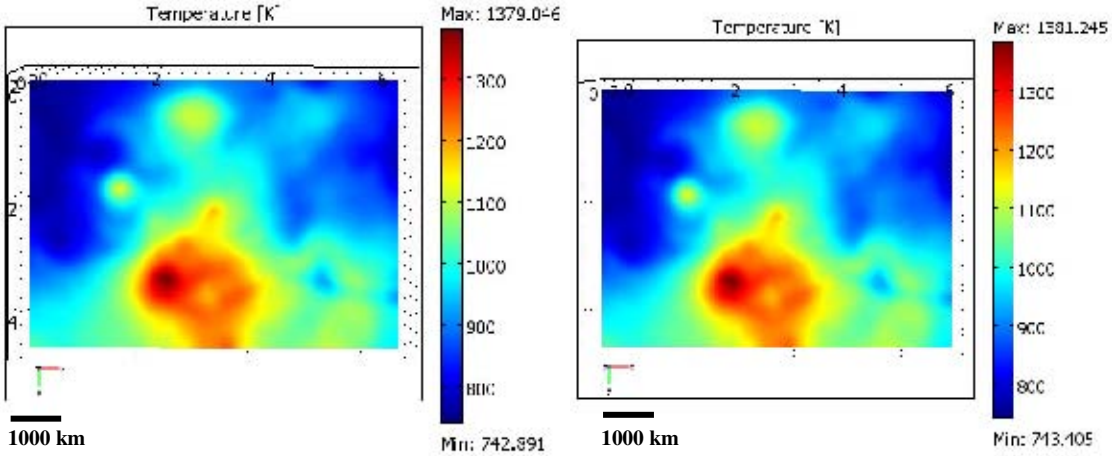

FIG 1 – *The temperatures were calculated using Model M7 parameters (from chapter 5), although for a period of time of 500 Ma ago (H=1.0976 – from chapter 4.3) on the left chart, and for 600 Ma ago (H=1.1075 – from chapter 4.3) on the right chart. The temperatures were measured at 120 km deep.*

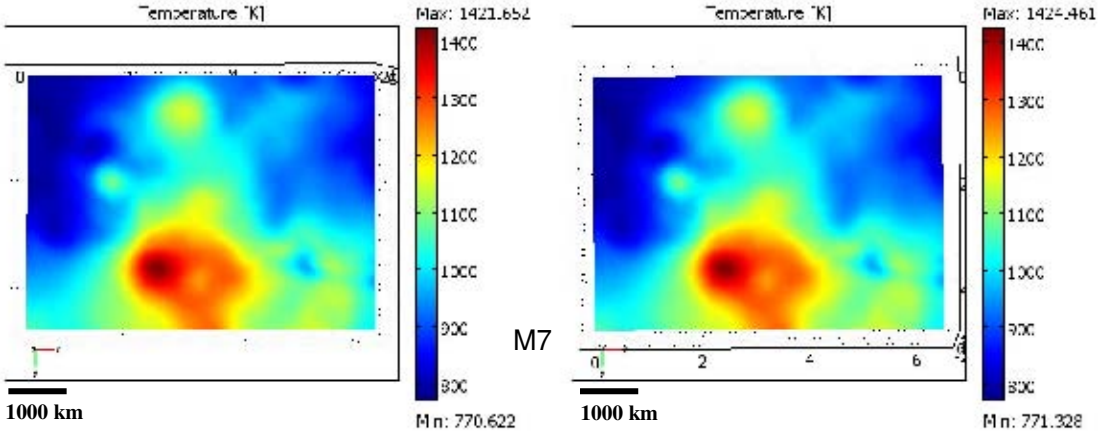

FIG 2 – *The temperatures were calculated using Model M7 parameters, for a period of time of 500 Ma ago (H=1.0976 – from chapter 4.3) on the left chart, and for 600 Ma ago (H=1.1075 – from chapter 4.3) on the right chart, where on the general heat sources, Q, it is included the heating fraction due the cooling effect of the planet. The temperatures were measured at 120 km deep.*

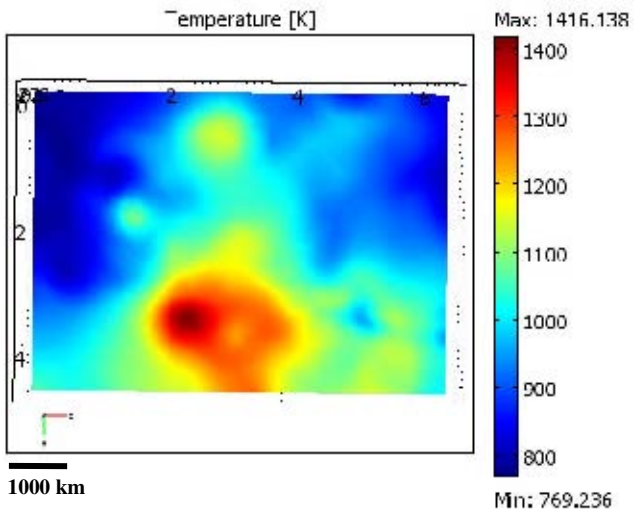

FIG 3 – *Model Mc. The temperatures were calculated using Model M7 parameters, for present-time, where on the general heat sources, Q, it is included the heating fraction due the cooling effect of the planet. The temperatures were measured at 120 km deep.*

Model Mc was obtained knowing that the cooling effect is determined by $-\rho C\frac{T_1-T_2}{t_1-t_2}$.

For a period between the present time (t_1) (see Figure 4 in annexes) and 100 Ma (t_2) (see Figure 4 in annexes), where, ρ=3100 kgm^{-3}, C=1000 JKg^{-1}K^{-1}, and T_1=1321.3 K, T_2=1324.5 K. The resulting heat due to the cooling effect is 6.50 x10^{-9} Wm^{-3}, which, considering the used general heat source for the steady-state regime Q=1.38x10^{-8} Wm^{-3}, is ~47% of the general heat, for this period of time.

Mc is then calculated using the new Q, which then takes into account the cooling effect.

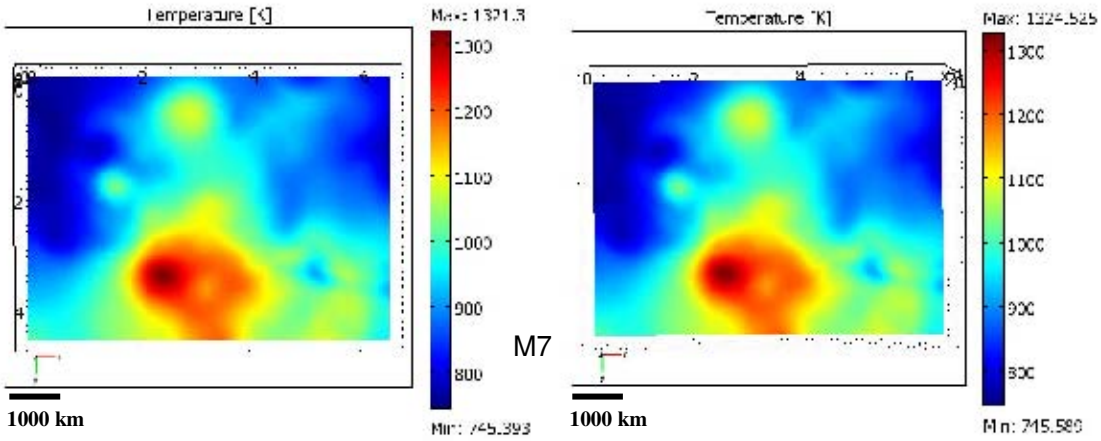

FIG 4 – *The temperatures were calculated using Model M7 parameters, for the present-time (H=1 – from chapter 4.3) on the left chart, and for 100 Ma ago (H=1.022 – from chapter 4.3) on the right chart. The temperatures were measured at 120 km deep.*

TAB. 1 – *The Temperatures were calculated in Arsia Mons, resulting from the iterative process described in Equations 5.8 - 5.11.*

M7	0	100 Ma	200 Ma	300 Ma	400 Ma	500 Ma	600 Ma	700 Ma	800 Ma	900 Ma
Temp 1	1324,728	1328,944	1333,16	1337,376	1341,591	1345,807	1350,023	1354,238	1358,454	1362,67
Q cooling	7,09553E-09	7,09553E-09	7,09553E-09	7,09384E-09	7,09553E-09	7,09553E-09	7,09385E-09	7,09553E-09	7,09553E-09	7,09553E-09
Temp 2	1435,11	1441,496	1447,882	1454,269	1460,655	1467,042	1473,428	1479,814	1486,201	1492,587
Q cooling	1,07476E-08	1,07476E-08	1,07493E-08	1,07476E-08	1,07493E-08	1,07476E-08	1,07476E-08	1,07493E-08	1,07476E-08	1,07476E-08
Temp 3	1491,93	1499,433	1506,937	1514,458	1521,962	1529,466	1536,953	1544,474	1551,978	1559,482
Q cooling	1,26275E-08	1,26292E-08	1,26578E-08	1,26292E-08	1,26292E-08	1,26006E-08	1,26578E-08	1,26292E-08	1,26292E-08	1,26292E-08
Temp 4	1521,176	1529,271	1537,55	1545,575	1553,626	1561,605	1569,632	1577,746	1585,826	1593,905
Q cooling	1,36239E-08	1,39336E-08	1,35061E-08	1,35498E-08	1,34287E-08	1,35094E-08	1,36559E-08	1,35986E-08	1,3597E-08	1,3597E-08
Temp 5	1534,67	1543,087	1551,433	1559,778	1568,124	1576,624	1584,989	1593,338	1601,687	1610,036
Q cooling	1,41658E-08	1,40463E-08	1,40446E-08	1,40463E-08	1,43055E-08	1,40783E-08	1,40514E-08	1,40514E-08	1,40514E-08	1,40514E-08
Temp 6	1542,519	1551,018	1559,517	1568,015	1576,614	1586,209	1594,555	1603,072	1611,589	1620,106
Q cooling	1,43038E-08	1,43038E-08	1,43021E-08	1,44721E-08	1,61484E-08	1,40463E-08	1,43341E-08	1,43341E-08	1,43341E-08	1,43341E-08
Temp 7	1545,631	1554,19	1564,367	1572,958	1605,396	1590,139	1598,729	1607,32	1616,09	1624,684

- Baptista, A. R., N. Mangold, V. Ansan, D. Baratoux, P. Lognonné, E. I. Alves, D. A. Williams, J. E. Bleacher, P Masson, and G. Neukum (2008), A swarm of small shield volcanoes on Syria Planum, Mars, *J. Geophys. Res*., 113, E09010, doi:10.1029/2007JE002945.

- **Liste des acronymes et notations**

- **Liste des figures et légendes**

- **Liste des tableaux et légendes**

JOURNAL OF GEOPHYSICAL RESEARCH, VOL. 113, E09010, doi:10.1029/2007JE002945, 2008

A swarm of small shield volcanoes on Syria Planum, Mars

Ana Rita Baptista,[1,2] Nicolas Mangold,[2] Véronique Ansan,[2] David Baratoux,[3] Philippe Lognonné,[1] Eduardo I. Alves,[4] David A. Williams,[5] Jacob E. Bleacher,[6] Philippe Masson,[2] and Gerhard Neukum[7]

Received 25 May 2007; revised 6 May 2008; accepted 21 July 2008; published 26 September 2008.

[1] This study focuses on the volcanism in Syria Planum, located at the center of the Tharsis bulge at an altitude of 6 to 8 km above Mars datum. Syria Planum was previously recognized as a center for the tectonic activity of Tharsis, but not as a major locus for volcanic activity, despite its centrality over the bulge. Using high-resolution images from the high resolution stereo camera on Mars Express combined with Mars Observer Laser Altimeter data, we have characterized a volcanic system that reveals a number of very interesting aspects of Mars volcanism. We identified a swarm of tens of coalesced shallow volcanic edifices, typically 10–30 km diameter, 0.1–0.2 km high, and with slopes around 0.5°. These characteristics are similar to those of small shield volcanoes found in Iceland. In addition, an intermediate-sized volcano, which is the source of lava flows that extend over >200 km, is observed west of this shield swarm. Our study characterizes a previously unrecognized volcanic assemblage on Mars which appears to be much more developed than was documented before, in terms of morphology, inferred origin, and periodicity of eruption. The estimated lava flux of the Syria Planum volcanoes is of the same order as the lava flux of Tharsis Montes. These characteristics suggest that Syria Planum experienced a very specific style of volcanism, which we dated to the Hesperian period.

Citation: Baptista, A. R., N. Mangold, V. Ansan, D. Baratoux, P. Lognonné, E. I. Alves, D. A. Williams, J. E. Bleacher, P. Masson, and G. Neukum (2008), A swarm of small shield volcanoes on Syria Planum, Mars, *J. Geophys. Res.*, *113*, E09010, doi:10.1029/2007JE002945.

1. Introduction

[2] Mars exhibits a great variety of volcanic landforms. Several types of edifices (Montes, Paterae, etc.), as well as volcanic plains, exist in both the northern and the southern hemispheres of Mars [e.g., *Carr*, 1975; *Mutch et al.*, 1976; *Carr*, 1981; *Greeley and Spudis*, 1981; *Mouginis-Mark et al.*, 1992; *Carr*, 1996]. The four most prominent shield volcanoes, Ascraeus, Pavonis, Arsia, and Olympus Mons, are located on the Tharsis province. Large volcanic edifices also occur in the Elysium region, ~4500 km west of Olympus Mons, although with significant contrasts in structure, composition, and eruptive style from those of the Tharsis province. The extensive lava flows associated with both the Tharsis and Elysium shields suggest that numerous smaller volcanic landforms of various types should also exist [e.g., *Plescia*, 1981; *Mouginis-Mark et al.*, 1992; *Hodges and Moore*, 1994]. Much of the knowledge of the physical volcanology of Mars comes from morphologic analyses of Mariner 9 and Viking Orbiter images [e.g., *Carr*, 1973, 1974; *Mouginis-Mark et al.*, 1992]. Using new imagery and altimetry data from the recent missions Mars Global Surveyor (MGS) and Mars Odyssey, many smaller volcanic features were detected in other regions, such as Tempe Terra, Cerberus Fossae, and the Tharsis region [e.g., *Tanaka and Dohm*, 1989; *Davis and Tanaka*, 1993; *Webb et al.*, 2001; *Hauber and Kronberg*, 2001; *Sakimoto et al.*, 2003; *Sakimoto*, 2003; *Vaucher et al.*, 2006; *Bleacher et al.*, 2007; *Hauber et al.*, 2007].

[3] In this study, we show that the high resolution stereo camera (HRSC) images allow us to identify, characterize, and map a suite of volcanic landforms in the Syria Planum region, a plains-style volcanic region where the identification of these landforms was limited in detail with Viking imagery. Syria Planum is a broad plateau located at the summit of the Tharsis rise (>6 km high above Mars Observer Laser Altimeter (MOLA) datum). *Plescia and Saunders* [1982] first recognized Syria Planum as a center of tectonic activity. This magmatic/tectonic driven province has been interpreted to have been active from the Noachian to the late Hesperian [*Frey*, 1979; *Plescia and Saunders*,

[1]Géophysique Spatiale et Planétaire, Institut de Physique du Globe de Paris, Saint Maur des Fossés, France.
[2]IDES, Université Paris XI, Orsay, France.
[3]Laboratoire Dynamique Terrestre et Planétaire, UMR5562 Observatoire Midi-Pyrénées, Université de Toulouse III, Toulouse, France.
[4]Centro de Geofísica da Universidade de Coimbra, Coimbra, Portugal.
[5]School of Earth and Space Exploration, Arizona State University, Tempe, Arizona, USA.
[6]Planetary Geodynamics Laboratory, NASA Goddard Space Flight Center, Greenbelt, Maryland, USA.
[7]Institut für Geologische Wissenschaften, Freie Universität Berlin, Berlin, Germany.

0148-0227/08/2007JE002945$09.00

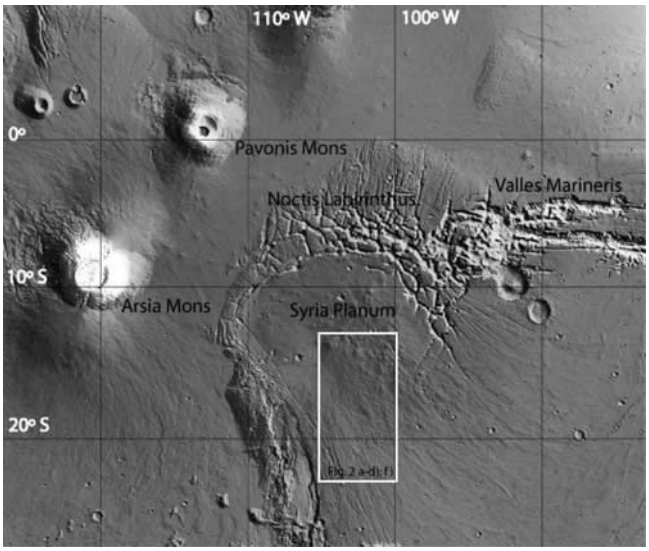

Figure 1. Shaded relief map from MOLA 1/128° DEM. The white rectangle delineates the THEMIS mosaic of Figures 2a–2c and the maps obtained from HRSC and THEMIS mosaics in Figures 2d and 2f.

1982; *Anderson et al.*, 2001]. *Anderson et al.* [2004] proposed that the long-lived magmatic activity of Syria Planum was related to a distinct episode of intensive tectonic activity during the late Noachian/early Hesperian, which declined and transitioned into a more volcanic style of activity [*Dohm et al.*, 2001]. *Scott and Wilson* [2003] suggested that Syria Planum is essentially representative of an end-member of the volcanic history of the Tharsis dome, involving the loss of a volcanic root followed by consequent uplift and then final subsidence.

[4] The topographic map [*Zuber et al.*, 1998] obtained by MOLA shows that Syria Planum is not a flat plateau (Figure 1). *Webb et al.* [2001] and *Sakimoto* [2003] noted the presence of topographic protuberances in MOLA data that might correspond to low shield volcanoes, although no image could confirm this interpretation. Now the HRSC images from the Mars Express orbiter allow us to identify and characterize these features at a high resolution (up to 10 m/pixel) and large coverage ideal for volcanic systems (Figure 2). Our study characterizes the volcanic landforms of this region, which appear to be much more developed than previously recognized. We identify and characterize a swarm of small shield volcanoes in terms of its origin, morphology, and periodicity of eruption, which we suggest requires further detailed study, namely, to understand its relationships with the complex history of the Tharsis bulge. In addition, a larger shield volcano is also identified on Syria Planum. We report on estimates of the rheological properties of the Syria Planum lava flows, their age, duration, morphology, and chronological relation to the smaller shield volcanoes.

2. Data

[5] We used high-resolution images acquired by the HRSC camera (orbits 2021, 2032, and 2054), orthorectified in a sinusoidal projection centered at 100°W longitude, with a resolution of 15 m/pixel. We mosaicked them to cover the region included in Figure 1 (the white box), where the swarm of shield volcanoes is observed (Figure 2e). This mosaic of images allowed us to identify, map, and extract morphometric parameters of the volcanic features. We also used MOLA data at a resolution of 128 pixel/degree, about 500 m at the equator [*Smith et al.*, 2001], and a vertical precision around 35 cm [*Zuber et al.*, 1998] that have been rectified in the same projection as HRSC images to obtain altimetry (Figure 2a). The altimetry allowed us to determine the quantitative geometric shape of the shield volcanoes and lava flows. In addition, we used visible and thermal infrared (IR) images (mosaic of images I17865001, I17290014, I17552023, and I16953015) acquired by the spectrometer Thermal Emission Imaging System (THEMIS) during day or night with a spatial resolution of 100 m/pixel [*Christensen*, 2003]. The IR day and IR night data give the surface brightness temperature, which is relevant to the discussion of surface rock properties. Mosaics of IR day (Figure 2b) and IR night (Figure 2c) images were coregistered with the HRSC image coverage to observe the field of lava flows southwest of the shield volcanoes (white box in Figure 1). All these data allowed us to identify, map, and define the morphology, geometry, and age of the volcanic features of Syria Planum to propose a volcanic scenario in relation to the Tharsis region.

3. Identification of the Main Morphostructural Units

[6] The plateau of Syria Planum is about 450 × 700 km wide and is centered at 12°S, 104°W (Figure 1). It is separated from the Tharsis Montes volcanoes by Noctis Labyrinthus to the north and Claritas Fossae to the west [*Masson*, 1980; *Tanaka and Davis*, 1988; *Head et al.*, 2000]. On the basis of Viking images, Syria Planum has

Figure 2. (a) MOLA altimetry with height contour intervals of 50 m. Regionally, the topography decreases from the north to the south and from the east to the west. (b) THEMIS IR day images (I17865001, I17290014, I17552023, and I16953015) where the white rectangles place and localize the figures shown in this work. (c) THEMIS IR night images. (d) MOLA slope expressed in percent. Some ruptures of slope are observed on the northwest and southwest, evidence for the presence of oriented fractures. The axisymmetrical protuberances on the northeast show higher dip mainly on their western flanks. Note the 20 km diameter protuberances on the higher (from about 6.8 to 7.5 km altitude) lands of Syria Planum. (e) Mosaic of HRSC images (orbits 2021, 2032 and 2054). (f) Geomorphologic map of Syria Planum. The axisymmetrical protuberances (morphostructure 1) are in red with impact craters in brown. The lava flows (morphostructure 2) that follow the regional slope are represented in orange. These formations are dissected by two families of lineations in black. On the southern part, these lineations become wider (morphostructure 3). In blue, at the top, we can distinguish some features that are the result of collapsed terrain. In gray possible contours for the top of the volcano A are represented.

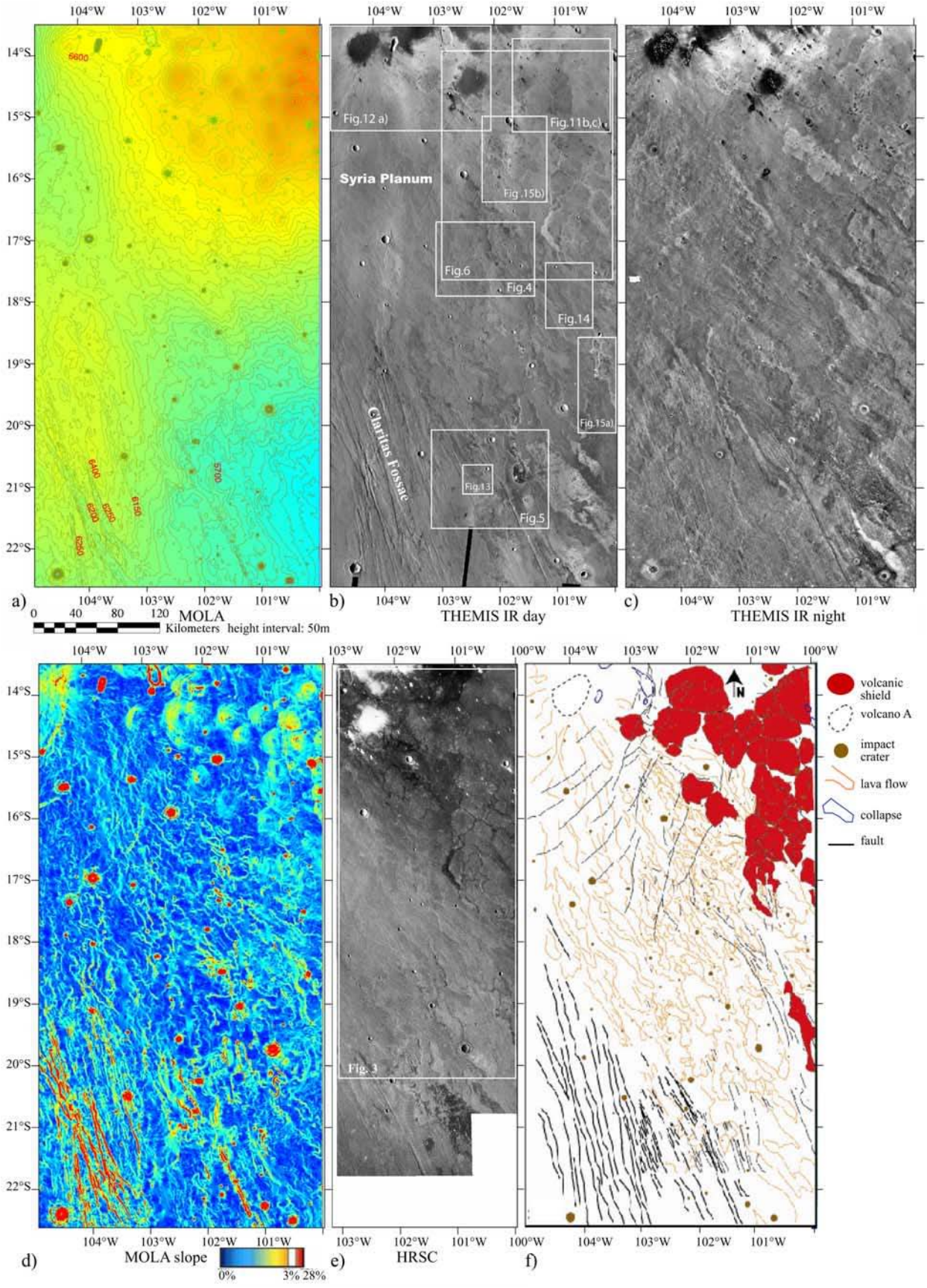
104°W
103°W
102°W
101°W
14°S
15°S
16°S
17°S
18°S
19°S
20°S
21°S
22°S
5600
6400
6300
6250
6200
6150
5700
6250
a)
0 40 80 120
MOLA
Kilometers height interval: 50m
b)
THEMIS IR day
c)
THEMIS IR night
Fig.12 a)
Fig.11b,c)
Syria Planum
Fig .15b)
Fig.6
Fig.4
Fig.14
Fig.15a)
Claritas Fossae
Fig.13
Fig.5
100°W
d)
MOLA slope
0% 3% 28%
e)
HRSC
Fig. 3
f)
N
volcanic shield
volcano A
impact crater
lava flow
collapse
fault

Figure 2

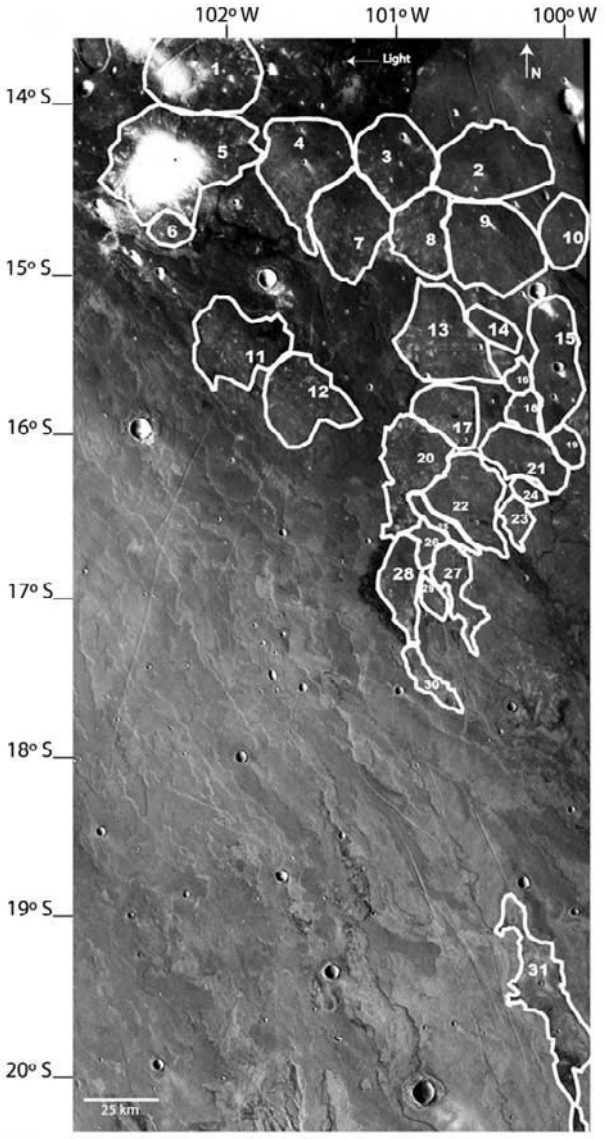

Figure 3. HRSC mosaic of the Syria Planum studied region. The context of this area is shown on Figure 2e. The higher albedo surfaces show areas highly covered by dust, while the lower albedo surfaces reveal contours of some circular features (on the East), extensive lava flows (coming from the Northwest), and two families of faults, more visible on the southern terrains. Several impact craters are also distinguished. Each single circular protuberance is circumscribed by a white contour and numbered (see Table 1).

been mapped as a volcanic plain of Hesperian age, with lava flows interpreted to originate from both the summit area and the flanks of a topographic high in northern Syria Planum and Noctis Labyrinthus [*Tanaka and Davis*, 1988; *Scott and Tanaka*, 1998]. Syria Planum also displays radial volcanic flow patterns [e.g., *Tanaka and Davis*, 1988] and volcanic eruptions along tube- fed and vent-fed flows [e.g., *Chadwick et al.*, 2004; *Webb et al.*, 2001]. Within this tectonovolcanic province, possible small edifices were locally found using Viking images [*Hodges and Moore*, 1994]. Some possible edifices are more broadly observed using MOLA altimetry [*Webb et al.*, 2001; *Sakimoto*, 2003]. They were named "protuberances" because of the lack of good imagery to certify the volcanic origin. These landforms stand at elevations >6 km and are several tens of kilometers in diameter and several hundreds of meters high (Figure 2a).

[7] New images allow us to better characterize the landforms observed in Syria Planum. Figure 2 shows mosaics of THEMIS and HRSC images and a simplified geomorphic map drawn from these mosaics. We detail hereinafter the following three main morphostructural units deduced from these data and mapped in the simplified geomorphic map: (1) in the northern and eastern regions, a group of conical features that resemble small volcanoes and correspond to the protuberances seen on MOLA data; (2) in the western and central regions, extensive lobate shaped lava flows; and (3) in the southern region, a highly fractured terrain displaying graben-like structures.

[8] In the NE region of Syria Planum, HRSC and THEMIS images show a group of 10 to 60 km diameter, relatively circular features corresponding to the topographic protuberances seen in the MOLA map (Figure 2a). This swarm of protuberances displays a distinct pattern of coalesced landforms, as seen on Figures 3, 6, and 11, (between 12°–21°S and 96°–100°W). A total of 30 individual protuberances are identified on these images (Table 1). They stand at the highest elevations on the plateau (>7 km). Some of these protuberances (e.g., numbers 1 and 5) located to the northern edge of the swarm have a higher albedo, interpreted as a dust cover, as confirmed by the low brightness in THEMIS IR night images (Figure 2c). Using the MOLA slope map expressed in percentage (Figure 2d), we observe that these protuberances have a central axisymmetry slope less than 3%, indicating shallow slope cones. Some protuberances display a central vent or radial fractures (Figures 2f and 3). The combination of topography and imagery suggests that these topographic protuberances correspond to small volcanic edifices. We studied these landforms and discuss in section 4 how our results evidence this volcanic interpretation.

[9] In the central part of the HRSC image mosaic (Figure 3), we observe an intermediate albedo feature, ~10 km wide and >100 km long, with elongated shapes bounded by lobate fronts and scarps covering a widespread area oriented NW–SE. In THEMIS day IR, these landforms are characterized by an intermediate albedo with lobate shapes. These landforms are interpreted as lava flows that erupted from the NW of Syria Planum and flowed to the SE as indicated by the location of their lobate fronts. Their NW–SE trend is parallel to the SE regional topographic slope of 0.5% in this part of Syria Planum (Figures 2a and 2d). These lava flows stand between 5.4 and 6.8 km in altitude. They are poorly cratered and crosscut by tens of kilometers long, 2.5 km wide N–S trending linear fractures (Figure 4).

[10] On the southernmost part of the HRSC image mosaic (Figure 5), below altitudes of 5.4 km on the MOLA map, the lava flows are crosscut by a widespread field of NW–SE-trending grabens. In contrast to their smooth surface at the HRSC image scale, the darkest areas located eastward in Figure 5 correspond to rough bedrock that lava flows did not cover.

[11] In addition to these three main units, we observe that a few grabens cross both the protuberances (inferred small

Table 1. Morphometric Parameters of Some Small Volcanoes in Syria Planum[a]

Volcano	W-E Width (km)	Mean Slope (°)	Altitude (m)	Mean Relief (m)	Area (km^2)	Mean Volume (km^3)	Vent	Eccentricity
1	41	0,7	6965	133	1081	55,7	yes	0,7
2	40,9	1,0	7264	248	794	103,6	yes	0,4
3	28	0,5	7060	117	637	22,8	yes	0,4
4	32	0,6	7053	195	836	49,9	yes	0,5
5	50,4	0,7	7085	241	1431	152,7	yes	0,5
6	16,2	0,7	6933	81	139	5,3	no	0,4
7	28	0,6	6999	105	704	20,5	yes	0,5
8	19	0,7	7208	151	459	13,6	yes	0,5
9	31,4	0,8	6999	202	839	49,8	no	0,5
10	16,5	0,7	7208	110	318	7,5	no	0,4
11	32	0,5	6955	70	686	17,9	yes	0,8
12	29,5	0,4	6901	105	638	22,9	no	0,4
13	29	0,5	7113	118	927	24,8	yes	0,8
14	14	0,3	7051	30	157	1,5	no	
15	14	0,7	7059	87	630	4,3	yes	
16	9	0,4	7002	29	78	0,6	yes	0,4
17	22,4	0,4	6977	77	363	9,6	yes	
18	10,4	0,3	6920	36	131	1,0	no	
19	9,6	0,7	6961	94	118	2,2	yes	
20	23	0,6	6901	117	600	15,5	yes	0,7
21	59	0,2	6858	50	444	43,5	no	
22	26,4	0,3	6788	27	570	4,7	yes	
23	10	0,5	6712	59	120	1,5	yes	0,6
24	10	0,5	6657	40	264	1,0	yes	0,6
25	7	0,3	7045	31	161	0,4	no	
26	10	0,1	6737	10	112	0,2	yes	
27	11	0,5	6763	57	270	1,7	yes	0,8
28	14,5	0,4	6703	90	346	4,7	yes	0,9
29	8,5	0,3	6628	67	82	1,2	no	
30	8,7	0,2	6421	9	158	0,2	no	

[a]Averaged values of slope, relief, and volume were determined considering separately the northern, southern, western, and eastern flanks. In some cases, not all of the four orientations were measured. For the volcanoes 14, 17, 18, 21, 26, 28, 29, and 20 the northern slope and relief values were not considered for the mean slope average. Also, the eastern values of volcanoes 15, 19, 21, and 29 were not considered. The difficulty in measuring some of the flanks is due to the superposition of lavas from adjacent volcanoes, which obviously hides the real contours of each volcano. The volumes were calculated using $V = 1/3 \times \pi r^2 h$, where h is the average relief and r is half of the W-E width. Topographic data and images were used to determine the contact between the shields and the plains and the shape of this contact was then used to determine the eccentricity.

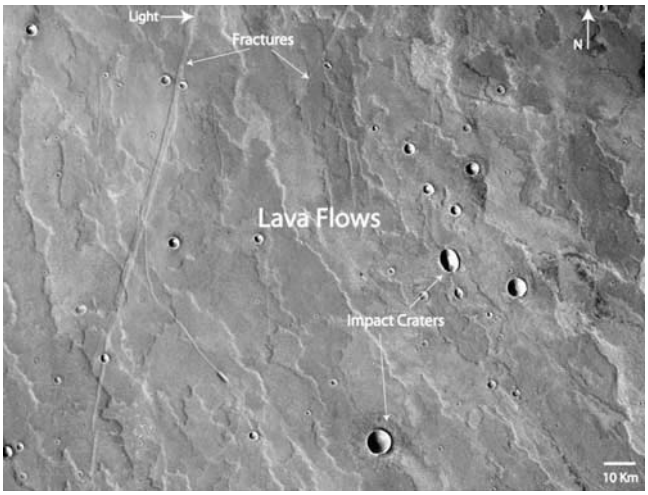

Figure 4. HRSC mosaic showing lava flow contours displayed in orange on Figure 2f. These lavas have a lobate and elongated shape, mainly oriented from NW to SE. Some of these flows are intersected by several lineations or faults. Illumination comes from the east. The image is centered at ~18.5°S, 102.7°W. See context on Figure 2.

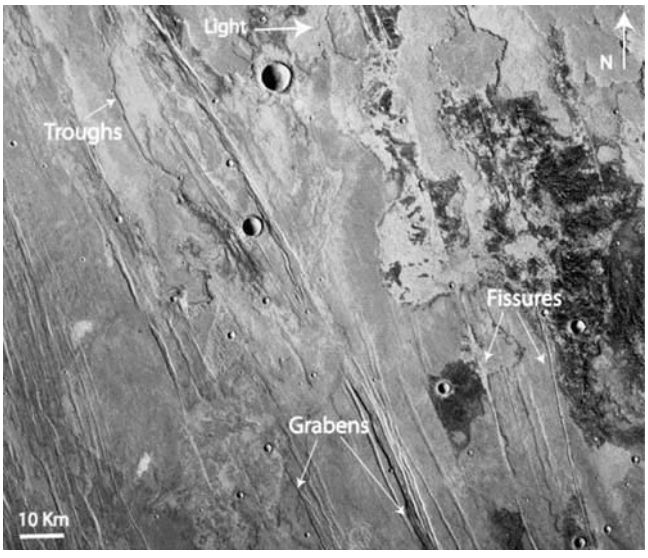

Figure 5. HRSC mosaic image showing several fractured lavas. Troughs are observed to be surrounded or filled in by lava. These fractured lava terrains show grabens of about 4 km width and several fissures that may be the result of ancient faults activated by volcanism. The image is centered at ~20.5°S, 101.5°W. See context on Figure 2.

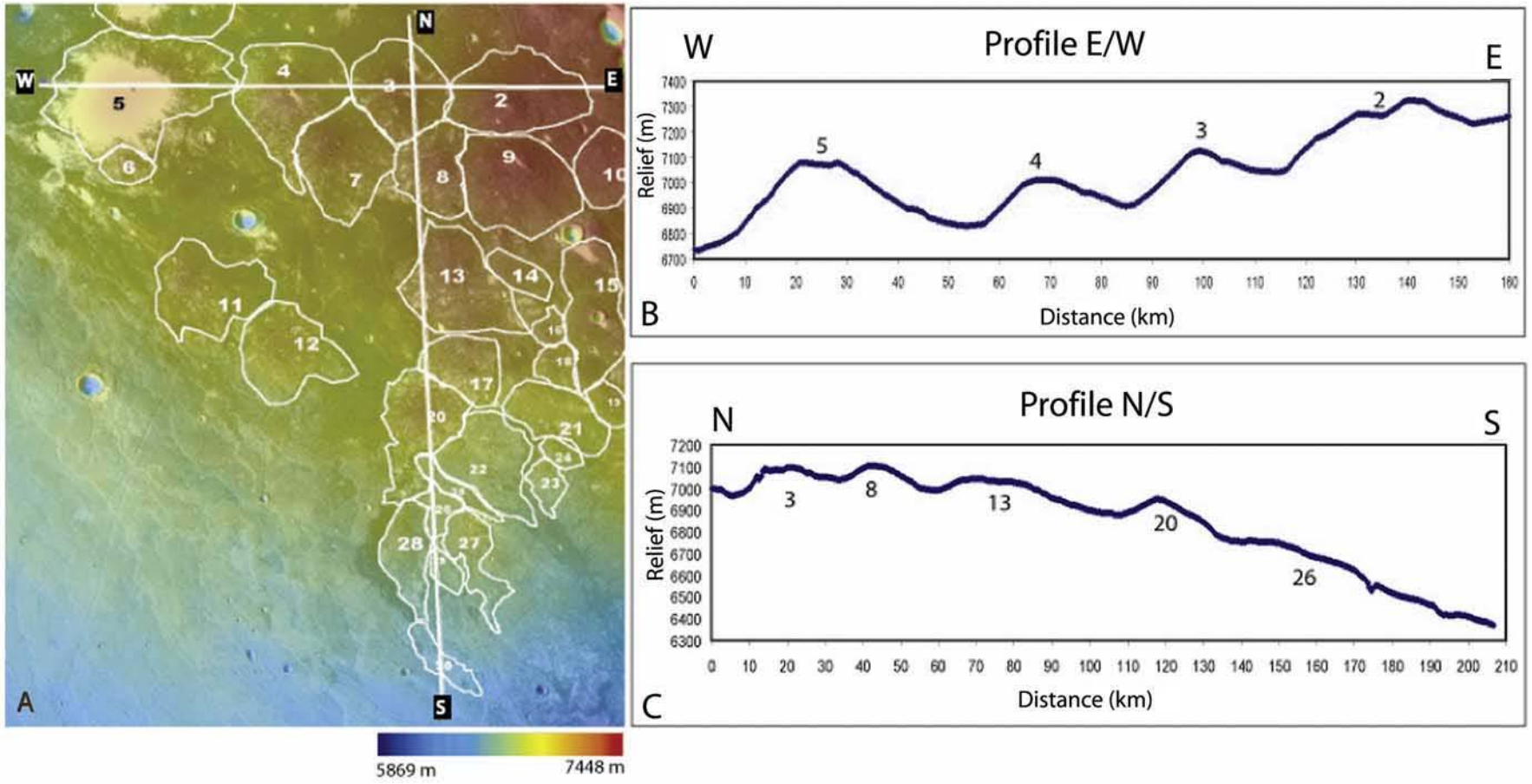

Figure 6. (a) HRSC image superimposed on MOLA data. The white contours limit the swarm of Syria Planum small shield volcanoes numbered from 1 to 31. The center of the image is ~15.40°S, 101.1°W. Profiles of (b) E–W and (c) N–S obtained from MOLA DTMs and located in Figure 6a. From north to south, the small shield volcanoes assume a more elongated shape, following the decreasing topography.

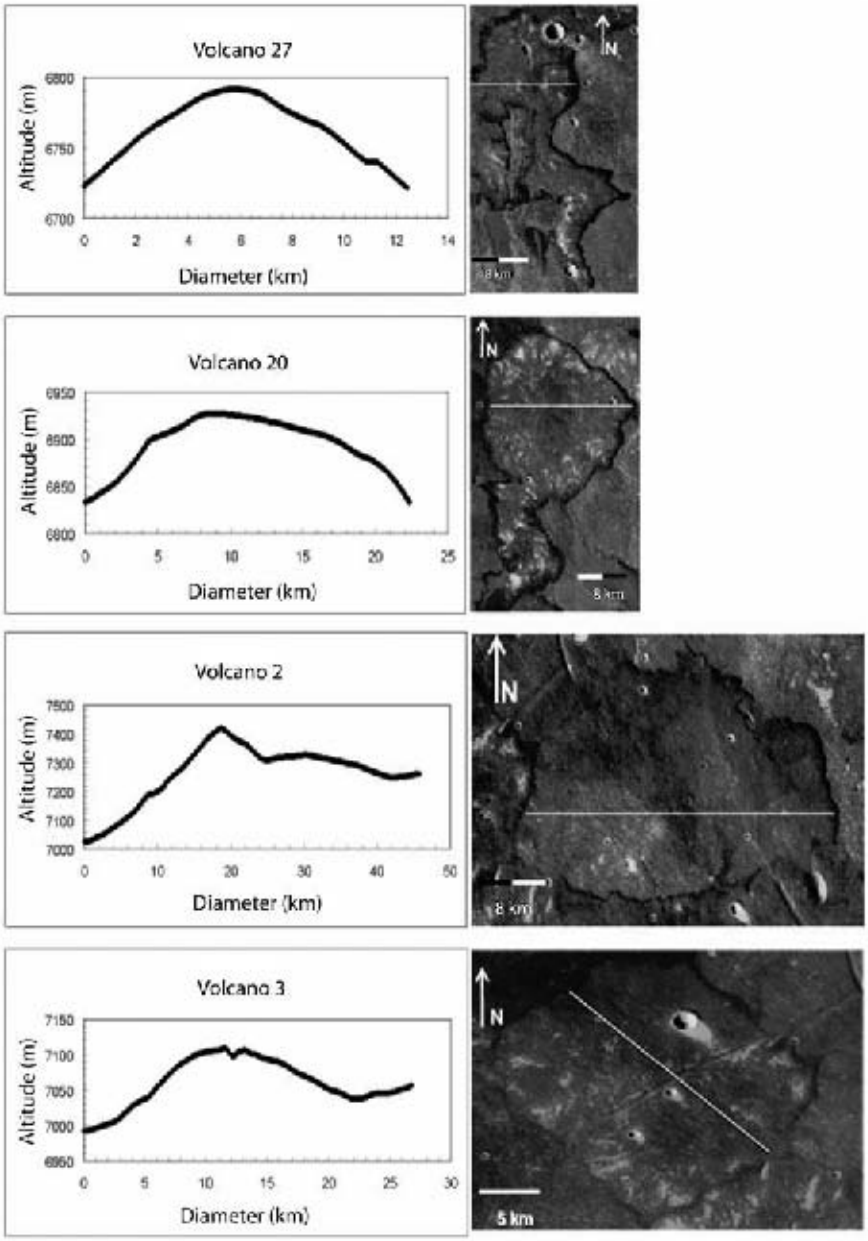

Figure 7. Detail of some shield volcanoes on Syria Planum as seen by HRSC and their correspondent profile from west to east (illumination from west). From the top to the bottom, we can see that volcanoes 27 and 20 show a N–S elongated shape, and volcano 2 shows different flank slopes from west to east. Volcano 3 shows a vent on its summit, which crosses its section NE–SW.

shields) and the lava flows. Ovoid depressions, apparently resulting from a collapsed surface, exist on the top west and east at the external margins of the plateau. A large number of impact craters are also visible from a few tens of meters to ~10 km diameter.

4. Characteristics and Origin of the Axisymmetrical Protuberances

4.1. Morphometry of the Protuberances

[12] The swarm of protuberances covers an area of about 250 km (N–S) × 150 km (E–W) (Figure 3). It is likely that other cones might exist east of the studied region because similar structures are observed with THEMIS and MOLA data. However, we limit our characterization to the features observed in HRSC images.

[13] The HRSC images outline the extent of each axisymmetrical landform, showing their individual shapes (Figures 3 and 6). The topographic profile of each protuberance observed in the MOLA data coincides with the imagery, except for some protuberances located at the northern edge of this area that are covered by dust (numbers 1 and 5 on Figure 3). A predominant central fissure is also present on most of these landforms (e.g., numbers 3 and 27 on Figure 6). This fissure is inferred to be a vent, similar to those observed on terrestrial volcanoes.

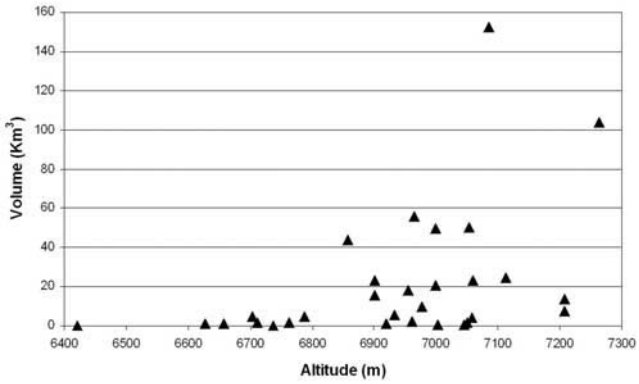

Figure 8. Distribution of Syria Planum small shield volcanoes volumes according to their summit altitude. There is a general tendency for the volcanoes with higher volumes of lava to concentrate at higher altitudes.

[14] These protuberances have flat conical shapes with basal diameters from 7 to ~60 km and individual heights from 10 to 250 m (measured using MOLA data). The flank slopes of the individual features are between 0.2° and 1.0°, with a median slope at 0.5° (see Table 1).

[15] The volume of the small shields (V) was calculated, assuming a conical shape, using their average relief (h) and their W–E basal width ($2r$) (Table 1): $V = 1/3\ \pi\ r^2\ h$. The volume of volcanic edifices ranges from 0.2 to 152.7 km^3 (Table 1). These values should be considered lower bounds on the volume because many of the volcanoes may be embayed by younger materials such as lavas from the adjacent volcanoes and any loading phenomena would have compressed the volcanic material.

[16] Although these volcanoes usually have a conical shape, there are some exceptions. Some of them (e.g., numbers 13 and 20 on Figure 6) display slightly asymmetrical E–W topographic profiles, with the steeper side often on the west. These steeper slopes occur at the intersection

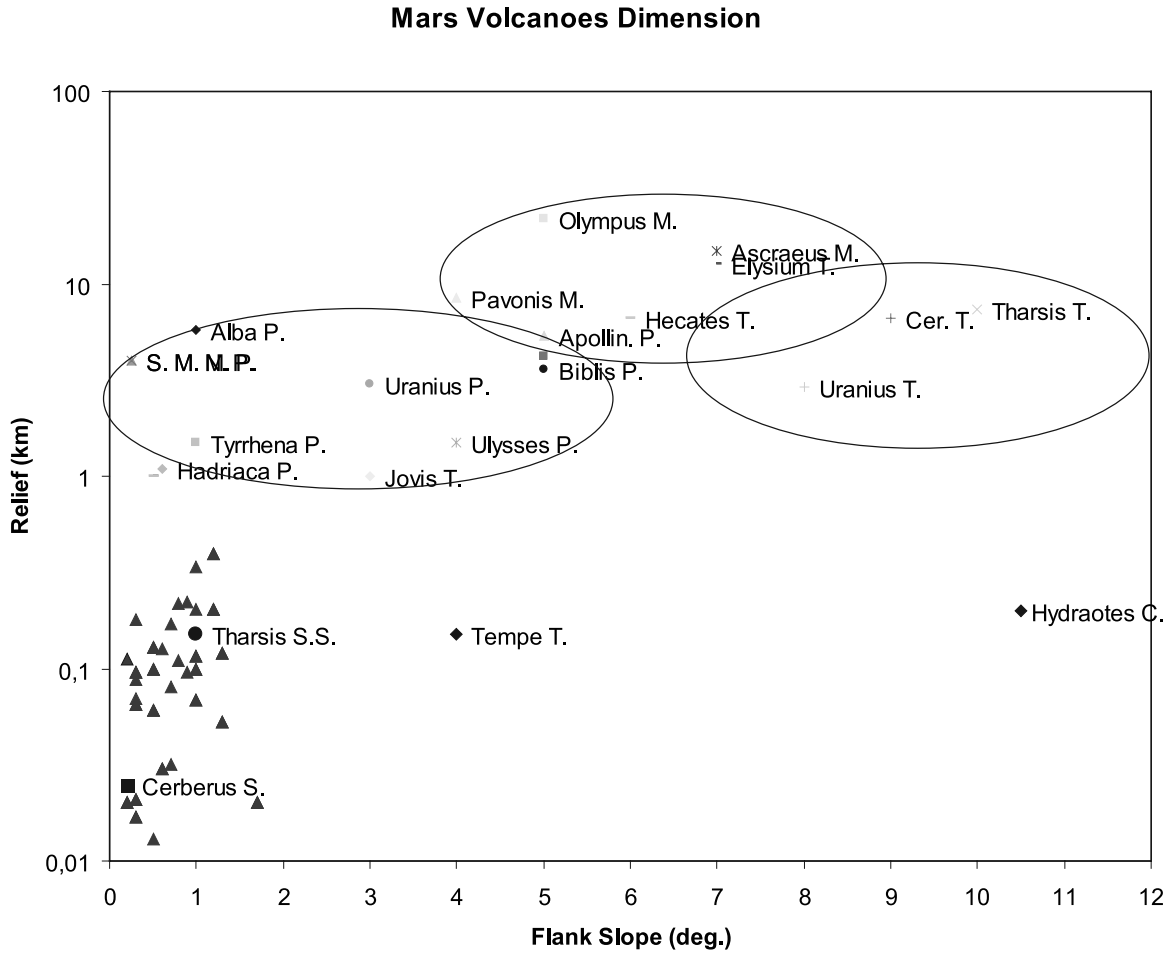

Figure 9. Dimension of Martian volcanoes. The highest topographies are dominated by the Tharsis Montes, while the Highland Paterae are characterized by their flatness [*Plescia*, 2004]. The highest volcano flank dip exists on the Tholii [*Plescia*, 2004] and on the little cones of Hydraotes Chaos [*Meresse et al.*, 2008]. The Cerberus shields (symbolized by a rectangle) represent the smallest shield volcanoes observed on Mars [*Vaucher et al.*, 2006] while those observed in Tempe Terra have higher thicknesses [*Davis and Tanaka*, 1993]. The Syria Planum small shield volcanoes (represented by the bigger triangles) are also flat and of low relief, similar to those shields observed close to the Tharsis Montes (symbolized by a small circle) [*Bleacher et al.*, 2007].

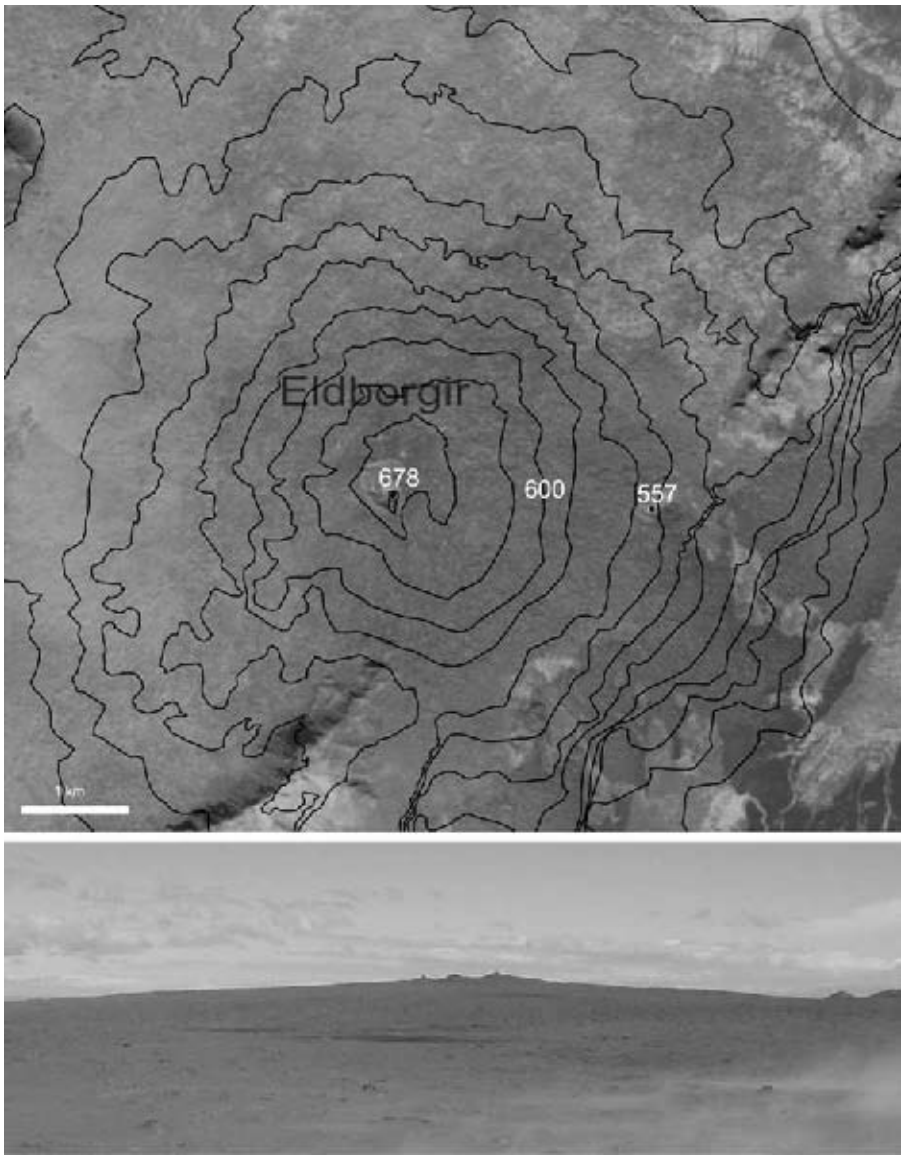

Figure 10. Icelandic small shield volcano. The volcano in the images is Eldborgir ((top) SPOT 5 satellite image with 20 m height contour intervals; (bottom) photography by authors), with a summit high of 200 m and a diameter of ~1000 m. Eldborgir is located in the south of Iceland in a periglacial cold desert area.

with the lava flows, as observed on our map of slopes (Figure 2d), whereas the volcanoes that are surrounded by other volcanoes tend to have a rounder shape and no preferential higher flank dip. Second, the volcanoes tend to be circular north of 15°S (Figure 7), but the shape can be N–S elongated, following the regional topography (e.g., number 20 on Figure 8). We observe that these volcanoes tend to have elongated shapes with the decrease in the regional topography and, consequently, the increased regional slope below 6.5 km. To support these observations, we tested the circularity of each volcano. The assessment of the circularity can be done using the eccentricity, a parameter of the distortion of a circle into an ellipse, which corresponds to the ratio of the linear eccentricity (square root of the difference between the square of the semimajor axis and the square of the semiminor axis) to the semimajor axis. To compute this, we extracted the altitude values of the largest closed contour (contours spaced of 20 m) of each volcanic feature from the MOLA contour data. The results are shown in Table 1. The absence of results for volcanoes 14, 15, 17–19, 21, 22, 25, 26, 29, and 30 is due to their flatter surface; the limited vertical resolution of MOLA data does not permit the isolation of their contours. On the basis of these calculations, we observe that the northern volcanoes (e.g., numbers 2–10) are rounder (eccentricity between 0.4 and 0.5) than the southern ones (e.g., numbers 13, 20, 23, 24, 27, and 28), which tend to be more elongated (eccentricity between 0.6 and 0.9).

[17] Each volcano increases in slope in the E–W direction (as shown on the profiles of Figure 7). Over all Syria Planum, the volcanoes increase in volume in the S–N direction, consistent with the increase in altitude (Figures 6–8). The slope increase to the west occurs closer to the units of large lava flows (e.g., number 5 on Figure 4 or Figure 7).

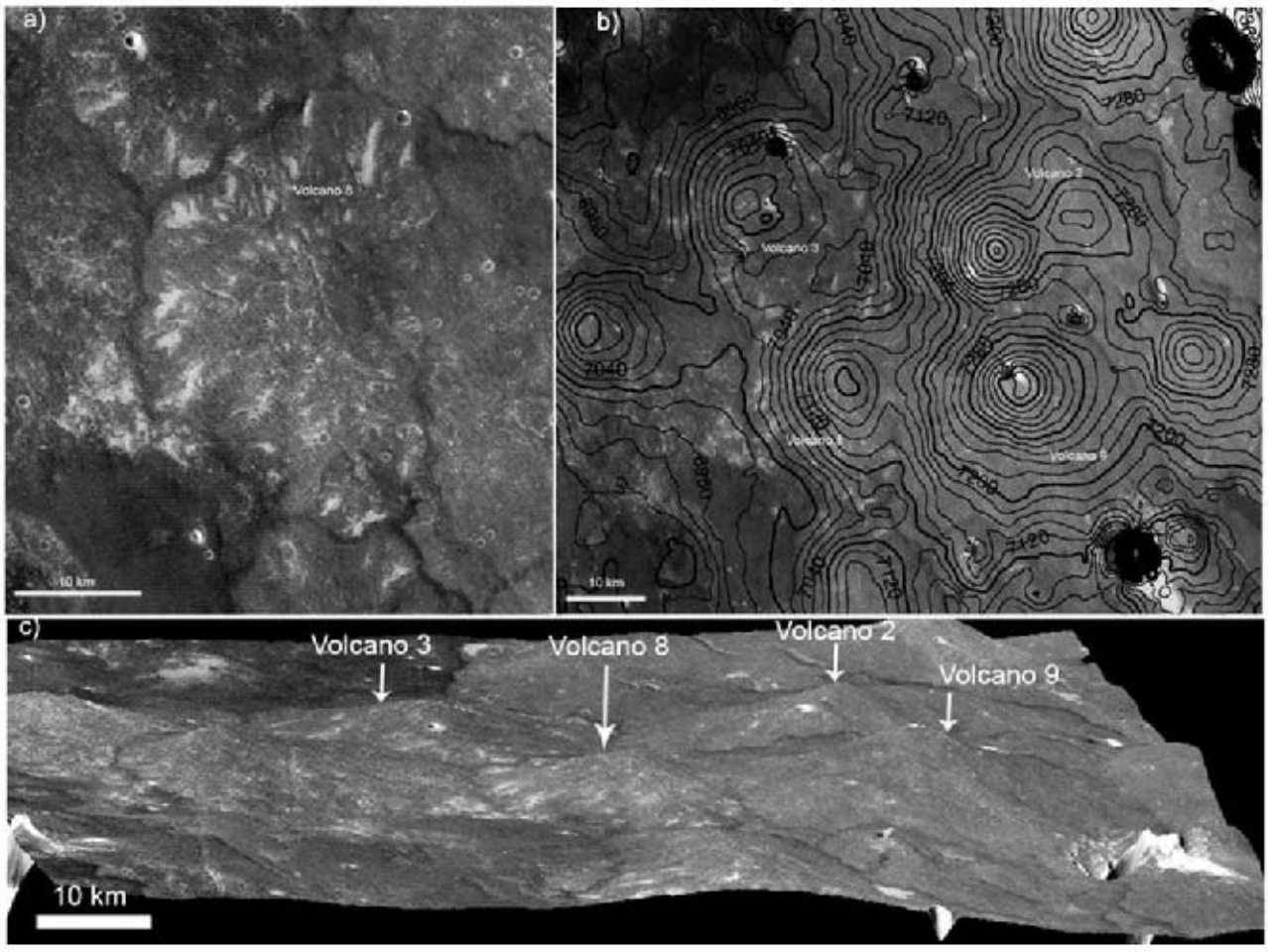

Figure 11. (a) Shield volcano 8 seen by HRSC, where a small vent is visible on the top. (b) HRSC image superimposed by MOLA data where the contour lines (spaced of 20 m) delineate each volcanic shield. The field of coalesced shield volcanoes is represented in a 3-D picture, with 10X vertical exaggeration. (c). The elevation of volcanoes 2, 3, 8, and 9 is shown on Figures 11b and 11c.

The volume decrease to the south is correlated to a decrease of elevation and an increase of the slope (Figures 6–8). This might be due to the fact that the slope impedes the development of a (well-developed) circular volcano creating more elongated edifices. As a consequence, the volcanoes with higher volumes and more circular shapes occur in the northern region, where the terrains are flatter and the elevation reaches a maximum (e.g., numbers 2 and 3 on Figures 7 and 8).

[18] The protuberances have a significant variability in their size, shape, volume, and the existence of an observable vent, but they have the mean shape of a flat cone that can be interpreted as being formed by the progressive accumulation of lavas, similar to terrestrial small shield volcanoes. We next test this hypothesis through comparison with other Martian volcanoes and analogs on Earth.

4.2. Comparison With Other Volcanoes on Mars and on Earth

[19] Figure 9 displays a graph of height versus slope for the main Martian volcanoes and the small volcanoes of Syria Planum. The small volcanoes observed in Syria Planum are different from the three main classes of volcanoes on Mars [e.g., *Plescia*, 2004]. The Tharsis Montes, which display a higher relief (>10 km), are characterized by moderate slopes (3–10°) and broad collapse calderas at their summits [*Malin*, 1977]. Close to their flanks, low thickness shields with few kilometers in diameter can also be observed [e.g., *Greeley*, 1977, 1982; *Hodges and Moore*, 1994; *Bleacher et al.*, 2007]. Tholii are smaller (1–10 km) than the Montes but they have steeper flank slopes (7–12°), much steeper than the Syria Planum volcanoes [e.g., *Mouginis-Mark et al.*, 1992]. Highland Paterae have gentle slopes (<5°) with shallow relief (1–8 km) [e.g., *Greeley and Crown*, 1990]. By comparison, the Syria Planum small edifices have a shape distinct from the three main classes of Martian volcanoes. While they have slopes similar to those of the Paterae (but much smaller in size), they are unlikely to be similar in terms of spatial extent and temporal activity. Syria Planum edifices, therefore, correspond to a distinct class of volcano that we may compare to small edifices found in Cerberus or Tempe Terra [e.g., *Hauber et al.*, 2007].

[20] Comparing the volume of erupted magma, *Plescia* [2004] determined values for the large Tharsis shields, like Olympus Mons (2.4×10^6 km^3), Alba Patera (1.8×10^6 km^3),

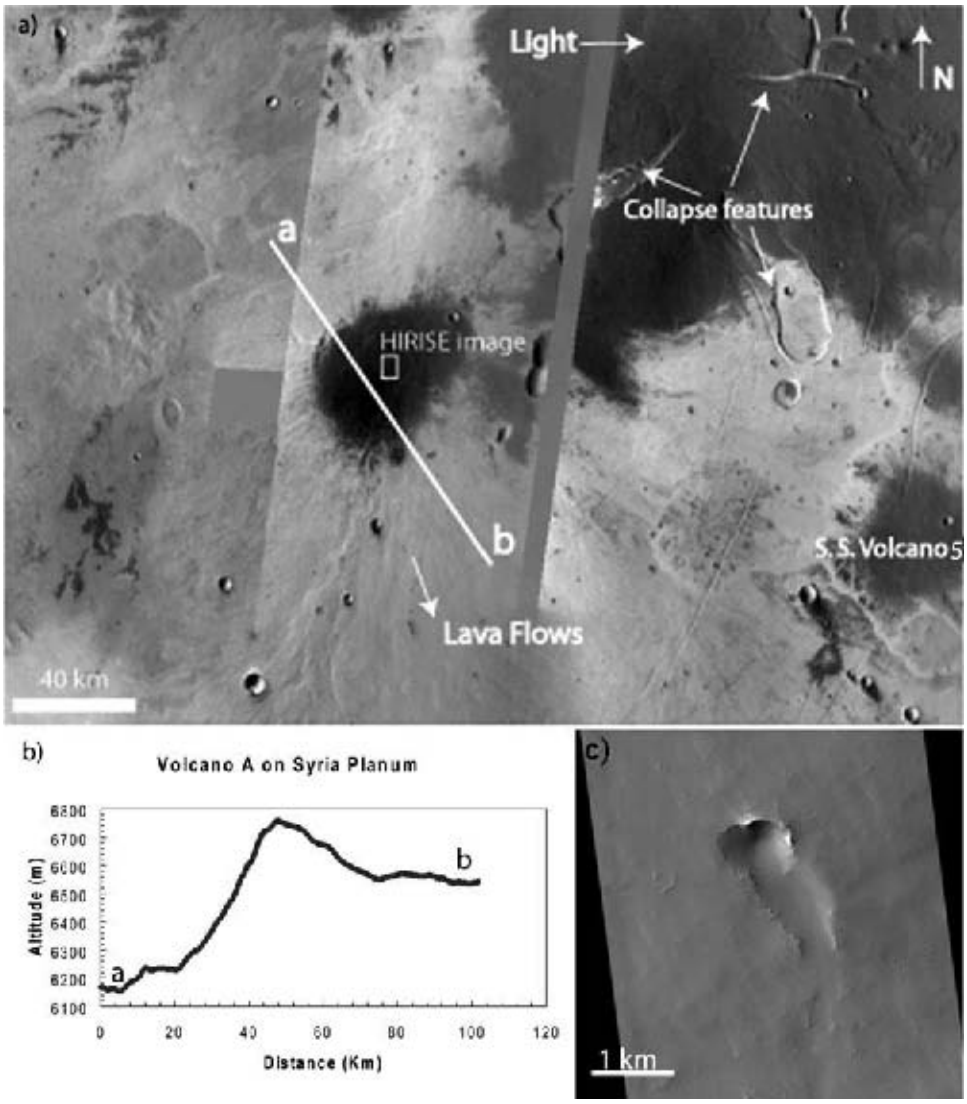

Figure 12. (a) On the center of this image one can observe volcano A, which is the eruption center of the described lava flows. The caldera is about 40 km wide. On the bottom right of the image the shield volcano 5 is visible. On the top right, several collapse features are noted. (b) The profile a–b. (c) HIRISE image (PSP_001840_1660) showing a volcanic vent, with about 700 m width, on the top of volcano A.

and Ascraeus Mons (1.1×10^6 km^3). The other volcanoes are all in the order between 10^3 and 10^5 km^3, with the exception of the Jovis Tholus (10^2 km^3), the minimum determined value. These volume amounts contrast with the Syria Planum small shields that are normally below 10^2 km^3.

[21] On Earth, similarly shaped small shield volcanoes are found in locations such as Iceland (Figure 10). *Rossi* [1996] presented a study of 24 basaltic postglacial shield volcanoes in Iceland. He found a median slope of 2.7° (from 0.6° to 8°), a median height of 60 m (from 12 to 520 m), and a median diameter of 3.6 km (from 500 m to 11 km). The shallow shape of these shields is due to the fluid lavas coming out of rift regions. Syria Planum cones can be compared to some of the Icelandic cones (Figure 11). A comparison is proposed with the Eldborgir shield volcano (also called Lambahraun), which formed 6000 years ago from a single long-duration eruption (Figure 10). The 10 km-diameter volcano has a mean slope of 2° with a summit vent. Its shape is not purely conical, as it formed over preexisting, nonflat topography. Several Icelandic cones have slopes smaller than 2°, or even 1°, such as Strandarheiði with a slope of 0.6° [*Rossi*, 1996], comparable to those of Syria Planum edifices. On average, the small edifices of Syria Planum have a median slope of 0.5°, thus 5 times smaller than in Iceland. A possible explanation of this difference is that it might come from a difference in viscosity of lavas slightly more fluid on Mars.

5. Characterization of the Lava Flows Unit

5.1. Morphology and Lavas Origin

[22] The extensive field of lava flows, identified between ~15°–19°S and 105°–102°W, covers an area of ~100,000 km^2 (Figure 2). Through the study of HRSC images and THEMIS IR day and IR night images, we can identify elongated and lobate shapes for these flows with preferential orientation NW to SE, following the regional slope.

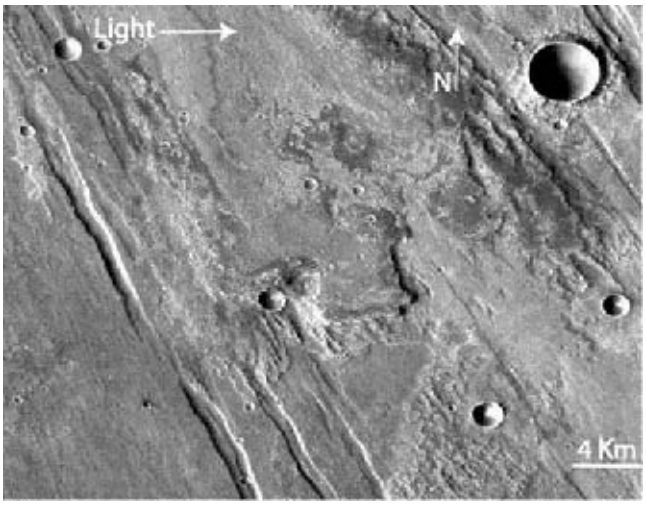

Figure 13. HRSC image centered at 20.5°S, 102.3°W, where some NW–SE oriented grabens are covered by lavas with the same orientation.

[23] Using THEMIS and MOLA data, we observe that these lava flows erupted from an isolated volcano, hereinafter named volcano A, on the northeast of Syria Planum (Figure 12, represented on the geomorphic map on Figure 2f). The summit cone of volcano A is about 40 km in diameter, and it lies at an elevation of ~6700 m. This volcano is located outside of the HRSC mosaic, although a new High Resolution Imaging Science Experiment (HiRISE) image enables its study (Figure 12). On Figure 12, we show a MOLA profile from "a" to "b." From the center of the volcano to the side a the slope is about 1.4°, while from the center to the side b the slope decreases to 0.7° to the side where the lava flows extend.

[24] We can observe the presence of postflow tectonic deformation. On Figure 12, note that the flanks facing east are much smoother than the western flanks, where the slope is much more accentuated. On the southern part of Syria Planum, and from an extension of some hundreds of kilometers SE of volcano A, we observe that the lava flows partially cover a field of grabens (Figure 13). We detail the fault system and its relationship with lava flows in section 6.

5.2. Lava Flow Rheology

[25] Using HRSC images, THEMIS IR day and MOLA data, we studied several lobate lava flows on Syria Planum. The results from its geometry and rheology are shown in Table 2. It is largely known that Martian volcanic edifices can produce several features such as lava tubes and channels [e.g., *Carr*, 1973, 1974; *Greeley*, 1973; *Greeley and Spudis*, 1981; *Cattermole*, 1987, 1990; *Sakimoto et al.*, 1997]. In terrestrial volcanology there exists a link between tube flows and a more steady flow rate and, conversely, the connection between channels and unsteady flow rates [e.g., *Sakimoto et al.*, 1997].

[26] We infer the Syria Planum lava channels are predominantly the result of constructional processes (flow confined by building of levees), often roofing over to form tube flows. The lava channels occur in the area immediately south of the Syria Planum shield volcanoes (Figure 14), an area where several periods of intensive fracturing are recognized (as described in section 6).

[27] The techniques described below consider alternatively the lava flows as Newtonian fluids (which allows the determination of the flow rate and viscosity) or as Bingham flows characterized by a yield stress. These techniques are useful in providing a comparison between terrestrial flows (of known composition) and Martian lava flows [e.g., *Hulme*, 1976]. However, given the fact that these rheological models are mutually inconsistent, the computed absolute values should be viewed with extreme caution.

5.2.1. Lava Flows Dimensions

[28] We isolated 10 lava flows where channel (or tube) flows are mostly present and their rheology was studied using MOLA DTM data. The size of the observed lava flows varies from a few hundred meters to about 200 km, with the mean length of about 150 km. Their width varies from 5 to 15 km, with the mean value of 9.4 km. The levees on the lava flow have a mean width of 5 km. Thicknesses of the lava flow vary from 15 to 70 m, with a mean value of 34.5 m. The average slopes of the studied flows are approximately to 0.2°, although in a few cases (in places with superposition of lavas) it can exceed 1°. This results in volumes of individual lava flows ranging from an average of 40 km^3 to a maximum of 200 km^3.

5.2.2. Effusion Rate

[29] The effusion rate of this system, or its volume flow rate (Q, m^3 s^{-1}), can be determined using the Graetz dimensionless number (Gz) [e.g., *Knudson and Katz*, 1979; *Pinkerton and Wilson*, 1994; *Warner and Gregg*, 2003; *Hiesinger et al.*, 2005]:

$$Q = \frac{Gz\ kxw}{b}. \tag{1}$$

The Graetz number that is related to the cooling of a warm fluid moving through a cold pipe [*Hulme and Fielder*, 1977; *Wilson and Head*, 1983; *Zimbelman*, 1985] assumes laminar flow and relates the heat lost by diffusion in a flow to the heat lost by advection along its length [*Warner and Gregg*, 2003], in which k is the thermal diffusivity (3.0×10^{-7} m^2 s^{-1}, a similar value for both Martian and terrestrial lavas) [e.g., *Gregg and Fink*, 1996; *Warner and Gregg*, 2003], x is the flow length (m), w is the width of the flow (m), and b is

Table 2. Geometric and Rheologic Parameters Measured From Topographic Data From Profiles on 10 Lava Flows

	Length (m)	Thickness (m)	Width (m)	Slope (°)	Effusion Rate (m^3 s^{-1})	Viscosity (Pa s)	Yield Stress (Pa)
Minimum	45×10^3	15	5×10^3	0.15	990	6.89×10^5	–
Maximum	200×10^3	70	15×10^3	1	6,075	4.23×10^6	–
Mean	150×10^3	34.5	9.4×10^3	0.2	3,300	–	1.2×10^{3a}

[a]Lengths between 100 and 200 km and thicknesses between 15 and 70 m were used. The mean value for the smaller size lavas is 7.9×10^2 and 1.7×10^7 for the larger ones.

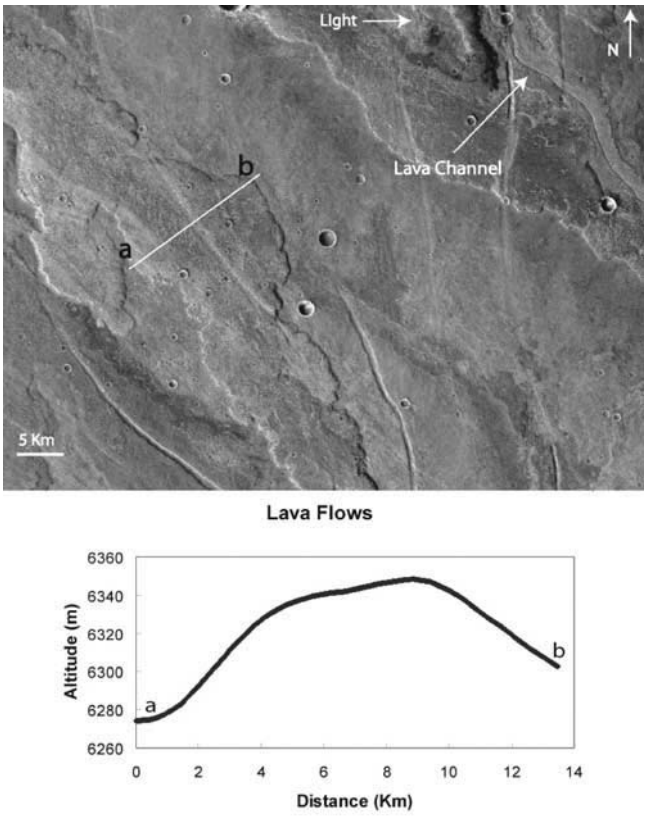

Figure 14. Image centered at 17.3°S, 100°W. Lava channels are visible on the described lava flows. The channel on the top right displays lava levees on its sides. The profile a–b is shown on the bottom graphic.

the thickness of the flow (m). In analogy to terrestrial lava flows, we assumed a value of 300 for the Graetz number [e.g., *Hiesinger et al.*, 2005]. As a result, we find that effusion rates range from 990 to 6075 $m^3\ s^{-1}$, and the mean value is 3300 $m^3\ s^{-1}$. These values are the same order of magnitude as the ones determined for Arsia Mons [*Warner and Gregg*, 2003], although they are of some orders of magnitude superior to those found on Ascraeus Mons (18–60 $m^3\ s^{-1}$ and a mean value of 35 $m^3\ s^{-1}$ from *Zimbelman* [1985]) or on Olympus Mons (400 $m^3\ s^{-1}$ from *Zimbelman* [1985]). Regarding the effusion rates and determining the volumes of individual lava flows, we calculated that the time necessary to emplace these flows is 140 days on average, with a maximum of 700 days.

5.2.3. Viscosity

[30] The viscosity can be determined using a model obtained from a steady laminar isothermal gravity-driven Newtonian flow, with no slip at the base and no shear stress at the top surface [*Sakimoto et al.*, 1997]. This flow system can be resolved in a rectangular flow solution (equation (2)) where flow depth and flow width are comparable. The surface velocity is independent of the cross-flow direction, likewise because there are no channel walls [*Sakimoto et al.*, 1997]. So, the flow rate per unit width is given by

$$\frac{Q}{w} = \frac{b^3 \rho g' \sin(\theta)}{3\mu}. \quad (2)$$

Here Q is the volume flow rate (i.e., eruption rate), w is full flow width (in sheet flow), b is the flow depth in a Newtonian channel and sheet flow, g' is the adjustment made for the acceleration of gravity on Mars (3.73 m s^{-2}), θ is the slope, μ the viscosity, and ρ is the density (we assumed 2800 kg m^{-3}, knowing that this value can change by 30–50% in the presence of bubbles/vesicles in lavas).

[31] Our estimate of the viscosity ranges from a minimum of 6.89×10^5 Pa s to a maximum of 4.23×10^6 Pa s (depending on the previous determined values of effusion rate). These values are in agreement with several other viscosities determined for Martian lavas [e.g., *Hiesinger et al.*, 2005, 2007; *Warner and Gregg*, 2003]. On Earth, terrestrial basalts and andesites have viscosities from 1.4×10^2 to 1.4×10^7 Pa s [e.g., *Hiesinger et al.*, 2005; *Wilson*, 2001; *Wilson and Head*, 1994]. So, the Syria Planum lava flows are in the range of relatively viscous basalt to andesite. Also, *Fink and Zimbelman* [1986], assembling different methods, determined values from $\sim 0.8 \times 10^6$ to 8×10^6 Pa s for the Kilauea lava flows.

5.2.4. Yield Stress

[32] Alternatively, we consider below that the lava flows can be approximated using Bingham fluids, which differ from Newtonian fluids by the existence of yield strength in addition to the viscosity.

[33] The yield stress may be estimated from the combination of the following three parameters: the flow depth b, the slope θ, and the width of the flow w, and also by assuming a density flow value equivalent to terrestrial basalt (2800 kg m^{-3}) [e.g., *Hiesinger et al.*, 2005]:

$$\sigma_s = \rho g b^2 / w \quad (3)$$

$$\sigma_s = \rho g b \sin\theta. \quad (4)$$

Using equations (3) and (4), for 10 lava channels of Syria Planum with lengths between 100 and 200 km and thickness between 15 and 70 m, we obtain mean values between 7.9×10^2 Pa (for the smaller sizes) and 1.7×10^3 Pa (for the larger sizes), and the overall mean value is 1.2×10^3 Pa. These values are consistent with terrestrial basaltic to andesitic lava flows and also with the Arsia Mons lavas [see *Moore et al.*, 1978]. Also, *Zimbelman* [1985] determined similar values for Arsia Mons ($1.0 \pm 0.8 \times 10^3$ Pa) and larger values for Ascraeus Mons ($2.1 \pm 1.8 \times 10^4$ Pa) and Olympus Mons ($2.0 \pm 0.3 \times 10^4$ Pa). *Fink and Zimbelman* [1986] determined different values of viscosity depending on the place that the measurements were made along the lava flow; higher with the increasing distance to the lava source. These authors analyzed lavas from the Kilauea volcano, in which lavas have lengths inferior to 3 km, so they have inferior size to the Martian ones, and obtained values from $\sim 4 \times 10^3$ to 40×10^3 Pa.

[34] Overall, rheologic parameters from Hawaiian and Arsia Mons flows are about the same order of magnitudes of those determined in Syria Planum.

6. Tectonic Patterns and Their Relationship With Volcanic Units

[35] In the studied area, we identify at least four tectonic episodes distinguishable from their different directions and

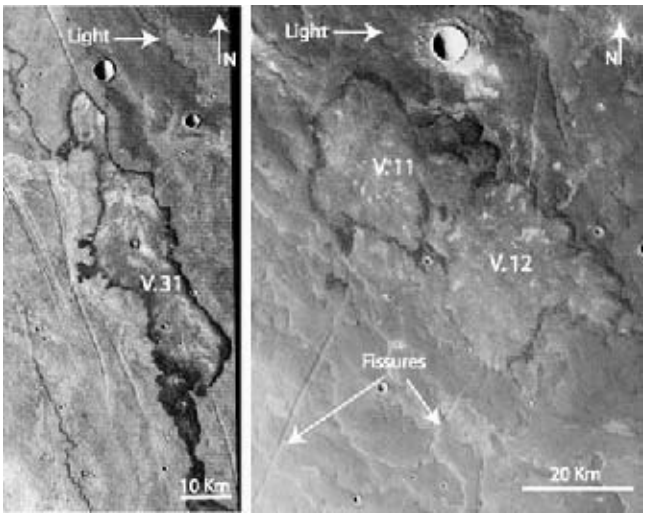

Figure 15. (left) HRSC image centered approximately at 19.8°S, 100.9°W showing the volcano 31, a fissure some tens of kilometers long from which lavas erupted. Its borders, which have a clearly darker tone, define well its shape. (right) HRSC image centered at 15.4°S, 101.5°W, where volcanoes 11 and 12 superimpose lavas that were intersected by fissures oriented NE–SW.

patterns. First, using MOLA and HRSC data, we observe NW–SE faults typically a few kilometers wide and hundreds of kilometers long, as seen at the bottom of the studied images (Figures 2 and 13). These fractures exhibit a very dense network of faults defining many small grabens, which are covered by lava flows related to volcano A in the northwest. These grabens might correspond to the most primitive tectonic pattern that affected the bedrock previously to the discussed volcanic events. Syria Planum was the center of tectonic activity before the emplacement of the volcanic plains at the surface. Those older faults are observed in Claritas Fossae and north of Noctis Labyrinthus. Presumably those faults underlie the present surface and can exhibit control on the area's volcanism.

[36] Second, the lava flows of volcano A have been intersected by faults, mainly oriented NE–SW, in the northern region of Syria Planum (Figure 15, right). We determine that these fractures are hundreds of kilometers long and approximately some tens of meters in depth. They are much more scattered and less densely distributed than the NW–SE oriented faults found to the south.

[37] Third, in the southern and eastern regions of Syria Planum (Figure 15, left), next to the NW–SE oriented grabens, there are fissures some hundreds of meters wide. Volcano 31 appears to have been created by such NW–SE reactivation. This activity thus clearly postdates the lava flows of volcano A and, therefore, the NW–SE faults that are buried beneath the lava flows. We interpret these faults and related activity to have resulted from a reactivation of the ancient NW–SE fractures possibly as a consequence of volcanic activity. It can be seen from the chronological relationships that the overall NW–SE features were formed earlier (without relation to this volcanic episode) and buried beneath lava flows from volcano A, whereas individual faults in same direction found over the lava flows formed later, probably in relation to the formation of the small shields.

[38] Finally, one can also identify several collapsed features (represented in blue on the geomorphologic map of Figure 2f) in the proximity of the isolated volcano A (Figure 12) and structural depressions that extend laterally to volcano 2 (e.g., Figure 3). These collapse features postdate all the different terrains of Syria Planum, affecting the small shields at their northern boundary.

[39] These four types of tectonic patterns can result from different volcanotectonic activities [e.g., *Masson*, 1980]. Faults with NW–SE preferential orientation correspond to the Noachian-Hesperian graben construction [e.g., *Plescia and Saunders*, 1982; *Tanaka and Davis*, 1988]. This activity is related to the first episode of faulting to the south, corresponding to a major stress field that crossed most of the Tharsis region. Faults with a NE–SW trend are more scattered, resembling individual fissures rather than a main tectonic episode. It has been shown that such features can be produced by near-surface stress fields associated with intrusive magma, which can fill in the existing fractures and sometimes increase their dimensions [e.g., *Wilson and Head*, 1981; *Tanaka and Davis*, 1988]. Because of the proximity of the small shield volcanoes, these faults might be interpreted as dikes from which several volcanic edifices were created. The ancient NW–SE fault direction might have been reactivated, possibly at the same time as the NE–SW faults formed, to localize the emplacement of the elongated volcanoes such as number 31. The collapse features that crosscut all units might be related to the period of main collapse of the Noctis Labyrinthus region north of Syria Planum.

[40] Chronologically, the sequence of tectonic and volcanic activity is very clear from relative stratigraphy. If we interpret the collapse features to have formed during the Noctis Labyrinthus event, then the age of these collapses would correspond to approximately the end of the late Hesperian and beginning of the early Amazonian [*Tanaka and Davis*, 1988]. This suggests that the volcanoes were all formed prior to that period. In the next section, we test this possibility by dating the volcanoes using crater counts.

7. Dating Volcanoes by Crater Counts

[41] Craters larger than 250 m in diameter were counted and classified over a surface of 7760 km^2 corresponding to the small shield volcanoes and over 20,945 km^2 on the lava flows. For the volcanoes, the craters were first counted for each isolated volcano and then summed over the entire surface in order to be able to date them both individually and as a whole.

[42] The cumulative number of impact craters with diameter $\geq$1 km is

$$N(1) = \frac{N}{S} \pm \frac{\sqrt{N}}{S}, \tag{5}$$

where N is the number of craters per surface S. We determined 0.0029 ± 0.0006 craters km^{-2} for the small shields and 0.0025 ± 0.0003 craters km^{-2} for the lava flows. These counts correspond to ages of 3.5–3.6 Ga for small

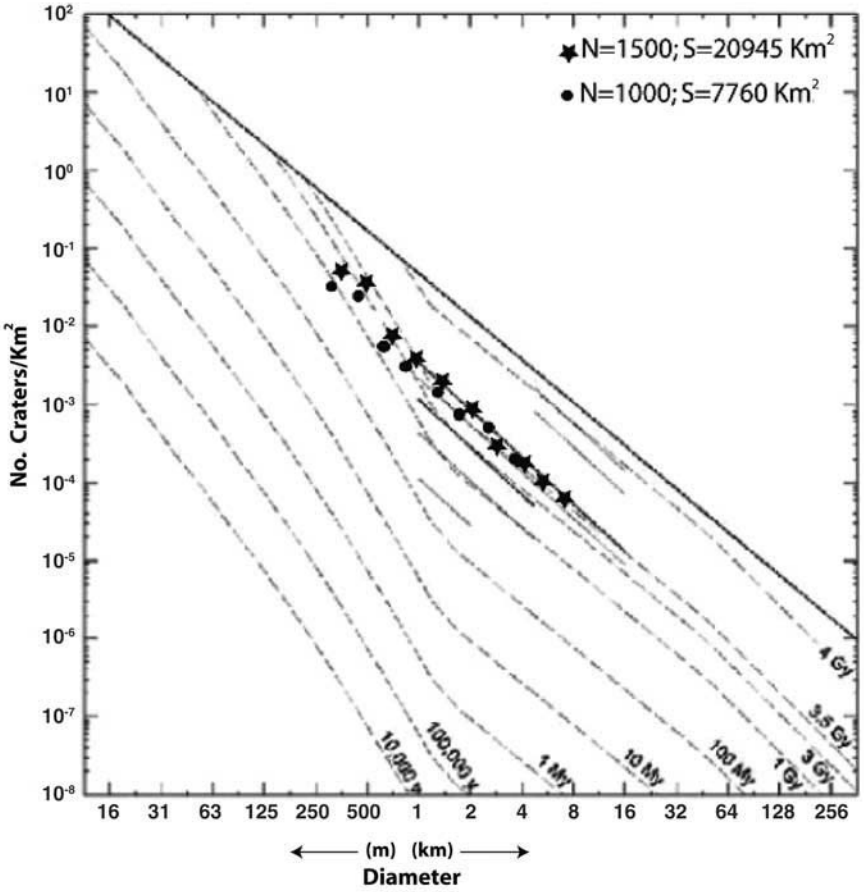

Figure 16. Crater distribution over the studied Syria Planum lava flows and shield volcanoes. Isochrones are plotted according to *Hartmann et al.* [2000]. We used only craters >250 m diameter for this study. The ages associated with the isochrones are given by the lunar rates modulated by a ratio of $R = 1.6$, corresponding to the ratio between the crater production function on Mars and the same rate on the Moon. However, these could all correspond to Hesperian ages. Dots correspond to volcanoes ages associated with a surface of 7760 km^2 and where ~1000 impact craters with a diameter >250 m were observed. Stars correspond to lava flow ages associated with a surface of 20945 km^2, where ~1500 impact craters with a diameter >250 m were observed.

shields and ~3.6 Ga for the lava flows from volcano A [*Hartmann and Neukum*, 2001]. The ages are not significantly different, suggesting that the period of time between the formation of volcano A and the small shields was limited.

[43] For a more accurate estimation, we plotted ages in increments of $\sqrt{2}$, as in the model of *Hartmann and Neukum* [2001]. The isochrones plotted on Figure 16 correspond to the density of craters that should be observable on a surface preserved from erosion and deposition since its formation.

[44] The model takes into account the crater production function of the Moon, adapted for Mars, which fixes the slope of craters smaller than 1 km and is adapted to show turndowns and variations of populations that could be interpreted in terms of obliteration, erosion, or deposition [*Hartmann et al.*, 2000]. On Figure 16, one can observe the frequency of each interval of crater size for the volcanoes (in dots) and for the lava flows (in stars). Both units follow isochrones of the Hesperian period with small shields appearing slightly younger than the lavas. The more recent ages for craters <500 m correspond, therefore, to surface degradation because of resurfacing since the formation of lava.

[45] We next tried to individually date each volcano, although statistically this estimate is not valid once recent resurfacing processes obliterate the smaller craters. The smaller-sized craters may be a good indicator of resurfacing and erosion periods, whereas to date bedrock (not surface) processes, the bigger sizes (up to 250–350 m) are better.

[46] The dating of these volcanoes, as well as their topographic analyses, confirm previous propositions [*Plescia*, 2004] of the fact that they might have occurred during a geologically short period of time, probably not more than some tens of millions of years. From this work, and using HRSC images and MOLA data on crater counting, we assume that these events may have lasted from the early Hesperian to the middle of the Hesperian, which

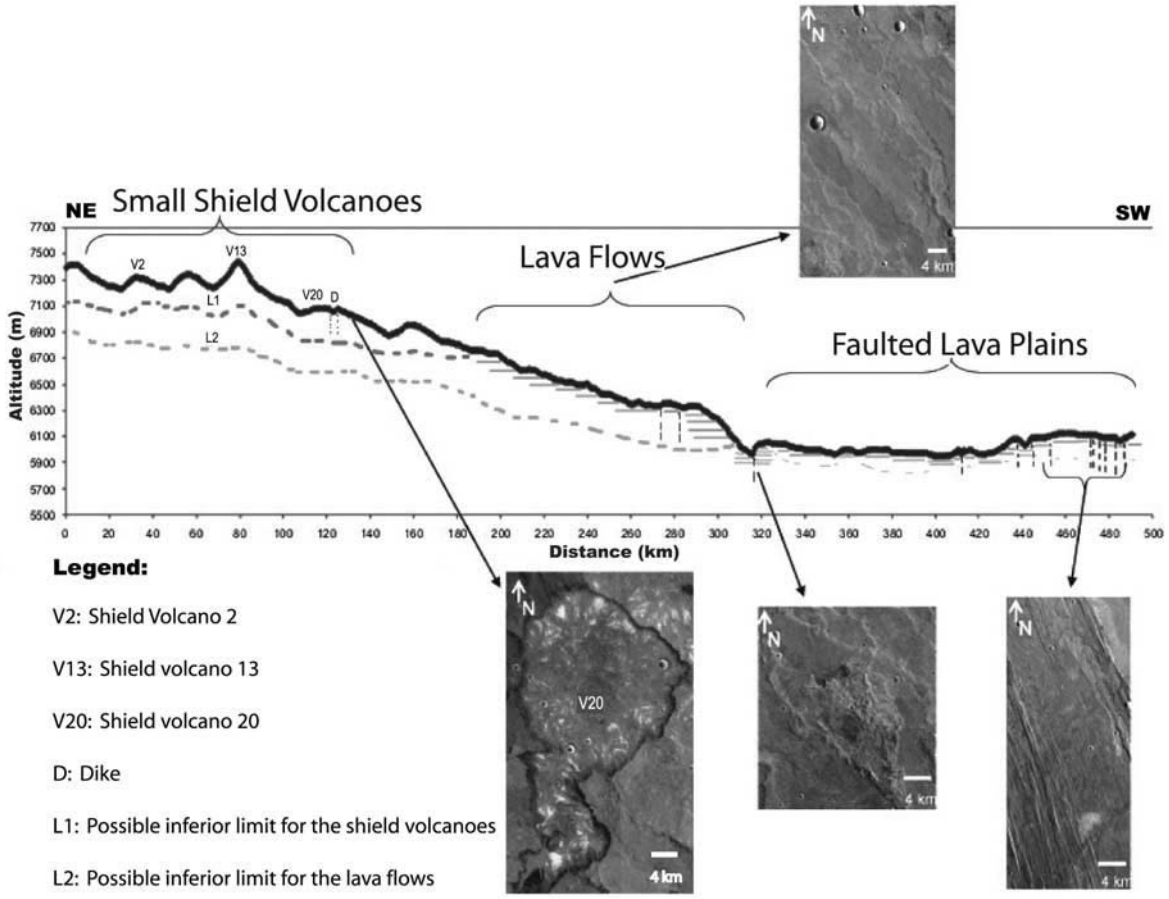

Figure 17. Profile NE–SW from the Syria Planum region. From highest to lowest altitudes we can observe the succession of the low shield volcanoes, the lava flows intersected by predominantly NE–SW fissures, and the highly faulted lava terrains.

means that the main volcanic activity in Syria Planum occurred during this period.

8. Synthesis: Chronology of Volcanic and Tectonic Episodes

[47] Our study of the HRSC images suggests that a much more complex geologic history of Syria Planum exists than was previously expected, especially in light of the identification of a unique swarm of small shield volcanoes that occur in the most elevated part of the region (Figure 17). Southwest of these edifices, ~200 km long lava flows erupted from a volcano also not previously identified. Both volcanic systems have embayed the highly faulted crust that is only visible in the southern part of the region (example on Figure 17).

[48] The geological episodes that existed in this location can be chronologically described in the following phases:

[49] 1. Formation of the grabens, with a few on the order of 4 km width, which is dated to the late Noachian to early Hesperian epoch [*Tanaka and Davis*, 1988].

[50] 2. Formation of volcano A in the early Hesperian, which partially covers the grabens of phase 1 (Figures 12–15), but are not cut by these grabens.

[51] 3. Lava flows from volcano A are cut by NE–SW faulting events of early Hesperian age. In some areas, the faults may serve as conduits for magma eruptions that postdate the lava flows from volcano A. In that case, phases 3 and 4 are almost contemporaneous (Figure 15).

[52] 4. A swarm of shield volcanoes (formed during the Hesperian period) are superimposed on these lava flows (Figure 17). Also, at least three volcanic shields are clearly superimposed on lava flows from volcano A (see volcano 5 on Figure 12a or volcanoes 11 and 12 on Figure 15).

[53] 5. A few depressions formed by collapse might signify the last episode of activity, perhaps generated by the Noctis Labyrinthus opening in, or after, the late Hesperian (Figure 12).

[54] The schematic cross section in Figure 17 also shows that the total unit of Hesperian-aged volcanic landforms does not have a large thickness. From the relationship with the fault system to the south, it is likely that the total thickness of this material does not exceed 2 km, although it is difficult to estimate a boundary that depends on preexisting terrains (now completely buried). This remark is important because it shows that the elevation acquired by Syria Planum predates the age of the visible surface, at least to the elevation of about 6 km over Mars datum, suggesting the

Noachian rise of the bulge reached this minimum value of 6 km.

9. Discussion

[55] The suite of volcanotectonic episodes identified in Syria Planum has two specific characteristics that require a few comments. First, swarms of coalesced small shield volcanoes are not usual in the Tharsis region. What kind of volcanic phase do they indicate? How are they related to volcano A? Second, our work shows that the volcanism in this area ended during the Hesperian epoch. Why did it end whereas the northern and western parts of the Tharsis region continued to display volcanic activity throughout the next 3 Ga?

[56] To answer the first question, we first note that both earlier studies of Martian volcanism [e.g., *Greeley and Crown*, 1990; *Crown and Greeley*, 1993] and more recent works [e.g., *Plescia*, 2004] proposed that the older volcanoes have smaller volumes and dimensions than the younger giant shields. Syria Planum small shield volcanoes are of a relative age older than the Tharsis shield volcanoes (at least to their current surfaces). Nevertheless, volcano A has many characteristics similar to the Tharsis Montes, such as the effusion rates, except that it did not grow as high as the Tharsis Montes. In addition, isolated small shield volcanoes were already observed in the flanks of Pavonis Mons and in the caldera of Arsia Mons as well as an extensive field of small vents on Ascraeus Mons [e.g., *Greeley and Spudis*, 1981; *Hodges and Moore*, 1994; *Bleacher et al.*, 2007]. *Greeley* [1977, 1982] characterizes it as a plains-style volcanic field area, where lava flows between the low shields and fissures were emplaced via a combination of lava tubes and extensive sheets. As they are distal to the caldera, or to the last volcanic episodes on the flanks, they might be a sign of late activity in the region of the large Tharsis Montes [*Bleacher et al.*, 2007], probably from the late Amazonian, an age much younger than the Syria Planum volcanoes. Syria Planum was dominated both by swarms of coalesced small shields and a single larger edifice (volcano A) as the source of long lava flows. The small shield volcanoes might signify late-stage activity that once began with the emplacement of volcano A, identified by long lava flows and a lava viscosity similar to the Tharsis Montes. This volcano A might never have reached the stage to enable the construction of a larger volcano at this location.

[57] This style of multistaged volcanic activity suggests that there is a need to examine the role of the local lithospheric structure. It is of note that the heights of volcanoes may provide significant constraints on the lithospheric thickness for terrestrial planets [e.g., *Blasius and Cutts*, 1976]. Assuming that the heights of the shield volcanoes are hydrostatically limited, there is a simple relationship between the height of the volcano and the base of the lithosphere considered to be the source of the magma. The region of Syria Planum is characterized by a thick crust of more than 80 km (from *Neumann et al.* [2004]) and the highest altitude of the Tharsis region [*Neumann et al.*, 2004]. Furthermore, according to *Neumann et al.* [2004], the deepest mantle, or the deepest Mars-equivalent Moho interface, occurs in southern Tharsis, near Syria and Solis Planum. Considering that the crust has a lower thermal conductivity ($\sim$2.5 W K^{-1} m^{-1}) than the mantle ($\sim$4 W K^{-1} m^{-1}) [*Schumacher and Breuer*, 2006], this fact implies that the present lithosphere is thinner below this region. The elastic thickness of the lithosphere (T_e) at the time of loading has been estimated independently from gravity/topography admittances [*McGovern et al.*, 2002]. Below Solis Planum, a region having a thick crust in the immediate vicinity of Syria Planum, T_e ranges from about 40–60 km corresponding to 10–15 K km^{-1}, whereas T_e has been estimated at twice this value below the Tharsis Montes. It is thus possible that the structure below Syria Planum is characterized by a thick crust associated with a thin lithosphere at the time of the magmatic activity, which has resulted in shallower magma sources in Syria Planum. As a consequence, the maximum height for the possible volcanic constructs in this region was more limited than in the other regions of the Tharsis plateau. We therefore suggest that the cessation of activity of a large volcano on Syria Planum might signify the presence of a thicker crust in that part of the bulge. This would explain the incomplete development of the larger volcano at this location by the end of the volcanism, early in the geologic history of the Tharsis region.

[58] In summary, we hypothesize that Syria Planum shield volcanoes played an important role in the primordial Tharsis volcanism and that their activity ceased early in the geologic history of this region. The progressive cessation of activity might be due to the enhanced crustal thickness in the magmatic processes of this region. The highest crustal thickness beneath Syria Planum led us to focus on its principal role in the origin, but also the decline, of volcanism in this area and its continuation on the northwestern side of Tharsis, leading to the formation of the present Tharsis Montes. However, in addition to the geological evidence, detailed geophysical studies are still needed to support this hypothesis.

[59] In previous works [e.g., *Anderson et al.*, 2004; *Scott and Wilson*, 2003] it was suggested that the thickened crust under Syria Planum is a result of the formation of the Syria plain volcanism itself. In our study, the thick crust is clearly not due to the accumulation of Hesperian lava flows, which we can limit to 1–2 km (see on Figure 17). Indeed, Noachian age terrain with faulted outcrops are observed at elevations of 5700–5900 m. Assuming that this terrain was flat below Syria, this implies a thickness of 1.5 km for the Hesperian lava flows. A possibility is that these terrains could be tilted by the bulge beneath the Syria Planum unit (as shown by dotted lines on Figure 17); in that case, the thickness of Hesperian lavas can be lower (<1 km). Nevertheless, the lack of Noachian crater rim outcrops in Syria Planum suggests the first hypothesis (1–2 km) is more likely. This also implies that Syria Planum was already an area at a high elevation at the end of the Noachian, in agreement with our proposed timing for the Tharsis bulge formation.

10. Conclusions

[60] HRSC images combined with MOLA and THEMIS data enable a better understanding of some geophysical processes and structures in the Syria Planum region of Mars. The Syria Planum region reveals the following

original pattern of volcanic features distinct from the other areas over the Tharsis bulge:

[61] 1. Syria Planum contains a swarm of small shield volcanoes centered in the northeast. Each volcano has a small height (<0.3 km) and relatively moderate diameter (10–60 km), with a small slope (<2°) compared to most other Martian volcanoes. They may have formed because of fissure-fed eruptions.

[62] 2. A larger volcano (volcano A) is identified west of the small shield swarm. It displays long lava flows (>200 km) resulting from high effusion rates. On the basis of our investigation, we conclude that these lavas flows are likely to be basaltic to andesitic in composition, similar to Montes lava flows.

[63] 3. The small shield volcanoes and the extensive lava flows of volcano A appear to be structurally different and chronologically distinct, despite that no precise timescale can be proposed. In comparison with the elongated lava flows, the small shield volcanoes imply a lower volcanic eruption volume that was subsequent to the flows from volcano A. We propose that this progressive cessation of activity might be due to the role of the enhanced crustal thickness in the magmatic processes of this region.

[64] 4. We can constrain the formation of Syria Planum to the following successive magmatic and tectonic events from the early to the late Hesperian period: (1) extensional field stress that produced grabens; (2) eruption of volcano A resulting in lavas that spread all over Syria Planum; (3) tectonic deformation of the emplaced lava flows by the formation of several fractured patterns such as NE–SW en echelon faults, troughs, and adjacent grabens; and (4) new episodes of volcanic activity, forming the coalesced small shield swarms that bury preexisting faults.

[65] **Acknowledgments.** We wish to thank J. Plescia, J.M. Byrnes, L. Keszthelyi, and an anonymous reviewer for careful and constructive reviews, H. Massol for her comments, and R. Bulow for the English corrections. We acknowledge the HRSC experiment teams for their successful planning, acquisition, and making the processed data available to the HRSC team. This work is supported by a FCT (Foundation for the Science and Technology, on the QCA III European Community Support Program for 2000–2010 in Portugal) grant to A.R.B. and grants from the Programme National de Planétologie (PNP) of Institut National des Sciences de l'Univers (INSU) and Centre National d'Etudes Spatiales (CNES) for French authors.

References

Anderson, R. C., J. M. Dohm, M. P. Golombeck, A. F. C. Haldemann, B. J. Franklin, K. L. Tanaka, J. Lias, and B. Peer (2001), Primary centers and secondary concentrations of tectonic activity through time in the western hemisphere of Mars, *J. Geophys. Res.*, *106*, 20,563–20,586, doi:10.1029/2000JE001278.

Anderson, R. C., J. M. Dohm, A. F. C. Haldemann, T. M. Hare, and V. R. Baker (2004), Tectonic histories between Alba Patera and Syria Planum, Mars, *Icarus*, *171*, 31–38.

Blasius, K. R., and J. A. Cutts (1976), Shield volcanism and lithospheric structure beneath the Tharsis plateau, Mars, *Proc. Lunar Sci. Conf.*, *7th*, 3561–3573.

Bleacher, J. E., R. Greeley, D. A. Williams, and G. Neukum (2007), Morphometric characterization and comparison among the Tharsis Montes-related low shield and fissure vent fields, *Lunar Planet. Sci.*, *XXXVIII*, Abstract 1314.

Carr, M. H. (1973), Volcanism on Mars, *J. Geophys. Res.*, *78*, 4049–4062, doi:10.1029/JB078i020p04049.

Carr, M. H. (1974), Tectonism and volcanism of the Tharsis region of Mars, *J. Geophys. Res.*, *79*, 3943–3949, doi:10.1029/JB079i026p03943.

Carr, M. H. (1975), The volcanoes of Mars, *Sci. Am.*, *234*, 32–43.

Carr, M. H. (1981), *The Surface of Mars*, chap. 7, 87–113, Yale Univ. Press, New Haven, Conn.

Carr, M. H. (1996), *Water on Mars*, Oxford Univ. Press, New York.

Cattermole, P. (1987), Sequence, rheological properties, and effusion rates of volcanic flows at Alba Patera, Mars, *Proc. Lunar Planet. Sci. Conf., 17th*, Part 2, *J. Geophys. Res.*, *92*, Suppl. E553–E560.

Cattermole, P. (1990), Volcanic flow development at Alba Patera, Mars, *Icarus*, *83*, 453–493, doi:10.1016/0019-1035(90)90079-O.

Chadwick, D. J., S. S. Hughes, and S. E. H. Sakimoto (2004), Deflections in lava flow directions relative to topography in the Tharsis region of Mars: Indications of post-flow tectonic motion, paper presented at *Second Conf. on Early Mars*, Lunar and Planet. Inst., Jackson Hole, Wyo., 11–15 Oct.

Christensen, P. R. (2003), Evidence for recent climate fluctuations on Mars: From cold to colder, *Eos Trans. AGU*, *84*(46), Fall Meet. Suppl., Abstract P32B-01.

Crown, D. A., and R. Greeley (1993), Volcanic geology of Hadriaca Patera and the eastern Hellas region of Mars, *J. Geophys. Res.*, *98*, 3431–3451, doi:10.1029/92JE02804.

Davis, P. A., and K. L. Tanaka (1993), Small volcanoes in Tempe Terra, Mars: Their detailed morphometry and inferred geologic significance, *Proc. Lunar Planet. Sci. Conf.*, *24th*, 379–380.

Dohm, J. M., K. L. Tanaka, and T. M. Hare (2001), Geologic map of the Thaumasia region of Mars, *U. S. Geol. Surv. Misc. Invest. Map, I-2650*, scale:1:5,000,000.

Fink, J. H., and J. R. Zimbelman (1986), Rheology of the 1983 Royal Gardens basalt flows, Kilauea volcano, Hawaii, *Bull. Volcanol.*, *48*, 87–96, doi:10.1007/BF01046544.

Frey, H. (1979), Thaumasia: A fossilized early forming Tharsis uplift, *J. Geophys. Res.*, *84*, 1009–1023.

Greeley, R. (1973), Mariner 9 photographs of small volcanic structures on Mars, *Geology*, *1*, 175–180, doi:10.1130/0091-7613(1973)1<175:MPOSVS>2.0.CO;2.

Greeley, R. (1977), Basaltic "plains" volcanism, in *Volcanism of the Eastern Snake River Plain, Idaho: A Comparative Planetary Geology Guidebook*, edited by R. Greeley and J. S. King, NASA Conf. Rep. 154621, 23–44.

Greeley, R. (1982), The Snake River Plain, Idaho: Representative of a new category of volcanism, *J. Geophys. Res.*, *87*, 2705–2712, doi:10.1029/JB087iB04p02705.

Greeley, R., and D. Crown (1990), Volcanic geology of Tyrrhena Patera, Mars, *J. Geophys. Res.*, *95*, 7133–7149. (Correction, J. Geophys. Res., 95, 15,657, 1990.)

Greeley, R., and P. D. Spudis (1981), Volcanism on Mars, *Rev. Geophys.*, *19*, 13–41, doi:10.1029/RG019i001p00013.

Gregg, T. K. P., and J. H. Fink (1996), Quantification of extraterrestrial lava flow effusion rates through laboratory simulations, *J. Geophys. Res.*, *101*, 16,891–16,900, doi:10.1029/96JE01254.

Hartmann, W. K., and G. Neukum (2001), Cratering chronology and the evolution of Mars, *Space Sci. Rev.*, *96*(1–4), 165–194.

Hartmann, W. K., J. A. Grier, D. C. Berman, and G. A. Esquerdo (2000), The case for youthful geological activity on Mars, *Bull. Am. Astron. Soc.*, *32*, 1111.

Hauber, E., and P. Kronberg (2001), Tempe Fossae, Mars: A planetary analogon to a terrestrial continental rift?, *J. Geophys. Res.*, *106*, 20587, doi:10.1029/2000JE001346.

Hauber, E., J. Bleacher, D. Williams, and R. Greeley (2007), Plains volcanism on Mars revisited: The topography and morphology of low shields and associated volcanic landforms, paper presented at European Mars Science and Exploration Conference: Mars Express & ExoMars, Eur. Space Agency, Noordwijk, Netherlands.

Head, J. W., III, M. A. Ivanov, H. Hiesinger, M. Kreslavsky, B. Thomson, and S. Pratt (2000), Oceans in the past history of Mars?: Evidence for recession and timing from MOLA data, *Lunar Planet. Sci.*, *XXXI*, Abstract 1750.

Hiesinger, H., et al. (2005), Rheological properties of late-stage lava flows on Ascraeus Mons: New evidence from HRSC, *Lunar Planet. Sci.*, *XXXVI*, Abstract 1727.

Hiesinger, H., J. W. Head, and G. Neukum (2007), Young lava flows on the eastern flank of Ascraeus Mons: Rheological properties derived from High Resolution Stereo Camera (HRSC) images and Mars Orbiter Laser Altimeter (MOLA) data, *J. Geophys. Res.*, *112*, E05011, doi:10.1029/2006JE002717.

Hodges, C. A., and H. J. Moore (1994), *Atlas of Volcanic Landforms on Mars*, U.S. Gov. Print. Off., Washington D. C.

Hulme, G. (1976), The determination of the rheological properties and effusion rate of an Olympus Mons lava, *Icarus*, *27*, 207–213, doi:10.1016/0019-1035(76)90004-X.

Hulme, G., and G. Fielder (1977), Effusion rates and rheology of lunar lavas, *Philos. Trans.R. Soc. London, Ser. A*, *285*, 227–234, doi:10.1098/rsta.1977.0059.

Knudson, J. G., and D. L. Katz (1979), *Fluid Dynamics and Heat Transfer*, 576 pp., R.E. Krieger, Huntington, N.Y.

Malin, M. C. (1977), Comparison of volcanic features of Elysium (Mars) and Tibesti (Earth), *Geol. Soc. Am. Bull.*, *88*, 908–919, doi:10.1130/0016-7606(1977)88<908:COVFOE>2.0.CO;2.

Masson, P. (1980), Contribution to the structural interpretation of the Valles Marineris-Noctis Labyrinthus-Claritas Fossae regions of Mars, *Moon Planets*, *22*, 211–219.

McGovern, P. J., S. C. Solomon, D. E. Smith, M. T. Zuber, M. Simons, M. A. Wieczorek, R. J. Phillips, G. A. Neumann, O. Aharonson, and J. W. Head (2002), Localized gravity/topography admittance and correlation spectra on Mars: Implications for regional and global evolution, *J. Geophys. Res.*, *107*(E12), 5136, doi:10.1029/2002JE001854.

Meresse, S., et al. (2008), Formation and evolution of the chaotic terrains by subsidence and magmatism: Hydraotes Chaos, Mars, *Icarus*, *194*, 487–500.

Moore, H. J., D. W. G. Arthur, and G. G. Schaber (1978), Yield strengths of flows on the Earth, Moon, and Mars, *Proc. Lunar Planet. Sci. Conf.*, *9th*, 750–751.

Mouginis-Mark, P. J., L. Wilson, and M. Zuber (1992), The physical volcanology of Mars, in *Mars*, pp. 424–452, Univ. of Ariz. Press, Tucson.

Mutch, T. A., R. E. Arvidson, J. W. Head III, K. L. Jones, and R. S. Saunders (1976), *The Geology of Mars*, chap. 4, pp. 151–201, Princeton Univ. Press, Princeton, N.J.

Neumann, G. A., M. T. Zuber, M. A. Wieczorek, P. J. McGovern, F. G. Lemoine, and D. E. Smith (2004), Crustal structure of Mars from gravity and topography, *J. Geophys. Res.*, *109*, E08002, doi:10.1029/2004JE002262.

Pinkerton, H., and L. Wilson (1994), Factors controlling the lengths of channel-fed lava flows, *Bull. Volcanol.*, *56*, 108–120.

Plescia, J. B. (1981), The Tempe volcanic province of Mars and comparisons with the Snake River Plains of Idaho, *Icarus*, *45*, 586–601, doi:10.1016/0019-1035(81)90024-5.

Plescia, J. B. (2004), Morphometric properties of Martian volcanoes, *J. Geophys. Res.*, *109*, E03003, doi:10.1029/2002JE002031.

Plescia, J. B., and S. Saunders (1982), Tectonic history of the Tharsis region, Mars, *J. Geophys. Res.*, *87*, 9775–9791, doi:10.1029/JB087iB12p09775.

Rossi, M. J. (1996), Morphology and mechanism of eruption of postglacial shield volcanoes in Iceland, *Bull. Volcanol.*, *57*, 530–540.

Sakimoto, S. E. H. (2003), Re-assessing plains-style volcanism on Mars, paper presented at 6th International Conference on Mars, Lunar and Planet. Inst., Pasadena, Calif., Abstract 3197.

Sakimoto, S. E. H., J. Crisp, and S. M. Baloga (1997), Eruption constraints on tube-fed planetary lava flows, *J. Geophys. Res.*, *102*, 6597–6614, doi:10.1029/97JE00069.

Sakimoto, S. E. H., T. K. P. Gregg, S. S. Hughes, and J. Chadwick (2003), Martian plains volcanism in Syria Planum and Tempe Mareotis as analogs to the eastern Snake River Plains, Idaho: Similarities and possible petrologic contributions to topography, *Lunar Planet. Sci.*, *XXXIV*, Abstract 1740.

Schumacher, S., and D. Breuer (2006), Influence of a variable thermal conductivity on the thermochemical evolution of Mars, *J. Geophys. Res.*, *111*, E02006, doi:10.1029/2005JE002429.

Scott, D. H., and K. L. Tanaka (1998), Geological map of the equatorial region of Mars, *U.S. Geol. Surv. Misc. Invest. Map I-1802-A*, scale:1:15,000,000.

Scott, E., and L. Wilson (2003), Did the Alba Patera and Syria Planum regions of Mars lose their lithospheric roots in convective overturn events?, *J. Geophys. Res.*, *108*(E5), 5035, doi:10.1029/2002JE001492.

Smith, D. E., et al. (2001), Mars Orbiter Laser Altimeter (MOLA): Experiment summary after the first year of global mapping of Mars, *J. Geophys. Res.*, *106*, 23,689–23,722, doi:10.1029/2000JE001364.

Tanaka, K. L., and P. A. Davis (1988), Tectonic history of the Syria Planum province of Mars, *J. Geophys. Res.*, *93*, 14,893–14,917, doi:10.1029/JB093iB12p14893.

Tanaka, K. L., and J. M. Dohm (1989), Volcanotectonic provinces of the Tharsis region of Mars: Identification variations, and implications, paper presented at MEVTV Workshop on Early Tectonic and Volcanic Evolution of Mars, Lunar and Planet. Inst., 79–81.

Vaucher, J., et al. (2006), Cerberus Plains, Mars: Chronology of volcanic event and evidence of recent tectonic activity, *Lunar Planet. Sci.*, *XXXVII*, Abstract 1851.

Warner, N. H., and T. K. P. Gregg (2003), Evolved lavas on Mars? Observations from southwest Arsia Mons and Sabancaya volcano, Peru, *J. Geophys. Res.*, *108*(E10), 5112, doi:10.1029/2002JE001969.

Webb, B., J. W. Head III, B. E. Kortz, and S. Pratt (2001), Syria Planum, Mars: A major volcanic construct in the early history of Tharsis, *Lunar Planet. Sci.*, *XXXII*, Abstract 1145.

Wilson, L. (2001), Evidence for episodicity in the magma supply to the large Tharsis volcanoes, *J. Geophys. Res.*, *106*, 1423–1434, doi:10.1029/2000JE001280.

Wilson, L., and J. W. Head (1981), Volcanic eruption mechanisms on Mars: Some theoretical constraints, *Lunar Planet. Sci.*, *XII*, 1194–1196.

Wilson, L., and J. W. Head (1983), A comparison of volcanic eruption processes on Earth, Moon, Mars, Io and Venus, *Nature*, *302*, 663–669, doi:10.1038/302663a0.

Wilson, L., and J.W. Head III (1994), Mars: Review and analysis of volcanic eruption theory and relationships to observed landforms, *Rev. Geophys.*, *32*, 221–263.

Zimbelman, J. R. (1985), Estimates of rheologic properties for flows on the Martian volcano Ascraeus Mons, *Proc. Lunar Planet. Sci. Conf. 16th*, Part 1, *J. Geophys. Res.*, *90*, suppl. D157–D162.

Zuber, M. T., D. E. Smith, R. J. Phillips, S. C. Solomon, W. B. Banerdt, G. A. Neumann, and O. Aharonson (1998), Shape of the northern hemisphere of Mars from the Mars Orbiter Laser Altimeter (MOLA), *Geophys. Res. Lett.*, *25*, 4393–4396, doi:10.1029/1998GL900129.

E. I. Alves, Centro de Geofísica da Universidade de Coimbra, Avenida Doutor Dias da Silva, P-3000-134 Coimbra, Portugal.

V. Ansan, N. Mangold, and P. Masson, IDES, Université Paris XI, Batiment 509, F-91405 Orsay CEDEX, France.

A. R. Baptista and P. Lognonné, Géophysique Spatiale et Planétaire, Institut de Physique du Globe de Paris, 4 Avenue de Neptune, F-94107 Saint Maur des Fossés, France. (baptista@ipgp.jussieu.fr)

D. Baratoux, Laboratoire Dynamique Terrestre et Planétaire, UMR5562, Observatoire Midi-Pyrénées, Université de Toulouse III, 14 Avenue Edouard Belin, F-31400 Toulouse, France.

J. E. Bleacher, Planetary Geodynamics Laboratory, NASA Goddard Space Flight Center, Code 698, Greenbelt, MD 20771, USA.

G. Neukum, Institut für Geologische Wissenschaften, Freie Universität Berlin, Malteserstrasse 74-100, D-12249 Berlin, Germany.

D. A. Williams, School of Earth and Space Exploration, Arizona State University, P.O. Box 871404, Tempe, AZ 85287, USA.

Liste des Acronymes et Notations

La liste suivante récapitule les principaux acronymes utilisés dans le texte :

BSVP - *Basaltic Volcanism Study Project*

ESA – *European Space Agency* (Agence Spatiale Européenne)

GCM – *Global Circulation Model* (Modèle de Circulation Globale de l'atmosphère)

HIRISE – *High Resolution Imaging Science Experiment*

HRSC – *High Resolution Stereo Camera* MAG-ER – *Magnetometer and Electron Reflectometer*

MEX – *Mars Express Mission*

MGS – *Mars Global Surveyor*

MO – *2001 Mars Odyssey* MOC – *Mars Orbital Camera*

MOLA – *Mars Orbiter Laser Altimeter*

NASA – *National Aeronautics and Space Administration*

OMEGA – *IR Mineralogic Mapping Spectrometer*

SNC – *Shergotty Nakhla Chassigny* (Shergotites Naklites Chassigny)

TES – *Thermal Emission Spectrometer*

UA – Unité Astronomique

USGS – *United States Geological Survey* (Institut de surveillance géologique des Etats-Unis)

Et finalement, la liste suivante récapitule les principales notations adoptées dans le texte :

Partie II :

N - Nombre de cratères per surface S

Q – Débit volumétrique

Gz – Nombre adimensionnel de Graetz

k – Diffusivité Thermique

b – Epaisseur de la coulée de lave

θ – Pente de la coulée de lave

μ – Viscosité de la coulée de lave

ρ – Densité de la coulée de lave

w – Largeur de la coulee

g' - Constante universelle de la gravité

σ_s - *Yield Stress* (Limite d'élasticité)

Partie III :

r - Rayon planétaire moyen

T_c - Epaisseur de la croûte

T_e - Epaisseur élastique

h, z - Hauteur du relief

ρ_c - Densité moyenne de la croûte

ρ_m - Densité moyenne du manteau

ρ - Densité moyenne de la planète

g - Constante universelle de la gravité

C_p – Capacité de Chaleur

k – Conductivité Thermique

Q_H – Chaleur Radiogénique per masse

Q – Flux de Chaleur

T_0 – Température à la surface

H – Source générale de Chaleur

Liste des Figures et Légendes

Part I

Part II

isochrones are given by the lunar rates modulated by a ratio of R=1.6 corresponding to the ratio between the crater production function on Mars and the same rate on the Moon. However, these could all correspond to Hesperian ages. Dots correspond to volcanoes ages, associated with a surface of 7760 km^2

FIG. 3.12 - *a) On the center of this image one can observe volcano A, which is the eruption center of the described lava flows. The caldera is about 40 km wide. On the bottom right of the image the shield volcano 5 is visible. On the top right several collapse features are noted. The profile a-b is shown on image b). c) HIRISE image (PSP_001840_1660) showing a volcanic vent, with about 700 m width, on the top of volcano A.*

FIG. 3.13 - *HRSC image centered at 20.5ºS; 102.3ºW, where some NW/SE -oriented grabens are covered by lavas with the same orientation.*

FIG. 3.14 - *Image centered at 17.3ºS, 100ºW. Lava channels are visible on the described lava flows. The channel on the top right displays lava levees on its sides. The profile a – b is shown on the bottom graphic.*

FIG 3.15 - *Left: HRSC image centered approximately at 19.8ºS; 100.9ºW, showing the volcano 31, a fissure some tens of kilometers long from which lavas erupted. Its borders, which have a clearly darker tone, define well its shape,. Right: HRSC image centered at 15.4ºS; 101.5ºW, where volcanoes 11 and 12 superimpose lavas that were intersected by fissures oriented NE/SW.*

FIG. 3.16 - *Profile NE–SW from Syria Planum. From highest to lowest altitudes we can observe the succession of the low shield volcanoes, the lava flows intersected by predominantly NE–SW fissures, and the highly faulted lava terrains. As it is observed by the profile, the thick crust in Syria is clearly not due to the accumulation of Hesperian lava flows, which we can limit to 1-2 km (Lava Flows Unit). These terrains could have been tilted by the bulge beneath the*

Part III

Liste des Tableaux

Partie II

Partie III

Abstract

In this work it was done a detailed study of the Syria Planum Volcanic Province on Mars. With the help of new set of data available from the most recent missions to this planet, we were then able to better understand this volcanic region formation and evolution. We described a set of coalesced shield volcanoes that concerning its morphology and rheology are not known anywhere else on Mars. Consequently, we hypothesized that Syria Planum shield volcanoes played an important role on the Tharsis main volcanism and also that ceased the volcanic activity early in its geological history. The progressive cessation of activity might be due to the enhanced crustal thickness in the magmatic processes of this region. The highest crustal thickness beneath Syria Planum led us to think on its principal role on the origin but also on the decline of the volcanism in this area, and it's continuation on the northwestern side of Tharsis, leading to the formation of the present Tharsis Montes. Moreover, analysis by Neukum et al. [2004] on Tharsis, leads to the conclusion that some of these flows are effectively very recent, about 2 Ma. Also, the evidence for recent volcanism, namely in the Tharsis province, is assumed by some other authors [e.g. Schumacher and Breuer, 2006] taking into account mantle convective heat parameterized models. Therefore, the mechanisms that cause the longstanding volcanic activity were still not well understood. For that purpose, in this dissertation we proposed the locally enhanced crustal thickness as the engine for the longstanding volcanic manifestation on the Tharsis province of Mars.

Résumé

Dans le cadre de cette étude, nous avons analysé le volcanisme de la région de Syria Planum sur Mars. La connaissance en détail de cette région, favorisée par les récentes données des missions spatiales sur cette planète, nous a conduits à mieux comprendre cette province volcanique. Nous avons analysé des groupes de volcans boucliers accolés, que par leurs caractéristiques morphologiques et rhéologiques ne sont pas connus ailleurs sur Mars. En conséquence, nous avons pu formuler l'hypothèse et démontrer que Syria Planum a joué un rôle important dans le développement du volcanisme de Tharsis.

Nous avons aussi montré que Syria Planum a arrêté son volcanisme tôt dans le passé géologique, par rapport au volcanisme global de Tharsis. La cessation progressive du volcanisme doit être due à un important épaississement crustal, résultat des intenses processus magmatiques primordiaux de cette zone.

L'épaisseur crustale la plus élevée au-dessous de Syria Planum nous a permis de remarquer son rôle principal dans l'origine mais aussi dans le déclin du volcanisme de cette région. Néanmoins, le volcanisme a poursuivi son activité dans la partie nord-ouest de Tharsis, en conduisant à la formation des Montes Tharsis jusqu'à l'époque actuelle. Particulièrement, des analyses d'imagerie menées par Neukum et al. [2004] sur Tharsis, montrent que Tharsis exhibe des coulées de lave récentes, âgées de 2 Ma. De même, des évidences d'un volcanisme récent sur Tharsis sont démontrées par des modèles de convexion thermique du manteau [ex. Schumacher and Breuer, 2006]. Cependant, les mécanismes internes qui favorisent la maintenance de ce volcanisme sont effectivement méconnus. Aussi dans cette étude, nous avons proposé l'influence des variations locales de l'épaisseur crustale comme étant le moteur des manifestations à long-terme du volcanisme.